UCRL-11338 Rev. 1

c.2

University of California

Ernest O. Lawrence Radiation Laboratory

TWO-WEEK LOAN COPY

This is a Library Circulating Copy which may be borrowed for two weeks. For a personal retention copy, call Tech. Info. Division, Ext. 5545

STUDIES IN THE LIQUID-DROP THEORY OF NUCLEAR FISSION

Berkeley, California

UCRL-11338 Rev. 1 c.2

DISCLAIMER

This document was prepared as an account of work sponsored by the United States Government. While this document is believed to contain correct information, neither the United States Government nor any agency thereof, nor the Regents of the University of California, nor any of their employees, makes any warranty, express or implied, or assumes any legal responsibility for the accuracy, completeness, or usefulness of any information, apparatus, product, or process disclosed, or represents that its use would not infringe privately owned rights. Reference herein to any specific commercial product, process, or service by its trade name, trademark, manufacturer, or otherwise, does not necessarily constitute or imply its endorsement, recommendation, or favoring by the United States Government or any agency thereof, or the Regents of the University of California. The views and opinions of authors expressed herein do not necessarily state or reflect those of the United States Government or any agency thereof or the Regents of the University of California.

Submitted to Annals of Physics

UCRL-11338 Rev. 1

UNIVERSITY OF CALIFORNIA
Lawrence Radiation Laboratory
Berkeley, California

AEC Contract No. W-7405-eng-48

STUDIES IN THE LIQUID-DROP THEORY OF NUCLEAR FISSION

James Rayford Nix and Wladyslaw J. Swiatecki

April 1, 1964

STUDIES IN THE LIQUID-DROP THEORY OF NUCLEAR FISSION

James Rayford Nix and Wladyslaw J. Swiatecki

Lawrence Radiation Laboratory
University of California
Berkeley, California

April 1, 1964

ABSTRACT

In connection with nuclear fission we study the division of an idealized charged drop, using a simplified version of the liquid-drop model. The degrees of freedom essential to a discussion of the division of a charged drop and the separation of the fragments to infinity are taken into account: a fragment-separation coordinate, a mass-asymmetry coordinate, a deformation coordinate for each fragment, and rotational coordinates for each fragment. To specify fragment deformation, the fragments are represented by spheroids; a nucleus prior to division is represented by two overlapping spheroids. The Hamiltonian for the idealized system consists of a sum of surface, Coulomb, and kinetic energies. A study of the saddle-point energies and shapes calculated in this two-spheroid approximation indicates that the approximation is most useful for discussing the fission of elements lighter than about radium. On the basis of this model, we calculate probability distributions for certain observable characteristics of fission fragments at infinity—their total translational kinetic energy, mass, individual excitation energies, and individual angular momenta. This is done by applying standard static, dynamical, and statistical methods to the Hamiltonian for the system. The present treatment, for the most part, is classical; quantum mechanics is considered only in the statistical-mechanics discussion of the behavior of the system near the saddle point.

The predictions of the model are compared with existing experimental data for distributions in fragment mass and total translational

kinetic energy, for nuclei lighter than radium. The comparisons are made without the use of any adjustable parameters. The theory is capable of accounting for the magnitudes of the most probable values and widths of the experimental distributions, as well as some, but not all, finer details of the distributions. The dependence of the experimental distributions upon nuclear temperature, and the dependence of the experimental most probable kinetic energies upon fissionability parameter are also approximately reproduced by the calculations.

I. INTRODUCTION

Nuclear fission was discovered by Hahn and Strassmann (1) in 1938, and yet, in the two and a half decades since its discovery, an adequate theory of the fission process has still not emerged. Numerous papers have been written dealing with various aspects of the theory, but in no instance has a definite model with a well-defined Hamiltonian been chosen and the implications of this model systematically worked out in detail. Such an approach would require that one select a model characterized by definite degrees of freedom; apply standard static, dynamical, and statistical methods to the resulting Hamiltonian; and compare the predictions of the model with experiment. In the present study we attempt to do this for a simplified version of the liquid-drop model. (A more detailed account of this work is given in Ref. 2; see also Ref. 3.)

Shortly after the discovery of nuclear fission, Meitner and Frisch emphasized the analogy between the fission process and the division of a charged drop of liquid(4). On the basis of the liquid-drop model, Bohr and Wheeler showed that a satisfactory account could be given of some of the phenomena observed in fission(5). These early successes of the liquid-drop model and its conceptual simplicity firmly established its popularity for discussing fission.

The major effort in the development of liquid-drop theory has been concerned with the static problem of calculating the potential energy of a deformed charged drop. The coordinates normally used to describe a deformed drop are the coefficients in the expansion of the drop's radius vector in spherical harmonics. The energy of a nearly spherical drop can then be calculated in terms of these coordinates as an expansion about a sphere(5-13). A similar technique, appropriate for shapes not far removed from spheroids (ellipsoids of revolution), is the expansion about a spheroid(8-13). For highly distorted shapes the deformation energy has to be calculated numerically(14-18). The potential energy of charged drops is now fairly well understood, particularly with regard to the variation of fission barriers throughout the periodic table.

Although statics has been extensively studied little is known about the dynamics of nuclear division. A fragmentary study of the dynamical aspects of fission was performed by Hill, and by Hill and Wheeler in connection with the question of mass asymmetry (19-21). For a few special cases, the division of a charged drop was traced out numerically to a short distance before the actual division of the drop into two fragments (scission). However, no relationship between initial conditions and final results was established. Some limited aspects of dynamics have also been considered by other authors (8, 22-25).

The statistical mechanics of fission has been investigated in some detail. Bohr and Wheeler formulated the calculation of fission probabilities by applying statistical transition-state methods at the saddle point (5). [See in particular the recent article by Wheeler (26).] The application of statistical mechanics in a somewhat different manner was discussed by Fong, whose starting point was the assumption of statistical equilibrium at the scission point (27-30). This theory suffers, however, from an arbitrariness in the definition of the scission configuration, which, unlike a saddle-point configuration, is not defined by the statics of the problem. Statistical aspects of fission have also been examined by several other authors (31-37).

We see that statics, dynamics, and statistical mechanics have all been considered to some extent in previous studies of fission. Never, however, have they been treated systematically for one and the same Hamiltonian.

In the present paper an attempt is made to study each of these steps for a simplified version of the liquid-drop model. The outline of

our program is as follows:

(1) Statics: After the coordinates specifying the system have been selected, the potential energy of the system (for a given nucleus) is mapped as a function of its coordinates, and the saddle point is located and its properties studied.

(2) Dynamics: The kinetic energy of the system is calculated as a function of the coordinates and their conjugate momenta. This makes it possible, by solving Hamilton's classical equations of motion for the system, to discuss the division of the nucleus and the separation of the fragments, from some given initial configuration to infinity.

(3) Statistical mechanics: In analogy to the method employed in discussing chemical reaction rates (38), attention is focused on the system at the saddle point (transition state), and statistical equilibrium is assumed to hold there. In the case of chemical reactions, this provides information regarding the rate of reaction, and it was for the calculation of rates that Bohr and Wheeler used the transition-state method (5). In our case, however, we use the transition-state method to calculate the probability for finding the system in a given state of motion close to the saddle point. These probability distributions are then combined in the sense of initial conditions with the dynamical calculations [step (2)] to trace out the separation of the fragments to infinity. This converts the probability distributions of the states of motion around the saddle point into the probability distributions of observable characteristics of fission fragments: their kinetic energies, excitations, and angular momenta.

Since the difficulty of solving dynamical equations of motion increases with the number of coordinates, it is desirable from the calculational point of view to have present in one's model as few degrees of freedom as possible. Let us therefore see what degrees of freedom it is essential to consider. Although we will be concerned with the liquid-drop model, the discussion that we are about to give for the degrees of freedom essential to fission is quite general and does not depend upon the assumption of the liquid-drop model.

A single fission fragment has three rotational degrees of freedom and three degrees of freedom associated with its center-of-mass motion. The specification of a fragment's extension in three dimensions requires three lengths (say three orthogonal axes a, b, c). This suffices to describe its size and leaves two dimensionless numbers to describe the fragment's intrinsic shape. [These numbers could be, for example, the β and γ deformations of the collective model or related parameters (39).] Thus to describe in this way the configuration of n fragments resulting from the division of a nucleus of given volume requires $(3 + 3 + 3)n - 1$ degrees of freedom. (The "minus one" reflects the fact that the total volume is given.) In the case of binary fission this gives $(9)(2) - 1 = 17$ as the number of coordinates required to describe a pair of separated fragments (see Fig. 1; in the caption to this figure an alternative enumeration of the 17 degrees of freedom is given).

It is necessary in a model of fission that one be able to describe in a continuous manner the sequence of shapes of a fissioning nucleus from the original sphere, through the saddle point and scission configuration, to the two fragments at infinity. If the number of

degrees of freedom is not to change in the course of the division, it follows that the number of degrees of freedom specifying fission shapes before division into separate fragments must also, in general, be 17 or more.

One could in principle continue introducing additional degrees of freedom to describe finer details of the dividing nucleus, including ultimately single-particle structure, until the number of degrees of freedom equaled the sum of the degrees of freedom of all the individual nucleons. We will consider explicitly, however, only the 17 basic degrees of freedom enumerated above. Although the remaining degrees of freedom will never be treated explicitly, they will, on the other hand, not be disregarded entirely. Their presence will be recognized implicitly when we consider the statistical mechanics of fission, when they will be assigned their statistical share of the total energy.

The question arises of how to choose the deformation coordinates for each fragment. We shall not be concerned here with effects arising from deviations of the fragments from axial symmetry. We will therefore restrict ourselves from the beginning to fragments that are axially symmetric, thus reducing the number of degrees of freedom to 15. Because spheroids can represent any desired degree of prolate and oblate elongation, and because their surface and Coulomb energies can be easily calculated, we will use spheroids to represent the fission fragments. We will represent a nucleus prior to division by two <u>overlapping</u> spheroids, with the interior surface of each simply "erased." With this parametrization, one is able to describe continuously in an

approximate way the sequence of shapes of a fissioning nucleus from the original sphere to the two fragments at infinity.

Of the 15 degrees of freedom required for specifying a system composed of two axially symmetric fragments, 3 are trivially eliminated by working in the center-of-mass system. Three more may be eliminated if, as will be done in the present work, one restricts the discussion to a system with zero total angular momentum.

This, then, leaves a system possessing nine degrees of freedom. In the neighborhood of the saddle point, these nine degrees of freedom correspond to certain characteristic motions of the system. The most important of these is the motion in the fission direction—an over-all separation of the system leading to its eventual division into fission fragments. The potential energy in this direction is of the form of a potential-energy barrier. For division of the drop to occur, the system must pass over this barrier.

Most of the remaining motions near the saddle point (motions in the non-fission direction) consist, in general, of bounded small oscillations, resulting from the potential energy increasing with deviations from the saddle point in these directions. These oscillations involve the relative sizes of the fragments, their eccentricities,

and their orientations in space. The various modes of oscillation that occur correspond roughly to (a) a change in the relative sizes of the nascent fragments, (b) an in-phase or out-of-phase stretching and contraction of the two halves of the saddle-point configuration, and (c) a bending and "wriggling" of the saddle-point configuration. In the treatment of these oscillations, the approximation that they are small will be made, although there will be some discussion of higher-order effects.

The separation of the fragments from the saddle point to infinity will be traced out dynamically. This converts the possible states of motion near the saddle point into states of motion of two fragments at infinity. The motion of the fragments at infinity, consisting of a translation of their centers of mass, and rotations and vibrations about their centers of mass, corresponds directly to observable properties of fission fragments: (a) The speed of separation of the fragments' centers of mass determines their translational kinetic energies. (b) The relative sizes of the fragments are directly observable. (c) The vibrations of the fragments are associated with their excitation (vibrational or deformation) energies.[1] (d) The rotations of the fragments are associated with their angular momenta.

We will find that for each of the above quantities we are able to discuss not only its most probable value, but also the distribution about its most probable value. In particular, our theory predicts the probability distribution $P(E, U, X_1, X_2, \underset{\sim}{L}_1, \underset{\sim}{L}_2)$ of simultaneously observing the two fragments at infinity with total translational kinetic energy E, fractional mass U, individual excitation energies X_1 and

---

[1] When used in this context, the term "excitation energy" refers to the energy of the collective vibrations and deformations of the fragment; it does not include the internal (excitation) energy of the individual nucleons.

X_2, and individual angular momenta $\underset{\sim}{L}_1$ and $\underset{\sim}{L}_2$. It proves convenient in practice to obtain from this distribution, by integrating over the quantities not of immediate interest, probability distributions involving a smaller number of observable quantities. Three such distributions are $P(E, U)$, $P(X_1, X_2)$, and $P(\underset{\sim}{L}_1, \underset{\sim}{L}_2)$.[2]

Our theory will also predict how these distributions should vary with the (internal) excitation energy of the compound nucleus undergoing fission, as well as with its charge and mass.

The immediate test of the theory will be the comparison of predictions with experiment for distributions in mass and total translational kinetic energy $[P(E, U)]$.[3] It is hoped that these comparisons, as well as those to be made when more experimental information becomes available, will yield a more accurate idea of the relevance of the liquid-drop model for discussing fission phenomena. Indeed, the entire purpose of undertaking this study was to trace out in detail the characteristics of the division of an idealized droplet whose size, surface tension, and charge are those of a nucleus, and to compare the results with what is observed experimentally in the fission of real nuclei. Stated in this way, there are <u>no adjustable parameters</u>

---

[2] The same symbol P is used throughout this paper to denote each of several probability distributions; the argument or subscript will indicate which explicit function is being referred to.

[3] Experimental information regarding the other distributions is at present not available for the fission of nuclei lighter than radium. We will see later that it is for these nuclei that our model is most nearly applicable.

in the problem.[4] Thus, when the comparison is made with experiment, we shall learn unambiguously to what extent an idealized liquid-drop model is capable of representing the characteristics of fission, as regards both over-all order-of-magnitude agreement and also more detailed aspects of the process.

Concerning the question of the validity of the liquid-drop model for discussing fission, we believe that the above clear-cut program of an unambiguous comparison of nuclear fission with the division of an idealized drop should be carried through irrespective of how good the liquid-drop model is thought to be. Nevertheless it is of interest to form some a priori judgment as to how well an idealized drop might be expected to represent nuclear fission. Some comments on this subject are made in the Appendix. Our conclusion is that although the liquid-drop theory of fission would not be expected to be accurate for a particular nucleus, it can be expected to yield the correct average behavior of nuclei throughout the periodic table, in analogy to the way the liquid-drop semiempirical mass formula reproduces the correct trends in the masses of nuclei, apart from oscillations due to shell structure.

---

[4] We have taken the constants of the Bethe-Weizsäcker semiempirical mass formula from Green's analysis of ground-state masses (40). The nuclear temperature at the saddle point is determined from the excitation energy and fission barrier of the compound nucleus. All other quantities are calculated directly from the model.

II. STATICS

We shall be concerned in this section with the static properties of our model—with mapping the potential energy of the system as a function of its coordinates, and with studying the properties of the saddle-point configuration. Before proceeding with this study, however, it will be advantageous for us to take care of some preliminaries.

A. Units, Notation, and Coordinates

For discussing fission within the framework of the liquid-drop model it is convenient to use a system of units based on the original spherical drop, rather than the conventional units of length, mass, and time. The three "natural" units to choose are the radius, mass, and surface energy of the original drop. Time is then no longer a fundamental unit, but is expressed in terms of a length, a mass, and an energy. This is analogous to the situation in elementary-particle physics, for example, where the speed of light, Planck's constant divided by 2π, and the pion mass are chosen as units.

In actual applications it is necessary to convert these liquid-drop units to conventional units. For the comparison of the theoretical and experimental results discussed here, this conversion is made with Green's values for the constants in the semiempirical mass formula(40).[5] We denote by A the number of nucleons in the compound nucleus undergoing fission. The radius of the original drop is then

$$R_0 = r_0 A^{1/3}, \quad \text{with } r_0 = 1.216\times10^{-13} \text{ cm}, \tag{1a}$$

and its surface energy is

$$E_S^{(0)} = a_S A^{2/3}, \quad \text{with } a_S = 17.80 \text{ MeV}. \tag{1b}$$

---

[5] When future determinations of these constants are made, the new values may be used since all theoretical quantities are given here in liquid-drop units.

The mass of the original drop, to an accuracy within one part per thousand, is equal to the mass unit times the number of nucleons; thus,

$$M_0 = m_0 A, \tag{1c}$$

with

$$m_0 = 1.660\times10^{-24}\ \mathrm{g} = 931\ \mathrm{MeV}/c^2\ \text{(Ref. 41)}.$$

In this discussion of units the symbol c denotes the speed of light.

The units for other familiar quantities may be readily derived from these three fundamental ones. For example, the unit of time is

$$T_0 = [M_0/E_S^{(0)}]^{1/2} R_0 = (m_0/a_S)^{1/2} r_0 A^{1/2}$$

$$= (2.933\times10^{-23}\ \mathrm{sec})A^{1/2}, \tag{2}$$

the unit of linear momentum is

$$P_0 = [M_0 E_S^{(0)}]^{1/2} = (m_0 a_S)^{1/2} A^{5/6} = (128.8\ \mathrm{MeV}/c)A^{5/6},$$

and the unit of angular momentum is

$$L_0 = [M_0 E_S^{(0)}]^{1/2} R_0 = (m_0 a_S)^{1/2} r_0 A^{7/6} = (0.793\,\hbar)A^{7/6}, \tag{3}$$

where $\hbar$ is Planck's constant divided by 2π. The unit of frequency is

$$\Omega_0 = 1/T_0 = (3.409\times10^{22}/\mathrm{sec})/A^{1/2}; \tag{4a}$$

when multiplied by $\hbar$ this becomes

$$\hbar\Omega_0 = 22.44\ \mathrm{MeV}/A^{1/2} = 1.261\ E_S^{(0)}/A^{7/6}. \tag{4b}$$

Although the unit of charge is formally $[R_0\ E_S^{(0)}]^{1/2}$, the charge on the drop is more conveniently specified through the dimensionless fissionability parameter x, defined by (5)

$$x = \frac{(\text{charge})^2}{10(\text{volume})\,(\text{surface tension})}. \tag{5a}$$

(The surface tension multiplied by $4\pi r_0^2$ is equal to a_S.) For a uniformly charged drop with a sharp surface,

$$x = E_C^{(0)}/[2E_S^{(0)}], \tag{5b}$$

where $E_C^{(0)}$ is the Coulomb energy of the original drop, given by

$$E_C^{(0)} = 3Z^2e^2/(5R_0) = a_C Z^2/A^{1/3},$$

with Z the number of protons, e the electronic charge, and the constant $a_C = 0.710$ MeV(40). A third conventional form for x is

$$x = (Z^2/A)/(Z^2/A)_{crit}, \tag{5c}$$

where

$$(Z^2/A)_{crit} = 2\,a_S/a_C = 50.13.$$

When these liquid-drop units are used, the results of our calculations can be displayed as functions of a single parameter (e.g., x) rather than as functions of two parameters (e.g., Z and A).

The notation of this paper will adhere, insofar as is practicable, to the following convention: Quantities referring to the left-hand fragment will be distinguished by the subscript 1, and to the right-hand fragment by the subscript 2. Furthermore, unless otherwise noted, any quantity that is the sum of two quantities, each referring to an individual fragment, will be designated by the same symbol but without subscripts; e.g., the total excitation energy of both fragments ($X_1 + X_2$) will be denoted by X.

For specifying the angles involved in our problem, we will adopt the following scheme (see the lower part of Fig. 2): We denote by Θ and Φ the two angles specifying the direction in space of the line connecting the centers of the two fragments. We define a right-handed coordinate system whose origin is at the center of fragment 1,

whose z_1 axis is along the line connecting the spheroid centers (positive in the direction fragment 2), and whose x_1 and y_1 axes are perpendicular to one another and to the z_1 axis. We define a second coordinate system whose origin is at the center of fragment 2, and whose x_2, y_2, and z_2 axes are parallel (with the same sense of direction) to the x_1, y_1, and z_1 axes, respectively. Then the orientation in space of fragment 1 is specified by the three Euler angles θ_1, ϕ_1, and ψ_1 [as defined, for example, by Goldstein(42)], and the orientation of fragment 2 by θ_2, ϕ_2, and ψ_2. These angles are defined as the (counterclockwise) angles of rotation about three mutually inclined axes necessary to bring a fragment from a position with its symmetry axis along the z_1 (or z_2) axis to its final position. For fragment 1, say, these rotations are: one through the angle ϕ_1 about the z_1 axis, one through the angle θ_1 about the new x_1 axis, and one through the angle ψ_1 about the new z_1 axis, made in that order. The angle θ_1 is the polar angle of spherical coordinates usually denoted by the same symbol: the angle between the z_1 axis and the symmetry axis of fragment 1. The angle ϕ_1 is related to the usual azimuthal angle of polar coordinates by an additive constant.

Because of the symmetry of the system, the potential energy is independent of all but the following three of the above angles: θ_1, θ_2, and the difference $\phi = \phi_1 - \phi_2$ between the azimuthal angles of the fragments' symmetry axes.

We choose the four remaining coordinates required for specifying a two-spheroid configuration (in the center-of-mass system) as follows: (a) the distance ℓ between the centers of the two spheroids, (b) the fractional mass (fractional volume) U of the left-hand fragment,[6] and (c) the semiaxes c_1 and c_2 of each fragment along its line of symmetry[7] (see again the lower part of Fig. 2).

---

[6] The fractional mass of the right-hand fragment is 1-U.

[7] For example, if spheroid 1 is prolate, then c_1 is its semimajor axis; its semiminor axis is determined by volume conservation.

Prior to division into separate fragments, the nucleus is represented by two overlapping spheroids. When the spheroids are overlapping, both the potential energy and the kinetic energy are much more difficult to calculate than when they are separated, and we then consider only the restricted case of symmetrical fragments, in which $U = 1/2$, $c_1 = c_2 \equiv c$, and $\theta_1 = \theta_2 = 0$. (The potential energy is for this case independent of ϕ.) For this restricted case, the two coordinates ℓ and c completely specify the system (see the upper part of Fig. 2).

B. Potential Energy of the System

The potential energy of the system is simply the sum of the surface energy E_S and the Coulomb energy E_C. The potential energy $\mathcal{V}$ of a deformed drop, relative to the original drop, is then

$$\begin{aligned}\mathcal{V} &= E_S - E_S^{(0)} + E_C - E_C^{(0)} \\ &= (B_S - 1)\, E_S^{(0)} + (B_C - 1) E_C^{(0)} \\ &= [\,(B_S - 1) + 2 \times (B_C - 1)]\, E_S^{(0)} \,. \end{aligned} \tag{6a}$$

The function B_S is the total surface energy of the system in units of the surface energy $E_S^{(0)}$ of the original drop, and B_C is the total Coulomb energy of the system in units of the Coulomb energy $E_C^{(0)}$ of the original drop. The definition (5b) is used in going from step 2 to step 3. When the system consists of two separated fragments, the potential energy is conveniently written as

$$\mathcal{V} = \left\{ [\, B_S^{(1)} + B_S^{(2)} - 1] + 2x\, [\, B_C^{(1)} + B_C^{(2)} + B_I - 1] \right\} E_S^{(0)} \,. \tag{6b}$$

The function $B_S^{(1)}$, for example, is the surface energy of fragment 1 in units of $E_S^{(0)}$, $B_C^{(1)}$ is the Coulomb self-energy of fragment 1 in units of $E_C^{(0)}$, and B_I is the Coulomb interaction energy between

fragments 1 and 2 in units of $E_C^{(0)}$. In terms of these appropriate units, the various energies denoted by B depend upon neither the value of A nor of Z of the original nucleus; they are functions only of the shape of the system.

Different formulae for calculating the energies are used, depending upon whether the system consists of separated spheroids or overlapping spheroids. The case in which the spheroids are separated is the simpler. The surface energies and Coulomb self-energies are then expressible in a closed form, and the interaction energy may be calculated by performing a triple multipole summation. Formulae for calculating $\mathcal{V}$ as a function of the coordinates specifying the system are given in Appendix B.1 of Ref. 2. For the restricted case of overlapping spheroids, specified by the two coordinates ℓ and c, the surface energy is again expressible in a closed form, but the Coulomb energy must now be calculated by numerically evaluating a double integral. The formulae given in Appendix B.2 of Ref. 2 for the symmetric overlapping case could be readily generalized to the case where $U \neq 1/2$ and $c_1 \neq c_2$, but not to the non-axially-symmetric case.

Let us now examine the appearance of the potential-energy surfaces calculated with these formulae. Since the results can be displayed easily in at most two dimensions, we present maps of the potential energy as functions of the two coordinates specifying symmetrical fragments: the separation coordinate ℓ and the deformation coordinate c. An examination of the potential energy for this restricted case will tell us many things of interest, including the location and energy of the saddle point. The potential energy is mapped in Fig. 3 for values of the fissionability parameter x between 0 and 1.0, at intervals of 0.2. (For potential-energy maps at intervals of 0.05 in x see Fig. 3 of Ref. 2.) In this figure are included maps of the surface energy B_S and the Coulomb energy B_C, as well as an illustration of configurations of the system for various values of the coordinates.

An expansion of the potential energy about the sphere indicates that for small distortions the contours are portions of ellipses whose major axes are tilted at angles of about 30.5° from the horizontal (see Appendix B.2 of Ref. 2). As the drop distorts in the direction of the saddle point, the potential energy increases until the saddle point is reached and then begins to decrease. For large values of x the potential-energy surface is much flatter in the overlapping region than in the separated region; the opposite is true for small values of x. The potential-energy surface in the separated region is a "trough" that drops off approximately as $1/\ell$ along the separation coordinate. At the scission line $\ell = 2c$ dividing the two regions there occurs a cusp in the energy surface.[8] This results from the discontinuous rate of change of the surface energy in passing from the region of overlapping spheroids, where the surface energy increases with separation, to the region of separated spheroids, where the surface energy is independent of separation.

The results of electronic computer studies of equilibrium configurations of idealized charged drops have recently become available (15-18). It is possible, then, to compare with these essentially exact results various properties of equilibrium configurations calculated in the two-spheroid approximation. This will provide us with some idea of the

---

[8] When all coordinates are considered, the cusp occurs at those values of the coordinates that correspond to the configuration of touching spheroids.

limitations of our model. The following properties of equilibrium configurations are compared as functions of fissionability parameter: the total potential energy $\mathcal{V}$, in Fig. 4; the individual surface and Coulomb energies B_S and B_C, in Fig. 5; the saddle-point shape of the drop, in Fig. 6; and the drop's maximum and minimum radii R_{max} and R_{min}, in Fig. 7.

There are several observations that may be made. One concerns the general appearance of the saddle-point shapes. A striking discrepancy between the true saddle-point shapes and those calculated in the two-spheroid approximation occurs in the central region of the drop (the neck). The restriction that the fragments maintain spheroidal shapes allows the drop very little freedom at its neck. In particular, a discontinuity is introduced in the surface of the drop, and the radius of the neck (R_{min}) in its dependence on x is reproduced very poorly. The two-spheroid model is thus not suitable for discussing phenomena that depend upon the properties of the neck.

In the two-spheroid approximation, when the fissionability parameter x is between 0 and 0.80, the saddle point lies on the scission line, possessing the shape of two tangent spheroids. For values of x between 0.80 and 1.0, the saddle point occurs for some value of $\ell < 2c$; i.e., the saddle-point shape is the configuration of two overlapping spheroids. The results of the exact calculations indicate that the saddle-point shapes change from dumbbell-like (approximated by two tangent spheroids) for $x \lesssim 0.67$ to cylinder-like (approximated by two overlapping spheroids) for $x \gtrsim 0.67$ (15). Thus the transition at $x \approx 0.80$ in the two-spheroid model, although qualitatively correct, occurs at a value of x that is somewhat too high.

In the short interval $0.79 \lesssim x \lesssim 0.85$ there are in the two-spheroid model three equilibrium configurations (apart from the original sphere): two saddle points and one stable minimum point.[9]

---

[9] This is clearly seen in Fig. 3 in the map for $x = 0.8$.

The occurrence of three configurations of equilibrium is associated with a "dip" in the potential energy as a function of distortion. For x close to the respective transition point in both the two-spheroid approximation and in the exact calculations, the potential energy becomes extremely flat. A very slight dip occurs in the two-spheroid model, resulting in three equilibrium configurations, but does not occur in the exact calculations.[10]

The dependence on x of the remaining properties calculated in the two-spheroid approximation is qualitatively correct. The two-spheroid model in addition reproduces the exact results both for x close to 1.0, where the saddle-point shape is a single spheroid (a single sphere at $x = 1.0$), and at $x = 0$, where the saddle-point shape is a pair of tangent spheres. However, it is clear from the figures that for the range of x roughly between 0.67 and 0.85 the two-spheroid model represents very poorly the true saddle-point properties. Thus, for $0.67 \lesssim x \lesssim 0.85$ this model should not be expected to accurately describe phenomena associated with saddle-point shapes.[11] Nevertheless, the model may still be useful for this range of x for discussing phenomena not related to the saddle point, such as the separation of the fragments after scission.

For $x \lesssim 0.67$ there is fair agreement between the exact saddle-point properties and those calculated in the two-spheroid approximation. The following major discrepancies should be noted. The fission barrier (saddle-point potential energy) calculated in the two-spheroid approximation is higher than the true liquid-drop barrier. This difference becomes as large as about 23 MeV, when the two-spheroid

[10] Historically, however, it was for a time believed that three equilibrium configurations possibly did exist for a short range of x close to 0.7 (15, 43).

[11] Unfortunately, most experimental information on fission is for nuclei that lie in this range of x. Some data exist, however, on the fission of nuclei where $x \lesssim 0.67$, and more are becoming available as time progresses.

barrier is roughly twice as high as the exact one. This means that the division of the total energy of the system at the saddle point into potential energy and internal excitation energy will be incorrect. The potential energy of deformation will be greater than it should be, and the internal excitation energy less by a corresponding amount.

Recall that for the lower values of x under consideration ($x \lesssim 0.67$) the saddle point lies on the scission line, where there is a cusp in the potential energy. In the direction of motion across the saddle point, then, there is a discontinuity in the rate of change of the potential energy. The second derivative, in particular, representing the (negative) "fission" stiffness constant, is not defined. Thus both the magnitude of the potential energy and the associated stiffness constant in the fission direction are not well reproduced by the two-spheroid model.

The failure of the model in these two respects (as well as its other failures, including the more drastic ones for the region $0.67 \lesssim x \lesssim 0.85$) is due to the lack of freedom of the drop at its neck. To remedy this we have tried a generalization of the two-spheroid model obtained by introducing a third conicoid of revolution (a hyperboloid of revolution of one or two sheets, or a spheroid) to connect the two end spheroids.[12] By thus including one additional coordinate to explicitly describe the neck degree of freedom, we found that all the saddle-point properties of Figs. 4-7 were reproduced with amazing accuracy. For example, over the entire range of x from 0 to 1.0, the fission barriers calculated in this generalization are accurate to within one-half an MeV. This is illustrated by the comparisons of saddle-point properties made in Figs. 8-11.

One would expect the two-spheroid model (without the conicoidal neck) to adequately describe those saddle-point properties not dependent upon details of the neck. The theory we develop depends in

---

[12] Formulae for calculating the potential energy of such a system are given in Appendix B.3 of Ref. 2.

part upon the variation of the potential energy in the neighborhood of the saddle point—in particular, upon the second derivatives of the potential energy evaluated at the saddle point (the stiffness constants). The increase in potential energy arising from changes in the fractional mass and in the length of the fragments' axes may be expected to be affected little by the presence or absence of a neck. We would thus expect the phenomena associated with the second derivatives with respect to fractional mass and semisymmetry axes—the distributions in mass, total translational kinetic energy, and excitation energies—to be described moderately well by the two-spheroid model. On the other hand, the crudeness of the neck makes the reliability of the stiffness constants for the angular coordinates less certain. We therefore do not have a clear idea of how well we should expect the distributions in fragment angular momenta (associated with the angular-coordinate stiffness constants) to be described by the model.

To summarize, we see that the two-spheroid model is inadequate in two important respects: First of all, it cannot be reliably used for $x \gtrsim 0.67$, where most of the experimental information on fission lies. Secondly, even for $x \lesssim 0.67$ it does not reproduce well those saddle-point properties associated with the neck—in particular, the fission barrier and the fission stiffness constant. It is thus unsuitable even in this range of x for discussing quantities dependent upon these properties, such as the probability of fission. On the other hand, the two-spheroid model is expected to be useful for estimating the distributions in mass, total translational kinetic energy, excitation energies, and perhaps, angular momenta of the fragments at infinity. The accuracy of the estimated distributions in angular momenta is uncertain. As regards the remaining distributions, we would expect the estimates to be fair —better than order of magnitude— and yet certainly not exact.

III. DYNAMICS

We considered in the last section one part of the Hamiltonian for the system: the potential energy; we now turn our attention to the other part: the kinetic energy. Although the potential energy of a liquid drop is uniquely determined as soon as the drop's boundary is given, the kinetic energy, on the other hand, is not uniquely determined by specifying the time rate of change of the boundary. One must in addition make some statement regarding the nature of the hydrodynamic flow of the fluid inside the drop, i.e., the curl (rotation or vorticity) in the system must be specified. A thorough treatment of the liquid-drop model would thus require that one study the system for various types of hydrodynamic flow, consistent with one and the same motion of the boundary.

We work out the details of the theory for the case of an incompressible fluid in which vibrations of a fragment are treated as irrotational, whereas rotations are treated as if the fragment were a rigid body. This means that the hydrodynamic flow within each fragment is taken to be a superposition of an irrotational flow and a flow corresponding to a uniform rotation; i.e., the curl within each fragment is equal to twice the angular-velocity vector (which is constant throughout the fragment). [For a brief discussion of such composite types of flow, see Lamb(44).]

The type of hydrodynamic flow that we have chosen to consider is, of course, only one of several types for which the theory should be worked out. For example, the case in which the flow is completely irrotational (as regards both vibrations and rotations), and the case in which the drop is very viscous should also be considered.[13] The actual situation in nuclei is presumably intermediate between these limiting cases.

---

[13] When we discuss the solutions to the equations of motion we will, whenever possible, also indicate the result for the case in which the fragments are infinitely viscous, and would therefore separate to infinity without oscillating.

It is of interest to have some a priori opinion as to how well the type of flow we are considering represents real nuclei. The deduction of vibrational inertial parameters and moments of inertia for nuclei in their ground states has been extensively considered. (See, for example, Ref. 45.) Estimates of the vibrational inertial parameters corresponding to quadrupole vibrations of even-even nuclei about spherical equilibrium shapes indicate that the actual values are considerably greater than the values corresponding to irrotational flow(45). These values, however, are strongly influenced by the effects of single-particle shell structure on ground-state nuclei. For the vibrations of interest in fission—small vibrations of the system about a deformed saddle-point shape, and relatively large vibrations of the fragments about their centers following scission—the effects of single particles would be expected to be less important.

Estimates of moments of inertia corresponding to rotations of deformed even-even nuclei indicate that the actual values are greater than the values corresponding to irrotational flow, and less than the values corresponding to rigid-body rotation. As the deformation of the nuclear equilibrium configuration increases, the ratio of the observed moment of inertia to the rigid-body value increases(45). This would imply that for the relatively large fragment deformations encountered in fission the fragment moments of inertia should not be too far from their rigid-body values.

In addition, the fragments in fission will, in general, possess some internal excitation, and, as we will discover, are typically rotating with several $\hbar$ units of angular momentum. One would expect each of these effects to increase the moment of inertia. (An argument for the approach of the moment of inertia to the rigid-body value at high spins is discussed in Ref. 46.)

In our dynamical study we shall be concerned with setting up and solving the classical equations of motion of the system.[14] This will make it possible to trace out dynamically the motion of the system from some given initial configuration near the saddle point to the final configuration of two fragments at infinity. The state of motion at infinity will correspond directly to observable characteristics of fission fragments—the speed of separation of fragment centers will correspond to their translational kinetic energies, the vibrations about their centers of mass will correspond to their excitation energies, and the rotations about their centers of mass will correspond to their angular momenta. Out of the dynamical study will come, then, the relationship between the initial configuration of the system near the saddle point and the observable quantities of interest at infinity. This relationship becomes extremely simple when the deviations of the initial configuration from the saddle point are small. (In practice, this turns out to be a good approximation.)

For the case in which the saddle point consists of two tangent spheroids ($x \lesssim 0.80$), we will find a simple equation that expresses very accurately the total translational kinetic energy E of the two fragments at infinity in terms of the initial coordinates and momenta.

---

[14] The use of classical equations of motion for discussing the separation of the fragments to infinity may be partially justified on the grounds that a short distance from the saddle point the de Broglie wavelength for translational motion has become relatively small, that the vibrations about each fragment's center of mass involve several quanta of energy, and that the angular momentum of each fragment is typically several $\hbar$ units in magnitude.

The value of E will be seen to depend primarily upon the initial distance between the fragment centers and the product of their charges.

Since the fractional mass does not change after division into two fragments, the fractional mass U at infinity will equal its original value at the saddle point.

The excitation energy of an individual fragment at infinity will be seen to depend primarily upon its initial elongation. We will content ourselves with establishing an equation for the excitation energy at infinity that is valid to first order in the small deviations of the configuration from its saddle-point shape.

We will find that the angular momentum of an individual fragment at infinity depends primarily upon the initial angular momentum it possessed near the saddle point. Fragments that are infinitely viscous and therefore separate without oscillating are capable of acquiring some additional angular momentum by virtue of the torque exerted by one fragment on the other through the electrostatic interaction.[15] The amount of such induced angular momentum depends primarily upon the fragment's initial angle θ_1 and upon its initial angular momentum p_{θ_1}. Fragments that oscillate with irrotational flow as they separate acquire very little angular momentum by this mechanism because the torque decreases as the symmetry axis shortens, and even changes sign as the spheroid changes from prolate to oblate. We will establish an equation for the angular momentum at infinity that is valid to first order in the initial coordinates and momenta, in analogy to what we did for the excitation energy.

---

[15] The angular momentum acquired by a rigid spheroid moving in the electrostatic field of a sphere has been discussed by Hoffman (47).

A. Kinetic Energy of the System

We shall in this subsection concern ourselves with the kinetic energy of the system. However, let us first consider another simplification arising from the smallness of the initial deviations from the saddle point.

Because—as regards angular momenta—we are working only to first order in the initial coordinates and momenta, it is sufficient when discussing the separation of the fragments to infinity to consider explicitly only configurations in which the symmetry axes are coplanar, and in which the spheroids are not spinning about their symmetry axes. This is true because of the symmetries of the saddle-point shape. Consider, say, the x component of angular momentum of a fragment at infinity. From symmetry, it will have no linear dependence upon an initial rotation of either fragment about its y or z axis. Similarly, it will not depend linearly upon the initial y or z components of angular momentum of either fragment. Analogous statements hold for the fragment's y and z components of angular momentum at infinity. Indeed, to first order, the fragment's z component of angular momentum at infinity is equal to its initial z component of angular momentum (near the saddle point). This means, then, that to first order in the initial coordinates and momenta, the result for the general noncoplanar configuration with rotations about the spheroids' symmetry axes is simply a superposition of the results for two special cases: (a) coplanar symmetry axes with no rotations about them, and (b) rotations about collinear symmetry axes, for which we know the result.

For the sake of clarity the exposition throughout this subsection will be as if the symmetry axes of the spheroids were coplanar and there were no rotations about them. Thus the difference $\phi = \phi_1 - \phi_2$ between the azimuthal angles of the symmetry axes (see Fig. 2) is taken to be zero. The results obtained by considering coplanar spheroids with no rotations about their symmetry axes will be subsequently generalized to the original case of two-spheroid configurations

described by nine degrees of freedom (in a center-of-mass system with zero total angular momentum). It must be borne in mind, however, that if one desired to discuss the solutions to a higher order than linear in the initial angles and their conjugate momenta, then it would be necessary to set up and solve the equations of motion for the general noncoplanar configuration with rotations about the spheroids' symmetry axes.

As we found to be true with the potential energy, the kinetic energy of the system is simpler when the fragments are separated than when they are overlapping. When the fragments are separated the total kinetic energy of the system is equal to the kinetic energy of the centers of mass of the two fragments, plus the kinetic energy of motion of each fragment relative to its own center of mass. The kinetic energy of a fragment relative to its center of mass is equal to an integral over its volume of one-half the mass density times the square of the local fluid velocity (relative to its center of mass). For the type of flow we are considering, the integration can be performed exactly (see Appendix C.1 of Ref. 2), yielding the sum of two terms: the kinetic energy of vibration of the fragment, and the kinetic energy of rotation of the fragment.

In general, the system's total kinetic energy is a function of the time rate of change of the angular coordinate Θ that specifies the orientation in space of the system as a whole (for coplanar fragments). However, for the case of a system with zero total angular momentum, the time rate of change of Θ is determined in terms of the time rates of change of θ_1 and θ_2. The result obtained for the system's total kinetic energy is (see Section III.A of Ref. 2 for details)

cap script tee

$$\mathcal{T} = \frac{1}{2}\left[\frac{p_\ell^{\,2}}{M_\ell} + \frac{p_{c_1}^{\,2}}{M_{c_1}} + \frac{p_{c_2}^{\,2}}{M_{c_2}} + \frac{p_{\theta_1}^{\,2}}{M_{\theta_1}} + \frac{p_{\theta_2}^{\,2}}{M_{\theta_2}} + \frac{(p_{\theta_1} + p_{\theta_2})^2}{M_\ell\,\ell^2}\right]. \tag{7}$$

We denote by p_ℓ the momentum conjugate to the coordinate ℓ, etc. The quantity M_ℓ is the reduced mass of the two fragments, given by

$$M_\ell = U(1 - U)M_0 \; ; \tag{8a}$$

the quantity M_{c_1}, say, is the vibrational effective mass of fragment 1, given by (44)

$$M_{c_1} = \frac{1}{5}\left(1 + \frac{1}{2}\,\frac{a_1^2}{c_1^2}\right)UM_0 = \frac{1}{5}\left(1 + \frac{U}{2}\,\frac{R_0^3}{c_1^3}\right)UM_0 \; ; \tag{8b}$$

and M_{θ_1} is the rigid-body moment of inertia of fragment 1 for rotations about a transverse axis, given by

$$M_{\theta_1} = \frac{1}{5}(c_1^2 + a_1^2)\,UM_0 = \frac{1}{5}\left(c_1^2 + \frac{UR_0^3}{c_1}\right)UM_0 \; . \tag{8c}$$

The transverse semiaxis of fragment 1 is denoted by a_1. We note that for the separated case there is no term in the kinetic energy involving the momentum conjugate to the fractional volume U ; this is because once the drop has split into two framents, the fractional volume U no longer changes with time.

Cap' script aich, tee, and vee

The Hamiltonian for the system is then

$$\mathcal{H} = \mathcal{T} + \mathcal{V}, \tag{9}$$

where $\mathcal{T}$ is given by (7), and $\mathcal{V}$ by (6b).

When the fragments overlap the kinetic energy of the system is much more difficult to calculate. We then specialize, as we did for the potential energy, to the restricted case of fragments that are symmetrical. The kinetic energy of the system can then be calculated approximately by using the method of Werner and Wheeler (48) (see Appendix C.2 of Ref. 2). A closed expression is obtained for the kinetic energy as a function of the coordinates ℓ and c, and their time derivatives $\dot{\ell}$ and $\dot{c}$. This method yields the exact result for two limiting cases: (1) when the system consists of two separated spheroids, and (2) for spheroidal distortions when the system consists of a single spheroid. The accuracy of the method for the general overlapping case is not known. However, for the lower values of x, where the saddle point consists of two tangent spheroids, this approximate method is never used, since we focus attention on the system only from the saddle point to infinity.

B. Transformation to Normal Coordinates

A fundamental aspect of the dynamical discussion of any physical system is the question of small oscillations about the positions

of equilibrium. In the normal fission process there are three equilibrium configurations: (1) the initial sphere, (2) the saddle point, and (3) the two spherical fragments at infinity. Both the initial sphere and the two spherical fragments at infinity are positions of stable equilibrium. The small oscillations about each of these spherical shapes can be readily discussed by expanding the drop's radius vector in spherical harmonics: The motion of the drop is a superposition of simple harmonic oscillations of different frequencies corresponding to the various spherical-harmonic distortions. The question of small oscillations about the remaining equilibrium position—the unstable configuration at the saddle point—will now be considered.

The first step in the discussion of the small oscillations about the saddle point is to transform from the original coordinate system to a system of normal coordinates.[16] In terms of the normal coordinates and their conjugate momenta, both the potential energy and the kinetic energy are simultaneously diagonalized at the saddle point; i.e., there appear through second order no cross terms of the form $c_1 c_2$, for example. The Hamiltonian for the system thus separates into a sum of terms, each involving only a single coordinate and its conjugate momentum. This means physically that the motion of the system in the vicinity of the saddle point separates into several independent modes that may be discussed separately.

We consider first the case in which the saddle point consists of two tangent spheroids. The normal-coordinate transformation for this case is not completely straightforward because of the cusp in the energy surface at the saddle point. The transformation to normal coordinates can nevertheless be performed by regarding the cusp as the limiting case of a regular (rounded) barrier. As the barrier becomes infinitely sharp, all but one of the normal coordinates come to lie in the subspace

---

[16] See the discussion of normal coordinates in any classical-mechanics textbook, for example, Goldstein (49).

of touching spheroids. In this subspace, the potential energy has no irregularities. The remaining normal mode of motion—the fission mode—retains a well-defined direction. The physical meaning of this direction is that it represents the initial mode of motion that would be acquired by the system if started with an arbitrary infinitesimal displacement from the saddle point.

For the discussion of the normal modes we again treat the more general case in which we consider the three angular degrees of freedom of each spheroid; i.e., the spheroids are permitted to rotate about their symmetry axes, and the symmetry axes are not required to lie in the same plane. (We are still considering a system with zero total angular momentum; this will introduce one condition on these six angular coordinates.) It is convenient in discussing small-angle oscillations to lowest order to use a set of angular coordinates defined more symmetrically with respect to the coordinate axes than the Euler angles. We denote by θ_{1x} and θ_{1y} the angles of rotation of fragment 1 away from the z_1 axis, the rotations being about the x_1 and y_1 axes, respectively. The angle of rotation of spheroid 1 about the z_1 axis is denoted by θ_{1z}. The angles θ_{2x}, θ_{2y}, and θ_{2z} are defined in an analogous manner with respect to coordinate system 2.

We expand the potential energy in the subspace of touching spheroids about the saddle point, retaining terms through second order in the coordinates. Let us denote by $K_{c_1c_2}$, for example, the second partial derivative in this subspace of the potential energy with respect to c_1 and c_2, evaluated at the saddle point. (Since the saddle point is a position of equilibrium, all first derivatives are zero.) In addition to the usual equalities between the stiffness constants (the K's) obtained by interchanging the order of differentiation, symmetry considerations at the saddle point yield the following equalities between the nonzero stiffness constants:

$$K_{c_2c_2} = K_{c_1c_1} ,$$

$$K_{\theta_{2x}\theta_{2x}} = K_{\theta_{2y}\theta_{2y}} = K_{\theta_{1x}\theta_{1x}} = K_{\theta_{1y}\theta_{1y}} \equiv K_{\theta_1\theta_1} ,$$

$$K_{\theta_{1x}\theta_{2x}} = K_{\theta_{1y}\theta_{2y}} \equiv K_{\theta_1\theta_2} ,$$

$$K_{Uc_1} = - K_{Uc_2} .$$

In addition, with the exception of K_{UU} and $K_{c_1c_2}$, all the remaining stiffness constants are seen from symmetry to be zero. We are left then with only six independent stiffness constants:

$$K_{UU}, K_{c_1c_1}, K_{\theta_1\theta_1}, K_{Uc_2}, K_{c_1c_2}, \text{ and } K_{\theta_1\theta_2} .$$

We denote the value of a coordinate at the saddle point by a superscript 0, and the difference between a coordinate and its saddle-point value by a δ preceding the coordinate; for example,

$$\delta\ell = \ell - \ell^0 = \ell - 2c_1^0 ,$$

$$\delta U = U - U^0 = U - \frac{1}{2} ,$$

$$\delta\theta_{1x} = \theta_{1x} - \theta_{1x}^0 = \theta_{1x} .$$

The coordinate ℓ, which in this subspace is the distance between the centers of the touching spheroids, is chosen as the dependent variable; it is thus expressed in terms of the other coordinates (see Appendix D.1 of Ref. 2). To second order, the potential energy of the system in the vicinity of the saddle point in this subspace can be written in matrix form as

$$\mathcal{V} - \mathcal{V}^0 = \frac{1}{2} (\delta U \ \delta c_1 \ \delta c_2 \ \delta\theta_{1x} \ \delta\theta_{2x} \ \delta\theta_{1y} \ \delta\theta_{2y})$$

$$\times \begin{pmatrix} K_{UU} & -K_{Uc_2} & K_{Uc_2} & 0 & 0 & 0 & 0 \\ -K_{Uc_2} & K_{c_1c_1} & K_{c_1c_2} & 0 & 0 & 0 & 0 \\ K_{Uc_2} & K_{c_1c_2} & K_{c_1c_1} & 0 & 0 & 0 & 0 \\ 0 & 0 & 0 & K_{\theta_1\theta_1} & K_{\theta_1\theta_2} & 0 & 0 \\ 0 & 0 & 0 & K_{\theta_1\theta_2} & K_{\theta_1\theta_1} & 0 & 0 \\ 0 & 0 & 0 & 0 & 0 & K_{\theta_1\theta_1} & K_{\theta_1\theta_2} \\ 0 & 0 & 0 & 0 & 0 & K_{\theta_1\theta_2} & K_{\theta_1\theta_1} \end{pmatrix} \begin{pmatrix} \delta U \\ \delta c_1 \\ \delta c_2 \\ \delta\theta_{1x} \\ \delta\theta_{2x} \\ \delta\theta_{1y} \\ \delta\theta_{2y} \end{pmatrix} .$$

The kinetic energy in the neighborhood of the saddle point,[17] to second order in the coordinates and velocities (or momenta), is

[17] When discussing the kinetic energy, we are not restricted to the subspace of touching spheroids.

obtained by evaluating at the saddle point the effective masses (8) of our previous expression for $\mathcal{T}$ [Eq. (7)] and generalizing the result to include general rotations of the spheroids about the x, y, and z axes (rather than in a plane).

Before listing the normal-coordinate transformation formulae, let us describe physically the normal modes of oscillation about the saddle-point configuration. We have tried to descriptively name each mode; the corresponding normal coordinate is designated by the first letter of the name. Figure 12 has been prepared to aid in visualizing the modes, which we now enumerate:

(a) Fission: This normal mode is distinguished from the others in that it is always unstable--the potential energy decreases rather than increases as we move away from the saddle point. Because of the cusp in the potential energy the stiffness constant for this mode is not defined; it would be negative for a saddle point in which there is no cusp. The motion of the system is a simultaneous separation of the centers of the spheroids and a decrease in their elongations, or vice versa.

(b) Mass-asymmetry: As will be discussed later, this normal mode is stable for x greater than x_{BG} (equal to 0.47 in the two-spheroid approximation), and unstable for x less than x_{BG}. The motion here is an increase in both the mass (volume) and elongation of one spheroid and a decrease in the mass and elongation of the other

spheroid, such that the distance between spheroid centers (as well as the total length of the drop) is constant.

(c) Stretching: The elongation of each spheroid increases (or decreases) by the same amount.

(d) Distortion-asymmetry: The elongation of one spheroid increases, and the elongation of the other spheroid decreases; the distance between spheroid centers (as well as the total length of the drop) remains constant.

(e) Bending: This mode is doubly degenerate (occurs twice), corresponding to rotations in the x-z plane and the y-z plane. For a given plane, one of the spheroids rotates clockwise about an axis through its center perpendicular to the plane, and the other counterclockwise through the same angle; the spheroids remain touching.

(f) Wriggling: This mode is also doubly degenerate, corresponding to rotations in the x-z and y-z planes. For a given plane, both spheroids rotate through the same angle either clockwise or counterclockwise about axes through their centers perpendicular to the plane; they remain touching. The entire system rotates in the opposite direction, ensuring conservation of the x and y components of total angular momentum.

(g) Twisting: One of the spheroids rotates about its symmetry axis clockwise and the other counterclockwise through the same angle. The restoring force (stiffness constant) for this mode is zero, resulting in a uniform, rather than oscillatory, rotation.

(h) Axial-rotation: This mode would correspond to a uniform rotation of the spheroids about their symmetry axes through the same angle in the same direction. Conservation of the z component of total angular momentum means that this mode is not excited.

The linear transformation that takes us from the original coordinates to the normal coordinates may be written as

$$f = \frac{\delta\ell - (\delta c_1 + \delta c_2)}{\sqrt{2}\,[1 + (2M_{c_1}^{0}/M_0)]} , \tag{11a}$$

$$m = \delta U , \tag{11b}$$

$$s = \frac{\delta\ell + 2(M_{c_1}^{0}/M_0)(\delta c_1 + \delta c_2)}{\sqrt{2}\,[1 + (2M_{c_1}^{0}/M_0)]} , \tag{11c}$$

$$d = (1/\sqrt{2})(-B\,\delta U + \delta c_1 - \delta c_2) , \tag{11d}$$

$$b_x = (1/\sqrt{2})(\delta\theta_{1x} - \delta\theta_{2x}) , \tag{11e}$$

$$w_x = (1/\sqrt{2})(\delta\theta_{1x} + \delta\theta_{2x}) , \tag{11f}$$

$$b_y = (1/\sqrt{2})(\delta\theta_{1y} - \delta\theta_{2y}) , \tag{11g}$$

$$w_y = (1/\sqrt{2})(\delta\theta_{1y} + \delta\theta_{2y}) , \tag{11h}$$

$$t = (1/\sqrt{2})(\delta\theta_{1z} - \delta\theta_{2z}) , \tag{11i}$$

$$a = (1/\sqrt{2})(\delta\theta_{1z} + \delta\theta_{2z}) , \tag{11j}$$

where the quantity B is defined by[18]

$$B = 2K_{Uc_2}/(K_{c_1c_1} - K_{c_1c_2}) . \tag{12}$$

---

[18] We will see later (Fig. 13) that K_{Uc_2} is always positive and that $K_{c_1c_1}$ is always greater than $K_{c_1c_2}$; hence, B is always positive.

These formulae may be verified by explicitly demonstrating that both $\mathcal{V}$ and $\mathcal{T}$ are diagonalized in terms of the new coordinates and their time derivatives (or conjugate momenta).[19] The normal coordinates are all identically zero at the saddle point.

In terms of the normal coordinates and their conjugate momenta the Hamiltonian (with respect to the saddle point) in the subspace of touching spheroids is given to second order by (the axial-rotation kinetic-energy term has been dropped)

$$\begin{aligned}\mathcal{H} = \frac{1}{2}\Bigg\{ & K_m m^2 + \left(K_s s^2 + \frac{p_s^2}{M_s}\right) + \left(K_d d^2 + \frac{p_d^2}{M_d}\right) \\ & + \left[K_b(b_x^2 + b_y^2) + \frac{p_{b_x}^2 + p_{b_y}^2}{M_b}\right] \\ & + \left[K_w(w_x^2 + w_y^2) + \frac{p_{w_x}^2 + p_{w_y}^2}{M_w}\right] + \frac{p_t^2}{M_t}\Bigg\}. \end{aligned} \tag{13}$$

The normal-coordinate stiffness constants are expressed in terms of the original stiffness constants by

$$K_m = K_{UU} - BK_{Uc_2} ,$$

$$K_s = K_{c_1c_1} + K_{c_1c_2} ,$$

$$K_d = K_{c_1c_1} - K_{c_1c_2} ,$$

---

[19] In verifying that $\mathcal{T}$ is diagonal in terms of the time derivatives of the normal coordinates, note that $\dot{U}$ is zero at the saddle point.

$$K_b = K_{\theta_1\theta_1} - K_{\theta_1\theta_2} ,$$

$$K_w = K_{\theta_1\theta_1} + K_{\theta_1\theta_2} ;$$

and the normal-coordinate effective masses are related to the original ones by

$$M_f = \left(1 + \frac{2M_{c_1}^{0}}{M_0}\right) M_{c_1}^{0} ,$$

$$M_s = \frac{1}{2}\left(1 + \frac{2M_{c_1}^{0}}{M_0}\right) M_0 ,$$

$$M_d = M_{c_1}^{0} ,$$

$$M_b = M_{\theta_1}^{0} ,$$

$$M_w = \left[1 - \frac{2M_{\theta_1}^{0}}{M_0 (c_1^0)^2 + 2M_{\theta_1}^{0}}\right] M_{\theta_1}^{0}$$

$$= \left[\frac{5}{6 + \frac{R_0^3}{2(c_1^0)^3}}\right] M_{\theta_1}^{0} ,$$

$$M_t = M_{\theta_{1z}}^{0} ,$$

$$M_a = M_{\theta_{1z}}^{0} .$$

The quantities $M_{c_1}^{0}$ and $M_{\theta_1}^{0}$ are the values of M_{c_1} and M_{θ_1} [see Eq. (8)], respectively, evaluated at the saddle point; and $M_{\theta_{1z}}^{0}$ is the rigid-body moment of inertia of spheroid 1 for rotations about the symmetry axis, evaluated at the saddle point:

$$M_{\theta_{1z}}^{0} = \frac{1}{5}\left(a_1^0\right)^2 M_0 = \frac{1}{10}\left(\frac{R_0^3}{c_1^0}\right) M_0 .$$

(In the first form of the equation for M_w, the second term within the brackets arises physically from the requirement that the total angular momentum be zero.)

The frequency for a particular normal mode is given by the square root of the appropriate stiffness constant divided by the appropriate mass. There are four well-defined nonzero frequencies (the bending and wriggling frequencies are, of course, doubly degenerate): ω_s, ω_d, ω_b, and ω_w. Since the (negative) fission stiffness constant K_f is not defined, the (imaginary) frequency ω_f is also not defined. It is shown in Appendix D.2 of Ref. 2 that, because the drop's minimum radius is zero, the mass-

asymmetry effective mass M_m is infinite.[20] The corresponding frequency ω_m is therefore zero.[21] The twisting frequency ω_t is also zero, because the stiffness constant K_t is zero.

A straightforward numerical method was used to locate the saddle point and calculate the stiffness constants (see Appendix G of Ref. 2). The results are presented as functions of fissionability parameter from 0 to 0.80 in a series of graphs. The value of c_1^0 defining the saddle-point shape (when the saddle point consists of two tangent spheroids) can be obtained from the R_{max} curve in Fig. 7 ($R_{max} = 2\ c_1^0$). The stiffness constants for the original coordinate system are given in Fig. 13.

The normal-coordinate stiffness constants are shown in Fig. 14. Four of these constants are always positive; the mass-asymmetry stiffness constant K_m changes sign at $x = x_{BG} \approx 0.47$. This value of x is the two-spheroid approximation to the true value of 0.39_4, where the Businaro-Gallone family of asymmetric equilibrium shapes bifurcates from the family of symmetric equilibrium shapes. (15, 43).[22]

---

[20] This result states physically that the kinetic energy associated with a finite flux of matter through an aperature of infinitesimal radius is infinite. This follows from the fact that the velocity of flow through the aperture is infinite, and that the kinetic energy depends upon the product of the amount of matter and the square of the velocity.

[21] The reason for the vanishing of ω_m is that in the two-spheroid model the neck radius of the saddle-point shape is zero. For the exact saddle point the neck radius is not zero but is small, and ω_m is not zero but is small in comparison with the other frequencies.

[22] The two-spheroid model thus predicts this bifurcation point at a value of x that is somewhat too high, in analogy to its prediction of a transition region at $x \approx 0.80$, when the true transition region occurs at $x \approx 0.67$.

For $x > x_{BG}$ the symmetric equilibrium shapes are stable against changes in asymmetry, and for $x < x_{BG}$ they are unstable. Thus, for $x > x_{BG}$ the symmetric equilibrium shapes are unstable with respect to displacements along only one normal coordinate (the fission coordinate), and for $x < x_{BG}$ they are unstable with respect to two (the fission coordinate and the mass-asymmetry coordinate). This means physically that for $x > x_{BG}$ the equilibrium configuration defines a barrier energy, whereas for $x < x_{BG}$ the equilibrium configuration is at the "top of a hill" and therefore does not define a barrier energy (15, 43).

The effective masses are shown in Fig. 15. The frequencies for the four nonzero modes of oscillation are given in Fig. 16 in liquid-drop units. In Fig. 17 the corresponding quantum energies ($\hbar$ times the frequencies) are given in units of MeV for nuclei along the line of beta stability (50). For the region in which we will be most interested ($x \approx 0.67$), the stretching and bending quantum energies are each about 1 MeV, the distortion-asymmetry quantum energy is about 1.5 MeV, and the wriggling quantum energy is about 2 MeV.

For values of $x \gtrsim 0.80$, where the saddle point is represented by overlapping spheroids, we again restrict ourselves to the case of symmetrical fragments, specified by the two coordinates ℓ and c. Since there is no cusp in the potential energy at the saddle point, the normal-coordinate transformation for this case is straightforward. There result two normal modes: a stable oscillation (stretching) and an unstable motion in the fission direction. We shall not present here the numerical results obtained for the frequencies of the normal modes.

C. Solution of Equations of Motion

We consider in this subsection the solution of Hamilton's classical equations of motion for the system. For given initial conditions, solution of these equations gives the subsequent motion of the system. The question naturally arises of what initial conditions to use. One could, for example, study the behavior of the system by always starting with the original sphere, giving it different sets of initial momenta. Because most of this work will be concerned with tracing out the consequences of assuming statistical equilibrium at the saddle point (see Section IV), we examine the solutions for initial conditions that are specified in the neighborhood of the saddle point. We will consider first the case in which the saddle point consists of two tangent spheroids ($x \lesssim 0.80$); then, in the region from the saddle point to infinity, the system consists of two separated spheroids.

We saw from the Hamiltonian (13) that four of the normal modes at the saddle point—stretching, distortion-asymmetry, bending, and wriggling—are simply bounded harmonic oscillations. The mass-asymmetry normal mode, on the other hand, was seen to be stable for $x > x_{BG}$ and unstable for $x < x_{BG}$. Since the effective mass for this mode is infinite, the mass-asymmetry coordinate changes with time infinitely slowly at the saddle point. Because the restoring force for the twisting mode is zero, this mode consists of uniform rotations of the fragments.

The remaining normal mode—the fission mode—is always unstable, taking us out of the subspace of touching spheroids. It is motion in the (positive) fission direction that causes the two fragments to start their separation to infinity. Attention is first focused on the system at the critical moment when it is passing over the saddle

point; i.e., the time is chosen to be zero when the fission coordinate f is zero. Our solutions to the equations of motion will then depend upon the values of the remaining normal coordinates and momenta when $f = 0$.

The equations of motion themselves are obtained for the separated case by differentiating the Hamiltonian (9) with respect to the coordinates and momenta. For the case of coplanar symmetry axes with no rotations of the spheroids about them, one obtains a system of ten simultaneous first-order differential equations, which are listed in Appendix C.1 of Ref. 2. These equations are given in terms of the original coordinates, since the normal coordinates have meaning as such only in the vicinity of the saddle point. The system of equations is solved numerically for given initial conditions, determing ℓ, c_1, c_2, θ_1, and θ_2, along with their conjugate momenta, as functions of time. By carrying a solution out to infinity (in practice, to $\ell = 25\ R_0$), one finds the values at infinity of the quantities of interest. A summary of the numerical procedure is given in Appendix G. of Ref. 2.

Let us now examine the qualitative features of the solutions for various initial conditions. We have indicated in Fig. 3, on each potential-energy map in the range $0.2 \leq x \leq 0.8$, the solution corresponding to starting from rest at the saddle point. For each case the points along the path are equally spaced in time at intervals of $0.1\ T_0$ [see Eq. (2) for the value of T_0]. The motion of the system is a fairly rapid oscillation of the fragments, superimposed on a separation of their centers.

Starting the system from the saddle-point configuration corresponds to the case in which all normal coordinates are initially zero. When a particular normal coordinate is initially nonzero, the solution is altered in a manner characteristic of that normal coordinate:

(a) Mass-asymmetry: The fragment with greater volume and larger semisymmetry axis oscillates with a larger amplitude but with a smaller frequency than the other fragment.

(b) Stretching: When s is positive (corresponding to fragments that are initially more elongated than at the saddle point), both fragments oscillate with greater amplitude and separate more slowly. Conversely, for negative s, the fragments oscillate with less amplitude and separate more rapidly.

(c) Distortion-asymmetry: The fragment with the larger semisymmetry axis oscillates with greater amplitude than the other fragment.

(d) Bending: In a bent configuration, each fragment experiences a torque from the electrostatic field, resulting in an induced angular momentum. One fragment rotates clockwise and the other counterclockwise. The period of rotation is much greater than the period of oscillation.

(e) Wriggling: Both fragments rotate clockwise, (or counterclockwise) simultaneously. (The relative orbital angular momentum of the two fragments is equal and opposite to the angular momenta of the individual fragments.) As with the bent case, the fragments oscillate many times during a single period of rotation.

In general, the initial conditions include several nonzero coordinates, and in addition several nonzero momenta. The corresponding solutions then consist of a superposition of the characteristic features arising from each normal coordinate, modified by the effects of the initial momenta. The motion of the system is thus in general a separation of the two fragments from the saddle point to infinity, with each fragment simultaneously oscillating fairly rapidly and rotating rather slowly.

What is desired is a relationship between the initial conditions and the observable properties of fission fragments at infinity. From this we will be able to obtain, by performing suitable integrations over probability distributions for the initial conditions (see Section IV), probability distributions for the observable quantities of interest. Each quantity of interest depends strongly upon only a few of the initial coordinates and momenta, and very weakly upon the remaining ones. Our approach will consist of neglecting the weak dependences of each quantity of interest on most of the initial conditions.

From a consideration of the numerical solutions corresponding to a large number of combinations of initial conditions, we have determined simple approximate equations expressing the quantities of interest in terms of the initial coordinates and momenta. The equations are, in general, valid for small deviations of the coordinates from the saddle point and for small values of the initial momenta. However, we were able to find for the total translational kinetic energy an equation that works well even for moderately large deviations from the saddle point. [The accuracy of each equation can be seen from Table E.I (in Appendix E) of Ref. 2, where there are listed forty-four sets of initial conditions for a particular value of x, along with the values for the quantities of interest determined exactly by solving the equations of motion and determined approximately from the equations listed below.] For a given x the constants appearing in each equation are calculated numerically from the solutions to the equations of motion, as described in Appendix G of Ref. 2.

The equation established for the translational kinetic energy E of both fragments at infinity is

$$E = \frac{4U(1-U)\,E^0}{1+\alpha s} + \frac{p_\ell^2}{2M_\ell}$$

$$= \frac{(1-4m^2)\,E^0}{1+\alpha s} + M_\ell \left(\frac{2M_{c_1}^{\,0}\,p_f}{M_0\,M_f} + \frac{p_s}{M_s} \right)^2 , \quad (14)$$

where E^0 and α are constants (for a given x). The second result is simply the first result expressed in terms of the normal coordinates and momenta. This equation can be interpreted physically as giving the final kinetic energy that would result from two effective point charges of relative strengths U and (1 - U) initially separated a certain distance and moving with relative momentum p_ℓ .

The fractional mass U at infinity is equal to the initial fractional mass, since after scission this coordinate does not change with time. Thus, the fractional mass at infinity is related to the mass-asymmetry normal coordinate m by the exact equation

$$U = \frac{1}{2} + m \,. \tag{15}$$

The relationship (14) for E reproduces the exact result extremely well—more accurately than do the equations we established for the individual excitation energies and angular momenta.[23] For these quantities we retain only terms linear in the more important initial coordinates and momenta:[24]

$$X_1 = X_1^0 + X_{1,s}\, s + X_{1,d}\, d + X_{1,m}\, m \,, \tag{16a}$$

$$X_2 = X_1^0 + X_{1,s}\, s - X_{1,d}\, d - X_{1,m}\, m \,, \tag{16b}$$

$$L_{1x} = L_{1,p_b}\, p_{b_x} + L_{1,p_w}\, p_{w_x} + L_{1,b}\, b_x + L_{1,w}\, w_x \,, \tag{17a}$$

$$L_{2x} = -\, L_{1,p_b}\, p_{b_x} + L_{1,p_w}\, p_{w_x} - L_{1,b}\, b_x + L_{1,w}\, w_x \,, \tag{17b}$$

$$L_{1y} = L_{1,p_b}\, p_{b_y} + L_{1,p_w}\, p_{w_y} + L_{1,b}\, b_y + L_{1,w}\, w_y \,, \tag{17c}$$

$$L_{2y} = -\, L_{1,p_b}\, p_{b_y} + L_{1,p_w}\, p_{w_y} - L_{1,b}\, b_y + L_{1,w}\, w_y \,, \tag{17d}$$

$$L_{1z} = p_{\theta_{1z}} = (1/\sqrt{2})\,(p_t + p_a) \,, \tag{17e}$$

$$L_{2z} = p_{\theta_{2z}} = (1/\sqrt{2})\,(-p_t + p_a) \,, \tag{17f}$$

---

[23] There is currently no experimental information on excitation energies and angular momenta for the fission of elements lighter than radium. We content ourselves at this time with treating these quantities to a lower order than the translational kinetic energy.

[24] It should be recalled that the excitation energy calculated here is the energy associated with the collective vibrations and deformations of the fragments. Any internal excitation energy that a fragment has at the moment of division would be added to the excitation energy we calculate, to obtain the final total excitation energy.

where the quantities X_1^0, $X_{1,s}$, $X_{1,d}$, $X_{1,m}$, L_{1,p_b}, L_{1,p_w}, $L_{1,b}$, and $L_{1,w}$ are constants (for a given x). We are denoting by $X_{1,s}$, for example, the partial derivative of X_1 with respect to s, evaluated at the saddle point. Symmetry arguments have been used to relate the constants in the equation for X_2 to those in the equation for X_1. Similarly, the constants in the equations for L_{1x}, L_{2x}, L_{1y}, and L_{2y} are related by symmetry. The equations for L_{1z} and L_{2z} express the approximate conservation of the z components of angular momentum, since to first order in the angles the z components of the torque are zero. Each of the remaining equations also has a simple physical significance, which we will discuss when we present graphs of the constants appearing in them.

Complete symmetry in the observable quantities of interest could be achieved by a simple transformation from E and U to the individual translational kinetic energies E_1 and E_2 of the two fragments at infinity. The conservation of linear momentum implies that

$$UE_1 = (1 - U)E_2 .$$

From this one finds that

$$E_1 = (1 - U)E,$$

$$E_2 = UE;$$

the inverse transformation is

$$E = E_1 + E_2 , \tag{18a}$$

$$U = E_2/(E_1 + E_2) . \tag{18b}$$

An expression for E to the same order as the equations for excitation energy and angular momentum can be obtained by expanding (14) and retaining only the linear term:

$$E = E^0 - (aE^0)s . \tag{19}$$

The individual rotational energies at infinity are of second order in the initial coordinates and momenta, since they are proportional to the square of the individual angular momenta at infinity, which in turn depend linearly upon the initial coordinates and momenta. Also, the (initial) energy of the system in the neighborhood of the saddle point is of second order in the initial coordinates and momenta. Therefore, to first order, the sum at infinity of the total translational kinetic energy and the individual excitation energies is a constant:

$$E + X_1 + X_2 = E^0 + 2X_1^0 = E^0 + X^0 . \tag{20}$$

The constant $X_{1,s}$ is thus not independent but is instead given by

$$X_{1,s} = \alpha E^0/2. \tag{21}$$

A series of graphs (Figs. 18-27) has been prepared giving each constant as a function of x from 0 to 0.80. The solid line in each figure represents the result for the case we have been considering: incompressible, nonviscous fragments with hydrodynamic flow consisting of a superposition of an irrotational flow and a flow corresponding to a uniform rotation. We also indicate (by a dot-dashed curve) the result for the limiting case of infinitely viscous fragments, which would separate to infinity (as rigid bodies) without oscillating. This limiting case would be approached physically if the fragments were sufficiently viscous that their period of oscillation was large in comparison with the time of separation to a few nuclear diameters.

Figure 18 gives the dependence on x of E^0, the total translational kinetic energy at infinity that would result from fragments initially starting from rest at the saddle point. Note that the translational kinetic energy that would result if the fragments were extremely viscous (top curve) is larger than the kinetic energy corresponding to nonviscous fragments with irrotational flow (middle curve). The difference between these two curves represents the portion of original interaction energy which, for the nonviscous

irrotational case, is converted into excitation energy rather than into translational kinetic energy. We also present the result (short-dashed curve) obtained using the very simple approximation that the kinetic energy is equal to the product of the charges of the spheroids divided by the initial distance between their centers. Of course, this is equivalent to replacing the oscillating spheroids by two rigid spheres whose centers initially coincided with the spheroid centers. That this procedure should give a result that is close to the nonviscous irrotational limit is physically very reasonable, since the fairly rapid oscillations of the fragments tend to cancel the opposing effects of the prolate and oblate shapes.

In Fig. 19 is shown the result for the constant α; as with E^0, we also present the result (short-dashed curve) that would be obtained by replacing the spheroids with rigid spheres whose centers initially coincided with the spheroid centers.

The constant X_1^0, the excitation energy of fragment 1 that would result from initially starting the fragments from rest at the saddle point, is given in Fig. 20. We note that the sum of E^0 and $2X_1^0$, which is the energy difference between the two-spheroid saddle point and the configuration of two fragments at infinity, is larger than the corresponding sum would be if calculated from the exact liquid-drop saddle point. This discrepancy is equal to the difference between the energy of the two-spheroid saddle point and the exact liquid-drop saddle point, which, as we noted before, is due principally to the inadequate representation of the neck in the two-spheroid model. One might argue that this discrepancy is therefore more likely to affect the estimates of fragment excitation energies rather than their kinetic energies, but this conclusion cannot be regarded as reliable.

The excitation-energy derivatives $X_{1,s}$, $X_{1,d}$, and $X_{1,m}$ are presented in Figs. 21 - 23, respectively. The physical content of the equations for X_1 and X_2 can be easily seen if we substitute the values of the constants and transform back to the original coordinate system. We find then that, for typical values of the initial

coordinates, the excitation energy of a fragment at infinity depends primarily upon its initial elongation, is less dependent upon the fractional mass, and is still less dependent upon the initial elongation of the other fragment. Note, as we discussed in connection with the result for E^0, that if the fragments were infinitely viscous they would have less excitation energy than nonviscous fragments oscillating with irrotational flow.

The angular-momentum derivatives L_{1,p_b}, L_{1,p_w}, $L_{1,b}$, and $L_{1,w}$ are shown in Figs. 24 - 27, respectively. By substituting these values for the constants in the equations for the x and y components of angular momentum, and transforming back to the original coordinate system,[25] we learn the physical content of these equations. For typical initial conditions, the x component of the angular momentum at infinity of fragment 1, say, is found to depend primarily upon its own initial value, is less dependent upon the initial angle θ_{1x}, and is still less dependent upon the initial x component of angular momentum of fragment 2 and the initial angle θ_{2x}. If the fragments did not acquire any additional angular momentum by virtue of the torque exerted by one fragment on the other through the electrostatic interaction, then L_{1,p_b} and L_{1,p_w} would each equal $1/\sqrt{2}$, and $L_{1,b}$ and $L_{1,w}$ would each be zero. Note that the torque mechanism is capable of inducing in infinitely viscous fragments roughly four times as much angular momentum as in nonviscous fragments oscillating with irrotational flow. This is because for an oscillating fragment the torque is reduced as the elongation of the spheroid

---

[25] The relationships $p_{b_x} = (1/\sqrt{2})\,(p_{\theta_{1x}} - p_{\theta_{2x}})$ and $p_{w_x} = (1/\sqrt{2})\,(p_{\theta_{1x}} + p_{\theta_{2x}})$ etc., obtained from the normal-coordinate transformation and the definitions of the momenta, are useful for this purpose. The value at infinity of $p_{\theta_{1x}}$, for example, is L_{1x}.

is reduced, even changing sign when the spheroid changes from prolate to oblate.

When the saddle point occurs for $\ell < 2c$ ($x \gtrsim 0.80$), it is necessary to consider the equations of motion for overlapping spheroids. As before, we specialize for the overlapping case to symmetrical fragments, specified by the two coordinates ℓ and c. Hamilton's equations of motion for this case are listed in Appendix C.2 of Ref. 2. In the vicinity of the saddle point, the motion of the system consists of a superposition of the two normal modes: bounded oscillations in one direction and unbounded motion in the fission direction.

The equations of motion for the overlapping case have been solved for only a few isolated values of x and initial conditions. We will here only briefly discuss the solution for $x = 0.90$ corresponding to initially starting the system from rest at the saddle point.[26] This solution is presented in Fig. 28. The semisymmetry axis c at first increases more rapidly than the distance ℓ between spheroid centers increases; this continues until the system has become fairly elongated. Then, as the distance between centers continues to increase, the semisymmetry axis starts to decrease. When scission occurs, the fragments are already moving apart with a translational kinetic energy of the order of 25 MeV. The scission configuration is less eccentric (and the fragment centers closer together) than the configuration obtained by minimizing the potential energy of symmetric tangent

---

[26] Since the saddle point is a position of (unstable) equilibrium, a system initially at rest at the saddle point would remain there (classically) for an infinite time; we imagine an infinitesimal push in the fission direction to start the system moving. An analytic solution, valid in the neighborhood of the saddle point, is used until the system is a short distance from the saddle point, where the numerical integration begins.

spheroids. This results in about a 20-MeV additional gain in translational kinetic energy at infinity over the kinetic energy that would result from initially starting the system at rest from the configuration of tangent spheriods whose eccentricities are obtained by minimizing the potential energy. For this $x = 0.90$ case, the total translational kinetic energy E was found to be $0.315_5\ E_S^{(0)}$, and the total excitation energy X was found to be $0.091_3\ E_S^{(0)}$.

For the higher values of x, where the saddle point is not near the scission configuration, the very subtle question of the dynamics of the motion from saddle to scission becomes important in determining what fraction of the total energy goes into translational kinetic energy and what fraction into excitation energy. Therefore, for the higher values of x, a calculation of the precise division of the total energy into kinetic and excitation energies based on optimum tangent spheroids is likely to be in error.

IV. STATISTICAL MECHANICS

We have obtained approximate formulae [(14), (15), (16), and (17)] relating the observable properties of fission fragments at infinity to the initial values of the coordinates and momenta (when the saddle point is the configuration of two tangent spheroids). We now consider the determination of the probability for the system possessing a given set of initial coordinates and momenta. These two results will be combined in the next section to yield the probability for the two fragments at infinity possessing given total translational kinetic energy, fractional mass, and individual excitation energies and angular momenta.

The conditions at the saddle point would in general depend upon the past history of the system—upon how the system was formed and upon the path it took in reaching the saddle point. However, the system typically undergoes about 10^6 oscillations after formation before it reaches the saddle point (if it ever does)(51). This provides ample opportunity for many interchanges of energy, making it unlikely that at the saddle point the system "remembers" the way it was formed or most of its previous motion. It is thus likely that at the saddle point thermal equilibrium is established. This is the central hypothesis of the transition-state method used for discussing the reaction rates of chemical or nuclear systems(38), and we will base our further considerations on this standard assumption.

The discussion of the statistical mechanics is essentially the same for both the case in which the saddle point is represented by tangent spheroids and the case in which it is represented by overlapping spheroids. In the following discussion we will explicitly consider probability distributions for the normal coordinates appropriate to the case in which the saddle point consists of two tangent spheroids; for the other situation (again considering the restricted case of symmetrical fragments) there are simply fewer probability distributions.

The determination of the probability of given initial conditions is very simple in classical statistical mechanics. The probability P

that the system possesses a given set of coordinates and momenta, with the corresponding total energy $\mathcal{H}$ given by (10), is simply

$$P = N \exp(-\mathcal{H}/\Theta) , \tag{22}$$

where Θ is the nuclear temperature at the saddle point (measured in energy units), and N is a normalization constant. (Use of the symbol Θ to denote nuclear temperature should cause no confusion with its earlier use in connection with angles.) When the actual Hamiltonian (10) is used, this expression for P is exact (classically) to all orders in the coordinates and momenta.

If one expands the Hamiltonian about the saddle point and retains only quadratic terms (harmonic approximation), then the probability distribution for each normal coordinate and its conjugate momentum is simply a Gaussian in the normal coordinate or momentum [with the exception of $P(p_a)$ and $P(f)$, which are discussed separately below].[27] Thus, for example,

$$P(s) = (2\pi\,\Theta/K_s)^{-1/2} \exp\left(-\frac{1}{2} K_s\, s^2/\Theta\right), \tag{23a}$$

$$P(p_s) = (2\,\pi\, M_s\,\Theta)^{-1/2} \exp\left[-p_s^2/(2M_s\,\Theta)\right] , \tag{23b}$$

$$P(p_f) = 2(2\,\pi\, M_f\,\Theta)^{-1/2} \exp\left[-p_f^2/(2M_f\,\Theta)\right] . \tag{23c}$$

Equations analogous to these hold for the remaining normal coordinates and momenta. For one of the momenta and two of the coordinates the Gaussian distributions become infinitely broad and hence reduce to constants. This occurs for $P(p_m)$ because the mass-asymmetry effective

---

[27] All probability distributions in this paper are normalized such that unity is obtained when the functions are integrated over the allowed range of variables, which is usually taken to be from $-\infty$ to $+\infty$. The range of integration for p_f is taken to be from 0 to ∞, since for negative values of p_f the system does not fission but instead returns to the pre-saddle-point configuration; this results in the additional factor of 2 in the expression for $P(p_f)$.

mass M_m is infinite,[28] and for $P(t)$ and $P(a)$ because the twisting and axial-rotation stiffness constants are zero.

Because of the condition that the total angular momentum of the system be zero, the distribution in the axial-rotation momentum is a Dirac delta function:

$$P(p_a) = \delta(p_a) .$$

We recall finally that we do not need a probability distribution in f because the transition-state method which we are using is formulated in terms of distributions in the subspace defined by $f = 0$.

As the nuclear temperature approaches zero, the classical distribution for each normal coordinate and momentum approaches a Dirac delta function. However, we know from the Heisenberg quantum-mechanical uncertainty principle that simultaneous localization of the system in a position and conjugate-momentum coordinate can be achieved only within limits. Even at zero temperature each of the distributions should, in general, have a nonzero width, associated with the quantum-mechanical zero-point vibrations. As we shall see, the quantum-mechanical effects may be important at typical nuclear temperatures.

Although the quantum-mechanical determination of the probability distributions would be difficult if one used the complete Hamiltonian (10), the problem can be readily solved in the harmonic approximation. Then, the individual terms in the Hamiltonian (13) are the Hamiltonians for simple harmonic oscillators. (The effect on the distributions of the infinite effective mass M_m and the zero

---

[28] The Gaussian distribution in the mass-asymmetry <u>velocity</u> becomes, on the other hand, infinitely narrow and hence reduces to a Dirac delta function. This means physically that the mass-asymmetry coordinate changes with time infinitely slowly at the saddle point.

stiffness constant K_t will be discussed later.) In our discussion below we will refer only to the stretching mode; results for the remaining modes are completely analogous.

In the coordinate representation the quantum-mechanical solution of the stretching mode yields the harmonic-oscillator wave functions $\psi_n(s)$, with corresponding energy levels $E_n^s = (n + \frac{1}{2})\hbar\omega_s$. When the oscillator is known to be in the quantum-mechanical state n, the probability that its position coordinate has a given value s is

$$P_n(s) = |\psi_n(s)|^2 .$$

In particular, when the oscillator is in the ground state $n = 0$, the probability distribution for the coordinate is (52)

$$P_0(s) = |\psi_0(s)|^2 = (\pi\hbar\omega_s/K_s)^{-1/2} \exp\left[- K_s s^2/(\hbar\omega_s)\right]. \tag{24a}$$

Analogous results for the momentum p_s are obtained just as readily by solving Schrödinger's equation for the stretching mode in the momentum representation(52). For example, the ground-state probability distribution for the momentum is

$$P_0(p_s) = (\pi M_s \hbar \omega_s)^{-1/2} \exp\left[- p_s^2/(M_s \hbar \omega_s)\right]. \tag{24b}$$

We note that for the stretching oscillator in the ground state, both the distribution in s and the distribution in p_s are Gaussians, with nonzero widths proportional to $(\hbar \omega_s/K_s)^{1/2}$ and $(M_s \hbar \omega_s)^{1/2}$, respectively.

Having thus determined probability distributions for an oscillator in a given quantum-mechanical state, we are now in a position to determine probability distributions for an oscillator in statistical equilibrium with its surroundings. The quantum-mechanical probability for finding the stretching oscillator, in statistical equilibrium with its surroundings at a temperature Θ, at position s is given by

$$P(s) = \sum_{n=0}^{\infty} P_n^s \, |\psi_n(s)|^2 ,$$

where

$$P_n^s = N \exp(-E_n^s/\Theta)$$

is the statistical probability that the oscillator is in the quantum-mechanical state n. Determination of the normalization constant N yields (the same symbol N is used in this paper to denote each of several normalization constants).

$$N = 2 \sinh[\hbar\omega/(2\Theta)] .$$

By using properties of the harmonic-oscillator wave functions, the infinite summation over n can be performed explicitly, yielding the remarkably simple result (53-55)

$$P(s) = (\pi C_s)^{-1/2} \exp(-s^2/C_s) , \tag{25a}$$

where the temperature-dependent constant C_s is given by

$$C_s = \frac{\hbar\omega_s}{K_s} \coth\left(\frac{\hbar\omega_s}{2\Theta}\right) \rightarrow \begin{cases} 2\Theta/K_s , & \Theta >> \hbar\omega_s \\ \hbar\omega_s/K_s , & \Theta << \hbar\omega_s \end{cases} .$$

The temperature dependence of C_s can be seen from the graph of $\coth[\hbar\omega/(2\Theta)]$ vs $2\Theta/(\hbar\omega)$ in Fig. 29. Note that for high temperatures the quantum-mechanical expression (25a) for $P(s)$ reduces to the classical result (23a), whereas in the low-temperature limit it reduces to

the distribution (24a) for the quantum-mechanical zero-point motion of a harmonic oscillator.

An analogous probability distribution for p_s is obtained from the momentum-representation solutions to Schrödinger's equation for the stretching mode. The result is (53)

$$P(p_s) = (\pi C_{p_s})^{-1/2} \exp\left(-p_s^2/C_{p_s}\right), \tag{25b}$$

where

$$C_{p_s} = M_s \hbar \omega_s \coth\left(\frac{\hbar \omega_s}{2\Theta}\right) \rightarrow \begin{cases} 2M_s \Theta, & \Theta >> \hbar\omega_s \\ M_s \hbar \omega_s, & \Theta << \hbar \omega_s . \end{cases}$$

For high and low temperatures this expression reduces to (23b) and (24b), respectively.

We saw earlier (Section III.B) that the mass-asymmetry and twisting normal modes have zero frequencies. Thus, $\hbar\omega_m$ and $\hbar\omega_t$ are always small in comparison with Θ, which means that for these modes we are always in the high-temperature (classical) limit. Hence the constants C_m and C_{p_t} are always given by [29]

$$C_m = 2\,\Theta/K_m ,$$

$$C_{p_t} = 2\,M_t\,\Theta .$$

---

[29] Recall that for $x < x_{BG}$ the mass-asymmetry stiffness constant K_m is negative. Thus for $x < x_{BG}$, the probability $P(m)$ increases rather than decreases with increasing absolute value of m.

We have thus derived in the harmonic approximation expressions that are valid quantum-mechanically at any temperature for the distributions in both coordinates and momenta for the normal modes (except the fission mode). Each distribution is a Gaussian with a temperature-dependent width that has simple high- and low-temperature limits.

The probability distribution for the fission momentum p_f is difficult to calculate quantum-mechanically both because this mode is unstable and because the stiffness constant K_f is not defined. For this distribution we use the classical result (23c); rewriting, this is

$$P(p_f) = 2\left(\pi\, C_{p_f}\right)^{-1/2} \exp\left(-p_f^2/C_{p_f}\right),$$

with

$$C_{p_f} = 2M_f\,\Theta\,.$$

Any attempt to improve this result should include an improved description of the shape of the fission barrier. The inaccuracies arising from using the classical expression for $P(p_f)$ are probably not serious for our purposes, since the equations relating the quantities of interest at infinity to the initial conditions are to first order independent of p_f. An error in $P(p_f)$ would thus affect the distributions of the quantities of interest only in second order.

For a given normal mode the probability distribution for the coordinate is independent of the probability distribution for the momentum. Also, each normal mode is completely independent of all the others. Therefore, the probability for observing the system with a given set of initial coordinates and momenta is simply the product of the individual probabilities for each coordinate and momentum.

The probability distributions for the initial conditions are in terms of stiffnesses, masses, and frequencies (all calculated and graphed as functions of x in Section III.B), and the nuclear temperature Θ at the saddle point. The temperature is a function of the internal nuclear excitation energy at the saddle point. The discussion of the determination of Θ in terms of the internal excitation energy will be given in Section VI.

V. PROBABILITY DISTRIBUTIONS FOR OBSERVABLE QUANTITIES OF INTEREST

In this section we derive expressions for the probability of simultaneously observing the two fragments at infinity with given values of the quantities of interest: total translational kinetic energy, fractional mass, individual excitation energies, and individual angular momenta. The derivation utilizes the results obtained in the two preceding sections: the equations relating the observable quantities of interest to the initial conditions, and the probability distributions for the initial conditions. Since the equations relating the quantities of interest to the initial conditions are for the case in which the saddle point is represented by two tangent spheroids ($x \lesssim 0.80$), the probability distributions that we derive for the quantities of interest will be for this case also.

A. The Distribution $P(E, U, X_1, X_2, \underset{\sim}{L}_1, \underset{\sim}{L}_2)$ to Lowest Order

We first consider the calculation of the probability $P(E, U, X_1, X_2, \underset{\sim}{L}_1, \underset{\sim}{L}_2)$ of simultaneously observing the two fragments at infinity with given total translational kinetic energy E, fractional mass U, individual excitation energies X_1 and X_2, and individual angular momenta $\underset{\sim}{L}_1$ and $\underset{\sim}{L}_2$. For this derivation we use the consistent set of lowest-order equations (15), (16), (17), and (19) expressing the quantities of interest in terms of the initial conditions. The resulting probability distributions will then be valid only to lowest order in the quantities of interest. We will later use (14) and (15) to calculate the distribution $P(E, U)$ to a higher order in E and U than that used in the present calculation.

The probability distribution for the observable quantities of interest is obtained by multiplying the probability distribution for the initial coordinates and momenta by the Jacobian for the transformation from the initial coordinates and momenta to the quantities

of interest, and then integrating over the remaining coordinates and momenta.

Since E, X_1, and X_2 are not independent, but are related to first order by the conservation-of-energy equation (20), the probability distribution $P(E, U, X_1, X_2, \underset{\sim}{L}_1, \underset{\sim}{L}_2)$ contains the Dirac delta function $\delta(E + X_1 + X_2 - E^0 - 2X_1^0)$. This probability distribution is then given by

$$P(E, U, X_1, X_2, \underset{\sim}{L}_1, \underset{\sim}{L}_2) = P(U, X_1, X_2, \underset{\sim}{L}_1, \underset{\sim}{L}_2)\, \delta(E + X_1 + X_2 - E^0 - 2X_1^0),$$

where a particular choice has been made for the remaining variables.

In order to calculate $P(U, X_1, X_2, \underset{\sim}{L}_1, \underset{\sim}{L}_2)$ we need to invert the set of equations (15), (16), and (17) to obtain nine of the initial conditions as functions of the nine quantities of interest and the remaining initial conditions. (Each component of angular momentum of each fragment is regarded here as a separate quantity of interest.) If we choose m, s, d, p_{b_x}, p_{w_x}, p_{b_y}, p_{w_y}, p_t, and p_a as dependent variables, this inversion gives

$$m = U - \frac{1}{2}, \tag{26a}$$

$$s = \frac{X_1 + X_2 - 2X_1^0}{2X_{1,s}}, \tag{26b}$$

$$d = \frac{X_1 - X_2 - 2X_{1,m}(U - \frac{1}{2})}{2X_{1,d}}, \tag{26c}$$

$$p_{b_x} = \frac{L_{1x} - L_{2x} - 2L_{1,b}\, b_x}{2L_{1,p_b}}, \tag{26d}$$

$$p_{w_x} = \frac{L_{1x} + L_{2x} - 2L_{1,w}\, w_x}{2L_{1,p_w}}, \tag{26e}$$

$$p_{b_y} = \frac{L_{1y} - L_{2y} - 2L_{1,b}\, b_y}{2L_{1,p_b}}, \tag{26f}$$

$$p_{w_y} = \frac{L_{1y} + L_{2y} - 2L_{1,w}\, w_y}{2L_{1,p_w}}, \tag{26g}$$

$$p_t = \frac{L_{1z} - L_{2z}}{\sqrt{2}}, \tag{26h}$$

$$p_a = \frac{L_{1z} + L_{2z}}{\sqrt{2}}. \tag{26i}$$

With this choice of dependent variables, the equation transforming the initial probability distribution into the desired probability distribution is

$$P(U, X_1, X_2, \underset{\sim}{L}_1, \underset{\sim}{L}_2) = \int_{-\infty}^{+\infty} db_x \int_{-\infty}^{+\infty} dw_x \int_{-\infty}^{+\infty} db_y \int_{-\infty}^{+\infty} dw_y$$

$$\times P(m, s, d, b_x, w_x, b_y, w_y, p_{b_x}, p_{w_x}, p_{b_y}, p_{w_y}, p_t, p_a)$$

$$\times \left| \frac{\partial(m, s, d, p_{b_x}, p_{w_x}, p_{b_y}, p_{w_y}, p_t, p_a)}{\partial(U, X_1, X_2, L_{1x}, L_{2x}, L_{1y}, L_{2y}, L_{1z}, L_{2z})} \right|;$$

we have already integrated over the initial coordinates and momenta not involved in the transformation, obtaining unity in each case. The probability distribution in the integrand is given by the product of the probability distribution for each normal coordinate and momentum appearing in its argument, as determined in Section IV. It is understood that this probability function has the set of equations(26) substituted for the variables $m, s, d, p_{b_x}, p_{w_x}, p_{b_y}, p_{w_y}, p_t$, and p_a.

The absolute value of the Jacobian for the transformation is given by

$$\left|\frac{\partial(m,s,d,p_{b_x},p_{w_x},p_{b_y},p_{w_y},p_t,p_a)}{\partial(U,X_1,X_2,L_{1x},L_{2x},L_{1y},L_{2y},L_{1z},L_{2z})}\right| = \left(\frac{1}{2X_{1,s}\,X_{1,d}}\right)\left(\frac{1}{2L_{1,p_b}\,L_{1,p_w}}\right)^2 .$$

We note that the transformation equations for m, s, and d are independent of $\underset{\sim}{L}_1$ and $\underset{\sim}{L}_2$; and the equations for p_{b_x}, p_{w_x}, p_{b_y}, p_{w_y}, p_t, and p_a are independent of U, X_1, and X_2. Because of this, the probability $P(U, X_1, X_2, \underset{\sim}{L}_1, \underset{\sim}{L}_2)$ splits into a product of two probability functions:

$$P(U, X_1, X_2, \underset{\sim}{L}_1, \underset{\sim}{L}_2) = P(U, X_1, X_2)\; P(\underset{\sim}{L}_1, \underset{\sim}{L}_2),$$

with

$$P(U,X_1,X_2) = \frac{1}{(4\pi^3 C_m X_{1,s}^2 C_s X_{1,d}^2 C_d)^{1/2}} \exp\left\{-\frac{(U-\frac{1}{2})^2}{C_m} - \frac{(X_1+X_2-2X_1^0)^2}{4X_{1,s}^2 C_s} - \frac{[X_1-X_2-2X_{1,m}(U-\frac{1}{2})]^2}{4X_{1,d}^2 C_d}\right\}, \quad (27)$$

and

$$P(\underset{\sim}{L}_1, \underset{\sim}{L}_2) = \frac{1}{(\pi^9 C_b^2 C_w^2 C_{p_b}^2 C_{p_w}^2 C_{p_t})^{1/2}} \left(\frac{1}{2L_{1,p_b}\,L_{1,p_w}}\right)^2 \int_{-\infty}^{+\infty} db_x \int_{-\infty}^{+\infty} dw_x \int_{-\infty}^{+\infty} db_y \int_{-\infty}^{+\infty} dw_y$$

$$\times \exp\left\{-\frac{(b_x^2+b_y^2)}{C_b} - \frac{(w_x^2+w_y^2)}{C_w} - \frac{[(L_{1x}-L_{2x}-2L_{1,b}b_x)^2+(L_{1y}-L_{2y}-2L_{1,b}b_y)^2]}{4L_{1,p_b}^2 C_{p_b}} - \frac{[(L_{1x}+L_{2x}-2L_{1,w}w_x)^2+(L_{1y}+L_{2y}-2L_{1,w}w_y)^2]}{4L_{1,p_w}^2 C_{p_w}} - \frac{(L_{1z}-L_{2z})^2}{2C_{p_t}}\right\} \delta\left(\frac{L_{1z}+L_{2z}}{\sqrt{2}}\right)$$

$$= \frac{\sqrt{2}}{(\pi C_{p_t})^{1/2}\pi^2 C'_{p_b} C'_{p_w}} \exp\left\{ - \frac{[(L_{1x}-L_{2x})^2 + (L_{1y}-L_{2y})^2]}{2C'_{p_b}} \right.$$

$$\left. - \frac{[(L_{1x}+L_{2x})^2 + (L_{1y}+L_{2y})^2]}{2C'_{p_w}} - \frac{(L_{1z}-L_{2z})^2}{2C_{p_t}} \right\} \delta(L_{1z}+L_{2z}). \qquad (28)$$

We have used the abbreviations[30]

$$C'_{p_b} = 2L_{1,p_b}^2 C_{p_b} + 2L_{1,b}^2 C_b,$$

$$C'_{p_w} = 2L_{1,p_w}^2 C_{p_w} + 2L_{1,w}^2 C_w.$$

The distribution $P(E, U, X_1, X_2, \underset{\sim}{L}_1, \underset{\sim}{L}_2)$ is of the form $\exp[-Q(E, U, X_1, X_2, L_{1x}, L_{2x}, L_{1y}, L_{2y}, L_{1z}, L_{2z})]$ times two Dirac delta functions, where $Q(E, U, X_1, X_2, L_{1x}, L_{2x}, L_{1y}, L_{2y}, L_{1z}, L_{2z})$ is a positive-definite quadratic function of its ten variables. In the language of statistics, $P(E, U, X_1, X_2, \underset{\sim}{L}_1, \underset{\sim}{L}_2)$ is a 10-variate normal distribution(56) multiplied by two delta functions. Similarly, the probability function $P(U, X_1, X_2)$ is a trivariate normal distribution, and $P(\underset{\sim}{L}_1, \underset{\sim}{L}_2)$ is a 6-variate normal distribution multiplied by a delta function.

1. Distributions Obtained from $P(E, U, X_1, X_2)$

We have derived the lowest-order result for the probability of observing the two fragments at infinity with given values of total translational kinetic energy, fractional mass, and individual excitation energies:

$$P(E, U, X_1, X_2) = P(U, X_1, X_2)\, \delta(E + X_1 + X_2 - E^0 - 2X_1^0),$$

where $P(U, X_1, X_2)$ is given by (27). By integrating over the quantities

[30] If there were no angular momentum induced by the torque arising from the presence of the electrostatic field, then C'_{p_b} would equal C_{p_b}, since for this case $L_{1,p_b} = 1/\sqrt{2}$, and $L_{1,b} = 0$. An analogous statement holds for C'_{p_w}.

not of immediate interest in this probability distribution, we obtain probability distributions for the observation of a smaller number of quantities. Each of the resulting probability functions is also a normal distribution (multiplied possibly by a delta function). For example, we obtain

$$P(X_1, X_2) = \frac{1}{[4\pi^2 X_{1,s}^2 C_s (X_{1,m}^2 C_m + X_{1,d}^2 C_d)]^{1/2}}$$

$$\times \exp\left[- \frac{(X_1 + X_2 - 2X_1^0)^2}{4X_{1,s}^2 C_s} - \frac{(X_1 - X_2)^2}{4(X_{1,m}^2 C_m + X_{1,d}^2 C_d)} \right],$$

$$P(U, -X_1) = \frac{1}{[\pi^2 C_m (X_{1,s}^2 C_s + X_{1,d}^2 C_d)]^{1/2}} \exp\left\{ - \frac{(U - \frac{1}{2})^2}{C_m} - \frac{[X_1 - X_1^0 - X_{1,m}(U - \frac{1}{2})]^2}{X_{1,s}^2 C_s + X_{1,d}^2 C_d} \right\},$$

$$P(X_1) = \frac{1}{[\pi (X_{1,m}^2 C_m + X_{1,s}^2 C_s + X_{1,d}^2 C_d)]^{1/2}}$$

$$\times \exp\left[- \frac{(X_1 - X_1^0)^2}{X_{1,m}^2 C_m + X_{1,s}^2 C_s + X_{1,d}^2 C_d} \right],$$

and

$$P(U) = \frac{1}{(\pi C_m)^{1/2}} \exp\left[- \frac{(U - \frac{1}{2})^2}{C_m} \right].$$

We can also obtain from (27) the probability distribution for mass and total excitation energy X by substituting

$$X_1 = X - X_2$$

and integrating over X_2:[31]

$$P(U, X) = \frac{1}{(4\pi^2 C_m X_{1,s}^2 C_s)^{1/2}} \exp\left[- \frac{(U - \frac{1}{2})^2}{C_m} - \frac{(X - X^0)^2}{4X_{1,s}^2 C_s} \right].$$

An integration over U in this equation then gives

$$P(X) = \frac{1}{(4\pi X_{1,s}^2 C_s)^{1/2}} \exp\left[- \frac{(X - X^0)^2}{4X_{1,s}^2 C_s} \right].$$

Since the total translational kinetic energy and the total excitation energy are related to first order by the conservation-of-energy equation (20), the two preceding equations are completely equivalent to

$$P(E, U) = \frac{1}{[\pi^2 C_m a^2 C_s (E^0)^2]^{1/2}} \exp\left[- \frac{(U - \frac{1}{2})^2}{C_m} - \frac{(E - E^0)^2}{a^2 C_s (E^0)^2} \right] \quad (29)$$

and

$$P(E) = \frac{1}{[\pi a^2 C_s (E^0)^2]^{1/2}} \exp\left[- \frac{(E - E^0)^2}{a^2 C_s (E^0)^2} \right];$$

---

[31] This equation is also obtainable directly from $P(m, s)$ and the equations $U = \frac{1}{2} + m$ and $X = X^0 + 2X_{1,s}\, s$ [obtained from (16) by adding X_1 and X_2].

we have also used the relationship (21) between $X_{1,s}$ and αE^0. Similarly, Eq. (27) is equivalent to

$$P(E, U, X_1) = \frac{1}{[\pi^3 C_m \alpha^2 C_s (E^0)^2 X_{1,d}^2 C_d]^{1/2}} \exp\left\{ - \frac{(U - \frac{1}{2})^2}{C_m} - \frac{(E - E^0)^2}{\alpha^2 C_s (E^0)^2} - \frac{[X_1 - X_1^0 + \frac{1}{2}(E - E^0) - X_{1,m}(U - \frac{1}{2})]^2}{X_{1,d}^2 \, C_d} \right\}.$$

This result is useful for discussing, for example, the excitation energy of a single fragment, for given values of the total translational kinetic energy and fractional mass.

From the expression (29) for $P(E, U)$ and the transformation (18) relating the total translational kinetic energy E and the fractional mass U to the individual translational kinetic energies E_1 and E_2, we obtain the probability distribution for individual translational kinetic energies:

$$P(E_1, E_2) = P(E, U) \left| \frac{\partial (E, U)}{\partial (E_1, E_2)} \right|$$

$$= \frac{1}{[\pi^2 C_m \alpha^2 C_s (E^0)^4]^{1/2}} \exp\left[- \frac{(E_1 + E_2 - E^0)^2}{\alpha^2 C_s (E^0)^2} - \frac{(E_1 - E_2)^2}{4 C_m (E^0)^2} \right] ;$$

the equation resulting from the transformation has been reduced to lowest order in E_1 and E_2. By integrating over E_2 in this equation we obtain the distribution in translational kinetic energy of a single fragment:

$$P(E_1) = \frac{1}{[\pi (4C_m + \alpha^2 C_s)(E_1^0)^2]^{1/2}} \exp\left[- \frac{(E_1 - E_1^0)^2}{(4C_m + \alpha^2 C_s)(E_1^0)^2} \right] .$$

It should be recalled that for $x < x_{BG}$, C_m is negative, resulting in the mass distribution increasing rather than decreasing with mass asymmetry. The distributions involving U then approach infinity for large values of U and are thus not normalizable. In a contour plot of P(E, U) vs. E and U, for example, the lines of constant probability are not ellipses for $x < x_{BG}$, but instead are two families of hyperbolas. One family represents lines of increasing probability for increasing mass asymmetry, whereas the other family represents lines of decreasing probability for deviations in the kinetic energy from its most probable value.

Since the above probability functions are normal distributions (of one or more variables), all the information they contain can be represented in terms of means, variances, and correlation coefficients (or alternatively, covariances) (56). For example, a monovariate normal (Gaussian) distribution is completely specified by two quantities: the mean and the variance (square of the standard deviation). From the standard form for a Gaussian distribution we can determine by inspection the mean and the variance of each of the Gaussian distributions above.

To specify a bivariate normal distribution, five quantities are required in general: the mean and variance of each variable, and the correlation coefficient (or alternatively, the covariance). The correlation coefficient ρ_{xy} of the distribution $P(x, y)$ is defined by (57)

$$\rho_{xy} = \frac{\int dx \int dy\ (x-\bar{x})(y-\bar{y})\ P(x, y)}{\sigma_x\ \sigma_y} .$$

The value of the correlation coefficient, which has a range of values from -1 to $+1$ (57), indicates the degree of correlation of the variables. A positive value of this coefficient means that the two variables are more likely to be simultaneously large or else simultaneously small; a negative value means that if one variable is large, the other is more likely to be small. The distributions $P(U, X)$ and $P(E, U)$ are seen to have correlation coefficients that are zero. On the other hand, the correlation coefficient for the distribution $P(X_1, X_2)$, for example, is nonzero; we find that it is given by

$$\rho_{X_1 X_2} = \frac{X_{1,s}^2\, C_s - X_{1,m}^2\, C_m - X_{1,d}^2\, C_d}{X_{1,s}^2\, C_s + X_{1,m}^2\, C_m + X_{1,d}^2\, C_d} . \qquad (30)$$

Coefficients of correlation could be similarly calculated for the other distributions.

To illustrate the magnitudes of the widths of these distributions, we present sample graphs of some of the more important functions derived above. The results are for nonviscous fragments with the type of hydrodynamic flow we have been considering: a superposition of an irrotational flow and a flow corresponding to a uniform rotation. All graphs refer to the fission of the compound nucleus ${}_{85}At^{213}$, with a nuclear temperature at the saddle point of $\Theta = 1.13$ MeV. (This situation may be obtained experimentally, for example, by bombarding ${}_{83}Bi^{209}$ with 65-MeV alpha particles.) In two of the graphs we

illustrate the effect of temperature on the widths by also presenting the result for $\Theta = 0$. In Fig. 30 is presented a contour map of $P(X_1, X_2)$ vs X_1 and X_2. Figure 31 shows the distribution in excitation energy of a single fragment: $P(X_1)$ vs X_1. The distribution in total excitation energy [$P(X)$ vs X], which is equivalent to the distribution in total translational kinetic energy [$P(E)$ vs E], is shown in Fig. 32. The lowest-order result (29) for the distribution in mass and total translational kinetic energy is presented in Fig. 33 as a contour map of $P(E, U)$ vs E and U.

An interesting feature of the theory is the prediction that the excitation energies should be anticorrelated—if one fragment has a large excitation energy, then the other fragment is more likely to have a small excitation energy, and vice versa. This can be seen either from the contour map of $P(X_1, X_2)$ in Fig. 30, or from evaluating Eq. (30) for the correlation coefficient. For ${}_{85}At^{213}$ and $\Theta = 1.13$ MeV, we find that $\rho_{X_1 X_2} = -0.46$. For this same nucleus in the high-temperature (classical) limit, $\rho_{X_1 X_2} = -0.44$, whereas in the zero-temperature limit, $\rho_{X_1 X_2} = -0.58$. Thus the excitation energies are predicted to be somewhat more strongly anticorrelated at low temperatures than at high temperatures.

The physical reason for the anticorrelation in the excitation energies is very simple in the classical limit. The result can be interpreted in terms of the relative amplitudes of the stretching and distortion-asymmetry modes, since the excitation energy of a fragment at infinity depends primarily upon its initial elongation. Pure stretching-mode oscillations correspond to completely correlated fragment excitation energies, whereas pure distortion-asymmetric oscillations correspond to completely anticorrelated fragment excitation energies. The potential energy in the neighborhood of the saddle point is found to be "stiffer" with respect to stretching than with respect to distortion-asymmetry. The distortion-asymmetric oscillations therefore possess larger amplitudes than the stretching oscillations—hence, anticorrelation.

The mean (or most probable) value of each of the quantities of interest is seen to be independent of nuclear temperature. However, since the constants C_s etc. are temperature-dependent, the widths (or variances) of the distributions are functions of nuclear temperature. As the temperature approaches zero, the widths of the distributions approach finite values determined by the quantum-mechanical zero-point vibrations of the appropriate oscillators. (Exceptions occur for the mass distribution and the distributions in the z-component of angular momentum. Since the mass-asymmetry and twisting frequencies are zero, the widths of these distributions approach zero as the nuclear temperature approaches zero.) For the fission of a typical lighter-than-radium nucleus, the zero-point full width at half maximum of the distribution in total translational kinetic energy is ≈ 10 MeV. The width of the kinetic-energy distribution arises primarily from oscillations in the distance between fragment centers (stretching mode). Because of the near cancellation of the opposing effects of the surface and Coulomb energies near the saddle point, the potential energy in the stretching direction is very flat. This means that a very small quantum-mechanical uncertainty in the stretching-mode potential energy (≈ 0.3 MeV) is "amplified" into a rather large zero-point width in the total translational kinetic-energy distribution. As the nuclear temperature increases, the uncertainty in the stretching-mode potential energy increases, resulting in a corresponding increase in the width of the kinetic-energy distribution.[3]

2. Distributions Obtained from $P(\underset{\sim}{L}_1, \underset{\sim}{L}_2)$

From Eq. (28) for $P(\underset{\sim}{L}_1, \underset{\sim}{L}_2)$ we can obtain several useful formulae involving the fragments' angular momenta. We first convert from cartesian coordinates to spherical coordinates through the transformation

$$L_{1x} = L_1 \sin\theta_1 \cos\phi_1,$$
$$L_{1y} = L_1 \sin\theta_1 \sin\phi_1,$$
$$L_{1z} = L_1 \cos\theta_1;$$

an analogous set of equations holds for fragment 2. The magnitude of $\underset{\sim}{L}_1$ is L_1, the angle between the angular-momentum vector of fragment 1 and the z_1 axis (the line connecting the fragment centers) is θ_1, and the azimuthal angle is ϕ_1. We further define

$$\phi = \phi_1 - \phi_2,$$
$$\phi' = (\phi_1 + \phi_2)/2;$$

if one looks along the line connecting the spheroid centers, then ϕ is the angle between the fragments' components of angular momentum perpendicular to this line.

Equation (28) becomes, after an integration over ϕ' (upon which the probability function does not depend) is performed (the normalization is such that the range of ϕ is from 0 to π),

$$P(L_1, L_2, \theta_1, \theta_2, \phi) = \frac{4\sqrt{2}\, L_1^2 L_2^2 \sin\theta_1 \sin\theta_2}{(\pi C_{p_t})^{1/2}\, \pi C'_{p_b} C'_{p_w}}$$
$$\times \exp\left[-\frac{1}{2}\left(\frac{1}{C'_{p_b}} + \frac{1}{C'_{p_w}}\right)(L_1^2 + L_2^2) \right.$$
$$-\frac{1}{2}\left(\frac{1}{C_{p_t}} - \frac{1}{C'_{p_b}} - \frac{1}{C'_{p_w}}\right)(L_1^2 \cos^2\theta_1 + L_2^2 \cos^2\theta_2)$$
$$+\left(\frac{1}{C'_{p_b}} - \frac{1}{C'_{p_w}}\right) L_1 L_2 \sin\theta_1 \sin\theta_2 \cos\phi$$
$$\left. + \frac{1}{C_{p_t}} L_1 L_2 \cos\theta_1 \cos\theta_2 \right] \delta(L_1 \cos\theta_1 + L_2 \cos\theta_2). \tag{31}$$

The integration over ϕ in this result can be performed explicitly to yield a probability distribution that is independent of azimuthal angles. Since (58)

$$\int_0^{\pi} \exp(x \cos\phi)\, d\phi = \pi\, I_0(x) = \pi\, J_0(ix), \tag{32}$$

where J_0 denotes the Bessel function of the first kind of order zero (I_0 is the modified Bessel function of the first kind of order zero); the expression for $P(L_1, L_2, \theta_1, \theta_2)$ can be obtained from (31) by inspection. Also, because of the presence of the delta function, an integration over any one of the four variables L_1, L_2, θ_1, θ_2 can be performed immediately.

In the zero-temperature limit the twisting mode is not excited, and the twisting-momentum constant C_{p_t} approaches zero. This means physically that the z component of angular momentum of each fragment is zero, and the angular-momentum vector of each fragment is perpendicular to its direction of motion. The integrations over both θ_1 and θ_2 in (31) can then be easily performed, yielding the zero-temperature result.[32]

$$P(L_1, L_2, \phi) = \frac{4L_1L_2}{\pi C'_{p_b} C'_{p_w}} \exp\left[-\frac{1}{2}\left(\frac{1}{C'_{p_b}} + \frac{1}{C'_{p_w}}\right)(L_1^2 + L_2^2) + \left(\frac{1}{C'_{p_b}} - \frac{1}{C'_{p_w}}\right) L_1 L_2 \cos\phi\right];$$

---

[32] This expression could also be obtained directly from the set of equations (17) and $P(b_x, w_x, b_y, w_y, p_{b_x}, p_{w_x}, p_{b_y}, p_{w_y})$ by integrating over the bending and wriggling angles, and transforming the result to cylindrical coordinates.

it is understood that the zero-temperature limits of C'_{p_b} and C'_{p_w} are to be used. By employing (32) the zero-temperature result for $P(L_1, L_2)$ can also be written down by inspection.

If, in the original expression (28) for $P(\underset{\sim}{L}_1, \underset{\sim}{L}_2)$, we integrate with respect to L_{2x}, L_{2y}, and L_{2z}, we obtain the probability distribution for the angular momentum of a single fragment:

$$P(\vec{L}_1) = \frac{2\sqrt{2}}{(\pi C_{p_t})^{1/2}\pi(C'_{p_b} + C'_{p_w})} \exp\left[-\frac{2(L_{1x}^2 + L_{1y}^2)}{C'_{p_b} + C'_{p_w}} - \frac{2L_{1z}^2}{C_{p_t}}\right].$$

If we transform to spherical coordinates and integrate over the azimuthal angle (upon which the probability function does not depend), we obtain

$$P(L_1, \theta_1) = \frac{4\sqrt{2}\, L_1^2 \sin\theta_1}{(\pi C_{p_t})^{1/2}(C'_{p_b} + C'_{p_w})} \exp\left[-\frac{2L_1^2}{C'_{p_b} + C'_{p_w}} - 2\left(\frac{1}{C_{p_t}} - \frac{1}{C'_{p_b} + C'_{p_w}}\right) L_1^2 \cos^2\theta_1\right].$$

An integration over θ_1 can be carried out to give the probability of observing a single fragment with given magnitude of angular momentum:

$$P(L_1) = \frac{4L_1}{[(C'_{p_b} + C'_{p_w})(C'_{p_b} + C'_{p_w} - C_{p_t})]^{1/2}} \exp\left[-\frac{2L_1^2}{C'_{p_b} + C'_{p_w}}\right] \times H\left\{\left[\frac{2(C'_{p_b} + C'_{p_w} - C_{p_t})}{C_{p_t}(C'_{p_b} + C'_{p_w})}\right]^{1/2} L_1\right\},$$

where $H(x)$ is the error function, defined by (59)

$$H(x) = \frac{2}{\sqrt{\pi}} \int_0^x \exp(-a^2)\,da.$$

In the zero-temperature limit, C_{p_t} approaches zero, and this expression reduces to

$$P(L_1) = \frac{4L_1}{C_{p_b}' + C_{p_w}'} \exp\left[- \frac{2L_1^2}{C_{p_b}' + C_{p_w}'} \right] .$$

The various probability functions obtained from $P(\underset{\sim}{L}_1, \underset{\sim}{L}_2)$ are useful as regards specific information on the fragments' angular momenta at infinity. One has available in these formulae predictions regarding the magnitudes of the angular momenta, the angles between the angular momenta and the line connecting fragment centers, and the angle between the components of angular momentum perpendicular to the line connecting fragment centers. These predictions include the correlations between the various quantities, as well as their dependences upon nuclear temperature and fissionability parameter.

As a single example, we present in Fig. 34 the curve $P(L_1)$ vs L_1 for the compound nucleus ${}_{85}At^{213}$ and $\Theta = 1.13$ MeV. The result for nonviscous fragments with hydrodynamic flow of the type we have been considering is given by the solid line, and the result for infinitely viscous fragments by the dot-dashed line. We also indicate the result (short-dashed line) that would follow if the torque exerted by one fragment on the other through the electrostatic interaction were zero—this represents the distribution of angular momentum at the scission configuration. At scission, the most probable magnitude of the angular momentum of a fragment is seen to be about $8.5\hbar$. The corresponding most probable value at infinity is about $10\hbar$ for the nonviscous case, and about $15\hbar$ for the viscous case. The relatively large difference in the predicted angular-momentum distribution between the case of viscous fragments and the case of nonviscous fragments will perhaps make it possible to estimate experimentally the degree of nuclear viscosity. For this to be practicable, of course, the

present theory of fragment angular-momentum distributions would have to be refined to the stage where predictions can be trusted to within considerably better than 50%.

B. The Distribution P(E, U) to Higher Order

We have seen [Eq. (29) and Fig. 33] that to lowest order in the variables E and U, the probability function P(E, U) is a bivariate normal distribution; in a contour map of P(E, U) the lines of constant probability are ellipses whose axes are along E and U. This lowest-order result for P(E, U) is completely specified by E^0 (the mean value of E; the mean value of U is one-half from symmetry) and the two variances σ_E^2 and σ_U^2, which measure the widths of the distributions in E and U, respectively. By use of this result we are able to discuss the distribution in mass and total translational kinetic energy in the immediate vicinity of the most probable values.

To discuss the deviations of the distribution in mass and total translational kinetic energy from a bivariate normal distribution, it is necessary to include in the expression for P(E, U) higher-order terms in the variables E and U. Whereas in the bivariate normal distribution the exponent contains only the two quadratic terms $(E-E^0)^2$ and $(U-\frac{1}{2})^2$, the exponent of the distribution to the next higher order contains in addition the two cubic terms $(E-E^0)(U-\frac{1}{2})^2$ and $(E-E^0)^3$, and the quartic term $(U-\frac{1}{2})^4$.[33] In addition to the mean E^0 and the two variances, three additional quantities, the coefficients of the two cubic terms and the quartic term, are needed to specify P(E, U) to this order. These coefficients have

---

[33] The other two cubic terms, $(E-E^0)^2(U-\frac{1}{2})$ and $(U-\frac{1}{2})^3$, are absent because P(E, U) is an even function of $(U-\frac{1}{2})$. The absence of the $(U-\frac{1}{2})^3$ term means that the $(U-\frac{1}{2})^4$ term is responsible for the first-order deviation of the distribution in mass from a Gaussian, and must then be considered to this order. The distribution P(E, U) would also, in general, have a pre-exponential dependence upon E and U.

simple physical significances: The coefficient of the $(E-E^0)^3$ term strongly affects the skewness(60) of the distribution in E, and determines the lowest-order deviation of the distribution in E from a pure Gaussian—whether the distribution has a high-energy or a low-energy tail, and by how much. Similarly, the coefficient of the $(U-\frac{1}{2})^4$ term strongly affects the kurtosis(60) (peakedness or flatness) of the distribution in U, and determines the lowest-order deviation of the distribution in U from a pure Gaussian—whether the distribution is more peaked than a Gaussian or has a flatter top. We will find that the coefficient of the $(E-E^0)(U-\frac{1}{2})^2$ term determines both how rapidly the most probable (or mean) value of E as a function of U falls off with $(U-\frac{1}{2})^2$, and also the derivative with respect to E (evaluated at $E=E^0$) of the variance of the mass distribution as a function of E. To the next higher order beyond including these three terms, the exponent of the P(E, U) distribution would contain the quartic term $(E-E^0)^4$, the sixth-order term $(U-\frac{1}{2})^6$, along with cross terms in E and U; and so on.

The derivation of the bivariate normal distribution (29) utilized a combination of two lowest-order results: (a) equation (19) relating E linearly to the initial conditions, and the exact equation (15) for U, and (b) the initial-conditions probability distributions obtained in Section IV by expanding the potential energy about the saddle point and retaining only quadratic terms (harmonic approximation). We have available [Eq. (14)] a much more accurate equation relating E to the initial conditions than the first-order equation (19). In addition to taking into account the dependence of E on the mass-asymmetry coordinate m and the fission and stretching momenta p_f and p_s, Eq. (14) also includes a more precise dependence of E on the stretching coordinate s. However, the harmonic-oscillator probability distributions that we have used for the initial conditions represent the most accurate quantum-mechanical result that can be easily obtained. In order to derive the best expression for P(E, U) that still incorporates initial conditions determined quantum-mechanically, we will use the same probability distributions for the initial conditions as before, but will

use the more accurate equation (14) for E and the exact equation (15) for U. Although the resulting expression for P(E, U) will be strictly accurate only to lowest order in E and U, it will in addition contain higher-order terms in E and U. The higher-order terms represent the effect of the nonlinear transformation (14) expressing E in terms of the initial conditions. Since there are two separate steps involved in the calculation of P(E, U), the treatment of one step essentially exactly and the other step to lowest order in E and U is not completely inconsistent.

We will later calculate an expression for P(E, U), valid in the classical limit, in which we use probability distributions for the initial conditions obtained by retaining certain anharmonic terms in the expansion of the potential energy about the saddle point.

1. P(E, U) for Initial Conditions Determined in the Harmonic Approximation

In order to calculate P(E, U) we need to invert the two equations (14) and (15) to obtain two of the initial conditions as functions of E and U and the remaining initial conditions. If we choose m and s as dependent variables, this inversion gives

$$m = U - \frac{1}{2}, \tag{33a}$$

$$s = \frac{1}{\alpha}\left[\frac{4U(1-U)\,E^0}{E - M_\ell\left(\frac{2M_{c_1}^0 p_f}{M_0 M_f} + \frac{p_s}{M_s}\right)^2} - 1\right]. \tag{33b}$$

With this choice of dependent variables, the transformation from the initial probability distribution to the desired probability distribution is given by

$$P(E, U) = \int_0^\infty dp_f \int_{-\infty}^{+\infty} dp_s \; P(m, s, p_f, p_s) \left|\frac{\partial(m, s)}{\partial(E, U)}\right| ;$$

we have already integrated over the initial coordinates and momenta not involved in the transformation. It is understood that the set of equations (33) is substituted for m and s in $P(m, s, p_f, p_s)$, which is given by the product of the probability distribution for each normal coordinate and momentum appearing in its argument, as determined in Section IV.

The double integral over p_s and p_f cannot be expressed in a closed form. (By an appropriate change of variables, the double integral can be reduced to a single integral in which the new integrand includes an error function; in practice, this transformation is not very useful.) However, if we expand the expression (33b) for s in powers of the small quantity

$$\frac{M_\ell \left(\frac{2M_{c_1}^0 p_f}{M_0 M_f} + \frac{p_s}{M_s} \right)^2}{E}$$

everywhere it appears in the integrand, we can integrate the resulting expansion term by term, obtaining an asymptotic series expansion for $P(E, U)$. The result is found to be

$$P(E, U) = \frac{4U(1-U)E^0 F(E, U)}{(\pi^2 C_m a^2 C_s)^{1/2} E^2} \exp\left\{ - \frac{(U - \frac{1}{2})^2}{C_m} - \frac{[E-4U(1-U)E^0]^2}{a^2 C_s E^2} \right\}, \tag{34}$$

where $F(E, U)$ is the asymptotic series

$$F(E, U) = 1 + \left\{ 1 + \frac{4U(1-U) E^0 [E - 4U(1 - U) E^0]}{a^2 C_s E^2} \right\}$$

$$\times \left[\frac{4(M_{c_1}^0/M_0)^2 C_{p_f}}{M_f^2} + \frac{C_{p_s}}{M_s^2} \right] \frac{M_\ell}{E} + \cdots . \tag{35}$$

The function $F(E, U)$ is close to unity, except where the term in braces becomes very large. This occurs only when E and/or U are far

from their most probable values. (Since this is an asymptotic series rather than a power series, the expansion converges for a definite range of the variables E and U rather than for an infinite number of terms retained in the expansion.) Thus, the approximation $F(E, U) = 1$ is a very good one. [Setting $F(E, U) = 1$ is equivalent to neglecting in (14) the dependence of E on the initial momenta p_f and p_s.]

An alternative way of writing $P(E, U)$ is more useful for some purposes than (34). If we collect terms in (34) according to powers of $(U - \frac{1}{2})$, we obtain

$$P(E, U) = \frac{E^0 F(E, U)}{(\pi^2 C_m a^2 C_s)^{1/2} E^2} \exp\left[- \frac{(E - E^0)^2}{a^2 C_s E^2} \right]$$

$$\times [1 - 4(U - \tfrac{1}{2})^2] \exp\left[- G(U - \tfrac{1}{2})^2 - H^2 (U - \tfrac{1}{2})^4 \right], \tag{36}$$

where the quantities G and H (functions of E) are defined by

$$G = \frac{1}{C_m} + \frac{8 E^0 (E - E^0)}{a^2 C_s E^2}, \tag{37a}$$

$$H = \frac{4 E^0}{(a^2 C_s)^{1/2} E}. \tag{37b}$$

It is instructive to compare the current higher-order result for $P(E, U)$ with the lowest-order expression (29) derived earlier. Whereas (29) is a bivariate normal distribution, the current result is not—in a plot of $P(E, U)$ vs E and U, the lines of constant probability are not ellipses. In Fig. 35 is presented a contour map of the current result for $P(E, U)$; this may be compared directly with the map of the lowest-order result shown in Fig. 33. Near the position of maximum probability the contour lines are close to ellipses, but in the region of smaller probability they tend toward a triangular shape.

From the distribution $P(E,U)$ one may obtain, by performing suitable integrations or by differentiating, other quantities of physical interest. We now list approximate analytical expressions for such quantities; the very good approximation $F(E,U) = 1$ is used in the derivation of these expressions (see Section V.B.1 of Ref. 2 for details).

By integrating over the total translational kinetic energy E, we obtain the distribution $P(U)$ of fractional mass:[34]

$$P(U) = \frac{1}{(\pi C_m)^{1/2}} \exp\left[-\frac{(U - \frac{1}{2})^2}{C_m}\right] . \tag{38}$$

The mean total translational kinetic energy, as a function of fractional mass, can be expressed in terms of an asymptotic series expansion in powers of $\alpha^2 C_s$:

$$\bar{E}(U) = 4U(1 - U)E^0(1 + \tfrac{1}{2}\alpha^2 C_s + \cdots) . \tag{39}$$

Similarly, the variance of the distribution in total translational kinetic energy, as a function of fractional mass, is given by

$$\sigma_E^2(U) = \tfrac{1}{2}[4U(1 - U)E^0]^2 \alpha^2 C_s(1 + 4\alpha^2 C_s + \cdots) . \tag{40}$$

Higher statistical moments of the distribution in total translational kinetic energy (as functions of fractional mass) could be calculated in a similar manner.

[34] This result follows directly from the equation $U = \frac{1}{2} + m$ and the distribution for $P(m)$, without the use of the approximation $F(E,U) = 1$. It may also be obtained by substituting (34) for $P(E,U)$, with $F(E,U) = 1$, and integrating.

The most probable total translational kinetic energy, as a function of fractional mass, is found to be

$$E_{MP}(U) = \frac{4U(1-U)E^0\left[(1+4\alpha^2 C_s)^{1/2} - 1\right]}{2\alpha^2 C_s}$$

$$= 4U(1-U)E^0(1 - \alpha^2 C_s + \cdots)$$

$$= E^0[1 - 4(U - \tfrac{1}{2})^2](1 - \alpha^2 C_s + \cdots) . \qquad (41)$$

It is interesting to note that the most probable total translational kinetic energy (for a given U) is slightly less than $4U(1-U)E^0$, whereas the mean value [Eq. (39)] is slightly greater. This is because the distribution $P(E,U)$ is not a normal distribution but instead has a small high-energy tail. The difference between $E_{MP}(U)$, $\overline{E}(U)$, and $4U(1-U)E^0$ is small, however, since $\alpha^2 C_s$ is typically ≈ 0.005.

We now consider the calculation of integrals with respect to U over the distribution $P(E,U)$. The distribution of total translational kinetic energy can be written as

$$P(E) = \frac{E^0}{(\pi^2 C_m \alpha^2 C_s)^{1/2} E^2} \exp\left[-\frac{(E-E^0)^2}{\alpha^2 C_s E^2}\right] \int_{-\infty}^{+\infty} dm(1-4m^2)\exp(-H^2m^4 - Gm^2) \qquad (42)$$

where G and H are defined by (37). The integral in (42) is not expressible in terms of elementary functions. We find it convenient for the present purposes to express it in terms of the functions $I_n(\beta)$ that are defined, for all values of n greater than $-\frac{1}{2}$, by the equation

$$I_n(\beta) = \int_{-\infty}^{+\infty} x^{2n} \exp(-x^4 - \beta x^2)dx$$

$$= \int_0^{\infty} y^{n-\frac{1}{2}} \exp(-y^2 - \beta y)dy \ . \qquad (43)$$

Properties of these functions, including the differential equation satisfied by $I_n(\beta)$, recurrence relations, and asymptotic expansion, as well as their relationship with the repeated integrals of the error function (61-63), are discussed in Appendix F of Ref. 2. We present in Fig. 36 graphs of the functions $I_n(\beta)$ vs β for $n = 0, 1,$ and 2.

The total translational kinetic-energy distribution can then be written in terms of these functions as

$$P(E) = \frac{E^0}{(\pi^2 C_m \alpha^2 C_s)^{1/2} E^2} \exp\left[-\frac{(E - E^0)^2}{\alpha^2 C_s E^2}\right]$$

$$\times \frac{1}{H^{1/2}} \left[I_0(G/H) - \frac{4 I_1(G/H)}{H} \right] , \qquad (44)$$

where the energy-dependent quantities G and H are defined by (37). The second term in the brackets is much smaller than $I_0(G/H)$ and can usually be neglected.

The variance of the distribution in fractional mass, as a function of total translational kinetic energy, is similarly found to be

$$\sigma_U^2(E) = \frac{1}{H}\left[\frac{I_1(G/H) - 4\, I_2(G/H)/H}{I_0(G/H) - 4\, I_1(G/H)/H}\right] . \tag{45a}$$

If we neglect the second term in the numerator and the second term in the denominator, we obtain the simple result

$$\sigma_U^2(E) \approx \frac{1}{H}\ \frac{I_1(G/H)}{I_0(G/H)} . \tag{45b}$$

A graph of the function $I_1(\beta)/I_0(\beta)$ vs (β) is given in Fig. 37. From the asymptotic expansion of $I_n(\beta)$ listed in Appendix F of Ref. 2, we find that for large values of G/H

$$\sigma_U^2(E) \rightarrow 1/(2G) . \tag{45c}$$

Higher statistical moments of the distribution in fractional mass (as functions of total translational kinetic energy) are obtainable just as readily as $\sigma_U^2(E)$. For example, the fourth central moment is given by

$$\mu_U^{(4)}(E) \approx \frac{1}{H^2}\ \frac{I_2(G/H)}{I_0(G/H)} ,$$

where we have neglected all but the leading terms. Then, the kurtosis of the distribution (60) is given by

$$\alpha_U^{(4)}(E) = \frac{\mu_U^{(4)}(E)}{\sigma_U^4(E)} - 3$$

$$\approx \frac{I_2(G/H)\ I_0(G/H)}{I_1^2(G/H)} - 3 . \tag{46}$$

A positive value of this coefficient means the distribution in mass is more peaked than a Gaussian, while a negative value means the distribution has a flatter top and is more rectangular than a Gaussian.

We consider finally quantities obtained by integrating over both E and U in $P(E,U)$. The mean total translational kinetic energy (integrated over fractional mass) is found to be given by

$$\bar{E} = E^0(1 - 2\,C_m)\,(1 + \tfrac{1}{2}\alpha^2\,C_s + \cdots)$$

$$= E^0(1 + \tfrac{1}{2}\alpha^2\,C_s - 2\,C_m + \cdots)\,,$$

and the variance of the total translational kinetic-energy distribution by

$$\sigma_E^{\,2} = \tfrac{1}{2}\alpha^2\,C_s(E^0)^2\,(1 + 4\,\alpha^2\,C_s - 4\,C_m + \frac{16\,C_m^{\,2}}{\alpha^2\,C_s} + \cdots)\,.$$

Since the distribution $P(E,U)$ is symmetric in U about $U = \frac{1}{2}$, the mean fractional mass (either as a function of E or integrated over E) is [illegible] $\frac{1}{2}$. The variance of the distribution in fractional mass is obtainable directly from the Gaussian (38) for $P(U)$:

$$\sigma_U^{\,2} = \tfrac{1}{2}\,C_m\,.$$

We shall postpone presenting any graphs of the quantities derived from $P(E,U)$ until we get to Section VI, where we compare the predictions with experimental data.

2. The Effect of Anharmonicity on $P(E,U)$

We are able to easily calculate quantum-mechanical probability distributions for the initial conditions only in the harmonic approximation. However, if the nuclear temperature is sufficiently high that classical statistical mechanics is valid for determining the initial conditions, then the probability distributions may be obtained to any desired order in the initial coordinates and momenta, or even exactly, from Eq. (22).

By expanding the potential energy about the saddle point and retaining anharmonic terms in the coordinates we are able to discuss classically the effect of the anharmonicity of the potential energy on the distribution $P(E,U)$. In order to discuss the distribution $P(E,U)$ to the next higher order beyond a bivariate normal distribution, we need keep only those terms in the expansion of the potential energy that will affect the coefficients of the $(E - E^0)(U - \frac{1}{2})^2$, $(E - E^0)^3$, and $(U - \frac{1}{2})^4$ terms in the exponent of the $P(E,U)$ distribution. Because the equations (14) and (15) for E and U depend only upon the mass-asymmetry coordinate m and the stretching coordinate s (disregarding, for the moment, the initial momenta p_f and p_s), it suffices to consider (in addition to the harmonic terms) only the three anharmonic terms m^2s, s^3, and m^4 in an expansion of the potential energy.[35]

[35] The two cubic terms ms^2 and m^3 are absent because $\mathcal{V}$ is an even function of m. Nonzero cubic terms of the form sd^2, for example, introduce only pre-exponential dependences on E and U after the integration over d is performed.

We therefore expand the potential energy about the saddle point with respect to the variables m and s, retaining terms as follows:

$$\mathcal{V} = \mathcal{V}^0 + \tfrac{1}{2} K_m m^2 + \tfrac{1}{2} K_s s^2 + \tfrac{1}{2} K_{mms} m^2 s + \tfrac{1}{6} K_{sss} s^3 + \tfrac{1}{24} K_{mmmm} m^4 .$$

The classical probability distribution for the coordinates m and s is therefore given to this order by

$$P(m,s) = N \exp\left[-(\tfrac{1}{2} K_m m^2 + \tfrac{1}{2} K_s s^2 + \tfrac{1}{2} K_{mms} m^2 s + \tfrac{1}{6} K_{sss} s^3 + \tfrac{1}{24} K_{mmmm} m^4)/\theta \right] , \tag{47}$$

where N is a normalization constant.

Figure 38 shows the third derivatives K_{mms} and K_{sss} (evaluated at the saddle point), as functions of fissionability parameter. In the range of x below 0.78 the third derivative K_{mms}, which couples the mass-asymmetry coordinate and the stretching coordinate, is positive. This means that the most probable value of s decreases with increasing m^2; i.e., the most probable distance between spheroid centers decreases as the mass asymmetry increases. This results in a greater translational kinetic energy at infinity than if the distance remained unchanged. Over the entire range of x (between 0 and 0.80) the stretching third derivative K_{sss} is negative. The effect of this is a contribution toward a low-energy tail on the distribution in E. A rough estimate of the mass-asymmetry fourth derivative K_{mmmm} (evaluated at the saddle point) indicates that it is negative and fairly independent of x. For $x = 0.677$ the estimate yields $K_{mmmm} \approx -15\, E_S^{(0)}$. The

effect of this term is a contribution toward a peaked mass distribution, but the effect is small, since this term accounts for only about 20% of the final value of the $(U - \frac{1}{2})^4$ term in the exponent of $P(E,U)$. (In all numerical results involving anharmonic terms that we present, the quantity K_{mmmm} is taken to be zero. On the scale of the graphs presented here, these results are indistinguishable from those calculated using the above estimate for K_{mmmm}.)

By using the set of equations (33) for m and s, and by taking into account also the classical probability distributions in the momenta p_f and p_s, we find for the desired distribution [we have collected terms according to powers of $(U - \frac{1}{2})$]

$$P(E,U) = \frac{NE^0 F(E,U)}{\alpha E^2} \exp\left[- \frac{K_s(E - E^0)^2}{2\,\theta\,\alpha^2 E^2} + \frac{K_{sss}(E - E^0)^3}{6\,\theta\,\alpha^3 E^3} \right]$$

$$\times [1 - 4(U - \tfrac{1}{2})^2] \exp\left[- G(U - \tfrac{1}{2})^2 - H^2(U - \tfrac{1}{2})^4 + \frac{32\,K_{sss}(E^0)^3(U - \frac{1}{2})^6}{3\,\theta\,\alpha^3 E^3} \right], \quad (48)$$

where G and H (functions of E) are now defined by

$$G = \frac{K_m}{2\theta} + \frac{4K_s E^0(E - E^0)}{\theta\,\alpha^2 E^2} - \frac{K_{mms}(E - E^0)}{2\,\theta\,\alpha\,E} - \frac{2K_{sss}E^0(E - E^0)^2}{\theta\,\alpha^3 E^3},$$

$$H = \left[\frac{8K_s(E^0)^2}{\theta\,\alpha^2 E^2} - \frac{2K_{mms}E^0}{\theta\,\alpha\,E} - \frac{8K_{sss}(E^0)^2(E - E^0)}{\theta\,\alpha^3 E^3} + \frac{K_{mmmm}}{24\,\theta} \right]^{1/2}.$$

The function $F(E,U)$ is given by (35), where it is understood that the classical limits are to be used for the constants C_s and C_{p_s} appearing in it.

We present in Fig. 39 a contour map of $P(E,U)$ vs E and U for the compound nucleus ${}_{85}At^{213}$ and $\theta = 1.13$ MeV, calculated using the completely classical result (48). (The nuclear temperature is sufficiently high that classical statistical mechanics is valid for determining the initial conditions.) By comparing this with Fig. 35, we can see the effect of the anharmonicity of the potential energy on the final distribution (see also Fig. 33). The lines of constant probability still tend toward rounded triangles, but not as markedly as in Fig. 35.

If we neglect the $(U - \frac{1}{2})^6$ term in the exponential of (48), the resulting expression is of the same form as (36). Thus, we are able to use the results previously derived for those quantities obtained by integrating over fractional mass: Eq. (44) for $P(E)$, Eq. (45) for $\sigma_U{}^2(E)$, and Eq. (46) for $\alpha_U{}^{(4)}(E)$. Closed expressions for the quantities that result from integrating over E are not so readily obtainable because of the presence of the cubic term in E in the exponential of $P(E,U)$.

The expression (48) for $P(E,U)$, although strictly correct only to the next higher order beyond quadratic in E and U, contains further higher-order terms representing the effects of the nonlinear equation (14) for E. If we retain in (48) only terms that are one order higher than quadratic in E and U, we obtain (we regard any pre-exponential factors as of higher order)

$$P(E,U) = \frac{N}{\alpha E^0} \exp\left[-\frac{K_m(U-\frac{1}{2})^2}{2\,\theta} - \frac{K_s(E-E^0)^2}{2\,\theta\,\alpha^2(E^0)^2} \right.$$

$$- \frac{(8K_s - \alpha K_{mms})(E-E^0)(U-\frac{1}{2})^2}{2\,\theta\,\alpha^2\,E^0} + \frac{\left(K_s + \frac{K_{sss}}{6a}\right)(E-E^0)^3}{\theta\,\alpha^2\,(E^0)^3}$$

$$\left. - \frac{\left(\frac{8K_s}{\alpha^2} - \frac{2K_{mms}}{\alpha} + \frac{K_{mmmm}}{24}\right)(U-\frac{1}{2})^4}{\theta} \right] . \qquad (49)$$

This result represents a consistent order of approximation in both the initial conditions and the equations for E and U.

The most probable total translational kinetic energy, as a function of fractional mass, is found from (49) to be

$$E_{MP}(U) = E^0 \left[1 - 4\left(1 - \frac{\alpha\,K_{mms}}{8K_s}\right)(U-\tfrac{1}{2})^2 + \cdots \right] . \qquad (50)$$

It is instructive to compare this classical result with the result (41) obtained by use of the harmonic approximation for the initial conditions. For x in the neighborhood of 0.67, $\alpha\,K_{mms}/(8K_s) \approx 1/5$; thus, the most probable total translational kinetic energy decreases with increasing $(U-\frac{1}{2})^2$ only about four-fifths as rapidly in (50) as in (41). The physical reason for this difference is that in (41) the decrease in total translational kinetic energy with increasing mass asymmetry results solely from the decrease in the product of the charges of the two fragments, whereas in (50) account is also taken of the decrease in distance between

spheroid centers (which tends to increase the kinetic energy) as the mass asymmetry increases.

In addition to determining the rate of decrease of $E_{MP}(U)$ with $(U-\frac{1}{2})^2$, the coefficient of the $(E-E^0)(U-\frac{1}{2})^2$ term also gives the derivative of the variance of the fractional mass at $E=E^0$. From (49) we find that

$$\sigma_U^2(E^0) = \Theta/K_m$$

and that

$$\frac{d\,\sigma_U^2(E^0)}{dE} = -\frac{\Theta(8K_s - aK_{mms})}{K_m^{\,2}\,a^2\,E^0}\,.$$

Since $8K_s > aK_{mms}$, the derivative is negative.

For values of x of interest in fission, the magnitude of the negative quantity $K_{sss}/(6a)$ is roughly one-half K_s; thus, the coefficient of the $(E-E^0)^3$ term in (49) is positive, indicating that the deviation of $P(E, 1/2)$ (the distribution in E for a symmetric mass division) from a pure Gaussian is toward a high-energy tail (positive skewness). The origin of the K_s term, which contributes toward the high-energy tail, is the nonlinear relationship (14) between E and s. The opposing contribution from the $K_{sss}/(6a)$ term toward a low-energy tail arises physically because the potential energy increases more rapidly as the fragments approach one another than as they separate.

An examination of the coefficient (including the over-all minus sign) of the $(U-\frac{1}{2})^4$ term in (49) indicates that it is negative. Thus, the prediction is that $P(E^0, U)$ (the distribution in mass for $E = E^0$) is less peaked and more rectangular than a Gaussian distribution (negative kurtosis).

In this section our concern has been the mathematical derivation and compilation of the formulae relevant to a discussion of the distributions in fragment total translational kinetic energy, mass, individual excitation energies, and individual angular momenta. By using these formulae and the graphs presented earlier for the constants appearing in them, curves expressing the theoretical predictions may be prepared for direct comparison with experiment. This will be done in the next section for distributions in total translational kinetic energy and mass.

VI. COMPARISON OF THEORY WITH EXPERIMENT

In the previous section we derived probability distributions for certain observable characteristics of fission fragments at infinity: their total translational kinetic energy, fractional mass, individual excitation energies, and individual angular momenta. From our earlier discussion regarding the applicability of the two-spheroid model (Section II.B), we know that these distributions are expected to describe only the fission of nuclei that have values of the fissionability parameter $x \lesssim 0.67$.

Experimentally, there is observed a marked transition in the properties of fission at about radium ($x = 0.684$)—mass divisions are predominantly symmetric for elements lighter than radium and predominantly asymmetric for elements heavier than radium. It is not clear whether this experimentally observed transition is associated with the transition in saddle-point properties at $x \approx 0.67$; no explanation of asymmetric fission for the heavier elements is foreseen within the framework of the two-spheroid model. We will nevertheless use the experimentally observed transition between symmetric and asymmetric mass divisions as the dividing point for determining what data the theory should be compared with.[36] We will therefore compare the theoretical predictions of the model with existing experimental data for the fission of nuclei lighter than radium.

---

[36] A recent experimental determination of the fission barrier of ${}_{81}Tl^{201}$ indicates that $(Z^2/A)_{crit}$ has a value(64) of 48.4 ± 0.5 [rather than Green's value(40) of 50.13 that is used here]. When this value of $(Z^2/A)_{crit}$ is used, the value of the fissionability parameter x for each compound nucleus is increased somewhat. For the comparisons between theory and experiment that are made here, the largest value of fissionability parameter that occurs is 0.677 when Green's value of $(Z^2/A)_{crit}$ is used, and 0.701 when the newly reported value is used.

Fission-fragment mass distributions, obtained by use of radiochemical techniques, are available for the fission of several of the lighter elements (65-70). Single-fragment translational kinetic-energy distributions have been determined for the fission of a number of light nuclei (71,72). In addition, two-dimensional distributions in mass and total translational kinetic energy, obtained by use of semiconductor detectors and two-dimensional analyzers,[37] have recently been reported for various nuclei lighter than radium (71, 73-78). On the other hand, for the fission of the lighter elements, there exists at the present time no experimental information regarding the distributions in individual excitation energies and individual angular momenta. The immediate test of the theory will therefore be the comparison of predictions with experiment for distributions in total translational kinetic energy and mass [P(E,U) and quantities derived from it].

The more detailed comparisons will be made with the data of Burnett (76) and with the data of Plasil (77). Burnett bombarded $_{83}Bi^{209}$ and $_{79}Au^{197}$ with alpha particles of energies 65.0 MeV and 70.0 MeV, respectively, to form the compound nuclei $_{85}At^{213}$ and $_{81}Tl^{201}$. The corresponding values of the fissionability parameter x are 0.677 and 0.651, respectively. Plasil studied the heavy-ion-induced fission of

[37] These experiments consist of measuring in coincidence the translational kinetic energies E_1 and E_2 of the two fission fragments at infinity and recording the corresponding number of events. From this experimentally constructed distribution $P(E_1, E_2)$, the experimental distribution $P(E,U)$ is obtained by use of the transformation (18).

the compound nuclei ${}_{76}Os^{186}$ (x = 0.619) and ${}_{82}Pb^{198}$ (x = 0.677) at several bombarding energies ranging from 102 MeV to 165 MeV. The former was produced in two ways from the reactions ${}_{68}Er^{170} + {}_{8}O^{16}$ and ${}_{70}Yb^{174} + {}_{6}C^{12}$, and the latter from the reaction ${}_{74}W^{182} + {}_{8}O^{16}$.

We will also refer frequently to the data of Britt, Wegner, and Gursky (75), and the date of Unik and Huizenga (78). The former have studied the 25.5-MeV ${}_{2}He^{3}$-induced fission of ${}_{79}Au^{197}$, ${}_{81}Tl^{nat}$, ${}_{82}Pb^{206}$, and ${}_{83}Bi^{209}$; for the ${}_{83}Bi^{209}$ case a bombarding energy of 22.1 MeV was also used. The latter authors have studied the 42-MeV helium-ion-induced fission of ${}_{83}Bi^{209}$. Comparisons will also be made with other data.

[A comparison of some of these experimental data with the predictions of the two-spheroid model is also made by Burnett, Plasil, and Thompson (79), whose experiments were carried out at the Lawrence Radiation Laboratory, Berkeley, simultaneously with the development of the theory.]

The theoretical distributions depend upon the nuclear temperature Θ at the saddle point, which is a function of the internal excitation energy E_{ex}^{SP} at the saddle point. The determination of Θ in terms of E_{ex}^{SP} is subject to an appreciable error. For the comparisons between theory and experiment made in this work, we use the semiempirical nuclear equation of state (80)

$$E_{ex}^{SP} = (A/8)\,\Theta^2 - \Theta\,,$$

where both θ and E_{ex}^{SP} are in MeV, and A is the number of nucleons in the compound nucleus. The excitation energy at the saddle point is in turn given by the total bombarding energy in the center-of-mass system, plus the binding energy of the projectile to the target, minus the fission-barrier energy. The fission-barrier energy is equal to the liquid-drop fission-barrier energy (15,17),[38] minus the shell correction to the ground-state mass (81, 82), plus the shell correction to the saddle-point mass. The saddle-point shell correction is not known, but probably does not exceed a couple of MeV—it was neglected here. These considerations are for a compound nucleus that is not rotating. The determination of the fission-barrier energy and the nuclear temperature for a rotating nucleus is discussed by Plasil (77); his procedure is briefly touched upon below.

Two complications present in the heavy-ion-induced fission reactions should be mentioned. First of all, because of the high excitation energies involved, it is possible that the compound nucleus will fission following partial de-excitation by the emission of one or more neutrons. If this occurs, there will be a spread in the saddle-point excitation energy (and hence the nuclear temperature θ) at the time of fission. Secondly, heavy ions are capable of creating compound

---

[38] A plot of the liquid-drop fission-barrier energy vs. x is given in Figs. 4 and 8. For the determination of θ, the true liquid-drop fission-barrier energy is used rather than the two-spheroid approximation to the barrier.

nuclei possessing large amounts of angular momentum. Because the ions strike the target with varying impact parameters, the angular momentum ranges from zero to some maximum value. Since the fission threshold is a sensitive function of angular momentum (77, 83), it will have a range of values, resulting in a spread in the saddle-point excitation energy (and hence Θ). The effect of both these complications on nuclear temperature was taken into account by Plasil (77). He obtained an average value of Θ by calculating the competition between fission and neutron emission throughout the de-excitation chain,[39] and by integrating over the distribution of angular momentum.

Although the effect of angular momentum on the nuclear temperature can be taken into account as described above, it should be recalled that the entire theory developed here is restricted to the case of a nonrotating compound nucleus. This must be borne in mind when comparing the theoretical predictions with the data for the heavy-ion-induced reactions. All conclusions drawn on the basis of such comparisons are thus subject to the provision that angular momentum has little effect on the fission process, except in affecting somewhat the average nuclear temperature at the saddle point.

The theoretical distributions are calculated for fragments observed (at infinity) before they have emitted any neutrons, whereas

[39] For the cases studied it was found that the average number of neutrons emitted before fission seldom exceeds one; this means that the uncertainty in the nuclear temperature arising from this effect is small.

the experimental kinetic-energy measurements are made after the emission of neutrons from the fragments. Fragment neutron emission decreases the average translational kinetic energy and introduces a dispersion in the distributions, thereby increasing the variances. When comparing theory and experiment, it is desirable to correct the experimental results for such neutron-emission effects. The problem of neutron-emission corrections has been discussed by Terrell (84), by Haines (85), and by Burnett (76). By making certain standard assumptions regarding the neutron emission, it is possible to derive formulae for correcting the mean total translational kinetic energy $\overline{E}(U)$, the variance $\sigma_E^2(U)$ of the total translational kinetic-energy distribution, and the variance $\sigma_U^2(E)$ of the mass distribution.

Using Burnett's neutron-correction formulae, Burnett and Plasil have corrected all statistical moments obtained from their data. (The formulae of Burnett differ slightly from those of Haines because certain higher-order terms are retained by Burnett.) With the exception of the mean total translational kinetic energies, the data of Britt, Wegner, and Gursky (75) have not been corrected for the effects of fragment neutron emission. The data of Unik and Huizenga (78) have been corrected for neutron-emission effects as regards the mean total translational kinetic energy and the full width at half maximum of the over-all total translational kinetic-energy distribution, but not otherwise.

Although neutron-emission corrections can be made for the statistical moments of the distributions, it is not possible to easily correct the distributions themselves. Thus, when comparing theoretical and experimental distributions, it must be borne in mind that the former refers to pre-neutron-emission and the latter to post-neutron-emission.

To distinguish these two cases we denote by a superscript asterisk a quantity measured after neutron emission has occurred; e.g., E^* is the total translational kinetic energy measured following neutron emission.

While making comparisons of the theoretical and experimental distributions it should be kept in mind that no arbitrary parameters have been adjusted—that the theoretical and experimental distributions have not been normalized to one another in any way. Also, it should be remembered that the theory is strictly valid only in the neighborhood of the most probable events; we will, however, extrapolate the theoretical curves to cover the entire region for which there are experimental data. [With the exception of Figs. 40 and 46, the figures that we will examine have been reproduced (with additions, and changes in notation and format) from Refs. 76 and 77.]

Figure 40 shows the experimental contour map of $P(E^*, U)$ vs E^* and U for the compound nucleus ${}_{85}At^{213}$, for which the nuclear temperature at the saddle point is $\Theta = 1.13$ MeV (86). Apart from the effects of neutron emission, as discussed above, this experimental contour map may be compared directly with the theoretical maps calculated for this experimental situation in each of the three successively

improved orders of approximation discussed in Section V—see Figs. 33, 35, and 39. (The same relative scales for E and U are used for all four graphs. However, the experimental contour lines are labelled differently from the theoretical ones.) Since the nuclear temperature is sufficiently high that classical statistical mechanics is valid for determining the initial conditions, the completely classical map calculated by including the effects of anharmonic terms on the initial conditions (Fig. 39) represents the best theoretical estimate available, and we will confine our discussion to a comparison with it.

The experimental and theoretical most probable values of total translational kinetic energy are seen to agree remarkably well. In addition the theory predicts that the most probable value of U should be one-half, and this is verified experimentally—the fission events are predominantly symmetric in mass rather than asymmetric. Furthermore, the widths of the distributions in E and U are seen to agree well. Finally, we compare the shapes of the distributions with the theoretical predictions of approximately bivariate normal distributions

modified by certain characteristic higher-order terms. The over-all agreement between the shapes of the experimental and theoretical contour lines is good. In the region of maximum probability the experimental contour lines are approximately ellipses, whereas in the region of smaller probability they tend to become rounded triangles, as predicted by the theory: The experimental mass distribution, as predicted, is broader for low values of the total translational kinetic energy than for high values. Other details of the agreement between the theoretical and experimental maps will be compared later in the form of statistical moments.

In Ref. 77 comparison is made by Plasil between theoretical and experimental contour maps of P(E, U) for fission following two heavy-ion-induced reactions. The agreement presented there is not as good as for the $_{85}At^{213}$ case we have discussed. However, the theoretical maps there are calculated using the intermediate approximation for P(E, U) in which the initial conditions are determined in the harmonic approximation. The agreement is significantly improved when the effects of anharmonicity on the initial conditions are taken into account. Also, the compound nuclei undergoing fission possessed considerable angular momentum, and the more highly excited fragments would have emitted more neutrons, which could possibly affect the experimental distributions.

Figure 41 shows the theoretical and experimental distributions in mass, P(U), and the theoretical and experimental distributions in total translational kinetic energy, P(E), for the compound nucleus $_{82}Pb^{198}$, each at two different nuclear temperatures. The theoretical curves are calculated in the intermediate approximation for P(E, U) in which the initial conditions are determined in the harmonic approximation.[40] As before, we first compare the most probable values of

[40] Although the approximate formulae derived in Section V for P(U), P(E), and the various statistical moments are sufficiently accurate for calculating the theoretical curves of this section, the curves have actually been calculated by numerical integrations over the full expression (36) [or the full expression (48)] for P(E, U), with F(E, U) retained.

the total translational kinetic energy, which are seen to agree favorably. Next, the widths of the experimental distributions in both kinetic energy and mass are seen to be reproduced well by the theory. In addition, as the nuclear temperature increases, the theory is seen to correctly predict an increase in width of each distribution. Finally, we note that the over-all shapes of the experimental and theoretical distributions in both E and U are in approximate agreement (each distribution is approximately Gaussian). Because of experimental uncertainties, including the uncertainty of the effects on the distributions of neutron emission from the fragments, we will not compare numerical results for skewness in P(E) and kurtosis in P(U).

We turn now to a comparison of the mean values of the total translational kinetic energy as functions of fragment mass. Shown in Fig. 42 is $\overline{E}(U)$ vs fragment mass AU for the compound nuclei ${}_{85}At^{213}$, ${}_{81}Tl^{201}$, and ${}_{82}Pb^{198}$, the latter for two temperatures. In this figure, as well as in the two succeeding ones, we indicate by a solid line the result obtained by use of the intermediate approximation (36) for P(E, U), in which the initial conditions are determined in the harmonic approximation. The dashed line represents the result calculated from the expression (48) for P(E, U), in which anharmonic terms are considered in determining the initial conditions. Since the nuclear temperature is sufficiently high that classical statistical mechanics is valid for determining the initial conditions, the dashed line in each case represents the better theoretical estimate, and we will confine our discussion to a comparison of the experimental results with it.

We note first of all in Fig. 42 that for three of the four cases the agreement between theory and experiment as regards the mean total translational kinetic energy at symmetry is excellent. For the remaining case (${}_{82}Pb^{198}$ at $\Theta = 2.07$ MeV) the experimental value is slightly higher than the theoretical one. For the ${}_{85}At^{213}$ and ${}_{81}Tl^{201}$ cases the experimental decrease in $\overline{E}(U)$ with increasing mass asymmetry is essentially as predicted by the theory, although the experimental points lie somewhat above the theoretical curves. However,

for the two $_{82}Pb^{198}$ cases (formed by heavy-ion bombardments), the experimental points do not drop off with increasing asymmetry nearly as fast as the theoretical curves. Indeed, for the case in which $\Theta = 2.07$ MeV, the experimental values are essentially independent of asymmetry.

The data of Britt, Wegner, and Gursky indicate that $\bar{E}(U)$ decreases with increasing mass asymmetry, although they find in some cases (in particular, $_{83}Bi^{209}$ + 25.5-MeV $_{2}He^{3}$) a tendency for $\bar{E}(U)$ to actually increase at large asymmetry(75). (Note that these authors plot their data as functions of fragment mass ratio rather than fragment mass or fractional mass.) The experimental $\bar{E}(U)$ curve of Unik and Huizenga also decreases with increasing mass asymmetry.(78).

As Haines has pointed out, the discrepancy between the calculated and experimental $\bar{E}(U)$ curves would be reduced somewhat if account were taken of the change in the mean charge density of fission fragments with a change in mass asymmetry(85). On the average, the lighter fragment acquires a slightly larger number of protons than its proportionate share, and the heavier fragment acquires a slightly smaller number. The product of the charges of the two fragments, and hence their translational kinetic energy at infinity, is thus increased somewhat over the corresponding value calculated here (in which both fragments have the same charge density). This effect is of the same order of magnitude as the effect of the anharmonicity of the potential energy, and in the case of $_{85}At^{213}$ and $_{81}Tl^{201}$ taking this effect into account would come close to removing the difference between the calculated and experimental $\bar{E}(U)$ curves. On the other hand, the large discrepancy between the calculated and experimental curves for the $_{82}Pb^{198}$ cases would still exist even if the effect arising from the difference in fragment charge densities were taken in account.

The suggestion has been made by Plasil that the angular momentum present in the $_{82}Pb^{198}$ cases is possibly responsible for the marked deviation of the experimental $\bar{E}(U)$ curves from the theoretical ones(77). This suggestion is consistent with the fact that for the two cases in which very little angular momentum is present ($_{85}At^{213}$

and $_{81}Tl^{201}$, formed by alpha-particle bombardments) the theory and experiment are in substantial agreement, and for the $_{82}Pb^{198}$ case in which there is less angular momentum present ($\Theta = 1.37$ MeV) the agreement is better than for the case of greater angular momentum present ($\Theta = 2.07$ MeV). To see if this actually is the explanation, the theory should be worked out taking into account angular momentum; this presents an interesting problem for the future.

In Fig. 43 we compare the theoretical and experimental variances of the total translational kinetic energy distributions as functions of fragment mass [$\sigma_E^2(U)$ vs AU] for the same experimental situations as in Fig. 42. The agreement near symmetry is excellent for the $_{85}At^{213}$ and $_{81}Tl^{201}$ cases. For $_{82}Pb^{198}$ (heavy-ion reactions) the agreement near symmetry is good for the $\Theta = 1.37$-MeV case, but for the $\Theta = 2.07$-MeV case the experimental points are somewhat higher than the theoretical values. In all cases the theoretical curves decrease with increasing mass asymmetry. This prediction is not borne out experimentally in the $_{85}At^{213}$ and $_{81}Tl^{201}$ cases—these experimental variances increase with increasing mass asymmetry. The trends of the two $_{82}Pb^{198}$ variances with mass asymmetry are rather uncertain.

Britt, Wegner, and Gursky have found in three of the four cases reported that the variance $\sigma_E^2(U)$ is essentially independent of fragment mass(75). In the fourth case ($_{83}Bi^{209}$ + 25.5-MeV $_2He^3$) $\sigma_E^2(U)$ was observed to remain essentially constant near symmetric mass divisions and to increase for more asymmetric divisions. The data of Unik and Huizenga also indicate that $\sigma_E^2(U)$ is essentially independent of fragment mass (78).

The comparisons made for $\sigma_E^2(U)$ indicate a fairly significant disagreement between theory and experiment. The theoretical curves would be scarcely changed if one were to take into account further anharmonic terms in the potential energy—any pure liquid-drop result that predicts that the mean total translational kinetic energy should decrease with increasing mass asymmetry (see Fig. 42) will also predict that the variance of the total translational kinetic energy should decrease

with increasing mass asymmetry. It thus appears that the experimental constancy or increase in $\sigma_E^2(U)$ with increasing mass asymmetry is caused by some effect other than those present in a pure liquid-drop model.

Burnett has suggested that the discrepancy between theory and experiment as regards $\sigma_E^2(U)$ may possibly arise from the effects of single-particle shell structure(76). If the doubly-closed shell at fragment mass 132 tended to make the heavier fragment nearly spherical a portion of the time, then the separation of the fragment centers would decrease a portion of the time, resulting in an increase in translational kinetic energy. Since only some fraction of the total fission events would be affected by the doubly-closed shell, there would also still be normal fissions with lower translational kinetic energy. This mixture of fission events—some predominantly low in kinetic energy and some predominantly high—would cause the variance to be greater than it otherwise would be. The suggestion that shell effects are responsible is consistent with two pieces of experimental evidence: First of all, as was pointed out by Burnett, the increase in $\sigma_E^2(U)$ begins for both ${}_{85}At^{213}$ and ${}_{81}Tl^{201}$ at fragment masses 120-125 rather than at a constant mass ratio. Secondly, the increase in $\sigma_E^2(U)$ with mass asymmetry becomes less pronounced as the nuclear temperature increases; indeed, for ${}_{82}Pb^{198}$ at $\Theta = 2.07$ MeV, $\sigma_E^2(U)$ is essentially independent of mass asymmetry. This disappearance of the marked disagreement between theory and experiment as the temperature increases would correlate with the disappearance of single-particle shell structure at high excitations.[41] Work on the cause of the discrepancy represents another interesting problem.

Variances of the mass distributions as functions of total translational kinetic energy [$\sigma_U^2(E)$ vs E] are shown in Fig. 44. The magnitudes of the theoretical and experimental variances of the mass

---

[41] The large amount of angular momentum present in the two ${}_{82}Pb^{198}$ cases could, of course, be responsible for the near-constancy of $\sigma_E^2(U)$ as a function of U (rather than a disappearance of shell structure).

distributions at the most probable total translational kinetic energy are in excellent agreement for the $_{85}At^{213}$ and $_{81}Tl^{201}$ cases, and in good agreement for the two $_{82}Pb^{198}$ cases. Furthermore, for the two former cases the theoretical curves correctly predict the over-all shape of the curves, including a flattening at high E and a very rapid rise at low E. At both high and low E, however, the experimental points deviate somewhat from the theoretical curves. The experimental curves for the two $_{82}Pb^{198}$ cases do not possess the characteristic "hyperbolic" shape predicted by the theory, and observed in the former cases. Indeed, for the $\Theta = 2.07$-MeV case the experimental curve is essentially linear. It is again possible that the discrepancies between theory and experiment for the two $_{82}Pb^{198}$ cases arise from the effects of angular momentum or fragment neutron emission; these possibilities should be investigated.

We have thus far been mainly concerned with comparing details of the distributions in mass and total translational kinetic energy for a given nucleus and excitation energy (or rather four such combinations). The theory we have developed also predicts the dependence of the distributions on nuclear temperature, and their dependence on fissionability parameter.

We turn now to a comparison of theory and experiment as regards the temperature dependence of the distributions. The mean total translational kinetic energy is prediced by the theory to be (for all practical purposes) independent of nuclear temperature. Plasil finds that for five different nuclear temperatures, ranging from $\Theta = 1.37$ MeV to $\Theta = 2.07$ MeV, the mean total translational kinetic energy $\bar{E}$ for the $_{82}Pb^{198}$ case varied by 3 MeV (with experimental errors on the values of $\bar{E}$ set at ± 5 MeV)(77). For $_{76}Os^{186}$ (formed in two ways) he found that for six different nuclear temperatures covering the range $1.49\ \text{MeV} \leq \Theta \leq 2.06$ MeV the values of $\bar{E}$ varied by 5 MeV (errors on $\bar{E}$ of ± 6 MeV). These data are thus in substantial agreement with the theory.

The variances of the distributions in E and in U are predicted to increase with increasing nuclear temperature. The comparison of theory and experiment as regards this point is made for the

$_{82}Pb^{198}$ and $_{76}Os^{186}$ cases in Fig. 45.[42] We again note the significant agreement between the magnitudes of the theoretical and experimental variances in both mass and total translational kinetic energy. Furthermore, theory and experiment are in substanital agreement as regards the dependence of the variances upon nuclear temperature.[43] This is especially true for the $_{82}Pb^{198}$ case; for $_{76}Os^{186}$ the experimental slopes for both σ_U^2 and σ_E^2 are somewhat smaller than the theoretical slopes.

The theoretical dependence of the most probable total translational kinetic energy on fissionability parameter is compared in Fig. 46 with the data of Viola and Sikkeland.[72] (This figure is reproduced from Ref. 3.) As in Fig. 18 the solid curve represents the result for nonviscous fragments with hydrodynamic flow of the type we have been considering (a superposition of an irrotational flow and a flow corresponding to a uniform rotation). The dot-dashed curve represents the result for infinitely viscous fragments (which would separate to infinity without oscillating), and the short-dashed line represents a simple approximation (see Section III. C) to the former curve. In addition to the data for nuclei with fissionability parameter $x \lesssim 0.67$, we have also included the data for heavier elements, with fissionability parameters up to $x = 0.807$. The experimental most probable kinetic energies for nuclei with $x \lesssim 0.67$ are seen to be reproduced well both

---

[42] For the benefit of those making a comparison between this figure and Fig. 6 of Ref. 3, the preliminary data presented there were overcorrected for the effects of neutron emission from the fragments; the agreement is better than indicated there.

[43] It should be recalled that the variance σ_U^2 retains its linear dependence upon Θ at low temperatures in the two-spheroid model because the mass-asymmetry frequency is zero (as a consequence of the zero neck radius of the saddle-point shape). In the actual situation, of course, the neck radius of the saddle-point shape and the mass-asymmetry frequency are not zero, but are small. The variance σ_U^2 of the mass distribution should therefore approach in the real case a small finite value, rather than zero, as the temperature goes to zero.

in magnitude and in their dependence on x by the solid line (nonviscous fragments). For $x \gtrsim 0.67$ the experimental points are higher than the theoretical estimate represented by the solid line. Recall that for $x \gtrsim 0.67$ the two-spheroid model is inadequate, among other respects, in that its saddle-point configuration is more elongated than the true liquid-drop saddle-point shape. Thus, the translational kinetic energies predicted by the model for $x \gtrsim 0.67$ are expected to be too low.

The comparison between theory and experiment as regards the variation of widths with fissionability parameter has not yet been made. There are insufficient data on either the widths of the mass distributions or the widths of the total translational kinetic-energy distributions to establish their dependence on x. However, the single-fragment translational kinetic-energy distributions of Viola and Sikkeland(72) cover a wide range of x. In the region $0.569 \leq x \leq 0.650$ they have reported the full widths at half maximum of single-fragment kinetic-energy distributions for nine nuclei. Since the reactions studied were formed by heavy-ion bombardments, considerable analysis [similar to that performed by Plasil(77)] is required to determine the average nuclear temperature at the saddle point. If the nuclear temperature for each of these reactions were determined, the experimental widths could then be compared directly with those predicted by the theory.

The remaining comparisons between theory and experiment will be made in a series of three tables. We compare in Table I for several compound nuclei and nuclear temperatures the over-all mean total translational kinetic energy $\overline{E}$, the over-all variance σ_E^2 of the total translational kinetic-energy distribution, and the over-all variance σ_U^2 of the mass distribution. Table II is a similar comparison, but in terms of full widths at half maximum of the distributions rather than variances. (For a Gaussian distribution, the full width at half maximum is equal to the square root of the variance multiplied by 2.3548.) In Table III we compare with theory the full widths at half maximum of mass distributions obtained by use of radiochemical techniques. From the comparisons made in these three tables we see that there are no unexpectedly large disagreements between theory and experiment.

To summarize this section, we have compared the predictions of our model with existing experimental data for the fission of nuclei lighter than radium—distributions in mass and total translational kinetic energy. From these comparisons we have learned that the two-spheroid model is capable of accounting for a large number of the observed properties of the distributions, but that some discrepancies remain. The significance of the comparisons will be discussed in Section VII.

VII. SUMMARY AND CONCLUSION

We have studied in connection with nuclear fission the division of an idealized charged drop, using a simplified version of the liquid-drop model. The coordinates for our model were selected so as to take into account the appropriate degrees of freedom essential to a discussion of the division of a charged drop and the separation of the fragments to infinity. To the Hamiltonian of our idealized system we have applied standard static, dynamical, and statistical methods in order to trace out the essential features of the process.

This has included, first of all, the calculation of the potential energy of the system (a sum of surface and Coulomb energies), and the location and study of the properties of the saddle point. From such a study we learned that our model is expected to be useful for discussing certain aspects of the fission of nuclei with fissionability parameter $x \lesssim 0.67$ (nuclei lighter than about radium), but not, in general, for discussing the fission of heavier elements.

The dynamical study was concerned with calculating the kinetic energy of the system, with setting up the equations of motion, and with solving them in terms of given initial conditions. This made it possible to trace out the division of the nucleus and the separation of the fragments from some given initial configuration to infinity. For the major portion of the study we worked out the theory for completely nonviscous fragments with hydrodynamic flow consisting of a superposition of an irrotational flow and a flow corresponding to a uniform rotation. For certain aspects of the theory we also considered the case of infinitely viscous fragments.

In the application of statistical mechanics we focused attention on the system at the saddle point, making the standard transition-state-method assumption of statistical equilibrium at the saddle point. This made it possible to calculate the probability of observing the system in a given state of motion close to the saddle point.

The results of the dynamical and statistical studies were then appropriately combined to give the probability of observing the two fragments in a given state of motion at infinity. This probability corresponds directly to the probability of certain observable characteristics of fission fragments: their total translational kinetic energy, fractional mass, individual excitation energies, and individual angular momenta.

As stated in the introduction, our purpose has been to study in detail the properties of the division of an idealized liquid drop whose size, surface tension, and charge are those of a nucleus; and to compare the results with what is observed experimentally in the fission of real nuclei. From this point of view there are no adjustable parameters in the problem.

Comparisons of calculations with experiment have been made for several nuclei lighter than radium as regards distributions in mass and total translational kinetic energy. These preliminary comparisons suggest the following conclusions. First and most important, the magnitudes of the experimental most probable kinetic energies and masses are reproduced by the calculations—the experimental and theoretical most probable (or mean) kinetic energies agree to within a few percent, and predominantly symmetric rather than asymmetric mass divisions are observed, as predicted. Secondly, the magnitudes of the experimental widths of the distributions in both kinetic energy and mass are essentially as calculated, usually to within several percent.

As far as the finer details of the distributions are concerned, the calculations are capable of reproducing the correct trend in two out of the three details that we have compared. With some exceptions there is essential agreement as regards the decrease in average total translational

kinetic energy with increasing mass asymmetry, and as regards the rapid broadening of the mass distribution at low values of the total translational kinetic energy. The experimental constancy or increase of the widths of the kinetic-energy distributions with increasing mass asymmetry is not reproduced by the theory, which predicts a slight decrease.

The dependence of the experimental distributions on the nuclear temperature of the system is in basic agreement with the theory. The theory predicts, and experiment seems to confirm, that the most probable kinetic energies should be essentially independent of temperature. The variances (squares of widths) of the distributions in both mass and total translational kinetic energy are predicted to increase in a characteristic way with increasing nuclear temperature. Experimentally, the variances of both the kinetic-energy distributions and the mass distributions were observed to increase with temperature, some with slopes in approximate agreement with theory. There were no experimental points in the interesting region of very low temperature, where the variances of the kinetic-energy distributions are predicted to become independent of temperature.

The experimental trend of the most probable kinetic energies with fissionability parameter x was approximately reproduced by the theory for nuclei with $x \lesssim 0.67$. No comparisons of theory and experiment have been made as regards the variation of the widths of the distributions with fissionability parameter.

On the whole, the preliminary comparison of theory with experiment suggests that the limitations of the liquid-drop model—in its simplified two-spheroid approximation—are not yet in evidence to a serious degree for the fission of the lighter nuclei. The model has stood the test of comparison with a number of properties of the distributions in mass and total translational kinetic energy, without the introduction of adjustable parameters. The model seems capable of accounting not only for the over-all orders of magnitudes of the most probable values and the widths of the distributions in kinetic energy and mass, but also more detailed properties of the distributions. It appears from preliminary comparisons that for the fission of elements lighter than about radium, single-particle effects are of little

importance in affecting the over-all characteristics of the distributions in kinetic energy and mass.

The conclusions drawn must not be regarded as final, however, since only a fraction of the full predictive power of the two-spheroid model has been subjected to experimental verification. Even as regards distributions in kinetic energy and mass, there are several remaining areas of exploration. The experiments that have been performed have provided us with information regarding the mean values and variances of the distributions, including the dependence of the mean value and variance of one distribution on the other variable, and vice versa. Future experiments of this type should aim at determining not only these quantities but, in addition, the further deviations of the distributions from normal distributions—the skewness of the kinetic-energy distribution, and the kurtosis of the mass distribution, for example. In addition, experimental points at higher and at lower nuclear temperatures are necessary to establish definitely the dependence of the variances of the distributions on nuclear temperature, in particular, whether or not the variance of the kinetic-energy distribution "flattens" to a constant value at low temperatures.

The extension of the measurements of mass and kinetic-energy distributions over a range of fissionability parameter is necessary to establish the trend of the widths with x, and to better confirm the trend of the most probable kinetic energies with x. It would be particularly desirable to perform experiments in the neighborhood of the Businaro-Gallone bifurcation point at $x = x_{BG} \approx 0.39_4$, which would include elements in the neighborhood of silver(15,43). At $x = x_{BG}$ there should be a transition in the qualitative features of the two-dimensional distributions in total translational kinetic energy and mass. For $x > x_{BG}$ the lines of constant probability should be ellipses (to lowest order), whereas for $x < x_{BG}$ they should consist of two families of hyperbolas. The distribution in mass should become extremely broad for $x \approx x_{BG}$, and for $x < x_{BG}$ the division process should become one of fragmentation, as distinguished from fission(43), with the probability for obtaining a given mass increasing with increasing mass asymmetry.

A major area of experimental exploration that is untouched for nuclei lighter than radium is the study of the distributions in individual fragment excitation energies. The most direct way of experimentally determining these distributions is to measure the distributions of the number of neutrons emitted from each fragment (87-89).[44] A less direct method of obtaining such information is the measurement of the distributions of kinetic energies of the neutrons emitted from each fragment (88-90); this method would involve the use of the relationship between fragment excitation energy and the resulting kinetic-energy distribution of the evaporated neutrons (80, 91-94).

Experimental information on distributions of individual fragment excitation energies would serve a twofold purpose. First of all, the information is needed for comparison with the theoretical predictions of the model. An important experiment would be the determination of the correlation coefficient of fragment excitation energies, which could be compared directly with the prediction that fragment excitation energies should be rather strongly anticorrelated. Secondly, such information could be used to accurately correct experimental distributions in mass and total translational kinetic energy for fragment neutron-emission effects. This would make the conclusions drawn from comparisons of these experimental distributions with theory more reliable.

The determination of the distributions of individual fragment angular momenta for the lighter elements represents another new area of experimental exploration. Experimental information regarding these distributions is potentially obtainable from at least three different types of experiments. One is a measurement of the distributions

---

[44] Note that a measurement of the distribution of the total number of neutrons emitted (from both fragments) would determine only the distribution in total excitation energy, which would be equivalent (to lowest order) to the distribution in total translational kinetic energy.

of the total prompt gamma-ray energy emitted by each fragment.[45] The distribution of individual fragment angular momenta could then be estimated from a knowledge of the effect of angular momentum on the competition between neutron emission and gamma-ray emission in the fragment de-excitation process(100-102).[46] The second method involves the measurement of the angular distributions of prompt gamma rays emitted from the fragments(47).[47] The third method, which would yield information only for specific fragment masses, is the study of shielded isomer ratios in the fission products(103,104).[48]

---

[45] For the heavier elements the average total gamma-ray energy per fission (for both fragments) has been found experimentally to be about 8 MeV(95-99). Fragment de-excitation calculations made for nonrotating fragments indicate that roughly one-half this amount of gamma-ray energy is expected(88-90,99). It has been suggested that this discrepancy is due to the presence of a total fragment rotational energy of several MeV.

[46] Recall (Section V.A. 2) that for the compound nucleus $_{85}At^{213}$ and a nuclear temperature at the saddle point of 1.13 MeV, the most probable value of the angular momentum of each fragment at infinity is estimated as about 10ħ if the fragments are nonviscous and about 15ħ if the fragments are infinitely viscous. If one uses for the moment of inertia of the fragments at infinity the rigid-body moment of interia of a sphere, for example, this corresponds to total rotational energies for both fragments of about 3 MeV for the nonviscous case and about 7 MeV for the viscous case.

[47] For the thermal-neutron-induced fission of heavier elements, this method (47) indicates that the average angular momentum per fragment is about 7 ħ.

[48] The angular momentum per fragment in the low- and medium-energy fission of heavy elements deduced by this method (104) is about 6 to 10 ħ.

The experimental determination of the distributions of individual fragment angular momenta could possibly be of value in helping decide the important question of the degree of nuclear viscosity.

The large number of predicted quantities for which there is little or no experimental information available calls perhaps for a re-examination of the directions in which basic experimental fission research should proceed. For the past quarter of a century experimentalists have concentrated on the more easily accessible region of the heavy elements, and have accumulated a prodigious amount of data. Until a more adequate theory of the fission of the heavy elements is worked out that is capable of explaining more of these data, it appears that a larger fraction of the future experiments might profitably be diverted to the region of the lighter elements.

Further progress in our understanding of fission involves, of course, not only further work on the experimental side but also on the theoretical. Ultimately, any theory of fission will have to take into account single-particle effects, but, even apart from that, there are several important refinements that should be studied within the liquid-drop model.

The present work has been concerned with tracing out the implications of the two-spheroid model on an essentially classical basis. The entire treatment of that stage of the fission process from the saddle point to infinity has involved the solution of classical equations of motion. Only in the neighborhood of the saddle point have we attempted to discuss the effects that quantum mechanics would be expected to have on the process, and it is not clear that quantum mechanics has been introduced in a consistent way. Our quantum-mechanical discussion involved the determination of the probability for initially finding the system in a given state of motion near the saddle point. These quantum-mechanical probability distributions were then combined in the sense of initial conditions with solutions to classical equations of motion.

The classical solution of the equations of motion corresponding to the two-spheroid Hamiltonian represents an essential step in our

understanding. An important next step would involve the completely consistent quantum-mechanical solution of Schrödinger's equation corresponding to the Hamiltonian—both in the vicinity of the saddle point and in the separated region. This would involve, among other things, a study of the restrictions imposed by symmetry upon the wave functions for the system, for which there are no classical analogues. From such a complete quantum-mechanical solution, the classical solutions discussed here could be obtained as a limiting case. (For most of the data compared here, however, the nuclear temperature is sufficiently high that classical statistical mechanics is valid for determining the initial conditions, and the ambiguities associated with this mixture of classical and quantum mechanics are not present. For these cases the entire treatment given here may be regarded as completely classical.)

There is a second important investigation that remains to be carried out for the two-spheroid model. The discussion in this paper was restricted to a system with zero total angular momentum. The theory should also be worked out in which account is taken of the three rotational degrees of freedom of the system as a whole. This would make it possible to draw stronger conclusions when comparing predictions of the theory with data from heavy-ion-induced reactions, in which there is considerable angular momentum present. Explicit consideration of the system's three rotational degrees of freedom would also make it possible to incorporate the existing discussions of angular distributions of fission fragments (51, 105-108).

A third extension of the work of this paper is possible. By relaxing the restriction that the charge density be constant throughout the nucleus, and by taking into account a charge-fluctuation degree of freedom, the discussion of fission-fragment charge distributions could be included (55).

To us the most exciting prospect for the future is the extension of the two-spheroid model by the introduction of a conicoid of revolution between the two spheroids (see Section II. B, and Appendix B.3 of Ref.2). By use of this extension of the model, one should be able to discuss certain aspects of the fission of nuclei over the entire range of fissionability parameter from 0 to 1. Since the saddle-point energies and shapes calculated in this extended model agree so remarkably well with the true liquid-drop saddle-point energies and shapes (see Figs. 8 - 11), the model should make practicable the calculation of the predictions of the liquid-drop model not only as regards the distributions discussed in this paper, but also as regards such questions as the probability for fission—cross sections for induced fission, and half lives for spontaneous fission.

The general version of the extended model has the capability of representing the transformation of the hyperboloidal neck into a spheroidal third body between the two side fragments. This provides the possibility for the division of the nucleus into three fragments. Thus it might be possible to discuss with this three-spheroid approximation the interesting questions of ternary fission and long-range alpha-particle emission, in particular the angular distributions and the kinetic-energy distributions of the long-range alpha particles.

In conclusion, we would like to suggest that the procedure to be adopted in discussing any extensions of the theory should be identical as far as possible with that underlying the present work—the writing down of the Hamiltonian describing the idealized situation, followed by the systematic application of standard static, dynamical, and statistical methods. In this way a degree of unity and continuity could be achieved in the development of fission theory.

ACKNOWLEDGMENTS

Appreciation is expressed to Stanley G. Thompson for his interest and encouragement, and for numerous discussions.

Thanks are extended to Donald S. Burnett and Franz Plasil for many discussions and for their cooperation in performing experiments to compare with the theory, and to Burnett for the use of his experimental contour map prior to publication. Thanks are also extended to John O. Rasmussen for a stimulating discussion regarding distributions of fragment angular momenta, and to several other individuals, particularly Eldon Lee Haines and William D. Myers, for stimulating discussions.

We are grateful to Paul Concus for advice on coding, to Stanley Cohen for the use of his saddle-point-searching computer code, to J. C. Douglas Milton for the use of his contour-plotting computer code and for the opportunity to compare results of some of our computer codes with his tables, and to Marvin M. Hoffman for the opportunity to compare with his calculations the results of our numerical integrations of the equations of motion for the special case of a rigid spheroid and a sphere.

The financial assistance of the U. S. Atomic Energy Commission, under whose auspices this work was performed, is also appreciated.

APPENDIX

Comments on the Validity of the Liquid-Drop Model for Discussing Fission[49]

A nucleus can be regarded for practical purposes as consisting of protons and neutrons held together by short-range nuclear forces. Solution of the resulting many-body problem would presumably yield an accurate description of all fission phenomena. However, this is at present not a practicable approach both because of the mathematical difficulties associated with the presence of a large number of particles and because the potential between nucleons is not accurately known.

The short-range character of the nuclear force provides a means for approximate solution. The dimensionless ratio characterizing the nuclear problem—the range of the nuclear force divided by the nuclear radius—is for all but the lightest nuclei a small quantity. The energy of the system (apart from the Coulomb energy) may then be calculated as an expansion in increasing powers of this dimensionless ratio. The coefficients of the various terms, which will in general depend upon nuclear composition (the relative number of neutrons and protons), may be determined, in principle, by fitting the resulting expansion to experimental masses. The four leading terms in such an expansion of the energy are of order $(R_0/r_n)^3$, $(R_0/r_n)^2$, $(R_0/r_n)^1$, and $(R_0/r_n)^0$, where R_0 is the radius of the undistorted nucleus, and r_n is the

[49] Some aspects of the foundations of the liquid-drop model have recently been discussed by Strutinskiĭ and Tyapin (109).

range of the nuclear force. With respect to the number of nucleons A, the expansion has leading terms of order A^1, $A^{2/3}$, $A^{1/3}$, and A^0.

A physical interpretation may be attached to the leading terms in the expansion of the energy. The term of order A^1 represents the approximation in which the size of the nucleus is infinite compared with the range of nuclear forces, i.e., the nuclear matter approximation. The contribution to the energy associated with the A^1 term is a negative quantity proportional to the volume of the nucleus; for a heavy nucleus its magnitude is a few thousand MeV. This volume energy, which is independent of the shape of the nucleus, represents the energy decrease arising from the binding of each nucleon with its close neighbors. Since it is a constant for a particular nucleus it need not be considered when discussing fission, where only shape-dependent energies are relevant.

The term of order $A^{2/3}$ represents the approximation in which the range of nuclear forces is no longer neglected in relation to the size of the nucleus. This term represents the loss of binding of nucleons near the surface of the nucleus, but since one is considering this effect only to lowest order, the approximation is equivalent to assuming a semi-infinite distribution of nuclear matter bounded by a <u>plane</u> surface. In this approximation the effect of the $A^{2/3}$ term may be represented as the loss of binding per unit area of the bounding surface, i.e., as a surface energy proportional to the surface area of the nucleus. The size of this term depends on the shape of the nucleus—a typical value for a heavy nucleus is several hundred MeV.

The actual value of the specific surface tension depends in a very complicated way on the details of nuclear forces and nuclear structure. On the other hand, the proportionality of the $A^{2/3}$ term to the nuclear surface area is a consequence only of the smallness of r_n in comparison to R_0, i.e., of the assumption that the causes for the decrease of binding at the surface can be localized to the immediate neighborhood of a given nucleon. The situation is analogous to the case of ordinary liquids—despite the immensely complicated nature of intermolecular forces the proportionality of the surface energy to the area of the drop is extremely accurate except for droplets whose radii become comparable to molecular distances.

The term of order $A^{1/3}$ represents a number of corrections to the volume and surface energies associated with the finite rather than infinite size of nuclei. In particular, the compressibility correction to the volume energy, and the curvature correction to the surface energy appear at this stage (18). The available information regarding these terms is very inadequate; in order of magnitude, they are some tens of MeV. Since these terms are smooth functions of the neutron and proton numbers, our ignorance regarding them is, in practice, compensated to a certain extent by a readjustment of the empirical coefficients of the volume-, surface-, and electrostatic-energy terms.

The correction terms of order A^0 are presumably even more subtle and less well understood. Insofar as these terms are smooth functions of the neutron and proton numbers they are also partly absorbed in the leading terms. We note, however, that single-particle effects

may be formally regarded to be of order A^0 —binding-energy anomalies associated with a single nucleon (a few MeV in practice) are of order A times smaller than the total binding of all nucleons. Because of the characteristic oscillating dependence of the single-particle binding anomalies on neutron and proton numbers, this correction is presumably the most important of the A^0 terms. Some information on this correction is directly available from the study of ground-state masses of nuclei in the periodic table and from theories of the observed oscillations (see, for example, Refs. 81 and 82).

We have thus far considered only the energy associated with the nuclear forces. The electrostatic repulsion of the positively charged protons gives rise to a Coulomb energy, which is also a function of the shape of the nucleus. This energy is of order $\alpha A^{5/3}$, where $\alpha \approx 10^{-2}$ is the ratio of the electromagnetic coupling constant to the nuclear coupling constant. For a heavy nucleus the Coulomb energy is of the order of a thousand MeV.

In connection with the Coulomb energy it should be pointed out that the discussion of the Coulomb energy of a deformed drop with a <u>thin</u> diffuse surface is as easy as that of a drop with a <u>sharp</u> surface (<u>81</u>); the lowest-order diffuseness correction to the Coulomb energy is a shape-independent constant and could be included by a re-definition of the fissionability parameter x.

We see that the leading terms of interest in fission—the shape-dependent ones—are of order $\alpha A^{5/3}$, $A^{2/3}$, $A^{1/3}$, and A^0. The liquid-drop model consists of treating only the first two, the Coulomb and surface energies. Barring accidental cancellations of the changes

in Coulomb and surface energies, the remaining terms should in general be less important. In the region of the heavy elements the changes in the Coulomb and surface energies do indeed tend to cancel, and, especially in the case of fission at low excitation energy, the single-particle effects may then be essential for discussing certain aspects of the process. On the other hand, in the region of the lighter elements, where the cancellation of the changes in the Coulomb and surface energies is not so close, single-particle effects should not have the same relative importance, particularly at higher excitation energies. A logical approach would seem to be to work out the details of the theory first considering only the surface and Coulomb energies, and later to incorporate single-particle effects.

The point of view that we are tying to bring out is that the liquid-drop model is not to be regarded as a "right" or a "wrong" model of fission, but as a first stage in the development of an approximate theory of nuclear fission that takes into account the principal components of the energy and that may be improved in a systematic way by the inclusion of corrections of higher order in $A^{-1/3}$.

REFERENCES

1. Otto Hahn and Fritz Strassmann, Über den Nachweis und das Verhalten der bei der Bestrahlung des Urans mittels Neutronen entstehenden Erdalkalimetalle, Naturwiss. 27, 11 (1939). For an English translation see Hans G. Graetzer, Discovery of Nuclear Fission, Am. J. Phys. 32, 9 (1964). See also Otto Hahn and Fritz Strassmann, Nachweis der Entstehung aktiver Bariumisotope aus Uran und Thorium durch Neutronenbestrahlung; Nachweis weiterer aktiver Bruchstücke bei der Uranspaltung, Naturwiss. 27, 89 (1939).

2. James Rayford Nix, Studies in the Liquid-Drop Theory of Nuclear Fission (Ph.D. Thesis), University of California Lawrence Radiation Laboratory Report UCRL-11338, April 1, 1964 (unpublished).

3. James Rayford Nix, Estimates of Fission-Fragment Kinetic-Energy Distributions on the Basis of the Liquid-Drop Model, Paper No. F-7, in Proceedings of the Third Conference on Reactions Between Complex Nuclei, edited by A. Ghiorso, R. M. Diamond, and H. E. Conzett (University of California Press, Berkeley, 1963), p. 366.

4. Lise Meitner and O. R. Frisch, Disintegration of Uranium by Neutrons: a New Type of Nuclear Reaction, Nature 143, 239 (1939).

5. Niels Bohr and John Archibald Wheeler, The Mechanism of Nuclear Fission, Phys. Rev. 56, 426 (1939).

6. R. D. Present and J. K. Knipp, On the Dynamics of Complex Fission, Phys. Rev. 57, 751, 1188 (1940).

7. R. D. Present, F. Reines, and J. K. Knipp, The Liquid Drop Model for Nuclear Fission, Phys. Rev. 70, 557 (1946).

8. U. L. Businaro and S. Gallone, On the Interpretation of Fission Asymmetry According to the Liquid Drop Nuclear Model, Nuovo Cimento 1, 629 (1955).

9. U. L. Businaro and S. Gallone, Saddle Shapes, Threshold Energies and Fission Asymmetry on the Liquid Drop Model, Nuovo Cimento 1, 1277 (1955).

10. U. L. Businaro and S. Gallone, Asymmetric Equilibrium Shapes in the Liquid Drop Model, Nuovo Cimento 5, 315 (1957).

11. V. G. Nossoff, On the Theory of Nuclear Fission Near Threshold, Paper No. P/653, in Proceedings of the International Conference on the Peaceful Uses of Atomic Energy, Geneva, 1955, Vol. 2, Physics; Research Reactors (United Nations, New York, 1956), p. 205.

12. W. J. Swiatecki, Deformation Energy of a Charged Drop. II. Symmetric Saddle Point Shapes, Phys. Rev. 104, 993 (1956).

13. Wladyslaw J. Swiatecki, Deformation Energy of a Charged Drop, III. Further Developments, Paper No. P/651, in Proceedings of the Second United Nations International Conference on the Peaceful Uses of Atomic Energy, Geneva, 1958, Vol. 15, Physics in Nuclear Energy (United Nations, Geneva, 1958), p. 248.

14. S. Frankel and N. Metropolis, Calculations in the Liquid-Drop Model of Fission, Phys. Rev. 72, 914 (1947).

15. Stanley Cohen and Wladyslaw J. Swiatecki, The Deformation Energy of a Charged Drop, Part V: Results of Electronic Computer Studies, Ann. Phys. (N. Y.) 22, 406 (1963).

16. V. M. Strutinskiĭ, Equilibrium Shapes of Nuclei in the Quasistatic Fission Model, Soviet Phys. JETP 15, 1091 (1962) [English translation of J. Exptl. Theoret. Phys. (U. S. S. R.) 42, 1571 (1962)].

17. V. M. Strutinskiĭ, N. Ya. Lyashchenko, and N. A. Popov, Symmetrical Equilibrium Shapes in a Sharp Surface Nucleus Model (The Liquid Drop Model), Soviet Phys. JETP 16, 418 (1963) [English translation of J. Exptl. Theoret. Phys. (U. S. S. R.) 43, 584 (1962)]; similar article published as Symmetrical Shapes of Equilibrium for a Liquid Drop Model, Nucl. Phys. 46, 639 (1963).

18. V. M. Strutinskiĭ, Results of Calculations of Nuclear Fission According to a Liquid-Drop Model, University of California Lawrence Radiation Laboratory Report UCRL-Trans 978, translated from a publication of Akademiia Nauk SSSR, Institut Atomnoi Energii, 1963 (Electro-Optical Systems, Inc., July, 1963).

19. David Lawrence Hill, Dynamical Analysis of Nuclear Fission (Ph. D. Dissertation), Princeton University, April 1951 (unpublished).

20. D. L. Hill, The Dynamics of Nuclear Fission, Paper No. P/660, in Proceedings of the Second United Nations International Conference on the Peaceful Uses of Atomic Energy, Geneva, 1958, Vol. 15, Physics in Nuclear Energy (United Nations, Geneva, 1958), p. 244.

21. David Lawrence Hill and John Archibald Wheeler, Nuclear Constitution and the Interpretation of Fission Phenomena, Phys. Rev. 89, 1102 (1953).

22. D. R. Inglis, Fission Asymmetry, Ann. Phys. (N. Y.) 5, 106 (1958).

23. W. D. Foland and R. D. Present, Hydrodynamic Theory of Spontaneous Fission, Phys. Rev. 113, 613 (1959).

24. B. T. Geĭlikman, Breakup of a Charged Liquid Drop and Nuclear Fission, Soviet Phys. JETP 36 (9), 168 (1959) [English translation of J. Exptl. Theoret. Phys. (U. S. S. R.) 36, 249 (1959)].

25. Osamu Miyatake, Dynamical Behavior of Pinch-Off in the Nuclear Fission, University of Osaka Prefecture, Sakai, Japan, preprint (no date).

26. John A. Wheeler, Channel Analysis of Fission, Fast Neutron Physics, Part II: Experiments and Theory, edited by J. B. Marion and J. L. Fowler (Interscience Publishers, Inc., New York, 1963), pp. 2051-2184.

27. Peter Fong, Asymmetric Fission, Phys. Rev. 89, 332 (1953); A Theory of Nuclear Fission (Ph. D. Dissertation), University of Chicago, 1953 (unpublished).

28. Peter Fong, Statistical Theory of Nuclear Fission: Asymmetric Fission, Phys. Rev. 102, 434 (1956); Calculations Relating to the Asymmetric Fission of Pu^{239}, Bull. Am. Phys. Soc., Series II, 1, 303 (1956).

29. Peter Fong, Mechanism of Fission of Heavy Nuclei, Phys. Rev. 122, 1542 (1961); Statistical Theory of Nuclear Fission and Prompt Neutron Distribution, Phys. Rev. 122, 1543 (1961); Nuclear Models and Nuclear Fission, Phys. Rev. 122, 1545 (1961).

30. Peter Fong, Statistical Theory of Nuclear Fission, Bull. Am. Phys. Soc., Series II, 8, 385 (1963); Kinetic Energy and Prompt Neutron Distributions in Fission, Phys. Rev. Letters 11, 375 (1963).

31. J. K. Perring and J. S. Story, Thermodynamic Theory of Fission, Phys. Rev. 98, 1525 (1955).

32. T. D. Newton, Statistical Weights and Coulomb Factors for Fission Modes, Paper D1, in Proceedings of the Symposium on the Physics of Fission Held at Chalk River, Ontario, May 14-18, 1956, edited by G. C. Hanna, J. C. D. Milton, W. T. Sharp, N. M. Stevens, and E. A. Taylor, Atomic Energy of Canada Limited, Chalk River Project Report CRP-642-A, p. 307 (unpublished).

33. William E. Stein and Stanley L. Whetstone, Jr., Prompt Neutron Emission from Spontaneous-Fission Modes of Cf^{252}, Phys. Rev. 110, 476 (1958).

34. A. G. W. Cameron, Semiempirical Correlation of Fission Yield and Kinetic Energy Distributions, Rev. Mod. Phys. 30, 553 (1958); similar article published as Paper No. P/198, in Proceedings of the Second United Nations International Conference on the Peaceful Uses of Atomic Energy, Geneva, 1958, Vol. 15, Physics in Nuclear Energy, (United Nations, Geneva, 1958), p. 425.

35. B. T. Geĭlikman, The Asymmetry of Nuclear Fission, Soviet J. At. Energy 6, 178 (1960); The Excitation Energy of Fragments in Nuclear Fission, Soviet J. At. Energy 6, 184 (1960) [English translations of At. Energ. (U. S. S. R.) 6, 290, 298 (1959)]. Similar articles published as Papers No. P/2474 and P/2473, in Proceedings of the Second United Nations International Conference on the Peaceful Uses of Atomic Energy, Geneva, 1958, Vol. 15, Physics in Nuclear Energy (United Nations, Geneva, 1958) pp. 273, 279. See also, Excitation of Fission Fragments and their Mass Distribution, Soviet Phys. JETP 11, 688 (1960) [English translation of J. Exptl. Theoret. Phys. (U. S. S. R.) 38, 955 (1960)].

36. N. A. Perfilov and V. P. Eismont, ed., Fizika Deleniya Atomnyi Yader (Physics of the Division of the Atomic Nucleus), (Gosatomizdat, Moscow, 1962).

37. E. Erba, U. Facchini, E. Saetta-Menichella, F. Tonolini, and L. Tonolini Severgnini, Statistical Model in Fission of U^{235} Induced by Thermal Neutrons, Phys. Letters 6, 294 (1963).

38. Samuel Glasstone, Keith J. Laidler, and Henry Eyring, The Theory of Rate Processes (McGraw-Hill Book Company, Inc., New York, 1941), Chap. III, "Potential-energy Surfaces," Chap. IV, "Statistical Treatment of Reaction Rates," pp. 85-201.

39. B. C. Carlson, Ellipsoidal Distributions of Charge or Mass, J. Math. Phys. 2, 441 (1961).

40. Alex E. S. Green, Coulomb Radius Constant from Nuclear Masses, Phys. Rev. 95, 1006 (1954).

41. Alex E. S. Green, Nuclear Physics (McGraw-Hill Book Company, Inc., New York, 1955), pp. 245, 519.

42. Herbert Goldstein, Classical Mechanics (Addison-Wesley Publishing Company, Inc., Reading, Mass., 1959), Chap. 4, Sec. 4, "The Eulerian angles," pp. 107-9.

43. Stanley Cohen and Wladyslaw J. Swiatecki, The Deformation Energy of a Charged Drop, IV. Evidence for a Discontinuity in the Conventional Family of Saddle Point Shapes, Ann. Phys. (N. Y.) 19, 67 (1962).

44. Sir Horace Lamb, Hydrodynamics, 6th ed. (Dover Publications, New York, 1945), Section 382, pp. 719-21.

45. K. Alder, A. Bohr, T. Huus, B. Mottelson, and A. Winther, Study of Nuclear Structure by Electromagnetic Excitation with Accelerated Ions, Rev. Mod. Phys. 28, 432 (1956).

46. Ben R. Mottelson and J. G. Valatin, Effect of Nuclear Rotation on the Pairing Correlation, Phys. Rev. Letters 5, 511 (1960).

47. Marvin M. Hoffman, Directional Correlation of Fission Fragments and Prompt Gamma Rays Associated with Thermal Neutron Fission, Phys. Rev. 133, B714 (1964).

48. Frederick G. Werner (University of Cincinnati) and John Archibald Wheeler (Princeton University), Superheavy Nuclei and the Kolesnikov-Larkin-Mottelson Effect in Spontaneous Fission, Appendix III, Approximate Procedure Used to Evaluate Inertial Deformation Parameter (unpublished, no date).

49. Herbert Goldstein, Classical Mechanics, Chap. 10, "Small Oscillations, "(Addison-Wesley Publishing Company, Inc., Reading, Mass.), pp. 318-46.

50. Alex E. S. Green, Nuclear Physics, (McGraw-Hill Book Company, Inc., New York, 1955), pp. 185, 250.

51. I. Halpern, Nuclear Fission, Ann. Rev. Nucl. Sci. 9, 245-342 (1959).

52. Lev Davidovich Landau and E. M. Lifshitz, Quantum Mechanics, Non-Relativistic Theory, translated by J. B. Sykes and J. S. Bell (Addison-Wesley Publishing Company, Inc., Reading, Mass., 1958), Sec. 21, "The linear oscillator," pp. 64-70.

53. Lev Davidovich Landau and E. M. Lifshitz, Statistical Physics, translated by E. Peierls and R. F. Peierls (Addison-Wesley Publishing Company, Inc., Reading, Mass., 1958), Sec. 30, "The probability distribution for an oscillator," pp. 86-89.

54. Albert Messiah, Quantum Mechanics, Vol. I, translated by G. M. Temmer (Interscience Publishers, Inc., New York, 1961), Chap. XII, Sec. 12, "Harmonic Oscillators in Thermodynamic Equilibrium," pp. 448-451.

55. Marshall Blann (University of Rochester) and Wladyslaw J. Swiatecki (University of California Lawrence Radiation Laboratory, Berkeley), unpublished work on fission-fragment charge distributions.

56. Samuel S. Wilks, Mathematical Statistics (John Wiley and Sons, New York, 1962), Sec. 7.4, "The k-Variate Normal Distribution," pp. 163-70.

57. Ibid., Sec. 3.4, "Moments of Two-Dimensional Random Variables," pp. 77-9.

58. Herbert Bristol Dwight, Tables of Integrals and Other Mathematical Data, 4th ed. (The Macmillan Company, New York, 1961), p. 249, Integral No. 866.03.

59. Tables of the Error Function and Its Derivative, U.S. National Bureau of Standards, Applied Mathematics Series 41 (U.S. Government Printing Office, Washington, D.C., 1954).

60. Samuel S. Wilks, Mathematical Statistics, (John Wiley and Sons, New York, 1962), p. 265.

61. D.R. Hartree, Some Properties and Applications of the Repeated Integrals of the Error Function, Manchester Lit. and Phil. Soc. Mem. and Proc. 80, 85 (1935).

62. Joseph Kaye, A Table of the First Eleven Repeated Integrals of the Error Function, J. Math. and Phys. 34, 119 (1955).

63. R.A. Fisher, Properties of the Functions, in Mathematical Tables, British Association for the Advancement of Science, Vol. I, 3rd. ed. (University Press, Cambridge, 1951), pp. xxviii-xxxvii.

64. Donald S. Burnett, Raymond C. Gatti, Franz Plasil, P. Buford Price, Wladyslaw J. Swiatecki, and Stanley G. Thompson, Fission Barrier of Thallium-201, Phys. Rev. 134, B952 (1964).

65. A. W. Fairhall, Fission of Bismuth with 15- and 22-MeV Deuterons, Phys. Rev. 102, 1335 (1956); Cyclotron Research, University of Washington, 1956 Annual Progress Report, "Mass Distributions in the Fission of Bismuth and Radium" (University of Washington, Seattle, Washington, 1956), p. 20 (unpublished).

66. A. W. Fairhall, R. C. Jensen, and E. F. Neuzil, Fission Studies of Elements Lighter than Thorium, Paper No. P/677, in Proceedings of the Second United Nations International Conference on the Peaceful Uses of Atomic Energy, Geneva, 1958, Vol. 15, Physics in Nuclear Energy (United Nations, Geneva, 1958), p. 452.

67. Cyclotron Research, University of Washington, 1959 Annual Progress Report, "Alpha Particle Induced Fission in Elements Between Tungsten and Bismuth" (University of Washington, Seattle, Washington, 1959), p. 18 (unpublished).

68. T. T. Sugihara, J. Roesmer, and J. W. Meadows, Jr., Asymmetric Fission of Bismuth, Phys. Rev. 121, 1179 (1961).

69. Cyclotron Research, University of Washington, 1962 Annual Progress Report, "Fission Studies in Bismuth and Lead Targets" (University of Washington, Seattle, Washington, 1962), pp. 26-7 (unpublished).

70. Cyclotron Research, University of Washington, 1963 Annual Progress Report, "Fission Study of Pb^{206}" (University of Washington, Seattle, Washington, 1963), p. 15 (unpublished).

71. R. Vandenbosch and J. R. Huizenga, Kinetic Energy Distributions of Fragments from the Fission of Au, Tl, Pb, and Bi, Phys. Rev. 127, 212 (1962).

72. Victor E. Viola, Jr. and Torbjørn Sikkeland, Fragment Kinetic Energy Release in Heavy-Ion-Induced Fission Reactions, Phys. Rev. 130, 2044 (1963).

73. H. C. Britt, H. E. Wegner, and J. Gursky, Energetics of the Charged Particle-Induced Fission of Ra^{226}, Bi^{209}, and Au^{197}, Phys. Rev. Letters 8, 98 (1962).

74. J. Unik, G. L. Bate, and J. R. Huizenga, Studies of Coincident Fragments in the Helium-Ion-Induced Fission of Bi^{209} and U^{238}, Bull. Am. Phys. Soc., Series II, 7, 303 (1962).

75. H. C. Britt, H. E. Wegner, and Judith C. Gursky, Energetics of Charged Particle-Induced Fission Reactions, Phys. Rev. 129, 2239 (1963).

76. Donald S. Burnett, Kinetic Energy and Mass Distributions for Nuclear Fission at Moderate Excitation Energy (Ph.D. Thesis), University of California Lawrence Radiation Laboratory Report UCRL-11006, Oct. 7, 1963 (unpublished).

77. Franz Plasil, Energy-Mass Distributions and Angular Momentum Effects in Heavy-Ion-Induced Fission (Ph.D. Thesis), University of California Lawrence Radiation Laboratory Report UCRL-11193, Dec. 31, 1963 (unpublished).

78. J. P. Unik and J. R. Huizenga, Binary Fission Studies of Helium-Ion-Induced Fission of Bi^{209}, Ra^{226}, and U^{238}, Phys. Rev. 134, B90 (1964).

79. Donald S. Burnett, Franz Plasil, and Stanley G. Thompson, work on mass and kinetic-energy distributions, to be submitted for publication to Phys. Rev.

80. K. J. LeCouteur and D. W. Lang, Neutron Evaporation and Level Densities in Excited Nuclei, Nucl. Phys. 13, 32 (1959).

81. Wladyslaw J. Swiatecki, Semi-Empirical Interpretation of Nuclear Masses and Deformations, in Proceedings of the Second International Conference on Nuclidic Masses, Vienna, Austria, July 15-19, 1963 (Springer-Verlag, Berlin).

82. William D. Myers and Wladyslaw J. Swiatecki (University of California Lawrence Radiation Laboratory, Berkeley), unpublished work on single-particle shell corrections to nuclear masses.

83. S. Cohen, F. Plasil, and W. J. Swiatecki, Equilibrium Shapes of a Rotating Charged Drop and Consequences for Heavy Ion Induced Nuclear Reactions, Paper No. F-1, in Proceedings of the Third Conference on Reactions Between Complex Nuclei, edited by A. Ghiorso, R. M. Diamond, and H.E. Conzet (University of California Press, Berkeley, 1963), p.325; and further work on equilibrium shapes of rotating charged drops, to be submitted for publication to Ann. Phys. (N. Y.).

84. James Terrell, Neutron Yields from Individual Fission Fragments, Phys. Rev. 127, 880 (1962) and 128, 2925 (1962) (errata).

85. Eldon Lee Haines, Mass-Energy Relations in the Fission of Highly Excited Heavy Nuclei (Ph. D. Thesis), University of California Lawrence Radiation Laboratory Report UCRL-10342, June 29, 1962 (unpublished).

86. Donald S. Burnett (University of California Lawrence Radiation Laboratory, Berkeley; currently at Kellogg Radiation Laboratory, California Institute of Technology), unpublished contour map; the data presented in reference 76 for the compound nucleus $_{85}At^{213}$ are obtained from this two-dimensional distribution.

87. James Terrell, Distributions of Fission Neutron Numbers, Phys. Rev. 108, 783 (1957).

88. R. B. Leachman, Emission of Prompt Neutrons from Fission, Phys. Rev. 101, 1005 (1956).

89. R. B. Leachman and C. S. Kazek, Jr., Neutron Emission from Fission Modes, Phys. Rev. 105, 1511 (1957).

90. James Terrell, Fission Neutron Spectra and Nuclear Temperatures, Phys. Rev. 113, 527 (1959).

91. V. Weisskopf, Statistics and Nuclear Reactions, Phys. Rev. 52, 295 (1937).

92. K. J. LeCouteur, Statistical Fluctuations in Nuclear Evaporation, Proc. Phys. Soc. (London) A65, 718 (1952).

93. J. M. B. Lang and K. J. LeCouteur, Statistics of Nuclear Levels, Proc. Phys. Soc. (London) A67, 586 (1954).

94. J. D. Jackson, A Schematic Model for (p, x n) Cross Sections in Heavy Elements, Can. J. Phys. 34, 767 (1956).

95. A. B. Smith, P. R. Fields, and A. M. Friedman, Prompt Gamma Rays Accompanying the Spontaneous Fission of Cf^{252}, Phys. Rev. 104, 699 (1956).

96. J. S. Fraser, Prompt Gamma Rays and Neutrons Emitted in Fission, Paper No. C2, in Proceedings of the Symposium on the Physics of Fission Held at Chalk River, Ontario, May 14-18, 1956, edited by G. C. Hanna, J. C. D. Milton, W. T. Sharp, N. M. Stevens, and E. A. Taylor, Atomic Energy of Canada Limited, Chalk River Project Report CRP-642-A, p. 239. (unpublished).

97. H. R. Bowman and S. G. Thompson, The Prompt Radiations in the Spontaneous Fission of Californium-252, Paper No. P/652, in Proceedings of the Second United Nations International Conference on the Peaceful Uses of Atomic Energy, Geneva, 1958, Vol. 15, Physics in Nuclear Energy (United Nations, Geneva, 1958), p. 212.

98. F. C. Maienschein, R. W. Peelle, W. Zobel, and T. A. Love, ibid., Gamma Rays Associated with Fission, Paper No. P/670, p. 366.

99. R. B. Leachman, ibid., The Fission Process—Mechanisms and Data, Paper No. P/2467, p. 229; Neutrons and Radiations from Fission, Paper No. P/665, p. 331.

100. G. A. Pik-Pichak, Nucleon Emission by a Rotating Nucleus, Soviet Phys. JETP 11, 557 (1960) [English translation of J. Exptl. Theoret. Phys. (U. S. S. R.) 38, 768 (1960)].

101. James Robb Grover, Effect of Competition between Gamma-Ray and Particle Emission on Excitation Functions, Phys. Rev. 123, 267 (1961).

102. John O. Rasmussen, Conference Summary, in Proceedings of the Third Conference on Reactions Between Complex Nuclei, edited by A. Ghiorso, R. M. Diamond, and H. E. Conzett (University of California Press, Berkeley, 1963), p. 441.

103. J. R. Huizenga and R. Vandenbosch, Nuclear Fission, in Nuclear Reactions, Vol. II, edited by P. M. Endt and P. B. Smith (Interscience Publishers, Inc., New York, 1962), Chap. 2, Sec. 5, "Isomeric Ratios for Shielded Fission Products," pp. 104-5.

104. H. Warhanek and Robert Vandenbosch, private communication to Marvin M. Hoffman (see footnote 16 of Ref. 47).

105. Aage Bohr, On the Theory of Nuclear Fission, Paper No. P/911, in Proceedings of the International Conference on the Peaceful Uses of Atomic Energy, Geneva, 1955, Vol. 2, Physics; Research Reactors (United Nations, New York, 1956), p. 151.

106. V. M. Strutinskiĭ, Angular Distribution of Fission Fragments, Soviet Phys. JETP 3, 638 (1956)[English translation of J. Exptl. Theoret. Phys. (U. S. S. R.) 30, 606 (1956)].

107. I. Halpern and V. M. Strutinskiĭ, Angular Distributions in Particle-Induced Fission at Medium Energies, Paper No. P/1513, in Proceedings of the Second United Nations International Conference on the Peaceful Uses of Atomic Energy, Geneva, 1958, Vol. 15, Physics in Nuclear Energy (United Nations, Geneva, 1958), p. 408.

108. James J. Griffin, Energy Dependence of Fission Anisotropy, Bull. Am. Phys. Soc., Series II, 3, 337 (1958).

109. V. M. Strutinskiĭ and A. S. Tyapin, Quasistatic Drop Model of the Nucleus as an Approximation to the Statistical Model, Soviet Phys. JETP 18, 664 (1964) [English translation of J. Exptl. Theoret. Phys. (U. S. S. R.) 45, 960 (1963)].

Table I. Moments of distributions in total translational kinetic energy and mass. The calculated mean total translational kinetic energy $\bar{E}$, the variance σ_E^2 of the distribution in total translational kinetic energy, and the variance σ_U^2 of the distribution in fragment mass are compared with the data of Britt, Wegner, and Gursky[75] for $_2He^3$ - induced fission reactions. The experimental values of σ_E^2 and σ_U^2 are not corrected for the effects of neutron emission from the fragments.

Target	Compound nucleus	x	Bombarding energy (MeV)	Θ (MeV)	$\bar{E}$ (MeV) Theory	$\bar{E}$ (MeV) Exp.	σ_E^2 $(MeV)^2$ Theory	σ_E^2 $(MeV)^2$ Exp.	σ_U^2 $(amu)^2$ Theory	σ_U^2 $(amu)^2$ Exp.
$_{79}Au^{197}$	$_{81}Tl^{200}$	0.654	25.5	0.65	143	140.3	39	55	73	96.7
$_{81}Tl^{nat}$	$_{83}Bi^{(208)}$	0.661	25.5	0.53	148	141.7	35	50	61	89.0
$_{82}Pb^{206}$	$_{84}Po^{209}$	0.673	25.5	0.57	149	145.4	38	50	62	79.1
$_{83}Bi^{209}$	$_{85}At^{212}$	0.680	25.5	0.54	151	147.3	37	57	58	85.0
$_{83}Bi^{209}$	$_{85}At^{212}$	0.680	22.1	0.40	151	146.5	30	48	43	72.7

Table II. Properties of distributions in total translational kinetic energy and mass. The calculated mean total translational kinetic energy $\overline{E}$, the full width at half maximum $(FWHM)_E$ of the distribution in total translational kinetic energy, and the full width at half maximum $(FWHM)_U$ of the distribution in fragment mass are compared with experimental data.

Target	Projectile	Compound nucleus	x	Bombarding energy (MeV)	Θ (MeV)	$\overline{E}$ Theory (MeV)	$\overline{E}$ Exp. (MeV)	$(FWHM)_E$ Theory (MeV)	$(FWHM)_E$ Exp. (MeV)	$(FWHM)_U$ Theory (amu)	$(FWHM)_U$ Exp. (amu)	Ref.
$_{83}Bi^{209}$	α	$_{85}At^{213}$	0.677	42	0.65[a]	151	150	15[a]	16[b]	20[a]	24[c,d]	78
$_{83}Bi^{209}$	α	$_{85}At^{213}$	0.677	43	0.68	151	148	15	20[d]	20	26[c,d]	71
$_{82}Pb^{nat}$	α	$_{84}Po^{(211)}$	0.667	43	—	149	146	—	—	—	—	71
$_{81}Tl^{nat}$	α	$_{83}Bi^{(209)}$	0.658	43	—	147	143	—	—	—	—	71
$_{79}Au^{197}$	α	$_{81}Tl^{201}$	0.651	43	—	143	138	—	—	—	—	71
$_{83}Bi^{209}$	d	$_{84}Po^{211}$	0.667	21.5	0.35	149	143	12	19[d]	—	—	71

[a] In Ref. 78 the experimental (rather than calculated) fission barrier is used to obtain Θ = 0.8 MeV; using this value, $(FWHM)_E$ = 16 MeV, and $(FWHM)_U$ = 22 amu.

[b] Value is corrected (in Ref. 78) for fragment neutron emission and experimental dispersion.

[c] Value is read off experimental curve.

[d] Value is not corrected for fragment neutron emission and experimental dispersion.

Table III. Widths of fragment-mass distributions. The calculated full width at half maximum $(FWHM)_U$ of the distribution in fragment mass is compared with data obtained by radiochemical techniques.

Target	Projectile	Compound nucleus	x	Bombarding energy (MeV)	Θ (MeV)	$(FWHM)_U$ Theory (amu)	$(FWHM)_U$ Exp. (amu)	Ref.
$_{82}Pb^{206}$	α	$_{84}Po^{210}$	0.670	42	0.62	20	21[a]	70
$_{83}Bi^{209}$	p	$_{84}Po^{210}$	0.670	36	0.76	22	18[a]	68
$_{83}Bi^{209}$	p	$_{84}Po^{210}$	0.670	58	1.20	27	24[a]	68
$_{79}Au^{197}$	α	$_{81}Tl^{201}$	0.651	42	0.72	21	34	67
$_{82}Pb^{204}$	α	$_{84}Po^{208}$	0.677	42	0.71	20	27[a]	67
$_{82}Pb^{206}$	α	$_{84}Po^{210}$	0.670	42	0.62	20	22	67
$_{83}Bi^{209}$	d	$_{84}Po^{211}$	0.667	22	0.38	15	17	65,66

[a]Value is read off experimental curve.

LIST OF SYMBOLS

β ,	lower case beta
γ ,	lower case gamma
$\mathbf{L}$,	boldface cap el
0 ,	zero
$\times$,	times
$\hbar$,	h bar
Ω ,	cap omega
Φ ,	cap phi
θ ,	lower case theta
Θ ,	cap theta
ϕ ,	lower case phi
ψ ,	lower case psi
ℓ ,	lower case script el
$\mathcal{V}$,	cap script vee
$\mathcal{T}$,	cap script tee
$\mathcal{H}$,	cap script aich
δ ,	lower case delta
$\sqrt{\ }$,	square root
ω ,	lower case omega
α ,	lower case alpha
π ,	lower case pi
∞,	infinity
$\lvert\ \rvert$,	absolute value

LIST OF SYMBOLS (cont.)

$\sum$,	summation
∂ ,	partial derivative
$\int$,	integral
$'$,	prime
σ ,	lower case sigma
μ ,	lower case mu

FOOTNOTES

[1] When used in this context, the term "excitation energy" refers to the energy of the collective vibrations and deformations of the fragment; it does not include the internal (excitation) energy of the individual nucleons.

[2] The same symbol P is used throughout this paper to denote each of several probability distributions; the argument or subscript will indicate which explicit function is being referred to.

[3] Experimental information regarding the other distributions is at present not available for the fission of nuclei lighter than radium. We will see later that it is for these nuclei that our model is most nearly applicable.

[4] We have taken the constants of the Bethe-Weizsäcker semiempirical mass formula from Green's analysis of ground-state masses (40). The nuclear temperature at the saddle point is determined from the excitation energy and fission barrier of the compound nucleus. All other quantities are calculated directly from the model.

[5] When future determinations of these constants are made, the new values may be used since all theoretical quantities are given here in liquid-drop units.

[6] The fractional mass of the right-hand fragment is 1-U.

[7] For example, if spheroid 1 is prolate, then c_1 is its semimajor axis; its semiminor axis is determined by volume conservation.

[8] When all coordinates are considered, the cusp occurs at those values of the coordinates that correspond to the configuration of touching spheroids.

[9] This is clearly seen in Fig. 3 in the map for $x = 0.8$.

[10] Historically, however, it was for a time believed that three equilibrium configurations possibly did exist for a short range of x close to 0.7 (15, 43).

[11] Unfortunately, most experimental information on fission is for nuclei that lie in this range of x. Some data exist, however, on the fission of nuclei where $x \lesssim 0.67$, and more are becoming available as time progresses.

[12] Formulae for calculating the potential energy of such a system are given in Appendix B.3 of Ref. 2.

[13] When we discuss the solutions to the equations of motion we will, whenever possible, also indicate the result for the case in which the fragments are infinitely viscous, and would therefore separate to infinity without oscillating.

[14] The use of classical equations of motion for discussing the separation of the fragments to infinity may be partially justified on the grounds that a short distance from the saddle point the de Broglie wavelength for translational motion has become relatively small, that the vibrations about each fragment's center of mass involve several quanta of energy, and that the angular momentum of each fragment is typically several $\hbar$ units in magnitude.

15 The angular momentum acquired by a rigid spheroid moving in the electrostatic field of a sphere has been discussed by Hoffman (47).

16 See the discussion of normal coordinates in any classical-mechanics textbook, for example, Goldstein (49).

17 When discussing the kinetic energy, we are not restricted to the subspace of touching spheroids.

18 We will see later (Fig. 13) that K_{Uc_2} is always positive and that $K_{c_1c_1}$ is always greater than $K_{c_1c_2}$; hence, B is always positive.

19 In verifying that $\mathcal{J}$ is diagonal in terms of the time derivatives of the normal coordinates, note that $\dot{U}$ is zero at the saddle point.

20 This result states physically that the kinetic energy associated with a finite flux of matter through an aperature of infinitesimal radius is infinite. This follows from the fact that the velocity of flow through the aperture is infinite, and that the kinetic energy depends upon the product of the amount of matter and the square of the velocity.

21 The reason for the vanishing of ω_m is that in the two-spheroid model the neck radius of the saddle-point shape is zero. For the exact saddle point the neck radius is not zero but is small, and ω_m is not zero but is small in comparison with the other frequencies.

22 The two-spheroid model thus predicts this bifurcation point at a value of x that is somewhat too high, in analogy to its prediction of a transition region at $x \approx 0.80$, when the true transition region occurs at $x \approx 0.67$.

23 There is currently no experimental information on excitation energies and angular momenta for the fission of elements lighter than radium. We content ourselves at this time with treating these quantities to a lower order than the translational kinetic energy.

24 It should be recalled that the excitation energy calculated here is the energy associated with the collective vibrations and deformations of the fragments. Any internal excitation energy that a fragment has at the moment of division would be added to the excitation energy we calculate, to obtain the final total excitation energy.

25 The relationships $p_{b_x} = (1/\sqrt{2})\,(p_{\theta_{1x}} - p_{\theta_{2x}})$ and $p_{w_x} = (1/\sqrt{2})\,(p_{\theta_{1x}} + p_{\theta_{2x}})$ etc., obtained from the normal-coordinate transformation and the definitions of the momenta, are useful for this purpose. The value at infinity of $p_{\theta_{1x}}$, for example, is L_{1x}.

[26] Since the saddle point is a position of (unstable) equilibrium, a system initially at rest at the saddle point would remain there (classically) for an infinite time; we imagine an infinitesimal push in the fission direction to start the system moving. An analytic solution, valid in the neighborhood of the saddle point, is used until the system is a short distance from the saddle point, where the numerical integration begins.

[27] All probability distributions in this paper are normalized such that unity is obtained when the functions are integrated over the allowed range of variables, which is usually taken to be from $-\infty$ to $+\infty$. The range of integration for p_f is taken to be from 0 to ∞, since for negative values of p_f the system does not fission but instead returns to the pre-saddle-point configuration; this results in the additional factor of 2 in the expression for $P(p_f)$.

[28] The Gaussian distribution in the mass-asymmetry <u>velocity</u> becomes, on the other hand, infinitely narrow and hence reduces to a Dirac delta function. This means physically that the mass-asymmetry coordinate changes with time infinitely slowly at the saddle point.

29 Recall that for $x < x_{BG}$ the mass-asymmetry stiffness constant K_m is negative. Thus for $x < x_{BG}$, the probability $P(m)$ increases rather than decreases with increasing absolute value of m.

30 If there were no angular momentum induced by the torque arising from the presence of the electrostatic field, then C'_{p_b} would equal C_{p_b}, since for this case $L_{1,p_b} = 1/\sqrt{2}$, and $L_{1,b} = 0$. An analogous statement holds for C'_{p_w}.

31 This equation is also obtainable directly from $P(m, s)$ and the equations $U = \frac{1}{2} + m$ and $X = X^0 + 2X_{1,s}\, s$ [obtained from (16) by adding X_1 and X_2].

32 This expression could also be obtained directly from the set of equations (17) and $P(b_x, w_x, b_y, w_y, p_{b_x}, p_{w_x}, p_{b_y}, p_{w_y})$ by integrating over the bending and wriggling angles, and transforming the result to cylindrical coordinates.

33 The other two cubic terms, $(E - E^0)^2(U - \frac{1}{2})$ and $(U - \frac{1}{2})^3$, are absent because $P(E, U)$ is an even function of $(U - \frac{1}{2})$. The absence of the $(U - \frac{1}{2})^3$ term means that the $(U - \frac{1}{2})^4$ term is responsible for the first-order deviation of the distribution in mass from a Gaussian, and must then be considered to this order. The distribution $P(E, U)$ would also, in general, have a pre-exponential dependence upon E and U.

34 This result follows directly from the equation $U = \frac{1}{2} + m$ and the distribution for $P(m)$, without the use of the approximation $F(E,U) = 1$. It may also be obtained by substituting (34) for $P(E,U)$, with $F(E,U) = 1$, and integrating.

35 The two cubic terms ms^2 and m^3 are absent because $\mathcal{V}$ is an even function of m. Nonzero cubic terms of the form sd^2, for example, introduce only pre-exponential dependences on E and U after the integration over d is performed.

36 A recent experimental determination of the fission barrier of ${}_{81}Tl^{201}$ indicates that $(Z^2/A)_{crit}$ has a value(64) of 48.4 ± 0.5 [rather than Green's value(40) of 50.13 that is used here]. When this value of $(Z^2/A)_{crit}$ is used, the value of the fissionability parameter x for each compound nucleus is increased somewhat. For the comparisons between theory and experiment that are made here, the largest value of fissionability parameter that occurs is 0.677 when Green's value of $(Z^2/A)_{crit}$ is used, and 0.701 when the newly reported value is used.

37 These experiments consist of measuring in coincidence the translational kinetic energies E_1 and E_2 of the two fission fragments at infinity and recording the corresponding number of events. From this experimentally constructed distribution $P(E_1, E_2)$, the experimental distribution $P(E,U)$ is obtained by use of the transformation (18).

38 A plot of the liquid-drop fission-barrier energy vs. x is given in Figs. 4 and 8. For the determination of Θ, the true liquid-drop fission-barrier energy is used rather than the two-spheroid approximation to the barrier.

39 For the cases studied it was found that the average number of neutrons emitted before fission seldom exceeds one; this means that the uncertainty in the nuclear temperature arising from this effect is small.

40 Although the approximate formulae derived in Section V for $P(U)$, $P(E)$, and the various statistical moments are sufficiently accurate for calculating the theoretical curves of this section, the curves have actually been calculated by numerical integrations over the full expression (36) [or the full expression (48)] for $P(E, U)$, with $F(E, U)$ retained.

[41] The large amount of angular momentum present in the two $_{82}Pb^{198}$ cases could, of course, be responsible for the near-constancy of $\sigma_E^2(U)$ as a function of U (rather than a disappearance of shell structure).

[42] For the benefit of those making a comparison between this figure and Fig. 6 of Ref. 3, the preliminary data presented there were overcorrected for the effects of neutron emission from the fragments; the agreement is better than indicated there.

[43] It should be recalled that the variance σ_U^2 retains its linear dependence upon Θ at low temperatures in the two-spheroid model because the mass-asymmetry frequency is zero (as a consequence of the zero neck radius of the saddle-point shape). In the actual situation, of course, the neck radius of the saddle-point shape and the mass-asymmetry frequency are not zero, but are small. The variance σ_U^2 of the mass distribution should therefore approach in the real case a small finite value, rather than zero, as the temperature goes to zero.

[44] Note that a measurement of the distribution of the total number of neutrons emitted (from both fragments) would determine only the distribution in total excitation energy, which would be equivalent (to lowest order) to the distribution in total translational kinetic energy.

37 These experiments consist of measuring in coincidence the translational kinetic energies E_1 and E_2 of the two fission fragments at infinity and recording the corresponding number of events. From this experimentally constructed distribution $P(E_1, E_2)$, the experimental distribution $P(E,U)$ is obtained by use of the transformation (18).

38 A plot of the liquid-drop fission-barrier energy vs. x is given in Figs. 4 and 8. For the determination of Θ, the true liquid-drop fission-barrier energy is used rather than the two-spheroid approximation to the barrier.

39 For the cases studied it was found that the average number of neutrons emitted before fission seldom exceeds one; this means that the uncertainty in the nuclear temperature arising from this effect is small.

40 Although the approximate formulae derived in Section V for $P(U)$, $P(E)$, and the various statistical moments are sufficiently accurate for calculating the theoretical curves of this section, the curves have actually been calculated by numerical integrations over the full expression (36) [or the full expression (48)] for $P(E, U)$, with $F(E, U)$ retained.

[41] The large amount of angular momentum present in the two $_{82}Pb^{198}$ cases could, of course, be responsible for the near-constancy of $\sigma_E^2(U)$ as a function of U (rather than a disappearance of shell structure).

[42] For the benefit of those making a comparison between this figure and Fig. 6 of Ref. 3, the preliminary data presented there were over-corrected for the effects of neutron emission from the fragments; the agreement is better than indicated there.

[43] It should be recalled that the variance σ_U^2 retains its linear dependence upon Θ at low temperatures in the two-spheroid model because the mass-asymmetry frequency is zero (as a consequence of the zero neck radius of the saddle-point shape). In the actual situation, of course, the neck radius of the saddle-point shape and the mass-asymmetry frequency are not zero, but are small. The variance σ_U^2 of the mass distribution should therefore approach in the real case a small finite value, rather than zero, as the temperature goes to zero.

[44] Note that a measurement of the distribution of the total number of neutrons emitted (from both fragments) would determine only the distribution in total excitation energy, which would be equivalent (to lowest order) to the distribution in total translational kinetic energy.

[45] For the heavier elements the average total gamma-ray energy per fission (for both fragments) has been found experimentally to be about 8 MeV(95-98). Fragment de-excitation calculations made for nonrotating fragments indicate that roughly one-half this amount of gamma-ray energy is expected(88-90,99). It has been suggested that this discrepancy is due to the presence of a total fragment rotational energy of several MeV.

[46] Recall (Section V.A. 2) that for the compound nucleus $_{85}At^{213}$ and a nuclear temperature at the saddle point of 1.13 MeV, the most probable value of the angular momentum of each fragment at infinity is estimated as about 10ħ if the fragments are nonviscous and about 15ħ if the fragments are infinitely viscous. If one uses for the moment of inertia of the fragments at infinity the rigid-body moment of interia of a sphere, for example, this corresponds to total rotational energies for both fragments of about 3 MeV for the nonviscous case and about 7 MeV for the viscous case.

[47] For the thermal-neutron-induced fission of heavier elements, this method (47) indicates that the average angular momentum per fragment is about 7ħ.

[48] The angular momentum per fragment in the low- and medium-energy fission of heavy elements deduced by this method (104) is about 6 to 10ħ.

[49] Some aspects of the foundations of the liquid-drop model have recently been discussed by Strutinskiĭ and Tyapin (109).

FIGURE CAPTIONS

Fig. 1. A two-fragment configuration described by 17 degrees of freedom. Three (Euler) angles describe the orientation in space of one fragment, three of the other, and two angles describe the orientation of the line joining their centers. One number specifies the relative sizes of the fragments, two specify the intrinsic shape of one fragment, two of the other, and one their separation. Three degrees of freedom describe the location in space of the common center of mass. Total: $3 + 3 + 2 + 1 + 2 + 2 + 1 + 3 = 17$.

Fig. 2. Coordinates used for describing a two-spheroid configuration. The three Euler angles θ_1, ϕ_1, ψ_1 describe the orientation in space of the left-hand spheroid (see description in text), and θ_2, ϕ_2, ψ_2 the right-hand spheroid; the two angles Θ and Φ describe the orientation in space of the line connecting their centers. The fractional mass (fractional volume) of the left-hand spheroid is denoted by U. The semisymmetry axis of the left-hand spheroid is denoted by c_1, and that of the right-hand one by c_2. The distance between their centers is ℓ. Illustrated in the upper part of the figure for overlapping spheroids are the two coordinates ℓ and $c \equiv c_1 = c_2$, used for discussing the restricted case of completely symmetrical fragments.

lower case

CAP theta, CAP phi

Fig. 3a. Symmetric two-spheroid configurations for selected values of the coordinates(marked by +), Coulomb energy B_C, surface energy B_S,

CAP script vee

and potential energy $\mathcal{V}$ for $x = 0.2$. The function B_C is the Coulomb energy in units of $E_C^{(0)}$, and B_S is the surface energy in units of $E_S^{(0)}$. The function $\mathcal{V}$ is in units of $E_S^{(0)}$. For the $x = 0.2$ case the solution of the equations of motion corresponding to starting from rest at the saddle point is indicated by the points, which are equally spaced in time at intervals of $0.1\ T_0$ [see Eq. (2) for value of T_0]. The dot-dashed line in each case corresponds to the scission configuration of tangent spheroids ($\ell = 2c$); the long-dashed line corresponds to the configuration of two separated spheres ($c/R_0 = 1/2^{1/3}$).

Fig. 3b. Maps of potential energy $\mathcal{V}$ for $x = 0.4$, 0.6, 0.8, and 1.0. The location of the overlapping saddle point for $x = 0.8$ is shown by the cross mark; for this value of x there are two saddles and a stable minimum point (apart from the original sphere). The function $\mathcal{V}$ is in units of $E_S^{(0)}$. For the $x = 0.4$, 0.6, and 0.8 cases the solutions of the equations of motion corresponding to starting from rest at the saddle points are indicated by the points, which are equally spaced in time at intervals of $0.1\ T_0$ [see Eq. (2) for value of T_0].

Fig. 4. The potential energy of equilibrium configurations, as a function of fissionability parameter x. The result calculated in the two-spheroid approximation is given by the solid line, the result of Cohen and Swiatecki (15) by the short-dashed line, and the result of Strutinskiĭ et al. (17) by the dot-dashed line.

Fig. 5. The surface energy B_S and Coulomb energy B_C of equilibrium configurations, as functions of fissionability parameter x. The function B_S is the surface energy in units of $E_S^{(0)}$, and B_C is the Coulomb energy in units of $E_C^{(0)}$. The results calculated in the two-spheroid approximation are given by the solid lines, and the results of Cohen and Swiatecki (15) by the dashed lines.

Fig. 6. Saddle-point shapes for various values of the fissionability parameter x. Shapes calculated in the two-spheroid approximation are given by the solid lines, and those calculated by Cohen and Swiatecki (15) by the dashed lines. For $x = 0.8$ the two saddle-point shapes ocurring in the two-spheroid approximation are shown.

Fig. 7. Maximum and minimum radii of equilibrium configurations, as functions of fissionability parameter x. The results calculated in the two-spheroid approximation are given by the solid lines, the results of Cohen and Swiatecki (15) by the dashed lines, and the results of Strutinskiĭ et al. (17) by the solid points. Note that the minimum radius calculated by Strutinskiĭ et al. for $x = 0.65$ is appreciably lower than that of Cohen and Swiatecki. The known limiting form of R_{min}/R_0 for $x \to 0$ is indicated by the straight line.

Fig. 8. The potential energy of saddle-point shapes, as a function of fissionability parameter x. The result calculated by using two spheroids connected by a conicoid of revolution is given by the solid line, the result of Cohen and Swiatecki (15) by the short-dashed line, and the result of Strutinskiĭ et al. (17) by the dot-dashed line.

Fig. 9. The surface energy B_S and Coulomb energy B_C of saddle-point shapes, as functions of fissionability parameter x. The function B_S is the surface energy in units of $E_S^{(0)}$, and B_C is the Coulomb energy in units of $E_C^{(0)}$. The results calculated by using two spheroids connected by a conicoid of revolution are given by the solid lines, and the results of Cohen and Swiatecki (15) by the dashed lines. The known values of B_S and B_C for $x = 0$ are indicated by open circles.

Fig. 10. Saddle-point shapes for various values of the fissionability parameter x. Shapes calculated by using two spheroids connected by a conicoid of revolution are given by the solid lines, and those calculated by Cohen and Swiatecki (15) by the dashed lines.

Fig. 11. Maximum and minimum radii of saddle-point shapes, as functions of fissionability parameter x. The results calculated by using two spheroids connected by a conicoid of revolution are given by the solid lines, the results of Cohen and Swiatecki (15) by the dashed lines, and the results of Strutinskiĭ et al. (17) by the solid points. Note that the minimum radius calculated by Strutinskiĭ et al. for $x = 0.65$ is appreciably lower than the other two results. The known limiting form of R_{min}/R_0 for $x \to 0$ is indicated by the straight line, and the value of R_{max}/R_0 for $x = 0$ by an open circle.

Fig. 12. Illustration of normal modes of oscillation about the saddle-point shape (when the saddle point is represented by two tangent spheroids). The fission mode is always unstable; the mass-asymmetry mode is

unstable for $x < x_{BG}$, and stable for $x > x_{BG}$. The bending and wriggling modes are each doubly degenerate, corresponding to rotations in two perpendicular planes. The twisting and axial-rotation modes consist of uniform (rather than oscillatory) rotation; for a system with zero total angular momentum the axial-rotation mode is not excited.

Fig. 13. Saddle-point stiffness constants (second derivatives of the potential energy, evaluated at the saddle point) for the original coordinate system, as functions of fissionability parameter x. The constant K_{UU} is in units of $E_S^{(0)}$; $K_{c_1c_1}$ and $K_{c_1c_2}$ are in units of $E_S^{(0)}/R_0^2$; K_{Uc_2} is in units of $E_S^{(0)}/R_0$; and $K_{\theta_1\theta_1}$ and $K_{\theta_1\theta_2}$ are in units of $E_S^{(0)}/\text{rad}^2$.

Fig. 14. Saddle-point stiffness constants (second derivatives of the potential energy, evaluated at the saddle point)for the normal-coordinate system, as functions of fissionability parameter x. The constant K_m is in units of $E_S^{(0)}$; K_s and K_d are in units of $E_S^{(0)}/R_0^2$; and K_b and K_w are in units of $E_S^{(0)}/\text{rad}^2$. The two-spheroid approximation to the Businaro-Gallone value of x is indicated by the arrow.

Fig. 15. Saddle-point effective masses, as functions of fissionability parameter x. The masses M_s, M_d, and M_f are in units of M_0; and M_b, M_w, M_t, and M_a are in units of $M_0 R_0^2$.

Fig. 16. Saddle-point frequencies of normal-mode oscillations, as functions of fissionability parameter x. The frequencies are in units of Ω_0 [see Eq. (4) for valuc of Ω_0].

Fig. 17. Saddle-point quantum energies of normal-mode oscillations for nuclei along the line of beta stability (50), as functions of fissionability parameter x.

Fig. 18. The total translational kinetic energy E^0 corresponding to the case in which the fragments initially start from rest at the saddle point, as a function of fissionability parameter x. The result calculated for nonviscous fragments is given by the solid line, the result for infinitely viscous fragments by the dot-dashed line, and a simple approximation to the former (see text) by the short-dashed line.

Fig. 19. The constant α [see Eq. (14)], as a function of fissionability parameter x. The result calculated for nonviscous fragments is given by the solid line, the result for infinitely viscous fragments by the dot-dashed line, and a simple approximation to the former (see text) by the short-dashed line.

Fig. 20. The excitation energy X_1^0 of a single fission fragment corresponding to the case in which the fragments initially start from rest at the saddle point, as a function of fissionability parameter x. The result calculated for nonviscous fragments is given by the solid line, and the result for infinitely viscous fragments by the dot-dashed line.

Fig. 21. The excitation-energy derivative $X_{1,s}$ [see Eq. (16)], as a function of fissionability parameter x. The result calculated for nonviscous fragments is given by the solid line, and the result for infinitely viscous fragments by the dot-dashed line.

Fig. 22. The excitation-energy derivative $X_{1,d}$ [see Eq. (16)], as a function of fissionability parameter x. The result calculated for nonviscous fragments is given by the solid line, and the result for infinitely viscous fragments by the dot-dashed line.

Fig. 23. The excitation-energy derivative $X_{1,m}$ [see Eq. (16)], as a function of fissionability parameter x. The result calculated for nonviscous fragments is given by the solid line, and the result for infinitely viscous fragments by the dot-dashed line.

Fig. 24. The angular-momentum derivative L_{1,p_b} [see Eq. (17)], as a function of fissionability parameter x. The result calculated for nonviscous fragments is given by the solid line, and the result for infinitely viscous fragments by the dot-dashed line. The short-dashed line represents the result that would follow if the torque exerted by one fragment on the other through the electrostatic interaction were zero.

Fig. 25. The angular-momentum derivative L_{1,p_w} [see Eq. (17)], as a function of fissionability parameter x. The result calculated for nonviscous fragments is given by the solid line, and the result for infinitely viscous fragments by the dot-dashed line. The short-dashed line represents the result that would follow if the torque exerted by one fragment on the other through the electrostatic interaction were zero.

Fig. 26. The angular-momentum derivative $L_{1,b}$ [see Eq. (17)], as a function of fissionability parameter x. The result calculated for nonviscous fragments is given by the solid line, and the result for infinitely viscous fragments by the dot-dashed line. For the value L_0 see Eq. (3).

Fig. 27. The angular-momentum derivative $L_{1,w}$ [see Eq.(17)], as a function of fissionability parameter x. The result calculated for nonviscous fragments is given by the solid line, and the result for infinitely viscous fragments by the dot-dashed line. For the value of L_0 see Eq. (3).

Fig. 28. Solution of equations of motion for $x = 0.90$ corresponding to initially starting the system from rest at the saddle point. The points are equally spaced in time at intervals of $0.107\ T_0$ [see Eq. (2) for value of T_0]. Note that the scission/configuration of tangent spheroids of minimum potential energy, whose location on the scission line is indicated by the open circle.

theta

Fig. 29. Coth $[\hbar\omega/(2\theta)]$, as a function of $2\theta/(\hbar\omega)$. The temperature dependence of the constants appearing in the probability distributions for the initial conditions is given by this function. Shown also is the asymptote of the function (dashed line).

Fig. 30. Contour map of the probability distribution of individual fragment excitation energies, $P(X_1, X_2)$ vs X_1 and X_2. The lines of constant probability (ellipses with axes rotated 45° with respect to the X_1 and X_2 axes) are labeled by relative probability. The value of X_1^0 is 21.3 MeV. The calculations are for the case of the compound nucleus ${}_{85}At^{213}$ ($x = 0.677$) at a nuclear temperature of 1.13 MeV (${}_{83}Bi^{209}$ + 65 - MeV α, for example).

Fig. 31. The probability distribution of excitation energy of a single fragment, $P(X_1)$ vs X_1. The value of X_1^0 is 21.3 MeV. The

calculations are for the case of nonviscous fragments and the fission of the compound nucleus $_{85}At^{213}$ ($x = 0.677$), at two different values of the nuclear temperature θ .

Fig. 32. The probability distribution of total fragment excitation energy, $P(X)$ vs X. The value of X^0 is 42.6 MeV. The calculations are for the case of nonviscous fragments and the fission of the compound nucleus $_{85}At^{213}$($x = 0.677$), at two different values of the nuclear temperature θ.

Fig. 33. Contour map of the probability distribution of total translational kinetic energy and fractional mass, $P(E,U)$ vs E and U, calculated to lowest order [Eq. (29)]. The lines of constant probability (ellipses with axes parallel to the E and U axes) are labeled by relative probability. The value of E^0 is 151.4 MeV. The calculations are for the case of nonviscous fragments and the fission of the compound nucleus $_{85}At^{213}$ ($x = 0.677$) at a nuclear temperature of 1.13 MeV ($_{83}Bi^{209} + 65$ - MeV α, for example).

Fig. 34. The probability distribution of the magnitude of angular momentum of a single fragment, $P(L_1)$ vs L_1 . The result that is calculated for nonviscous fragments (with hydrodynamic flow consisting of a superposition of an irrotational flow and a flow corresponding to a uniform rotation) is given by the solid line, and the result for infinitely viscous fragments by the dot-dashed line. The short-dashed line represents the result that would follow if the torque exerted by one fragment on the other through the electrostatic interaction were zero. The calculations are for the compound nucleus $_{85}At^{213}$ ($x = 0.677$) at a nuclear temperature of 1.13 MeV($_{83}Bi^{209}$+65-Mev α, for example).

Fig. 35. Contour map of the probability distribution of total translational kinetic energy and fractional mass, $P(E,U)$ vs E and U, calculated for initial conditions determined in the harmonic approximation [Eq. (36)]. The lines of constant probability are labeled by relative probability. The value of E^0 is 151.4 MeV. The calculations are for the case of nonviscous fragments and the fission of the compound nucleus ${}_{85}At^{213}$ ($x = 0.677$) at a nuclear temperature of 1.13 MeV (${}_{83}Bi^{209}$ + 65 - MeV α, for example).

Fig. 36. The functions $I_n(\beta)$ [defined by Eq. (43)] vs β, for $n = 0$, 1, and 2.

Fig. 37. The function $I_1(\beta)/I_0(\beta)$ vs β. The functions $I_n(\beta)$ are defined by Eq. (43).

Fig. 38. Third derivatives of the potential energy, evaluated at the saddle point, as functions of fissionability parameter x. The quantity K_{mms} is in units of $E_S^{(0)}/R_0$, and K_{sss} is in units of $E_S^{(0)}/R_0^3$.

Fig. 39. Contour map of the probability distribution of total translational kinetic energy and fractional mass, $P(E, U)$ vs E and U, including effects of anharmonicity [Eq. (48)]. The lines of constant probability are labeled by relative probability. The value of E^0 is 151.4 MeV. The calculations are for the case of nonviscous fragments and the fission of the compound nucleus ${}_{85}At^{213}$($x = 0.677$) at a nuclear temperature of 1.13 MeV (${}_{83}Bi^{209}$ + 65 - MeV α, for example).

Fig. 40. Experimental contour map of the probability distribution of total translational kinetic energy and fractional mass, $P(E^*,U)$ vs E^* and U. The superscript asterisk denotes that E is measured after neutron

emission from the fragments has occurred. The data are those of Burnett(86) for the compound nucleus $_{85}At^{213}$ (x = 0.677), formed from the reaction $_{83}Bi^{209}$ + 65 - MeV α , for which θ = 1.13 MeV. The labels on the lines of constant probability have the following significance: the contour labeled by 10, for example, passes through those regions of the E^* - U plane where an area of 6 MeV by 3 amu contains 1% of the total number of events.

Fig. 41. Probability distributions for fragment mass (top) and for total translational kinetic energy (bottom). The theoretical curves (solid lines) are calculated for initial conditions determined in the harmonic approximation [from Eq. (36)]. The data are those of Plasil(77) for the compound nucleus $_{82}Pb^{198}$ (x = 0.677), formed from the heavy-ion-induced reaction $_{74}W^{182}$ + $_{8}O^{16}$. The results for a bombarding energy of 102 MeV (θ = 1.37 MeV) are given by the solid points, and for a bombarding energy of 165 MeV (θ = 2.07 MeV) by the open circles. The superscript asterisk denotes that E is measured after neutron emission from the fragments has occurred.

Fig. 42. Mean total translational kinetic energies, as functions of fragment mass AU. The theoretical results that are calculated for initial conditions determined in the harmonic approximation [from Eq. (36)] are given by the solid lines, and the results that are calculated by including effects of anharmonicity [from Eq. (48)] are given by the dashed lines. The data (solid points) are as follows: Burnett (76): $_{83}Bi^{209}$ + 65-MeV α = $_{85}At^{213}$(x = 0.677, θ = 1.13 MeV), and

$_{79}Au^{197}$ + 70-MeV α = $_{81}Tl^{201}$(x = 0.651, θ = 1.28 MeV); Plasil (77): $_{74}W^{182}$ + 102-MeV $_{8}O^{16}$ = $_{82}Pb^{198}$(x = 0.677, θ = 1.37 MeV), and $_{74}W^{182}$+165-MeV $_{8}O^{16}$ = $_{82}Pb^{198}$(x = 0.677, θ = 2.07 MeV). Note that the left-hand scale and the right-hand scale are different.

Fig. 43. Variances in the distributions of total translational kinetic energy, as functions of fragment mass AU. The theoretical results that are calculated for initial conditions determined in the harmonic approximation [from Eq. (36)] are given by the solid lines, and the results that are calculated by including effects of anharmonicity [from Eq. (48)] are given by the dashed lines. The data (solid points) are as follows: Burnett (76): $_{83}Bi^{209}$ + 65-MeV α = $_{85}At^{213}$ (x = 0.677, θ = 1.13 MeV), and $_{79}Au^{197}$ + 70-MeV α = $_{81}Tl^{201}$(x = 0.651, θ = 1.28 MeV); Plasil (77): $_{74}W^{182}$ + 102-MeV $_{8}O^{16}$ = $_{82}Pb^{198}$(x = 0.677, θ = 1.37 MeV), and $_{74}W^{182}$ + 165-MeV $_{8}O^{16}$ = $_{82}Pb^{198}$(x = 0.677, θ = 2.07 MeV).

Fig. 44. Variances in the distributions of fragment mass, as functions of total translational kinetic energy E. The theoretical results that are calculated for initial conditions determined in the harmonic approximation [from Eq. (36)] are given by the solid lines, and the results that are calculated by including effects of anharmonicity [from Eq. (48)] are given by the dashed lines. The data (solid points) are as follows: Burnett (76): $_{83}Bi^{209}$+65-MeV α = $_{85}At^{213}$ (x = 0.677, θ = 1.13 MeV), and $_{79}Au^{197}$ + 70-MeV α = $_{81}Tl^{201}$ (x = 0.651, θ = 1.28 MeV); Plasil (77): $_{74}W^{182}$ + 102-MeV $_{8}O^{16}$ = $_{82}Pb^{198}$ (x = 0.677, θ = 1.37 MeV), and $_{74}W^{182}$ + 165-MeV $_{8}O^{16}$ = $_{82}Pb^{198}$(x = 0.677, θ = 2.07 MeV).

Fig. 45. Variances in the distributions of fragment mass (top), and variances in the distributions of total translational kinetic energy (bottom), as functions of nuclear temperature Θ. The theoretical curves (solid lines) are calculated for initial conditions determined in the harmonic approximation [from Eq. (36)]. The data are those of Plasil(77). The compound nucleus ${}_{82}Pb^{198}$ ($x = 0.677$) was formed from the reaction ${}_{74}W^{182} + {}_{8}O^{16}$, and the compound nucleus ${}_{76}Os^{186}$ ($x = 0.619$) from each of two reactions: ${}_{68}Er^{170} + {}_{8}O^{16}$ (solid points) and ${}_{70}Yb^{174} + {}_{6}C^{12}$ (open circles).

Fig. 46. Most probable total translational kinetic energy, as a function of fissionability parameter x. The result calculated for non-viscous fragments is given by the solid line, the result for infinitely viscous fragments by the dot-dashed line, and a simple approximation to the former by the short-dashed line. The data are those of Viola and Sikkeland (72).

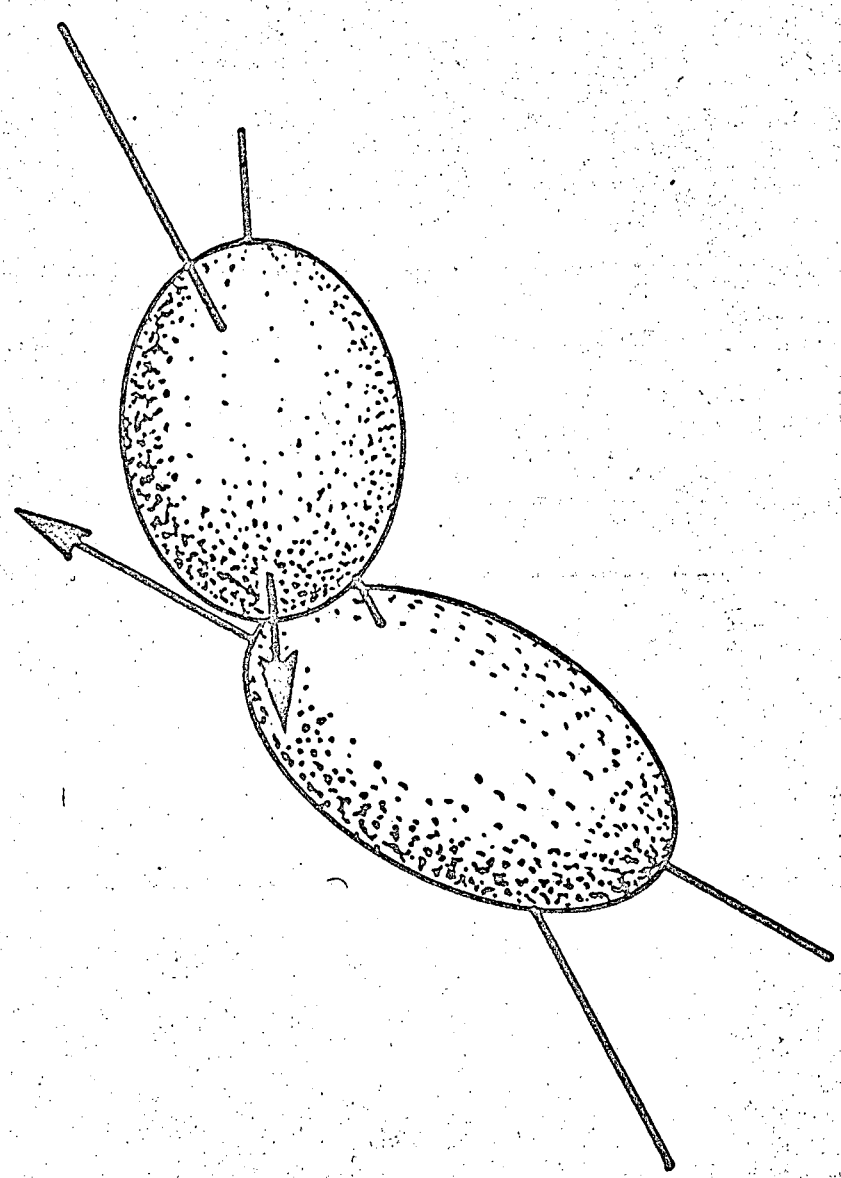

Fig. 1

MU-33372

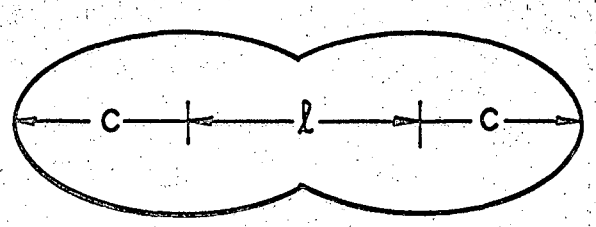

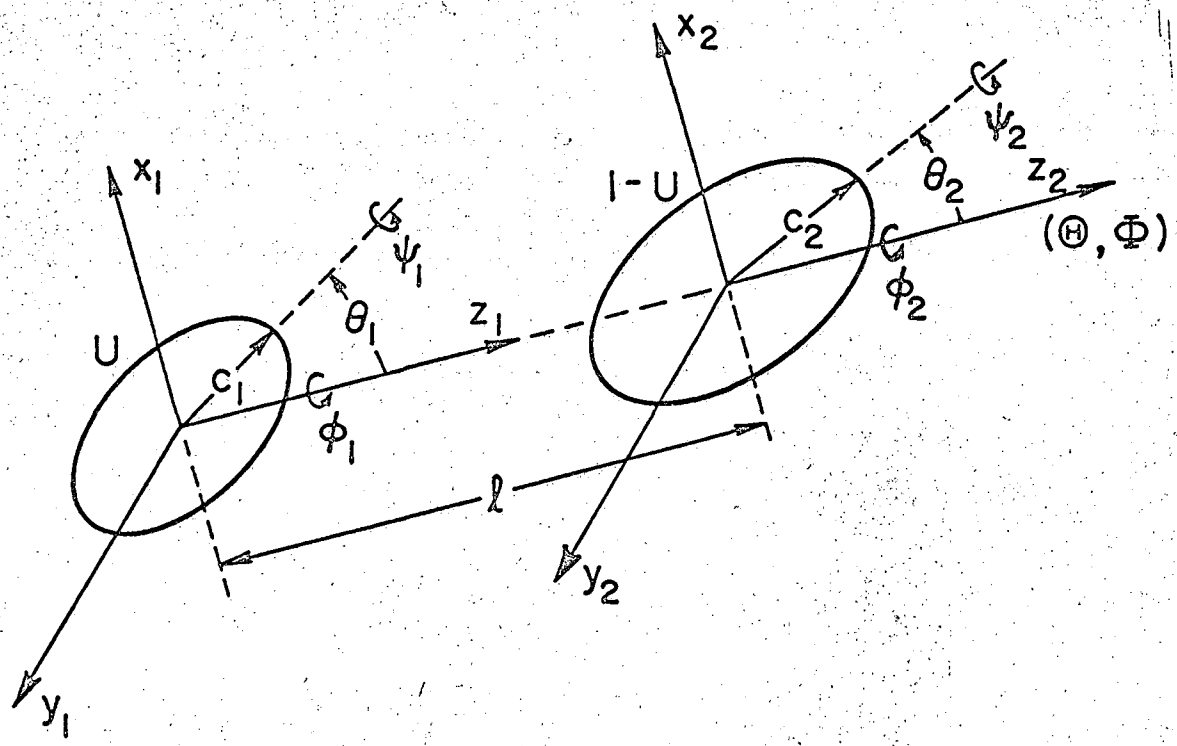

Fig. 2

MU-33547

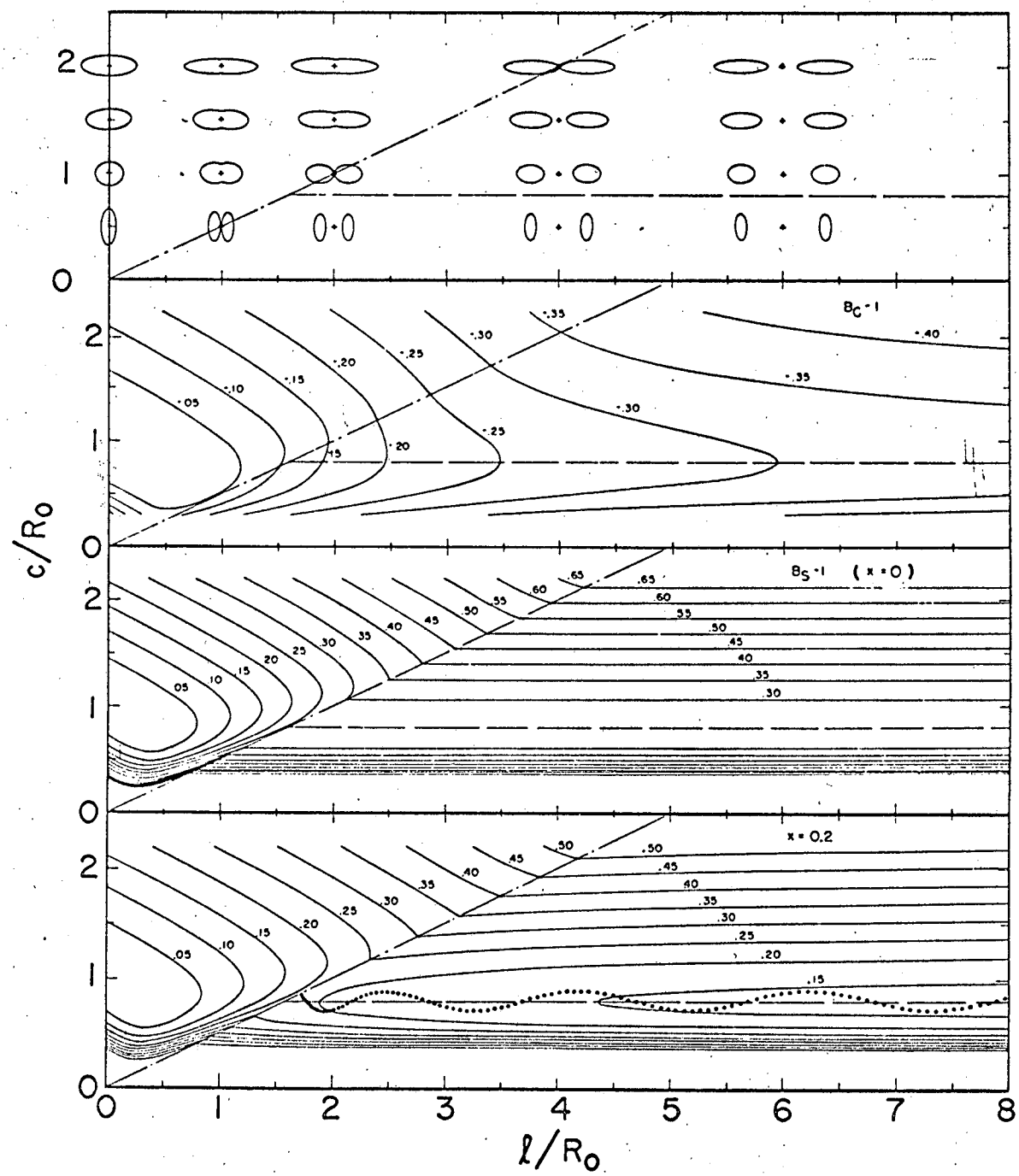

Fig. 3a

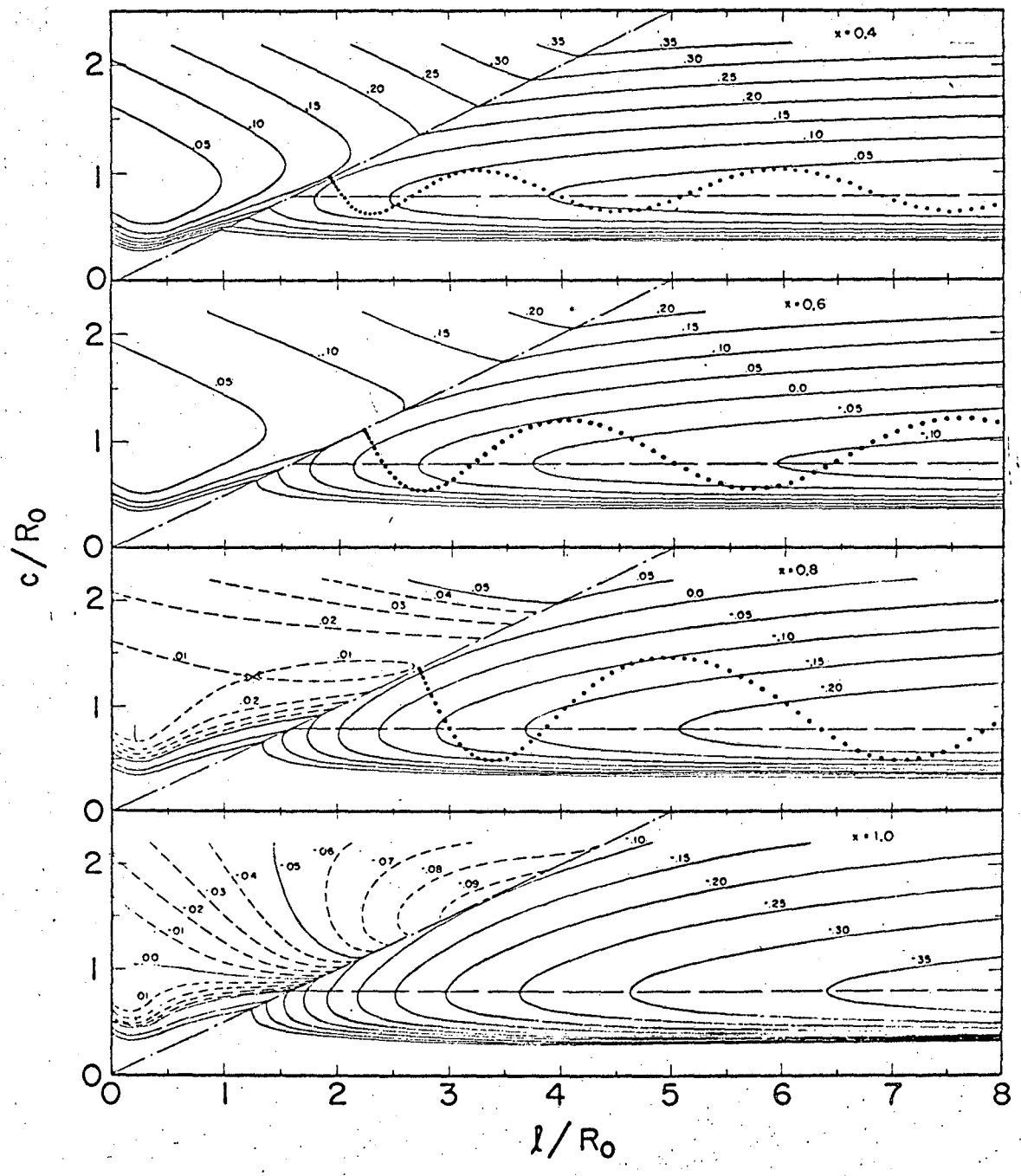

Fig. 3b

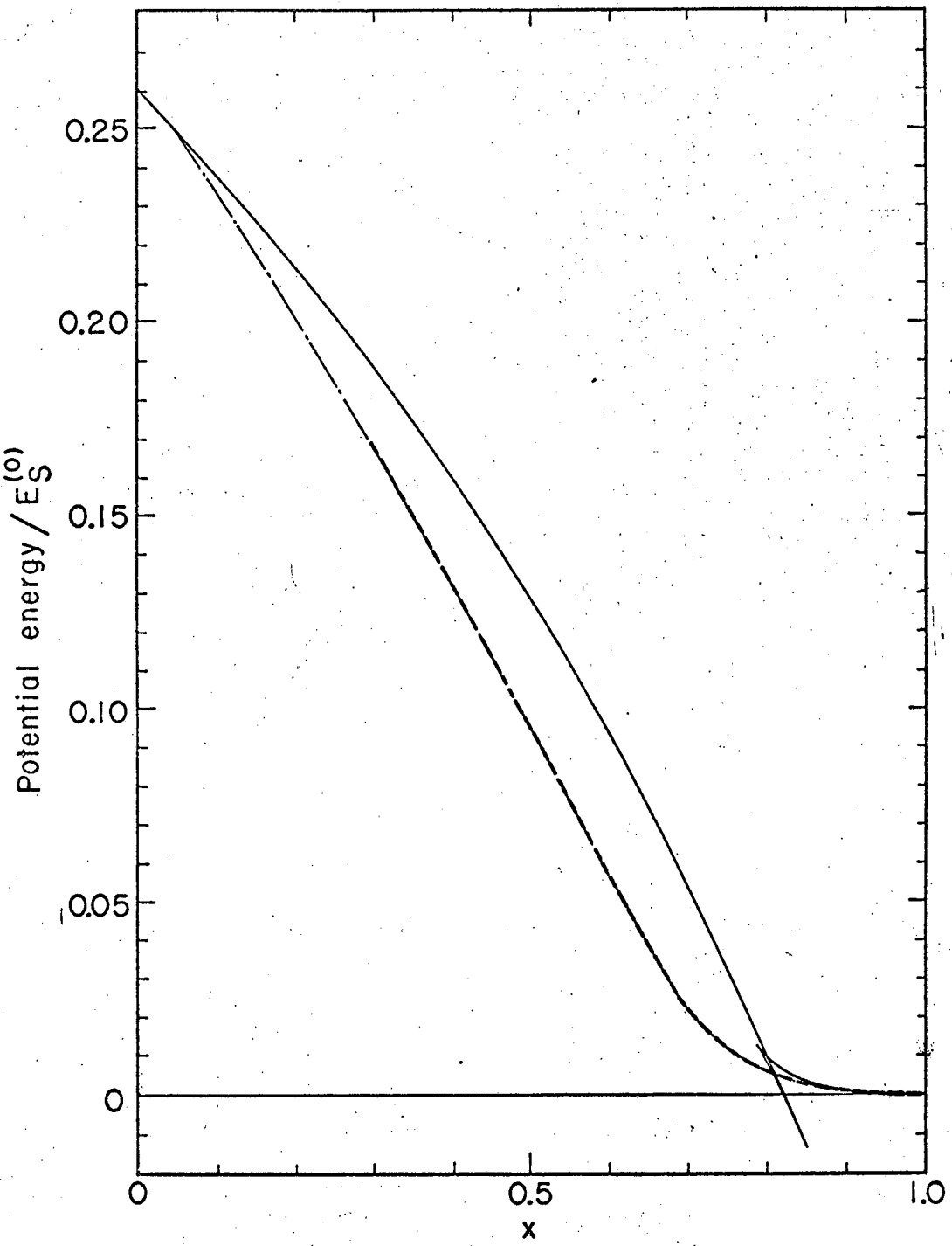

Fig. 4

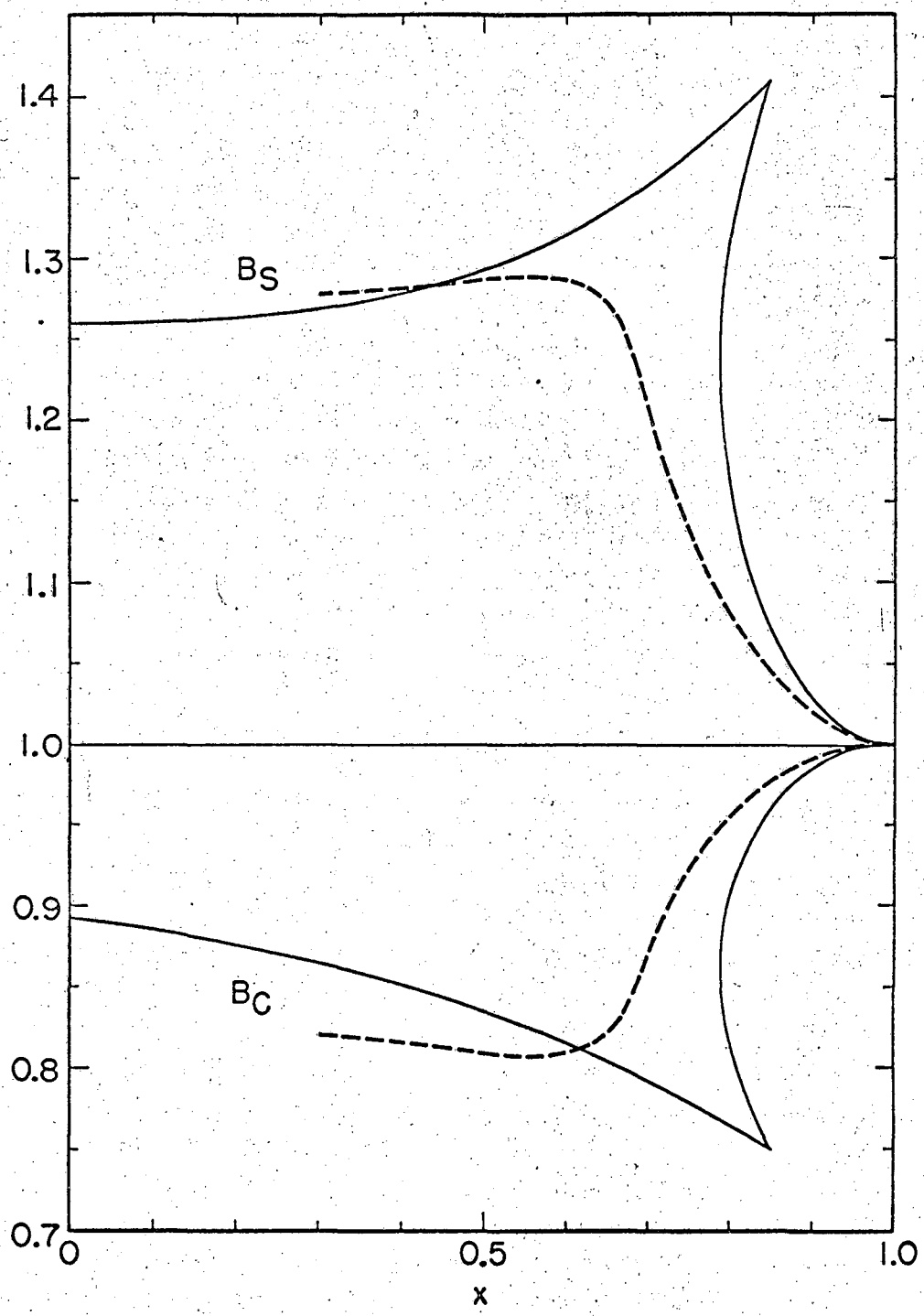

MUB-2393

Fig. 5

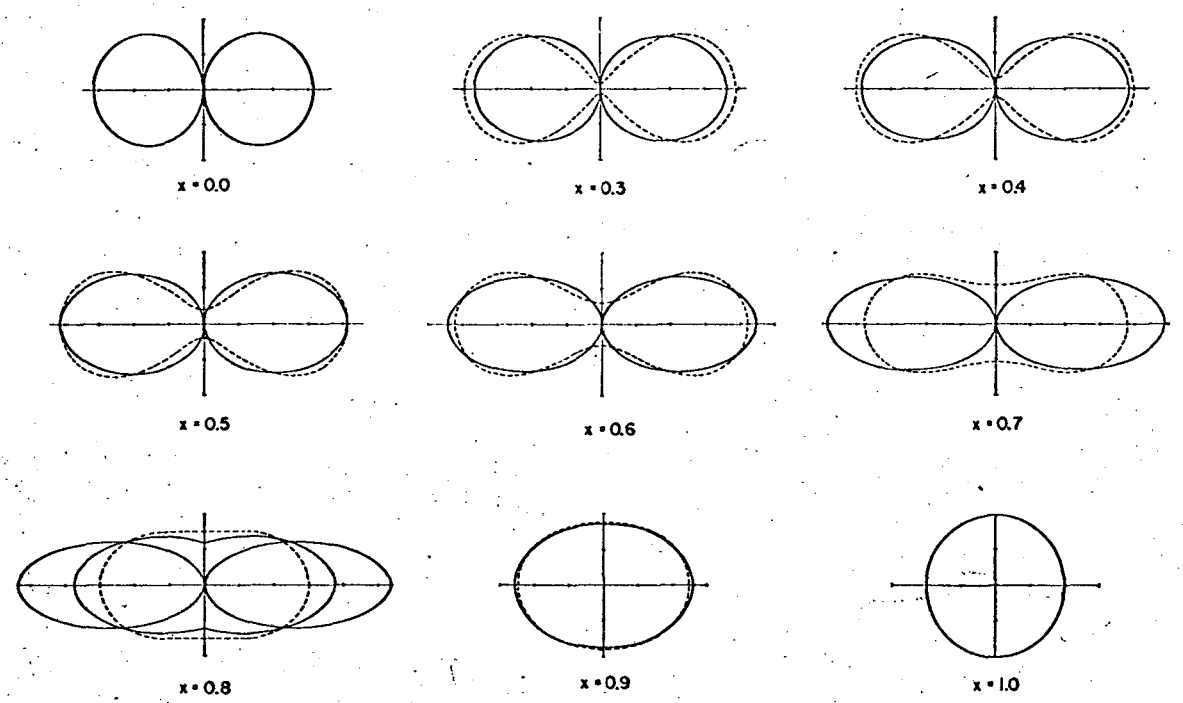

Fig. 6

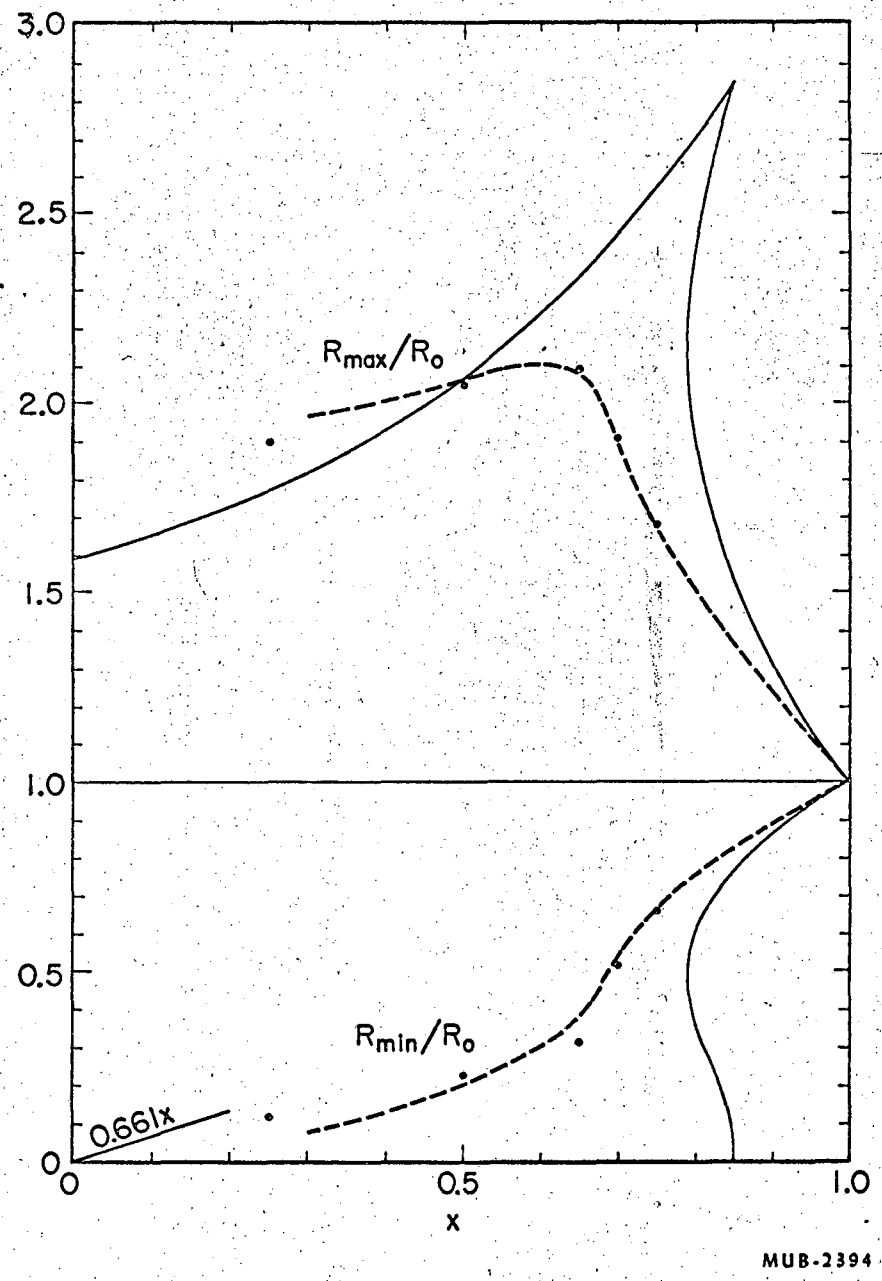

Fig. 7

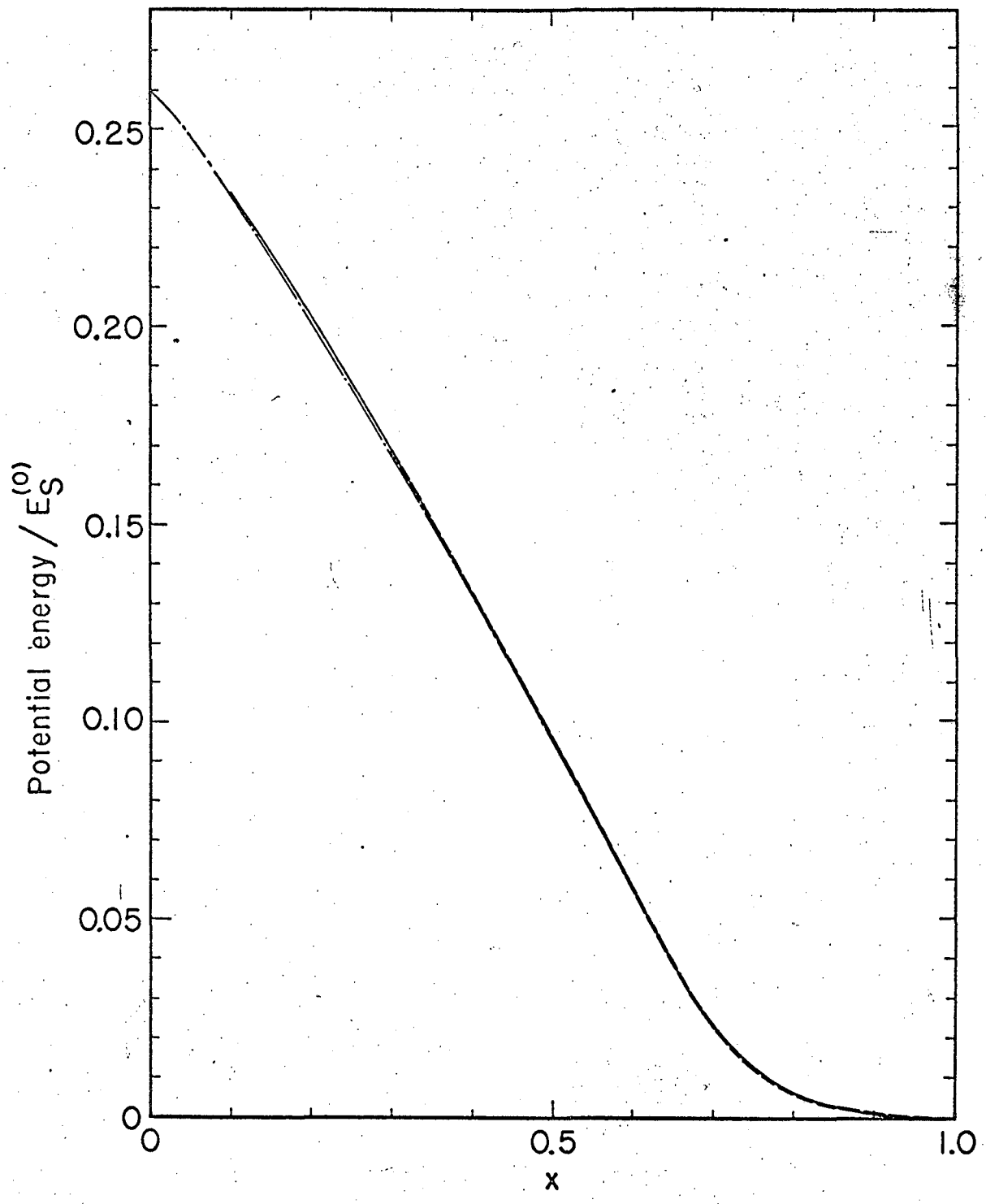

MUB-2422

Fig. 8

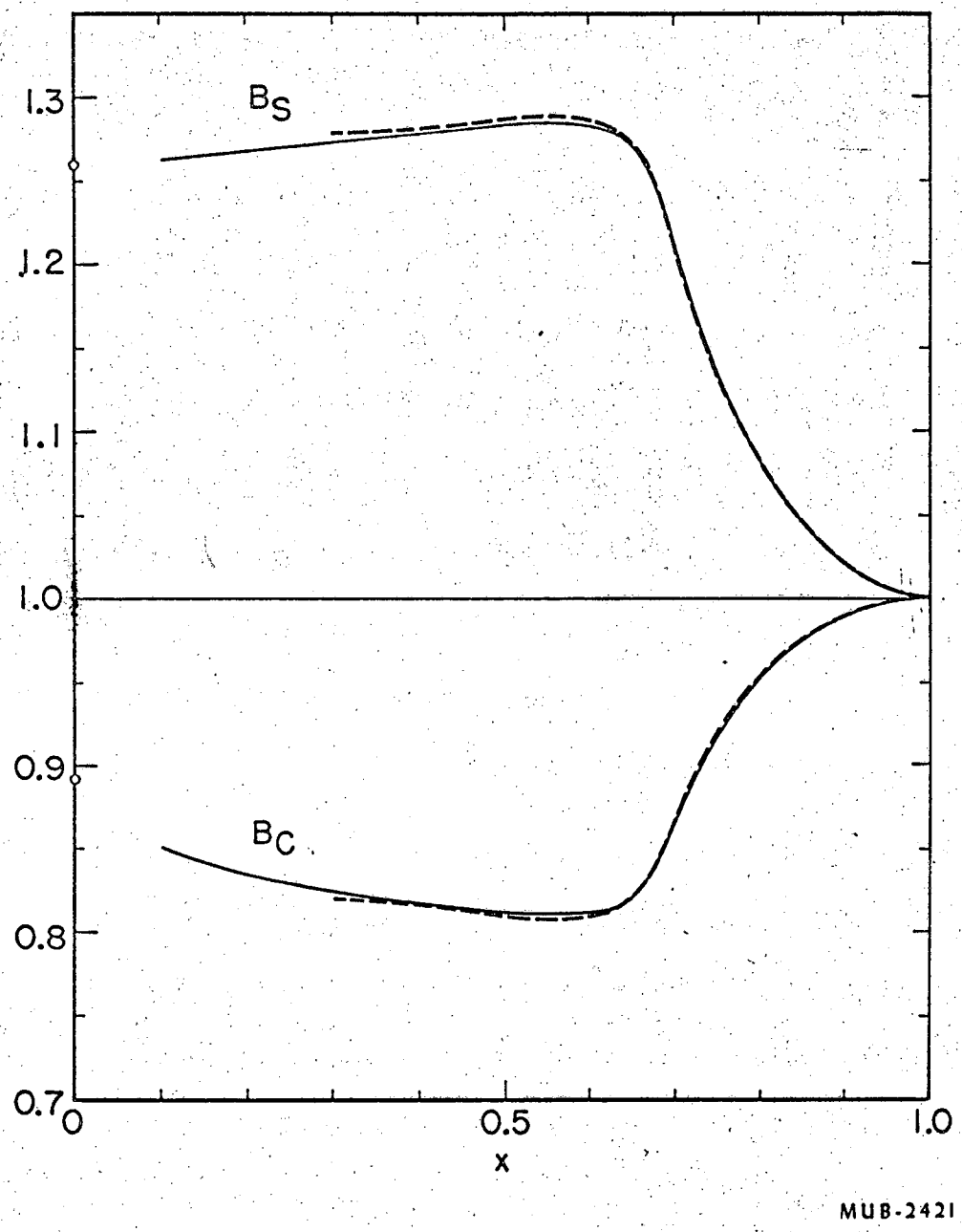

Fig. 9

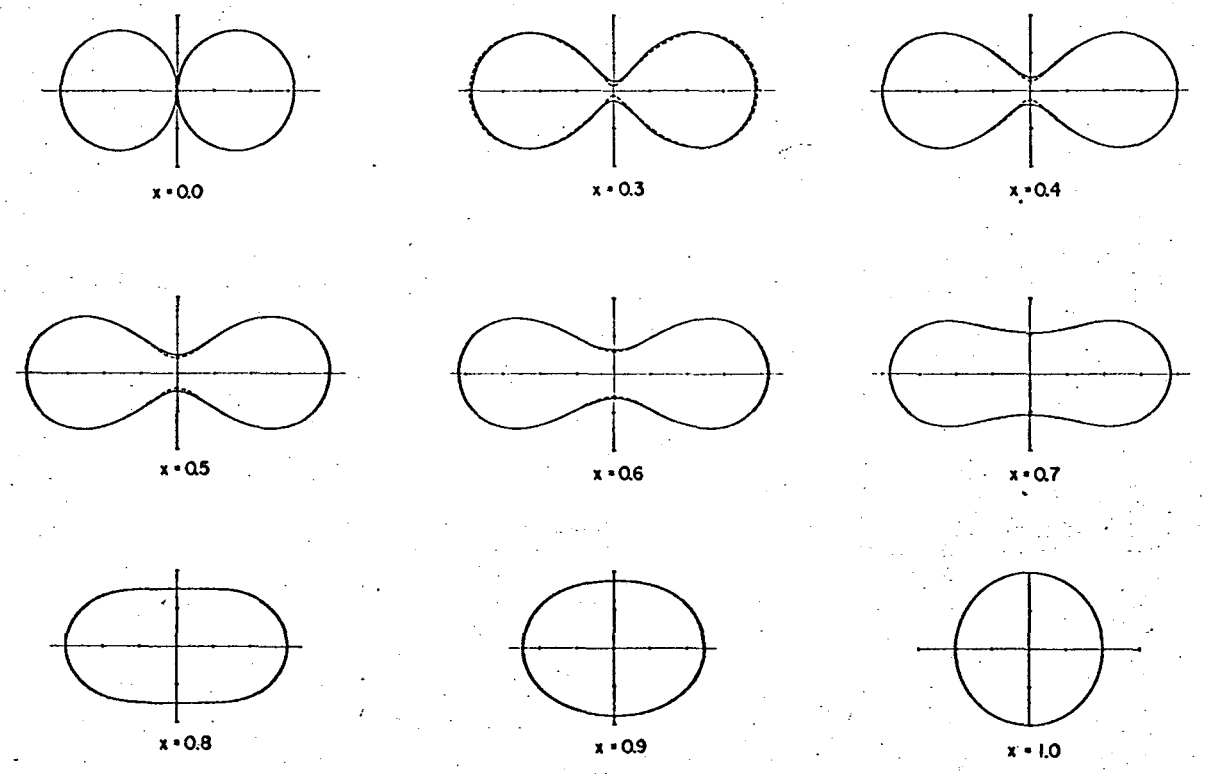

Fig. 10

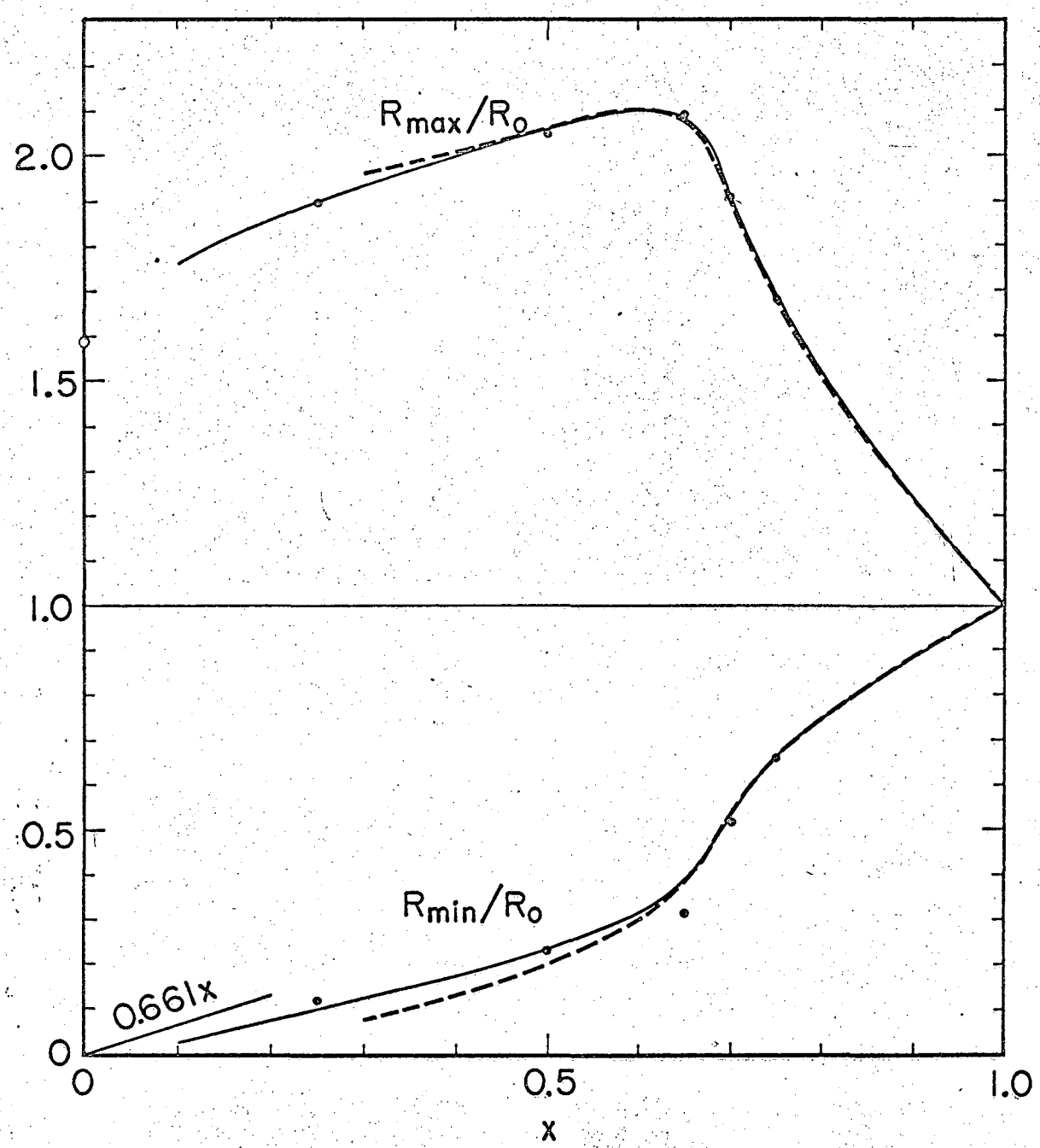

MUB-2420

Fig. 11

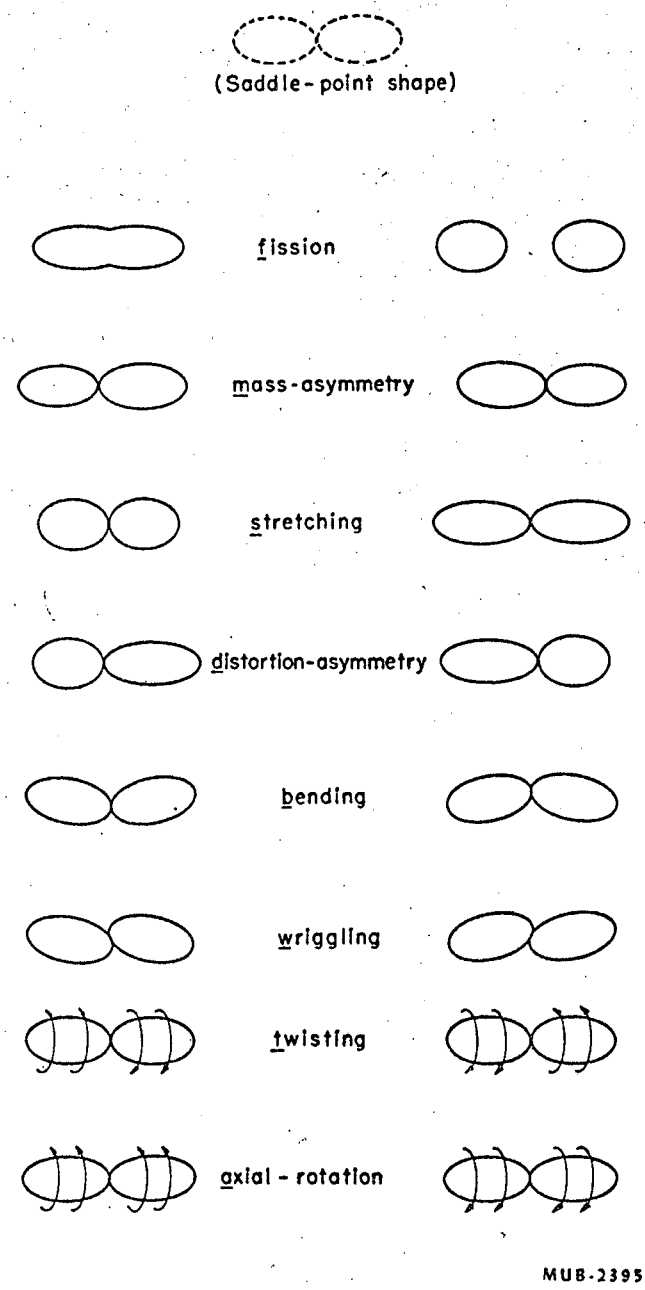
(Saddle-point shape)
fission
mass-asymmetry
stretching
distortion-asymmetry
bending
wriggling
twisting
axial-rotation
MUB-2395

Fig. 12

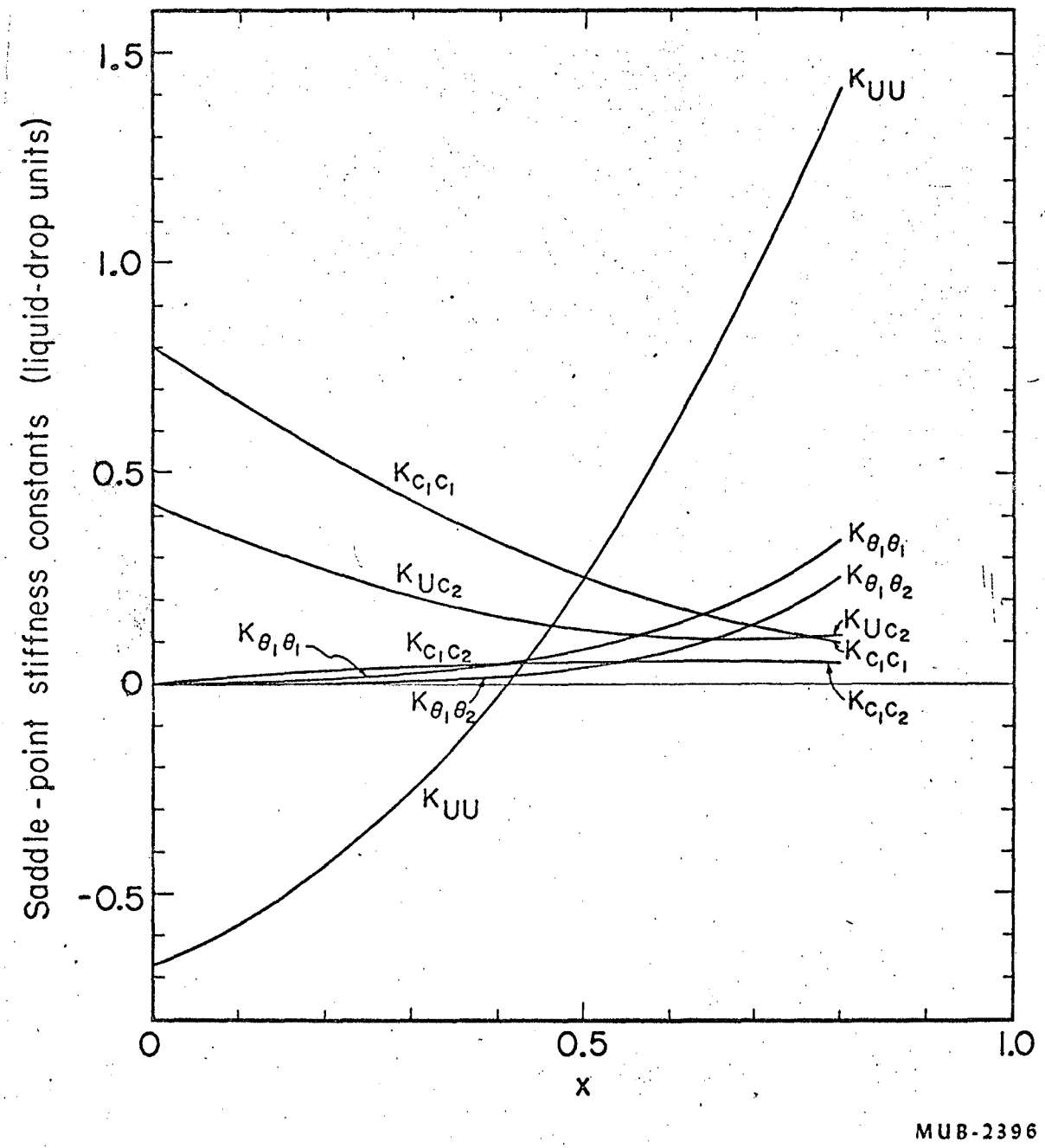

MUB-2396

Fig. 13

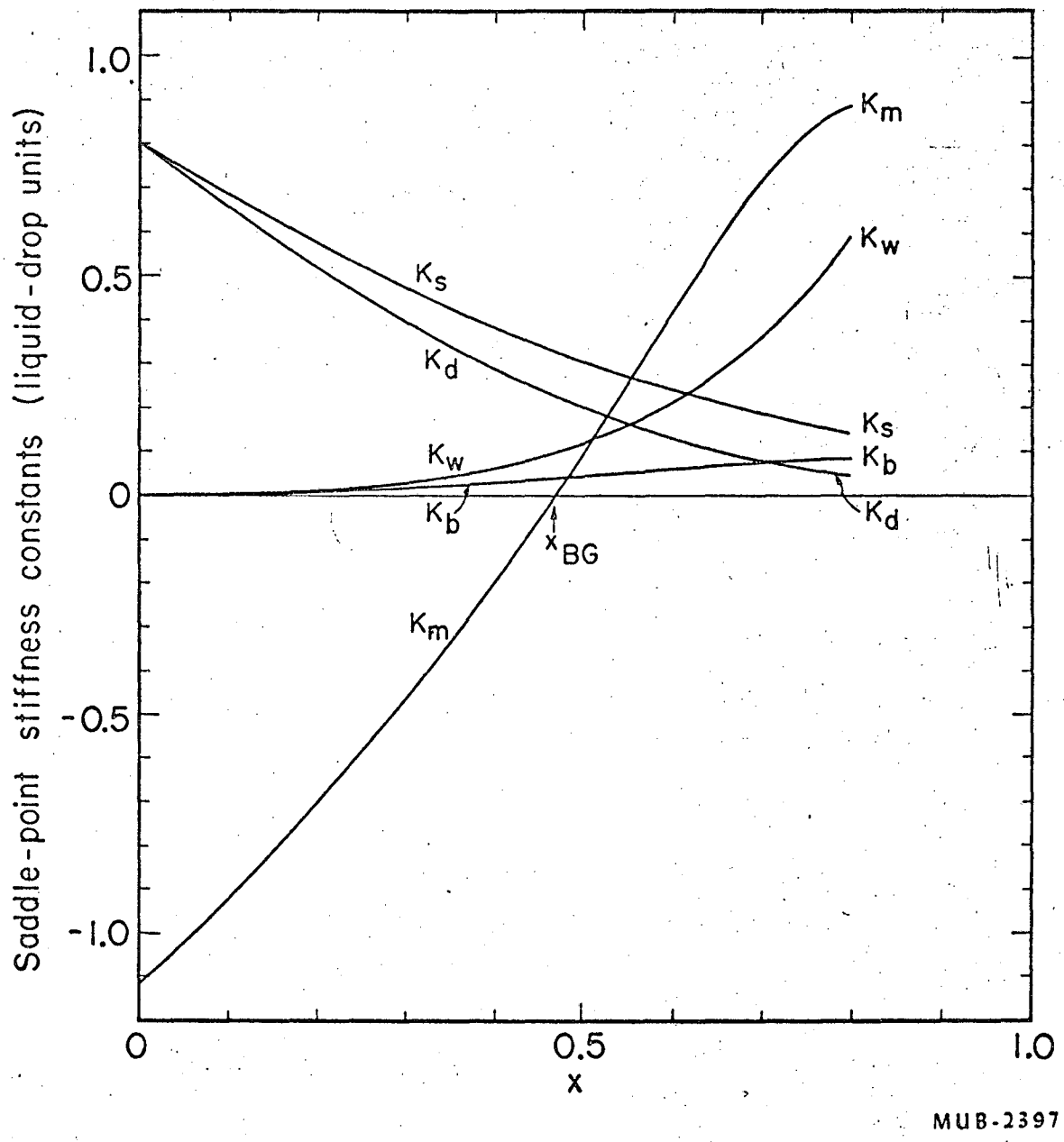
1.0
0.5
0
-0.5
-1.0
Saddle-point stiffness constants (liquid-drop units)
0
0.5
1.0
x
K_m
K_w
K_s
K_d
K_s
K_b
K_d
K_w
K_b
x_{BG}
K_m
MUB-2397

Fig. 14

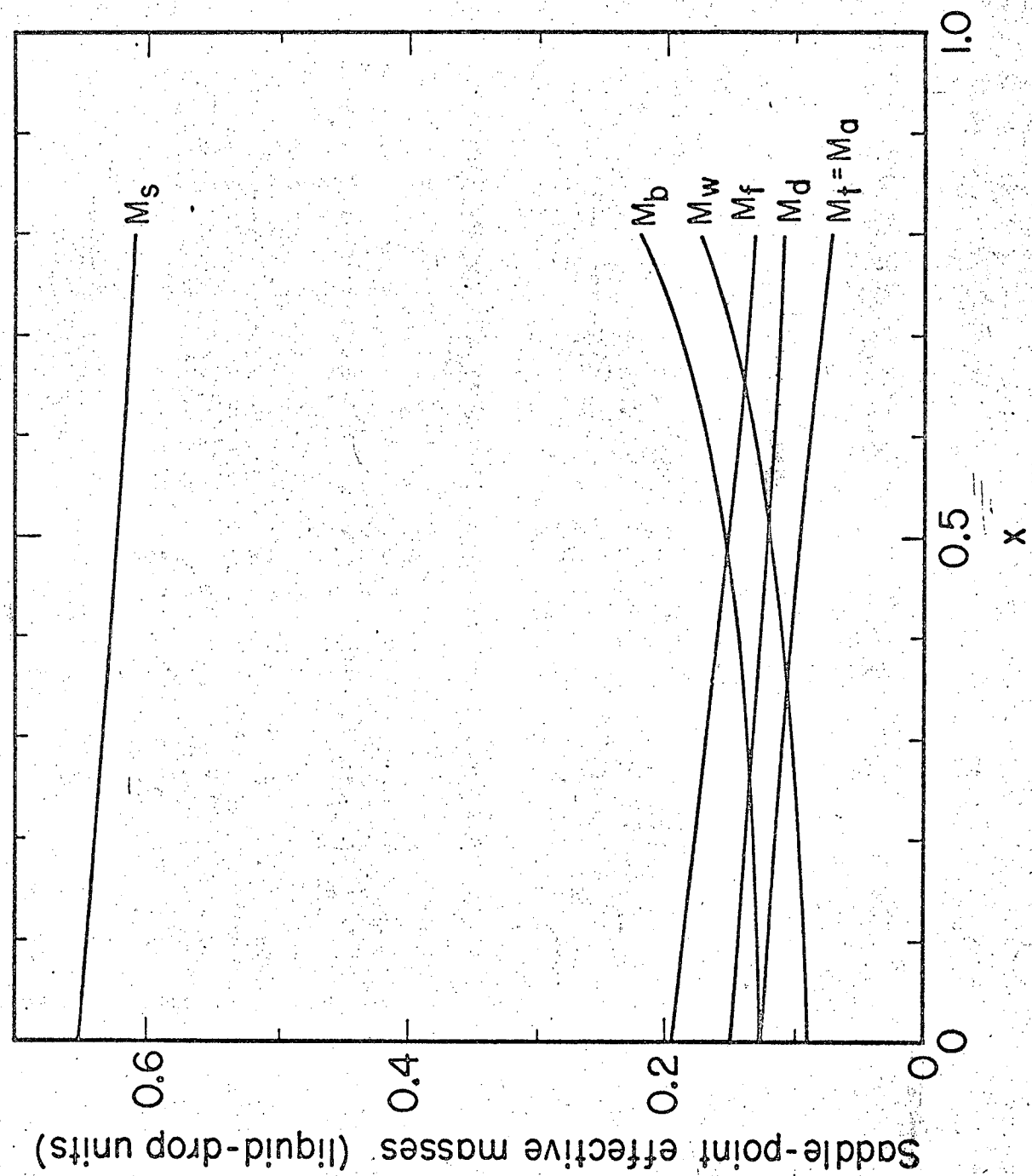
Saddle-point effective masses (liquid-drop units)
0.6
0.4
0.2
0
0.5
1.0
x
M_s
M_b
M_w
M_f
M_d
$M_t = M_a$
MU-33373

Fig. 15

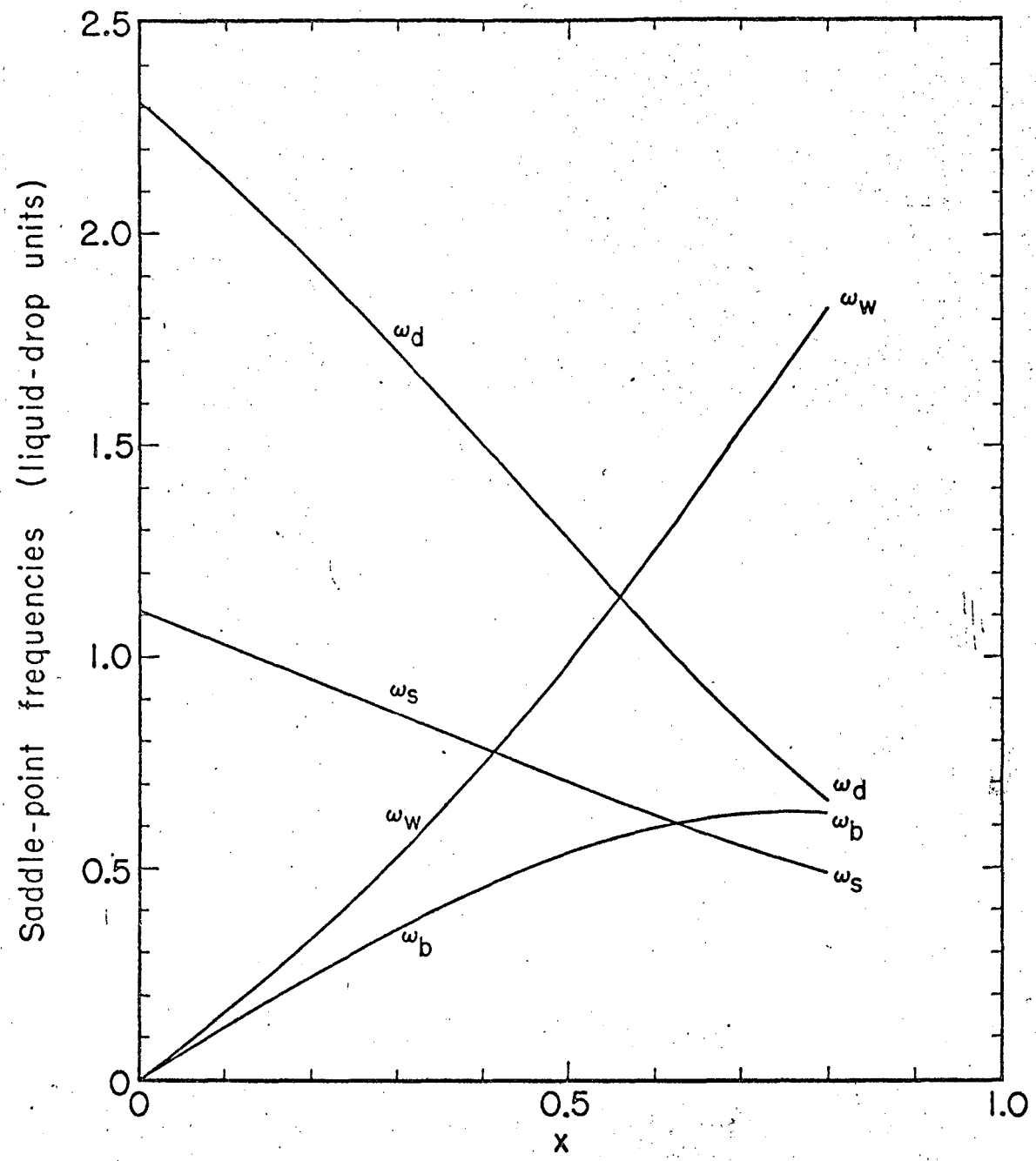

Fig. 16

MUB-2398

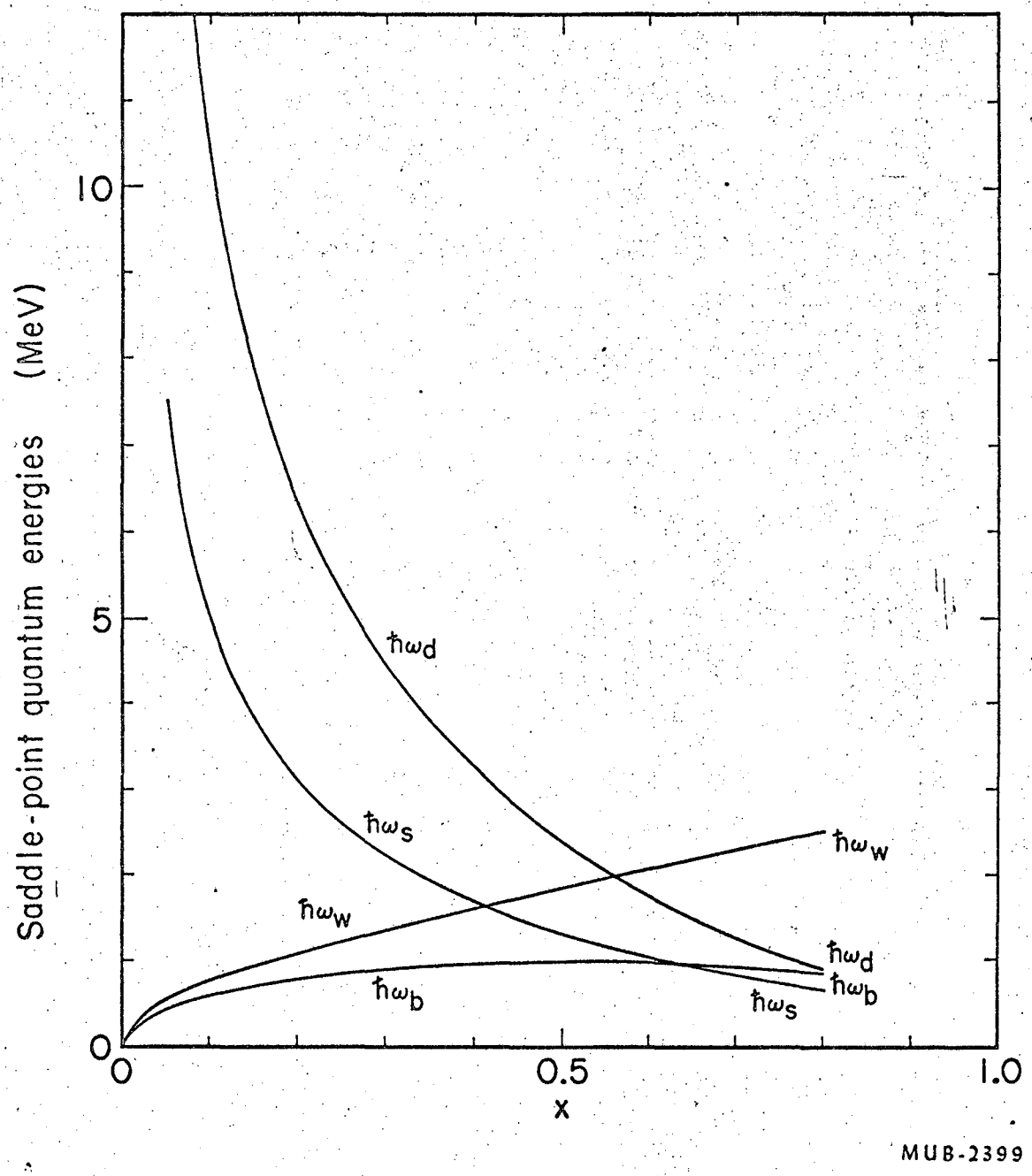
Saddle-point quantum energies (MeV)
10
5
0
0
0.5
1.0
x
ħωd
ħωs
ħωw
ħωw
ħωd
ħωb
ħωb
ħωs
MUB-2399

Fig. 17

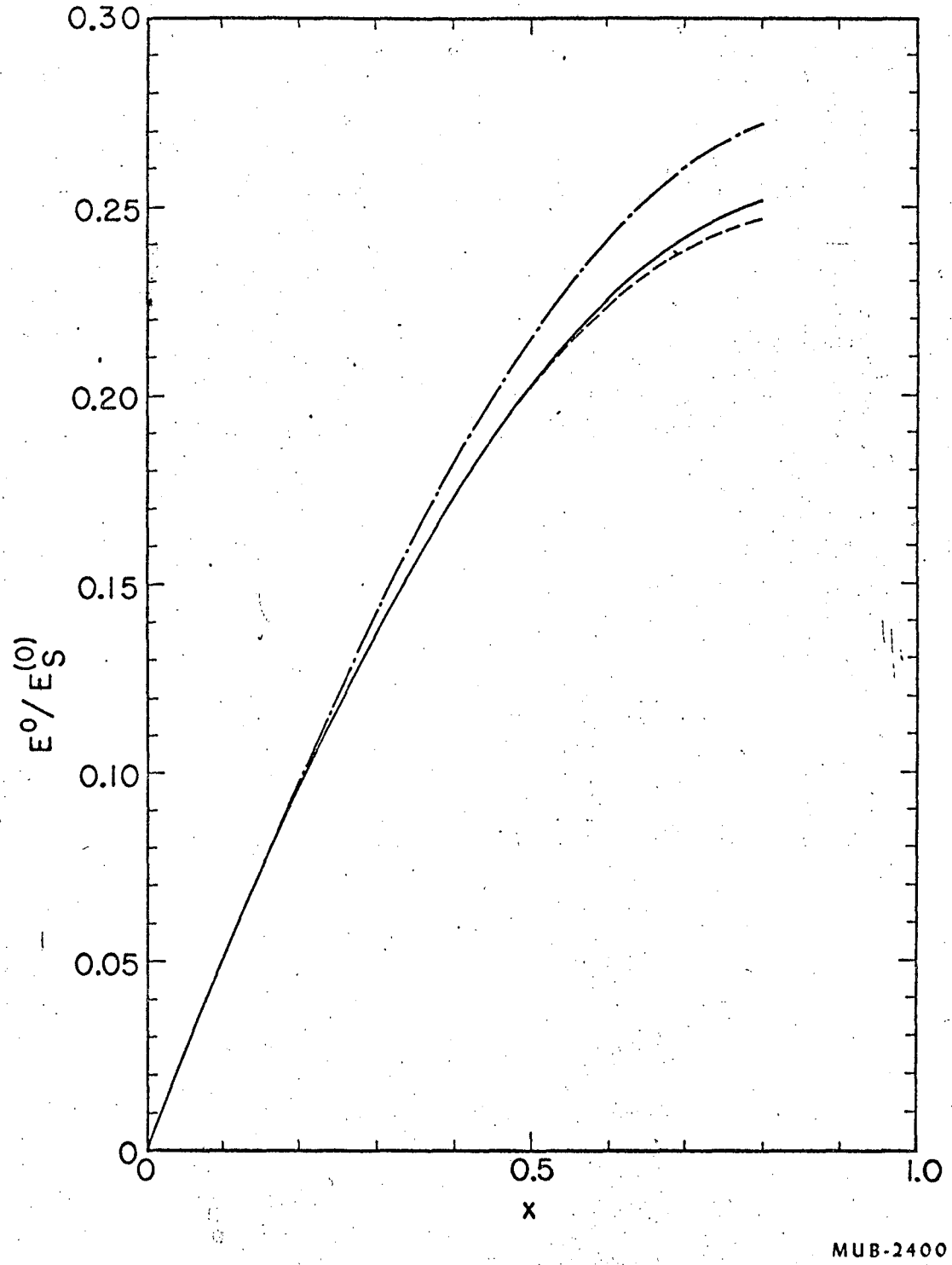

Fig. 18

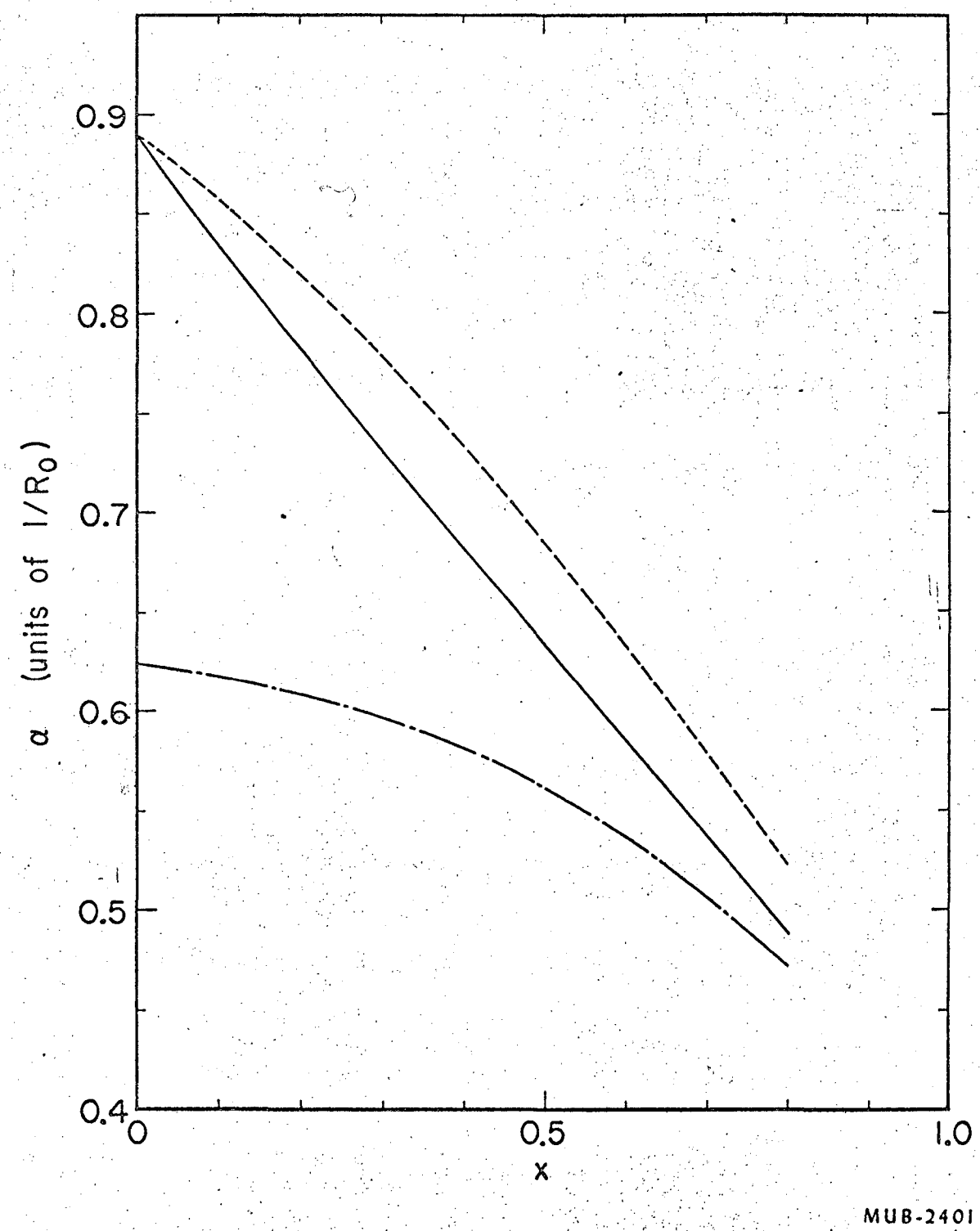

Fig. 19

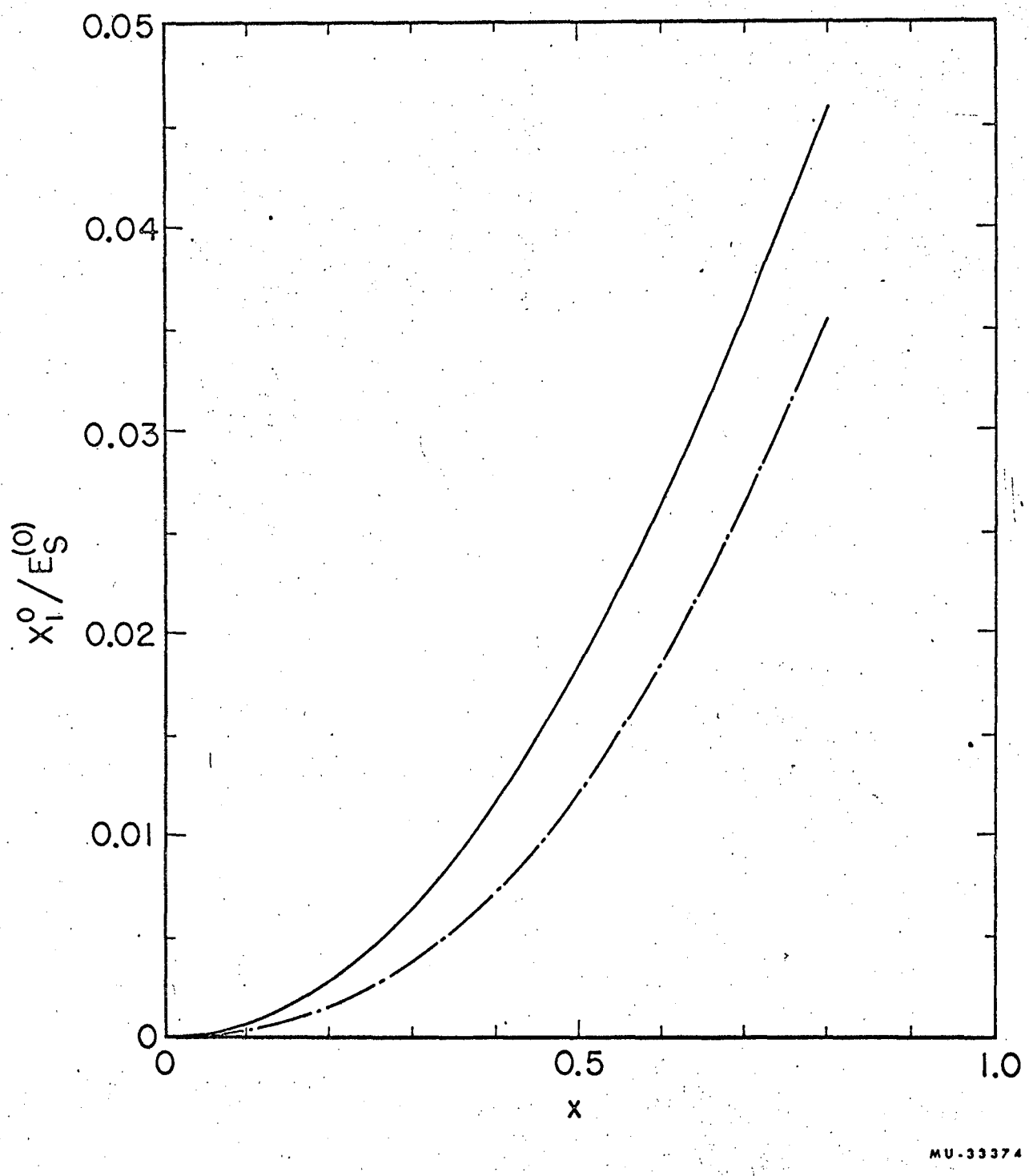

Fig. 20

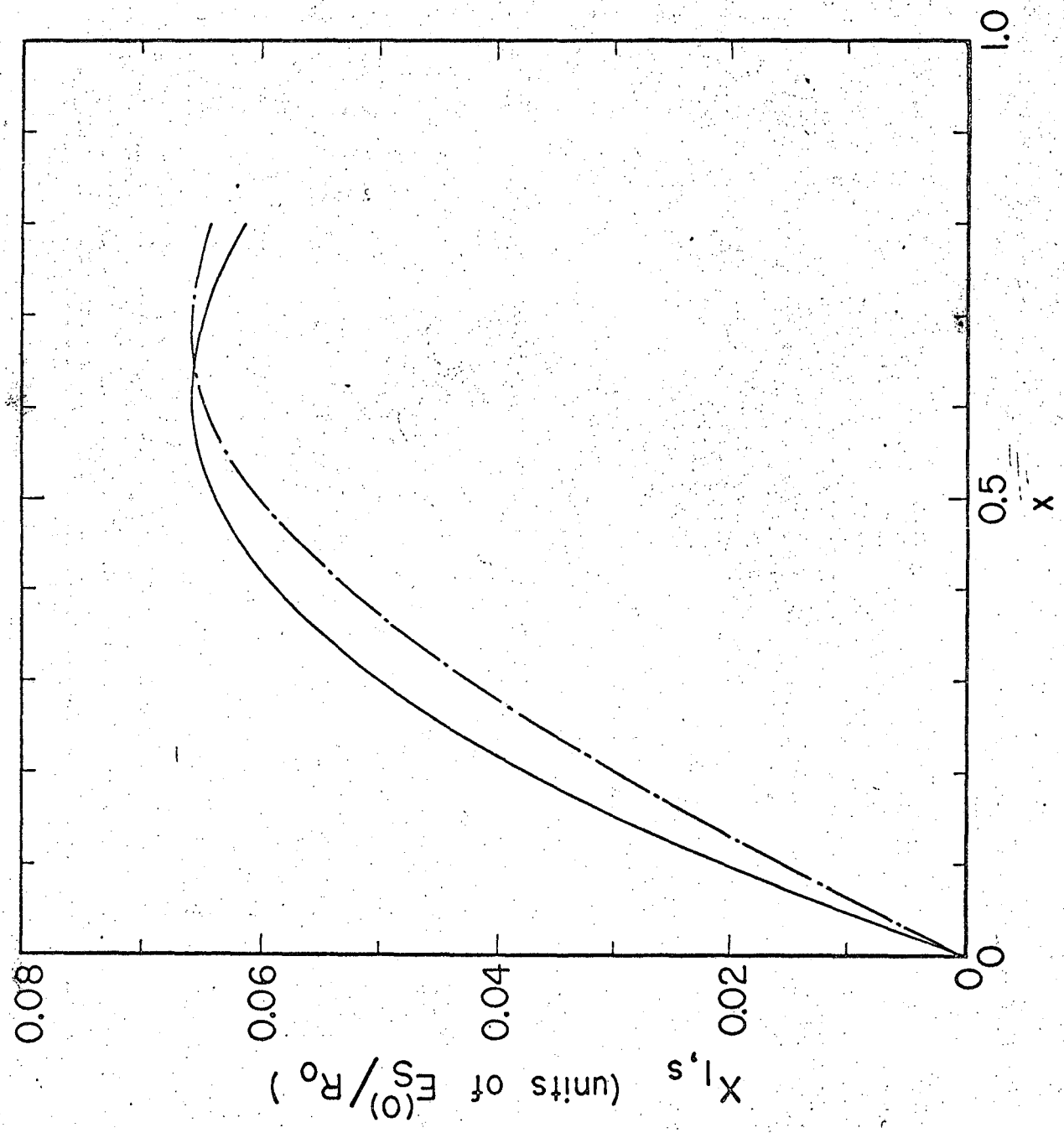
0.08
0.06
0.04
0.02
0
$X_{1,s}$ (units of $\varepsilon_S^{(0)}/R_o$)
0
0.5
1.0
x
MU-33375

Fig. 21

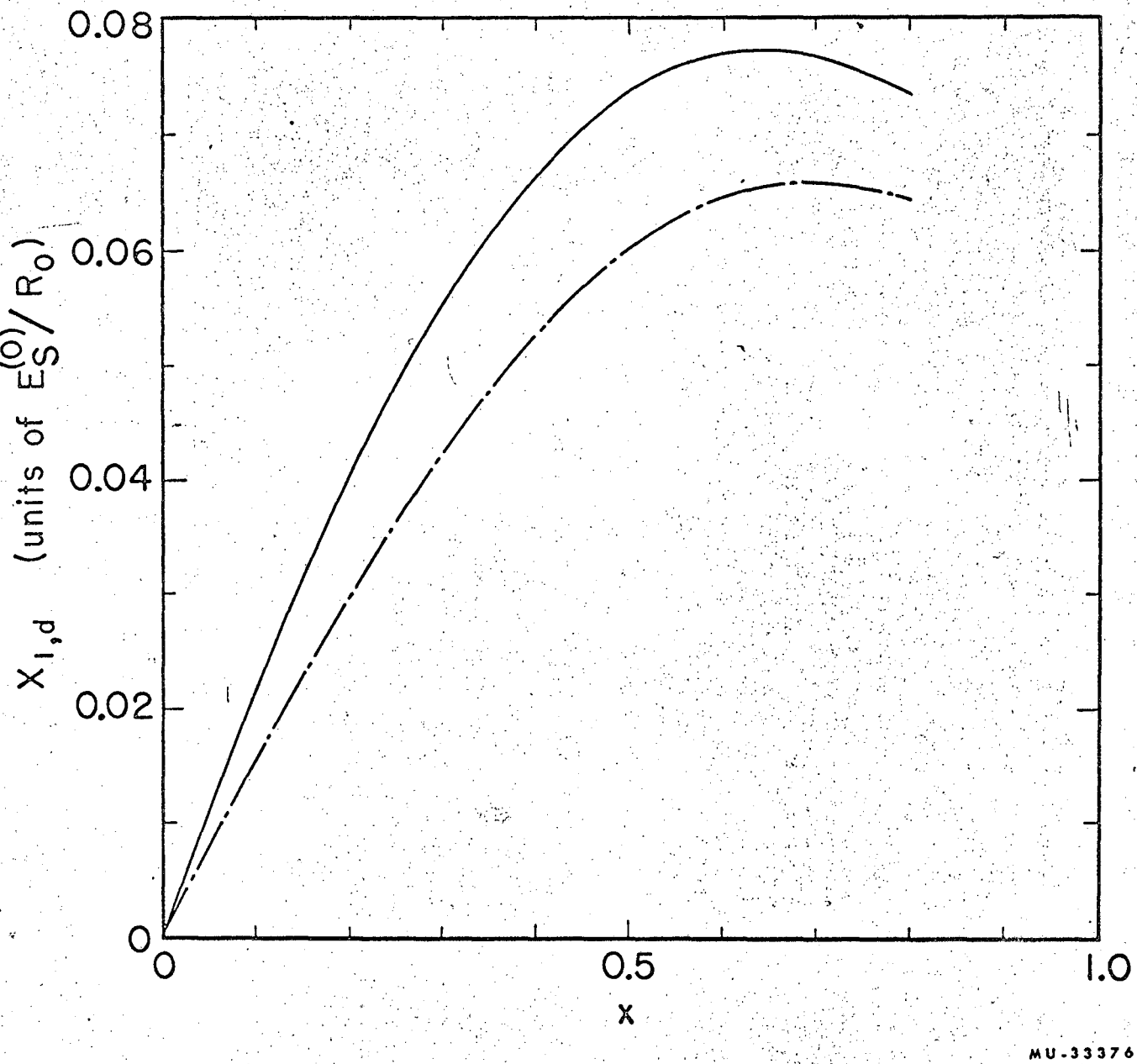

Fig. 22

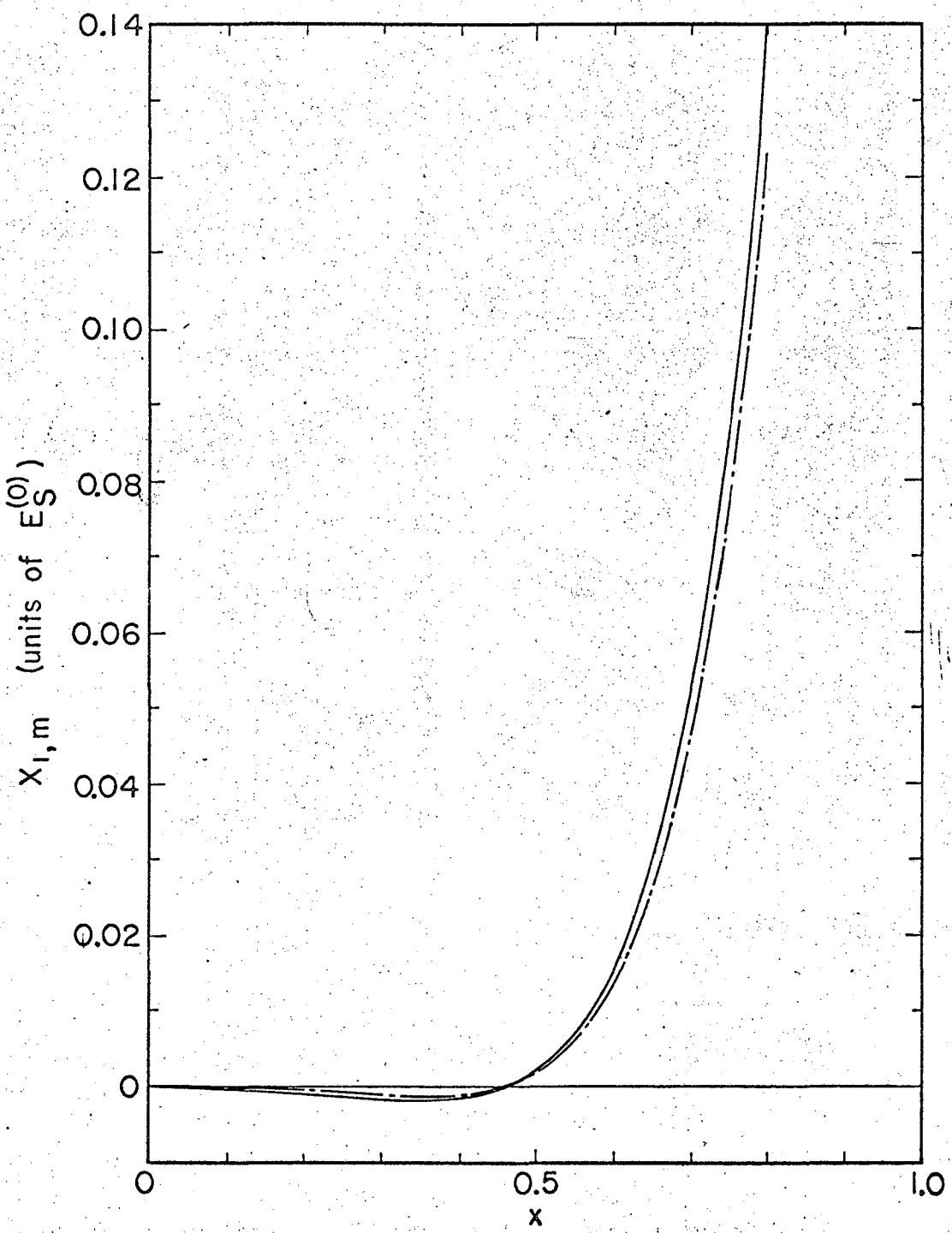

MUB-2402

Fig. 23

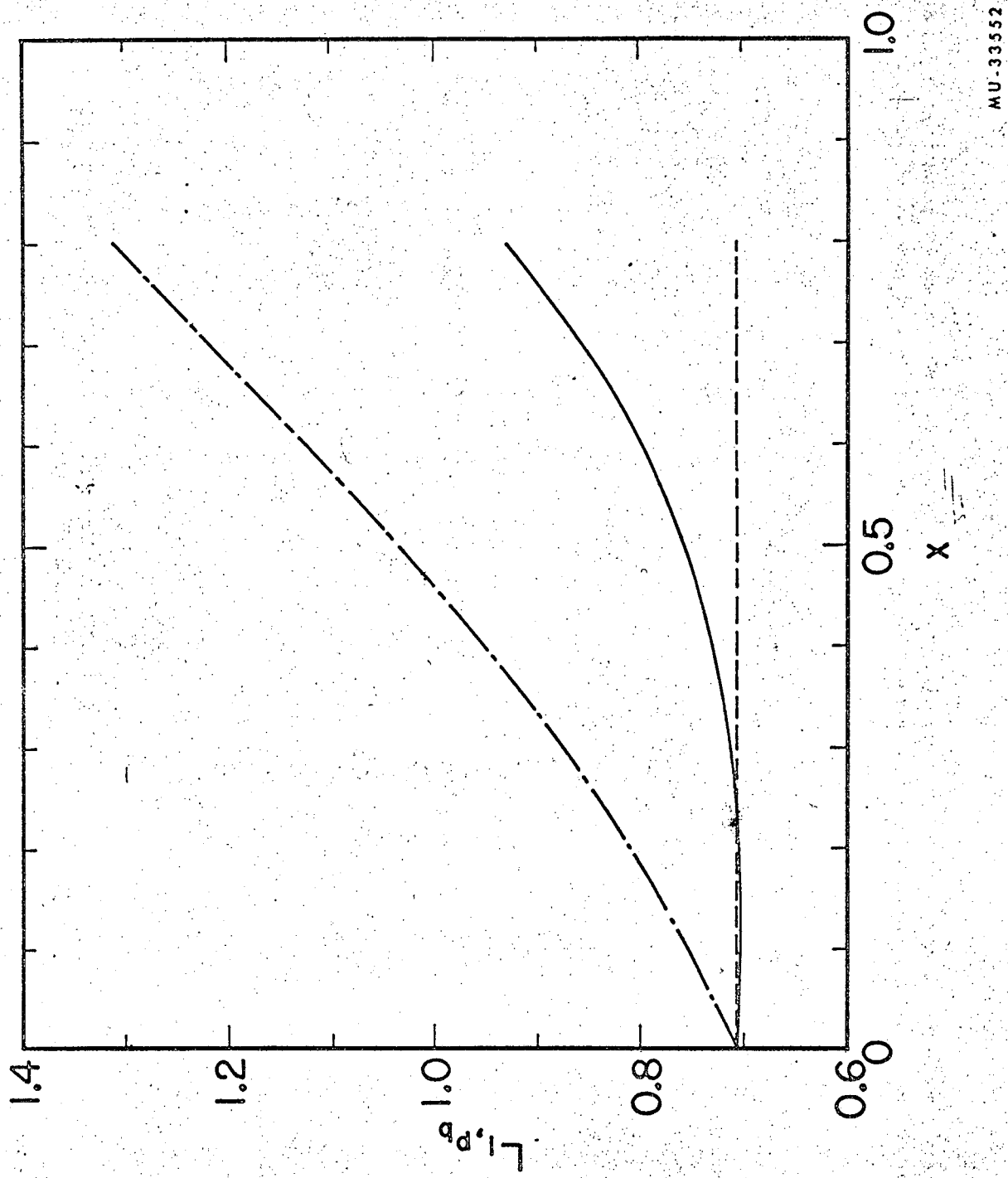

Fig. 24

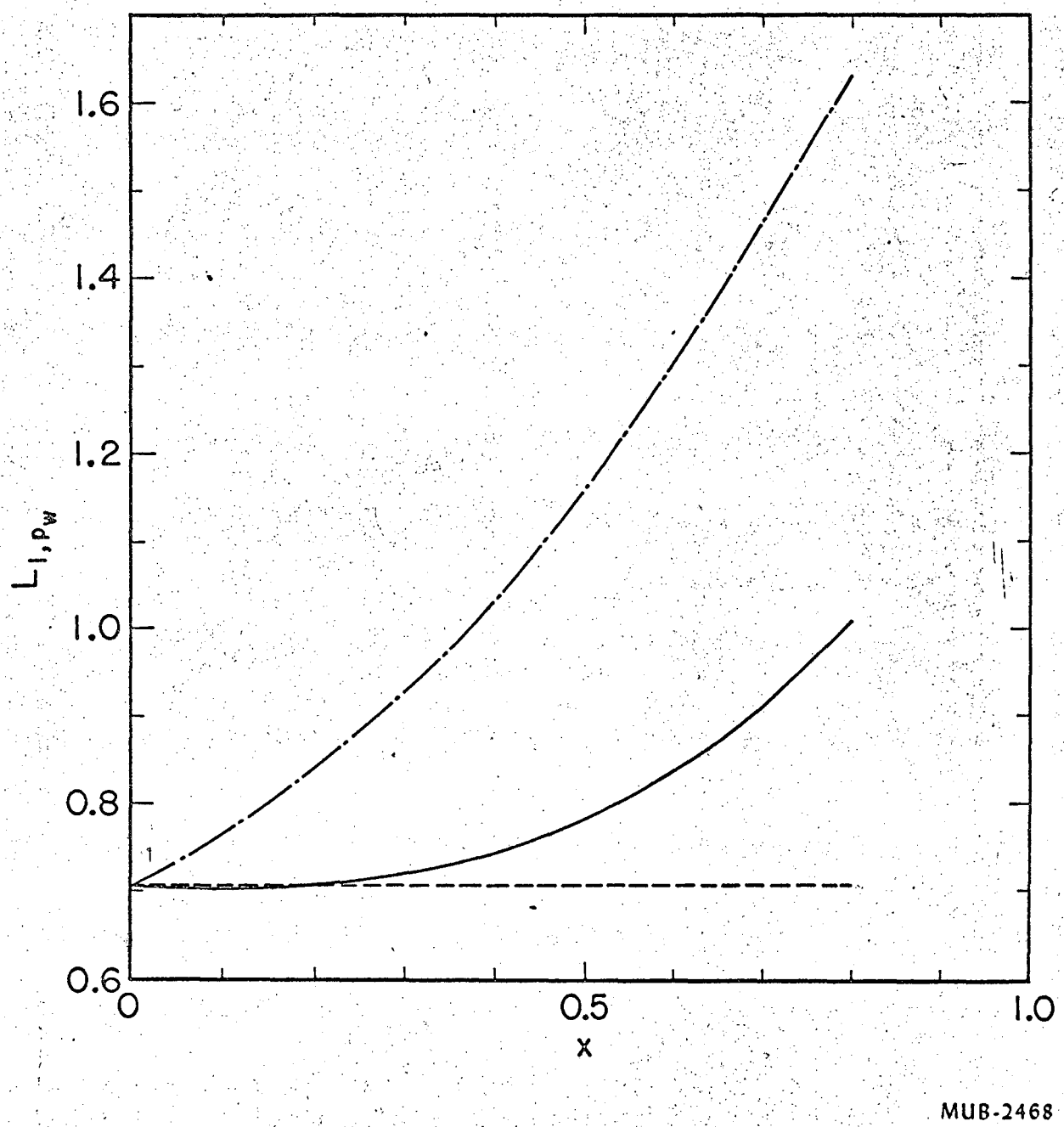

Fig. 25

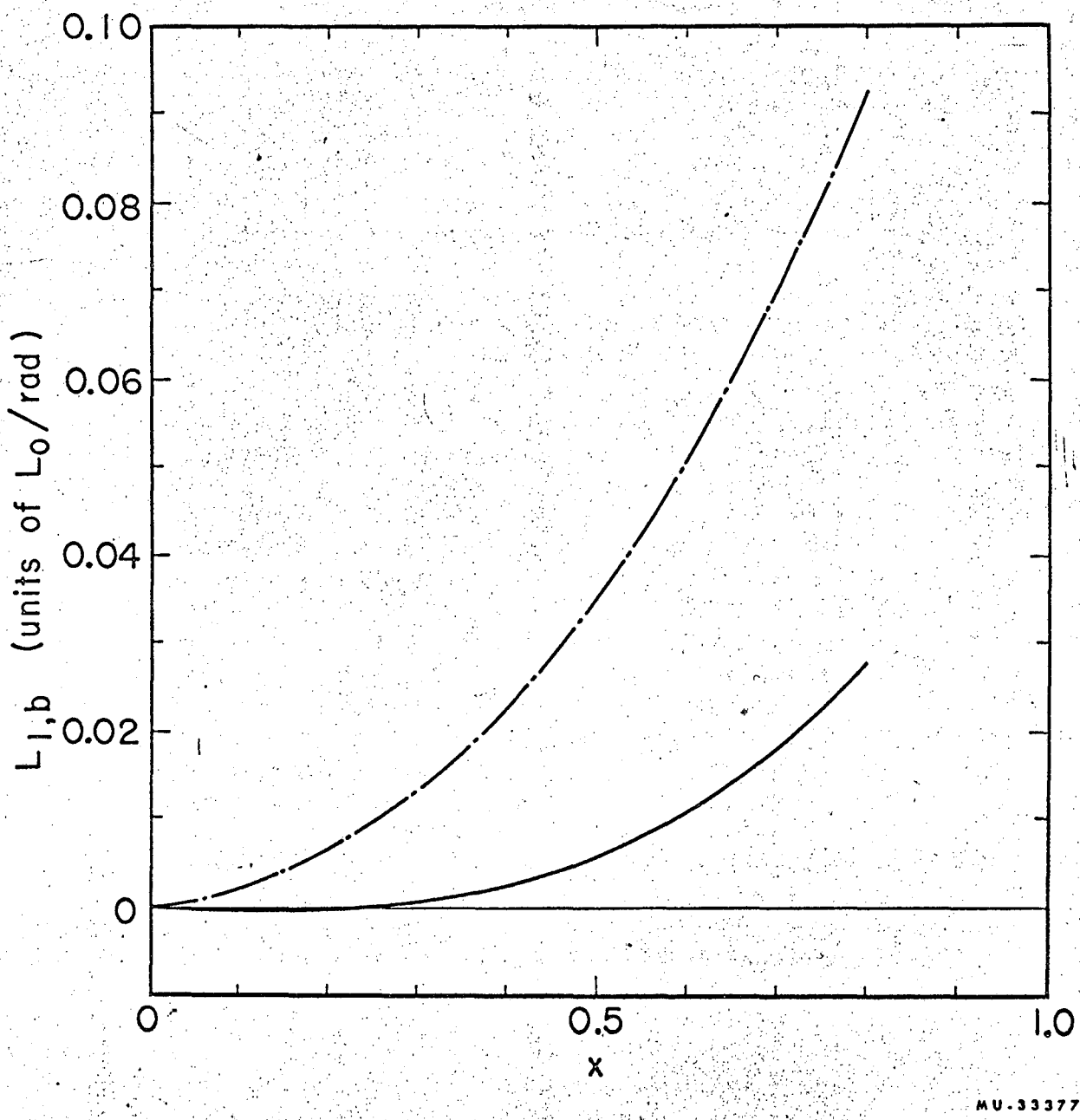

Fig. 26

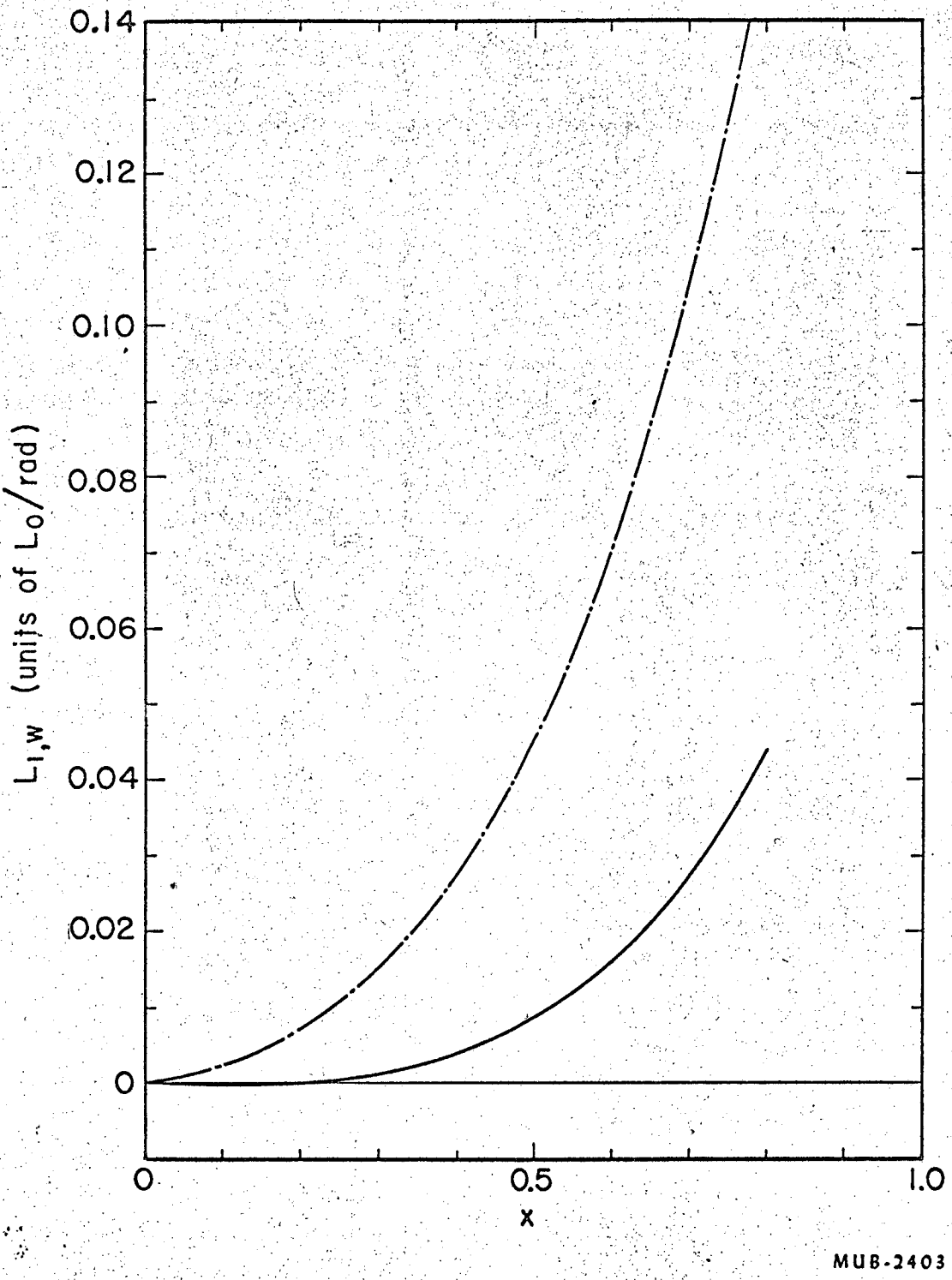
0.14
0.12
0.10
0.08
0.06
0.04
0.02
0
$L_{1,W}$ (units of L_0/rad)
0
0.5
1.0
x
MUB-2403

Fig. 27

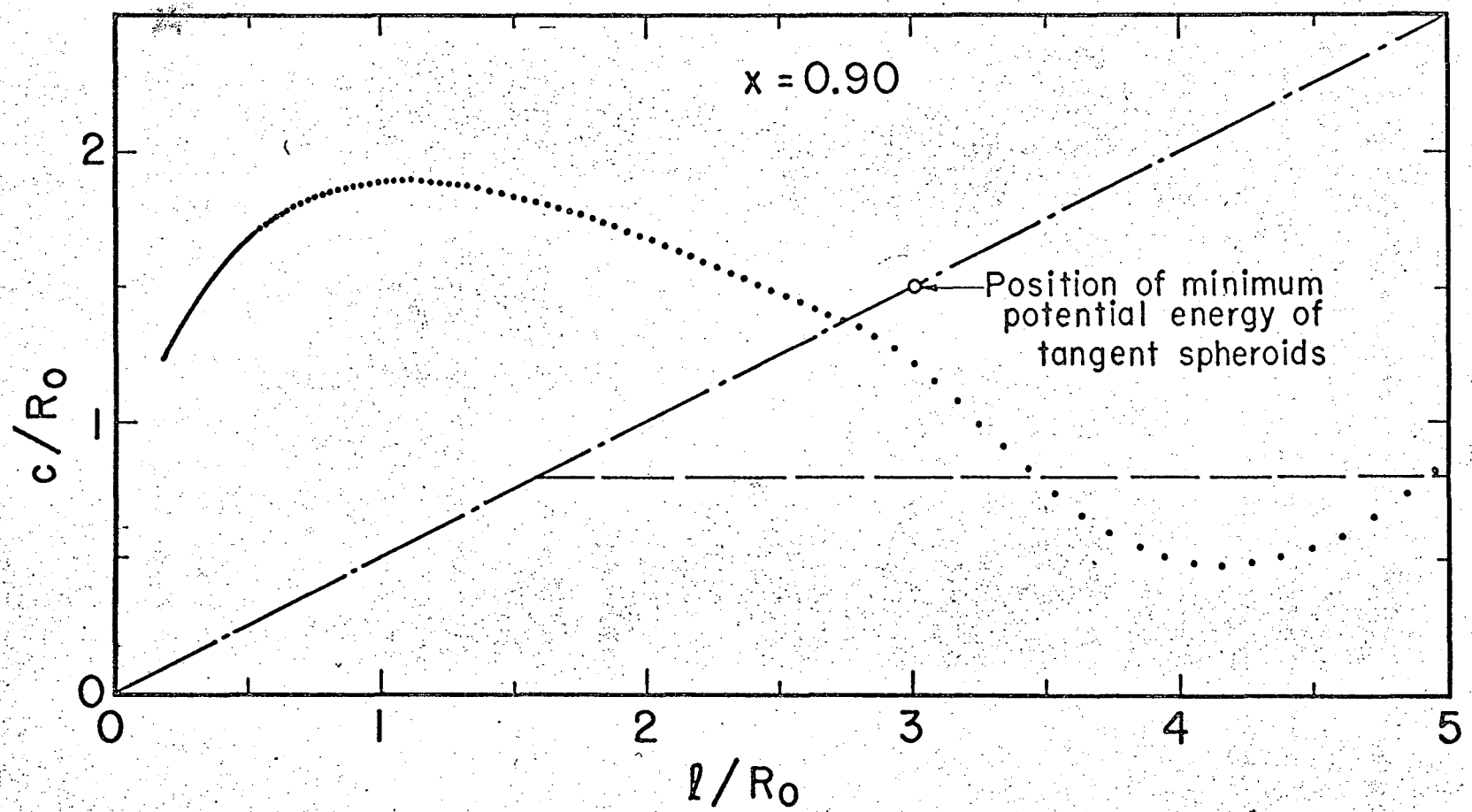

MU-33378

Fig. 28

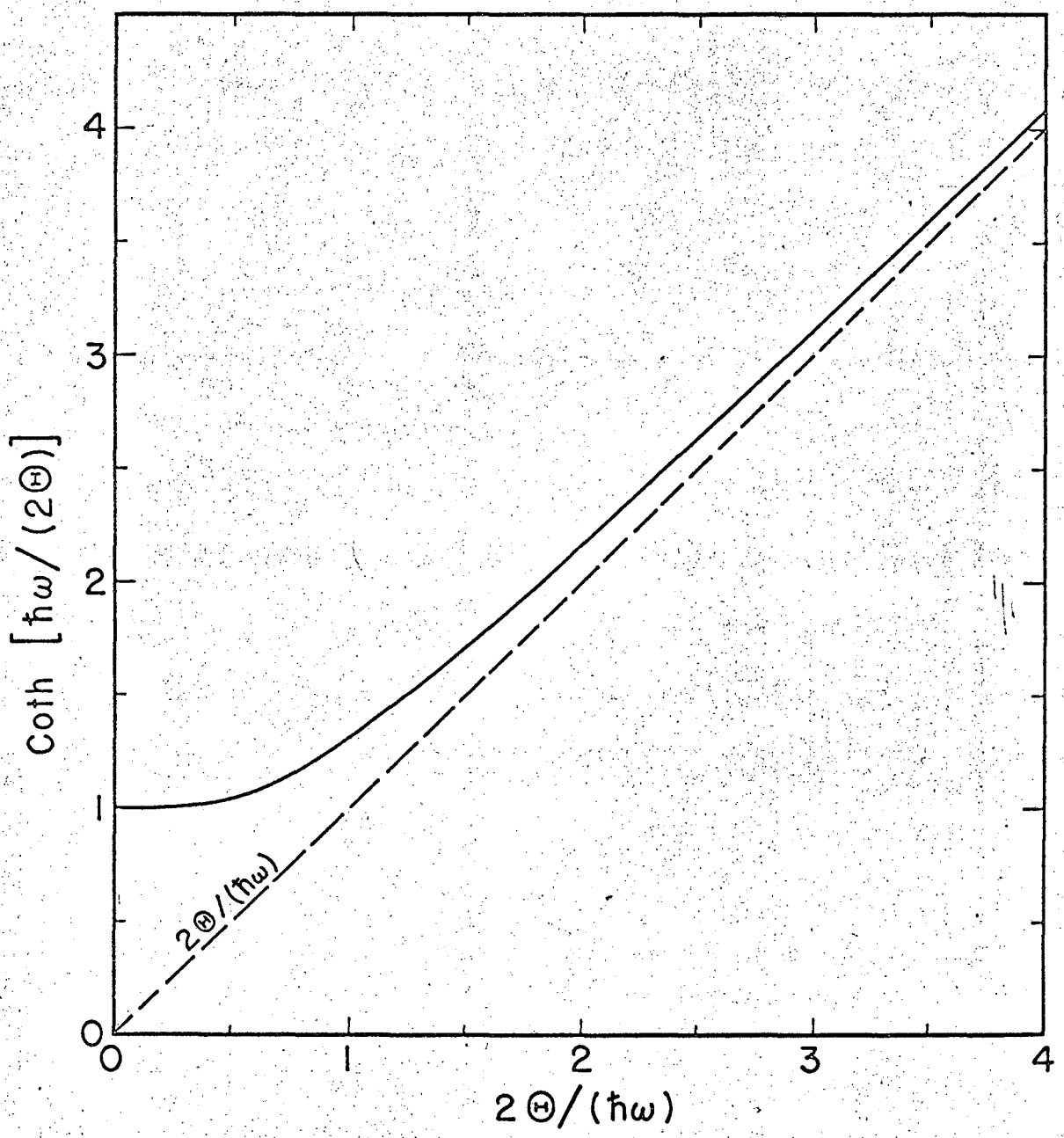

MUB-2404

Fig. 29

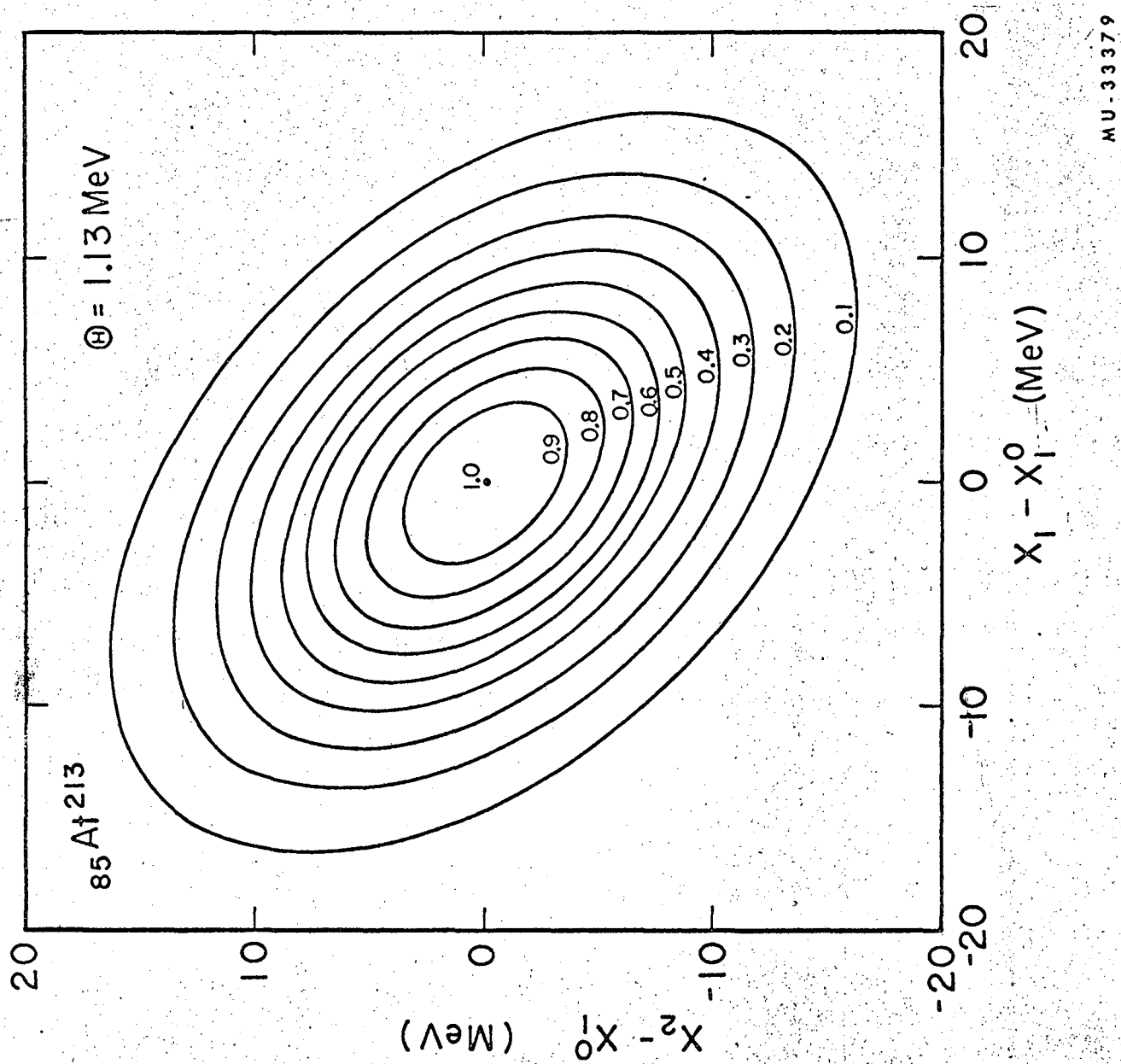
$_{85}At^{213}$
Θ = 1.13 MeV
1.0
0.9
0.8
0.7
0.6
0.5
0.4
0.3
0.2
0.1
$X_2 - X_1^0$ (MeV)
$X_1 - X_1^0$ (MeV)
20
10
0
-10
-20
MU-33379

Fig. 30

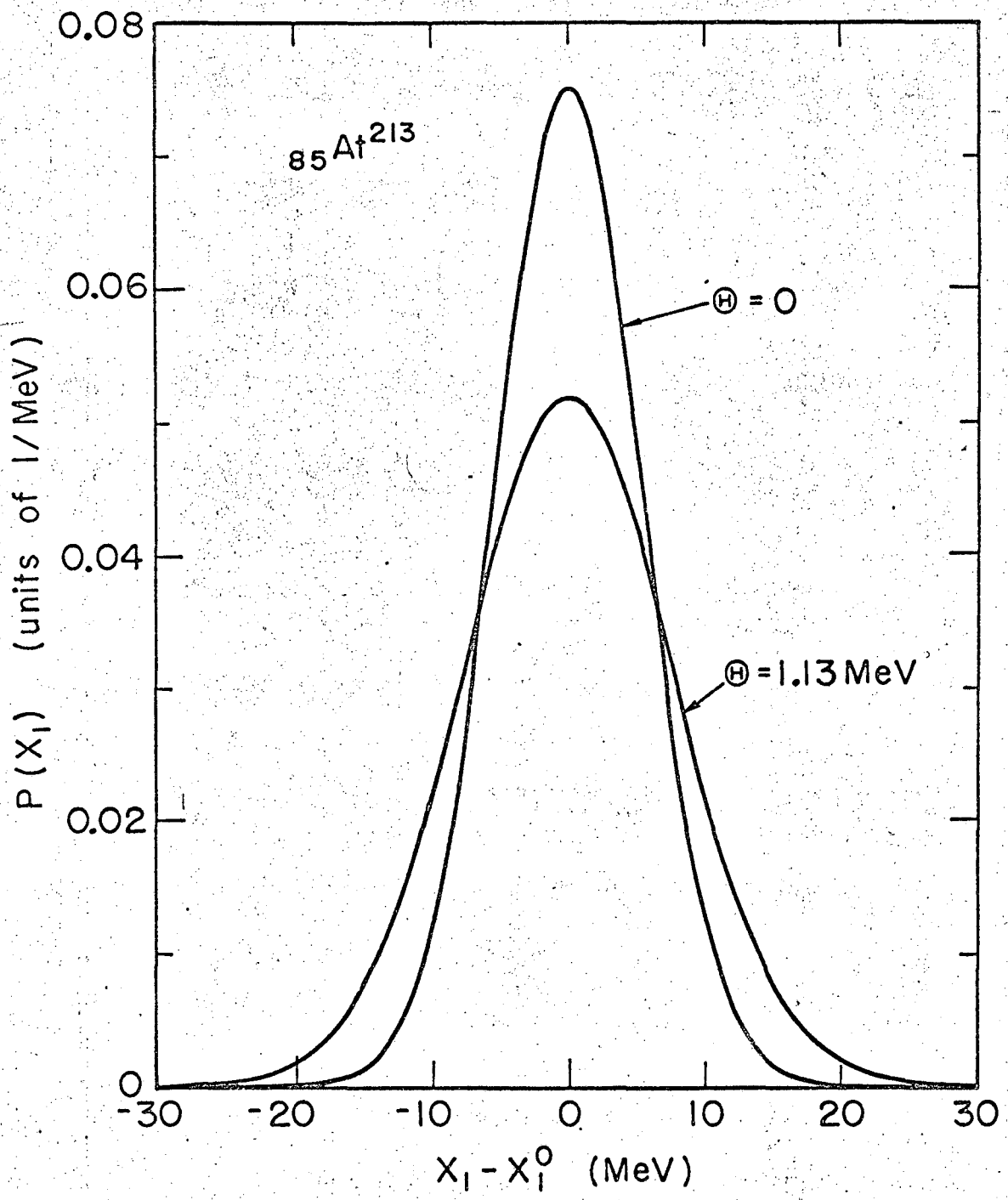

MU-33380

Fig. 31

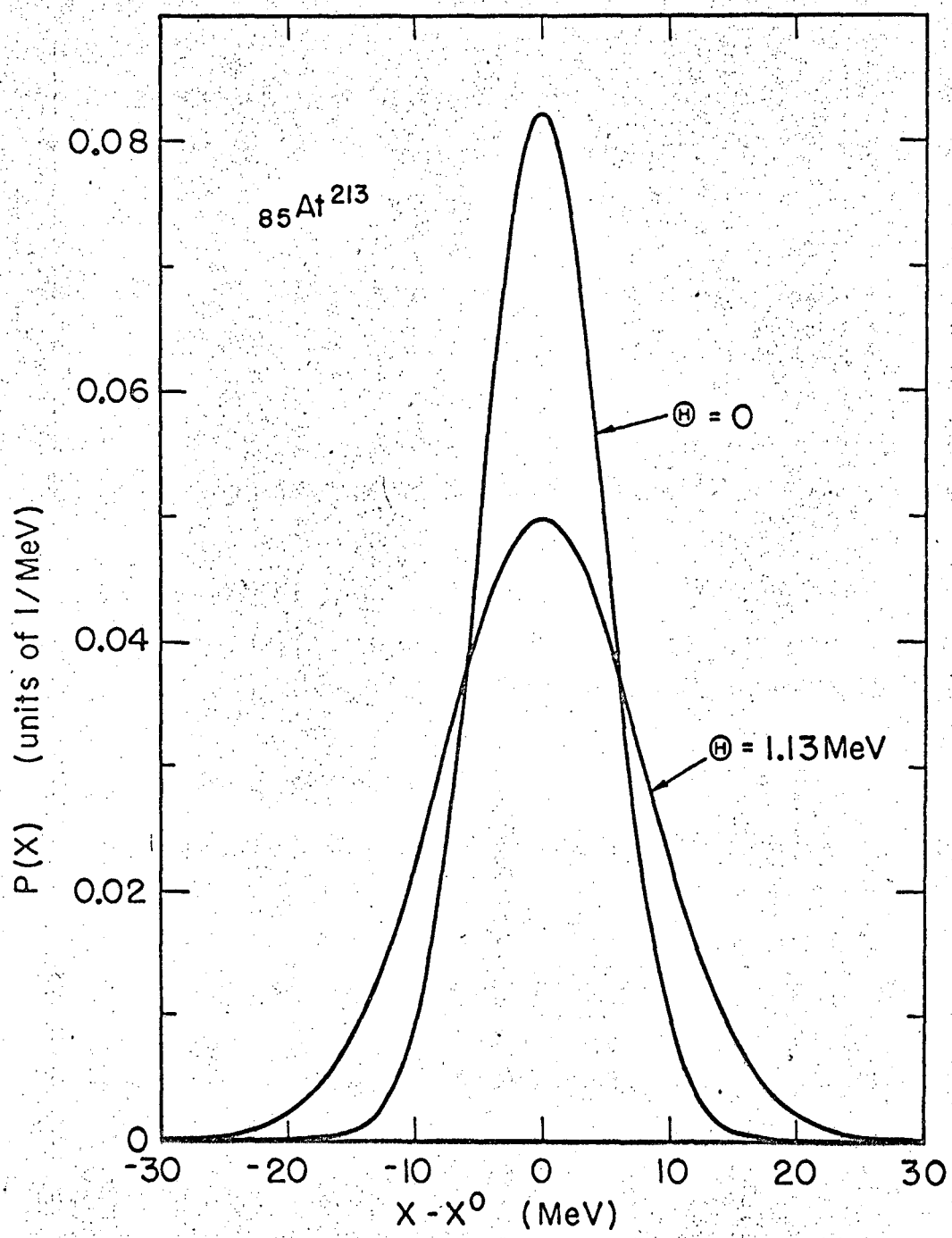

MU-33381

Fig. 32

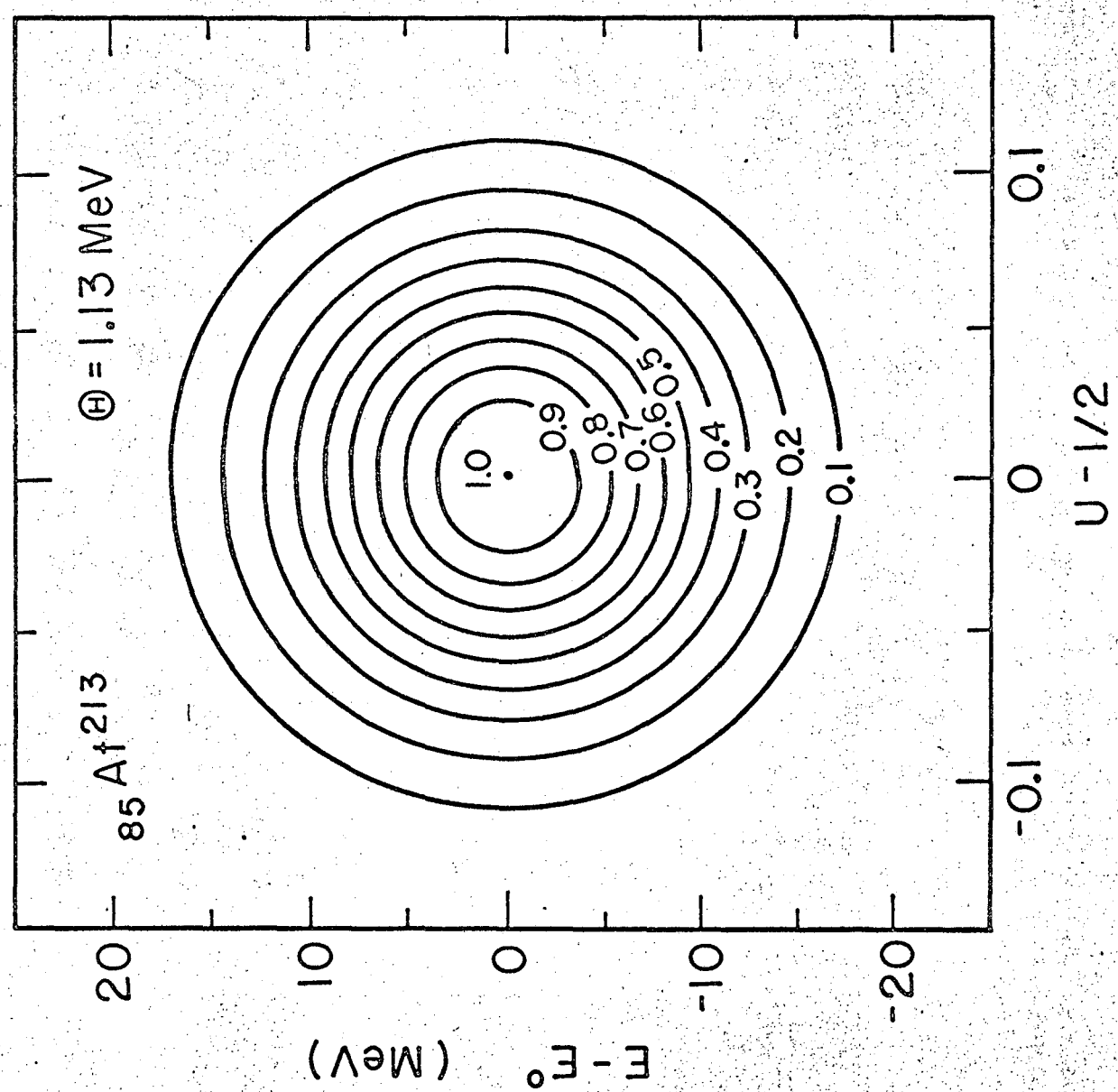

MU-33550

Fig. 33

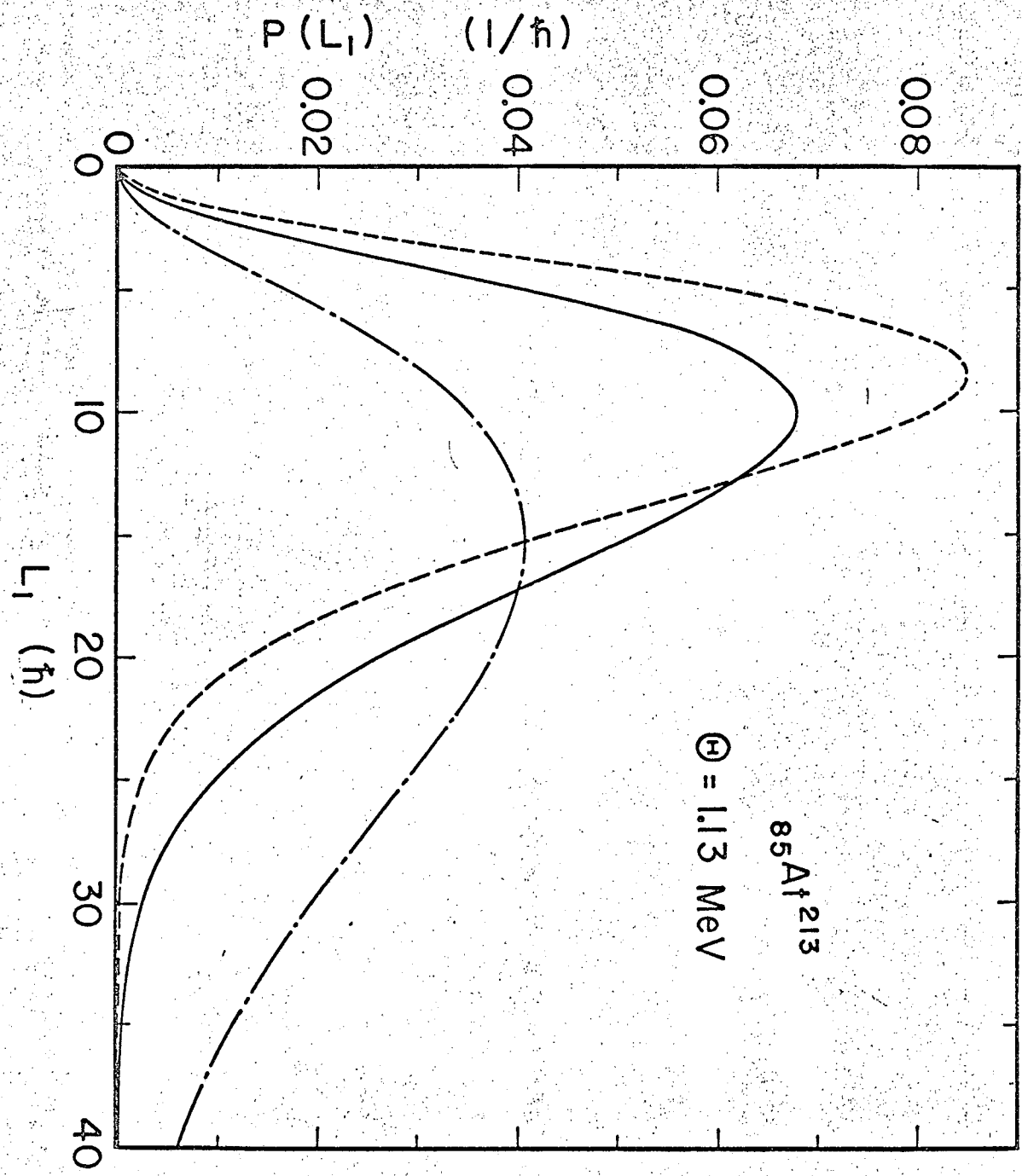

MU-33553

Fig. 34

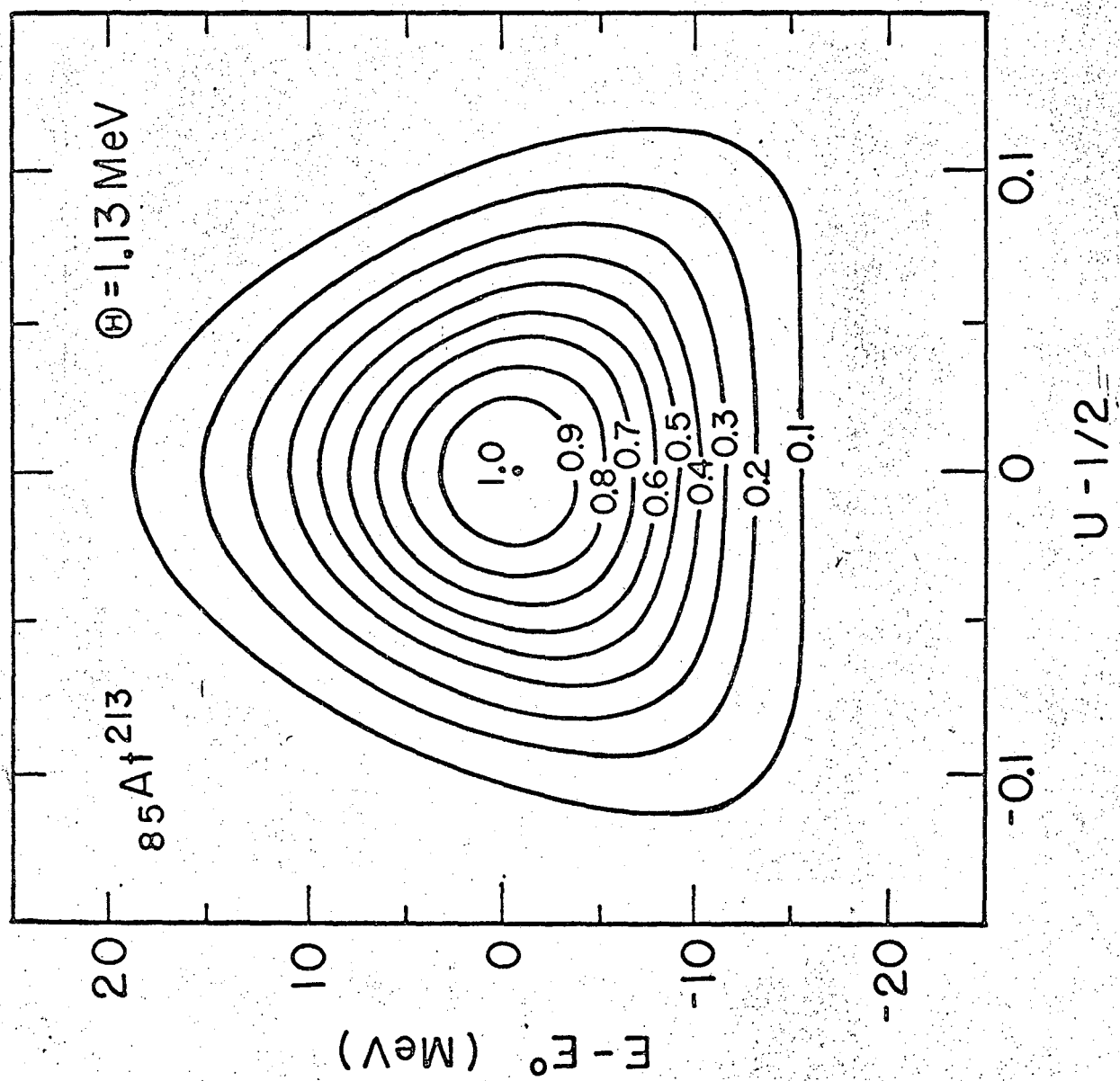

MU-33548

Fig. 35

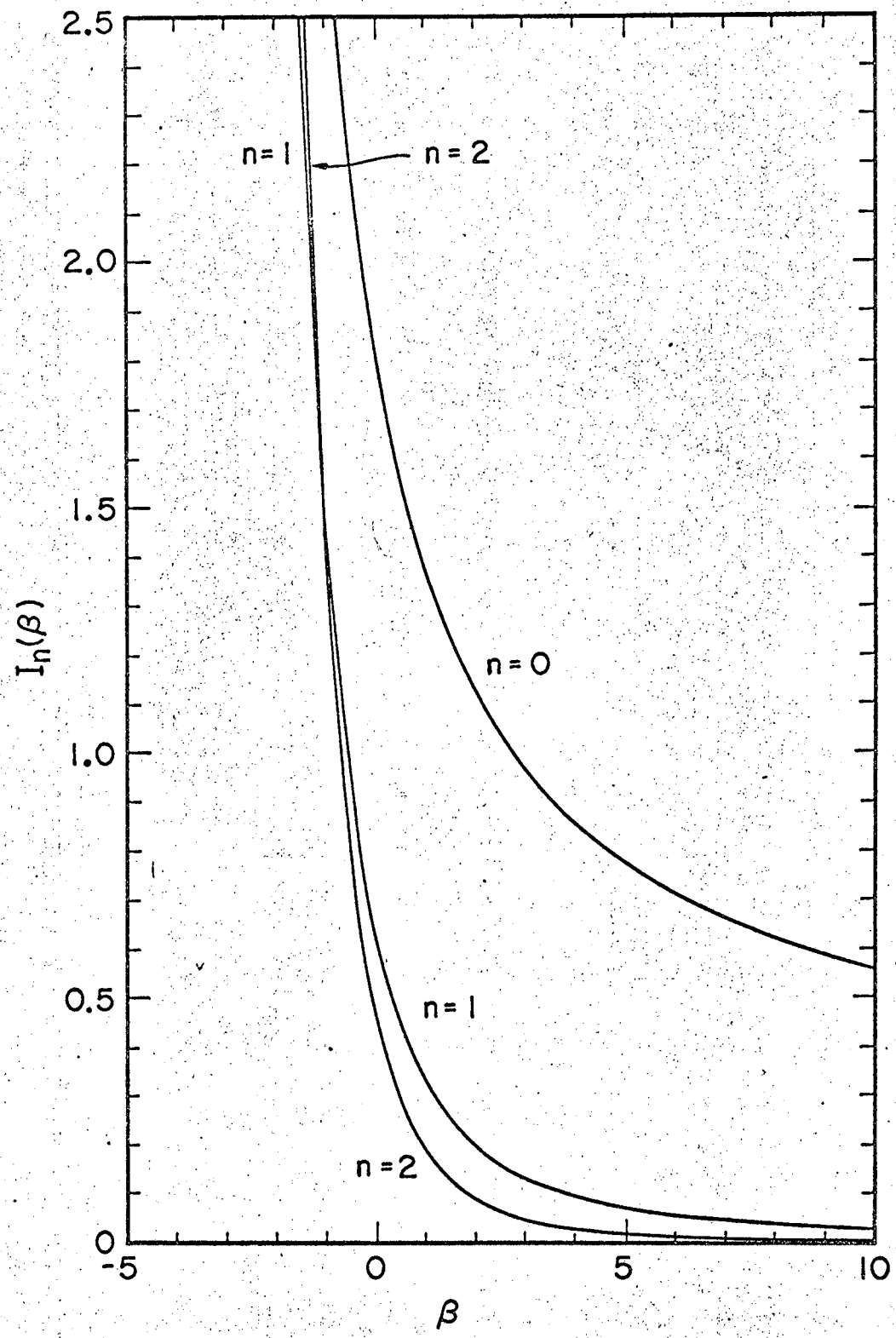

MU-33384

Fig. 36

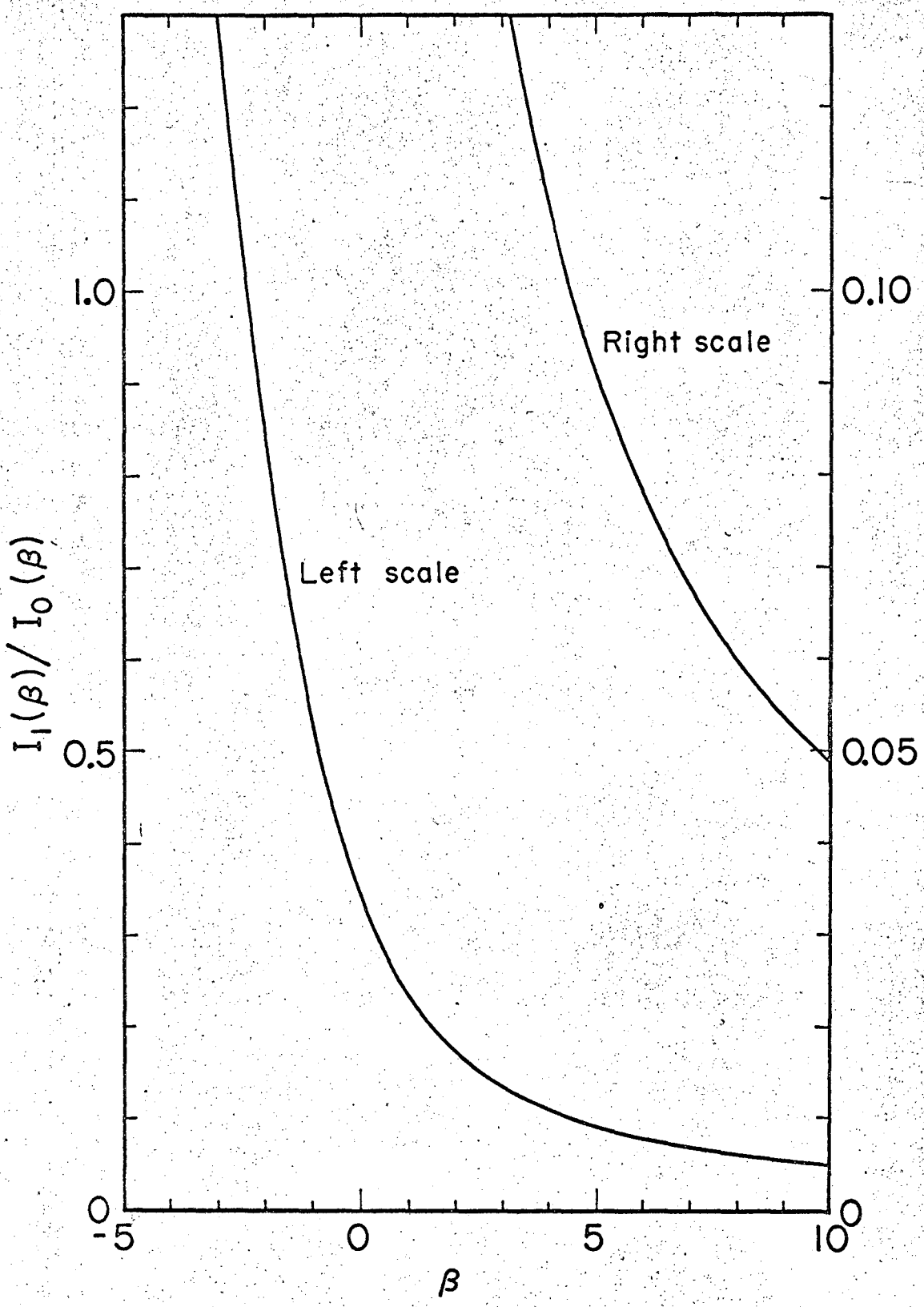

Fig. 37

MU.33385

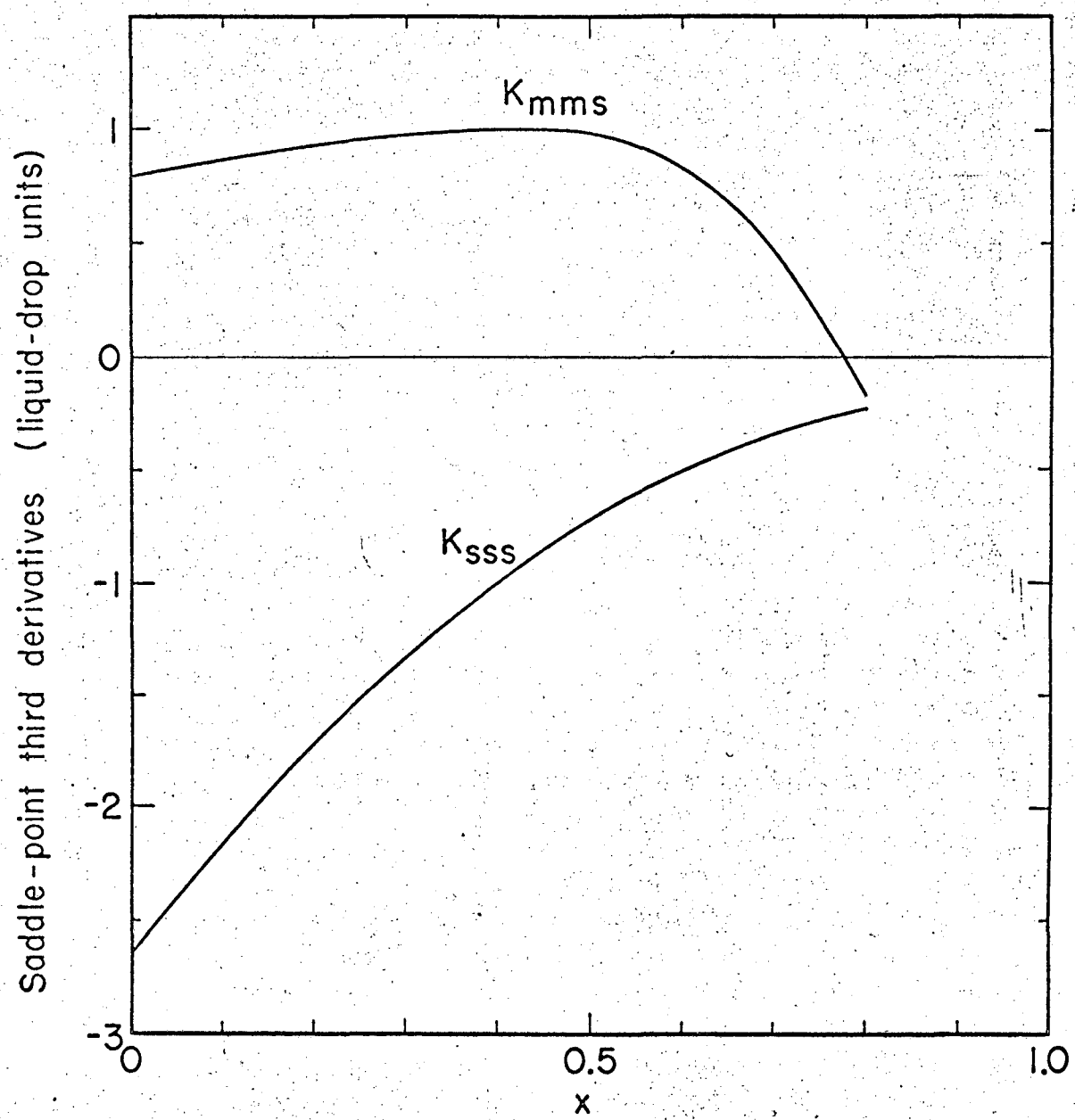

MUB-2425

Fig. 38

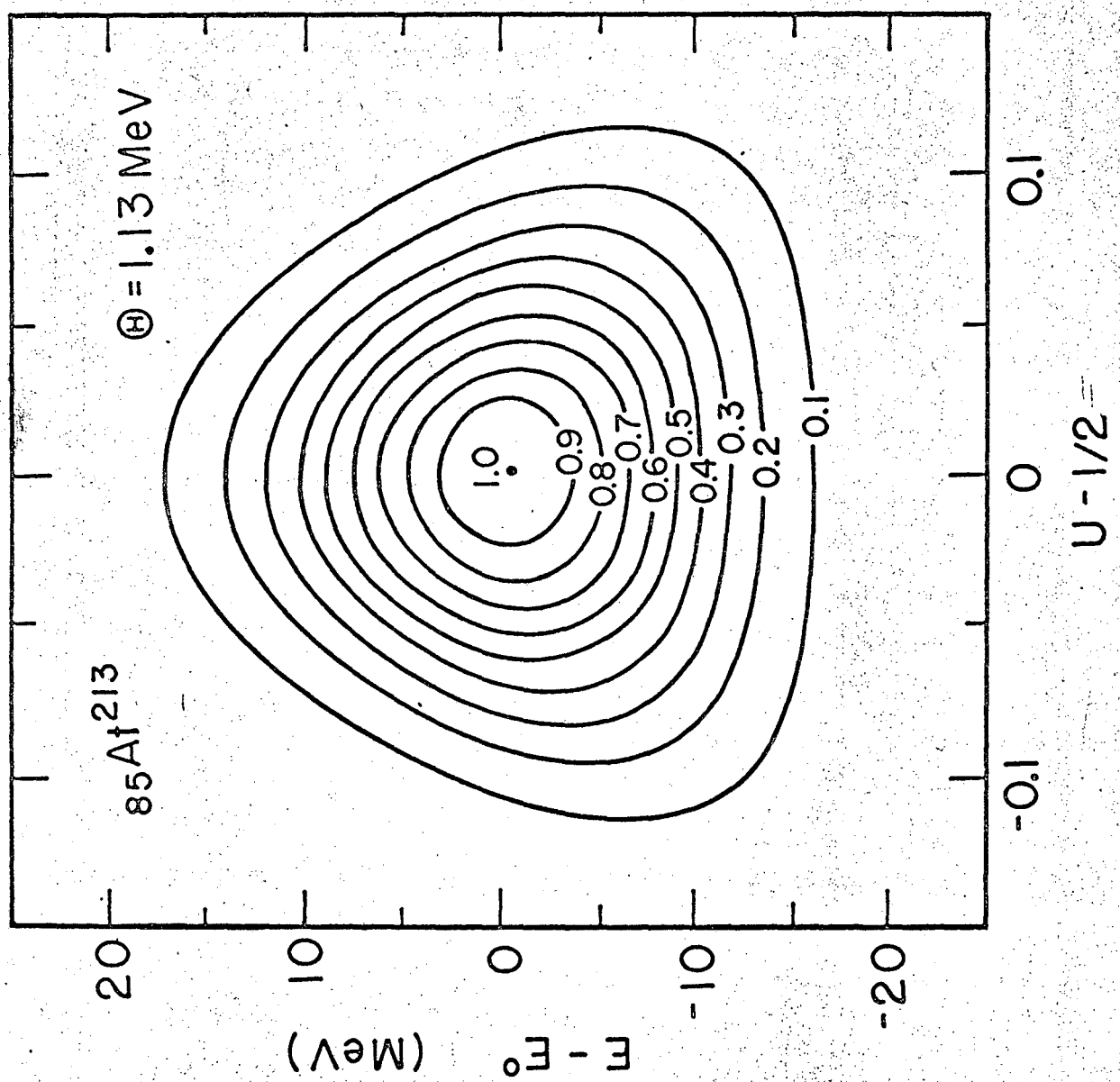

MU-33549

Fig. 39

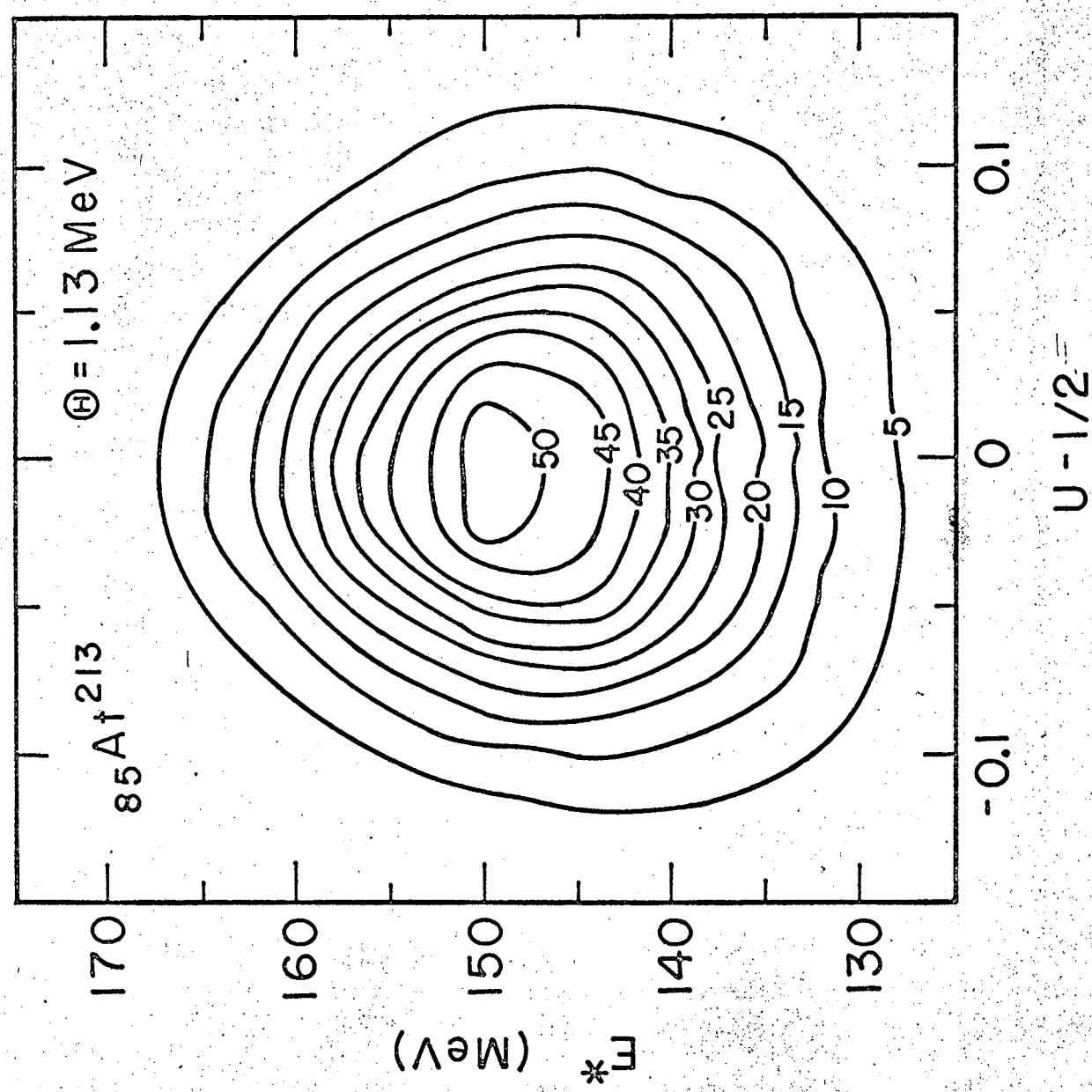

MU-33551

Fig. 40

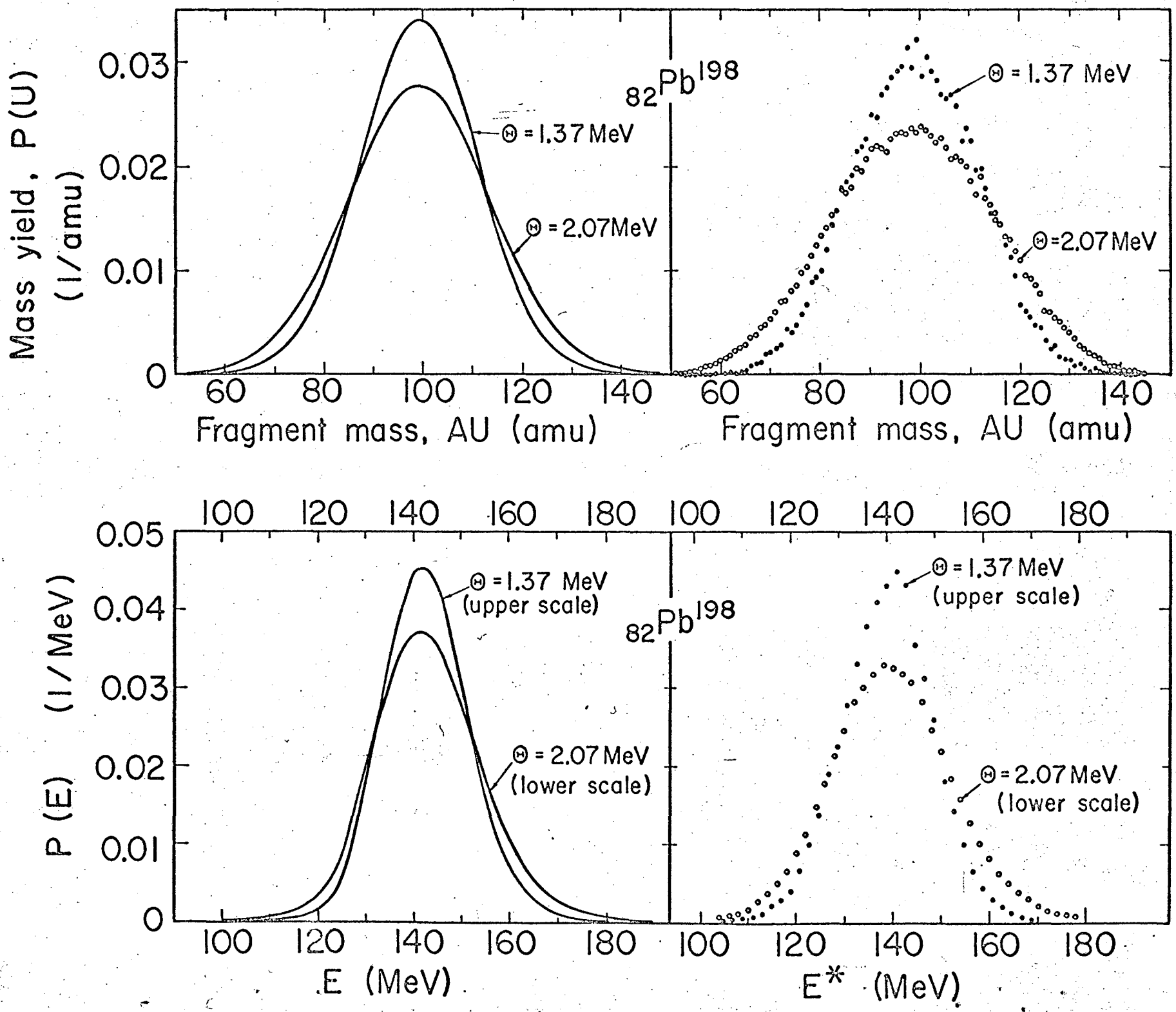
Mass yield, P(U) (1/amu)
0.03
0.02
0.01
0
60
80
100
120
140
Fragment mass, AU (amu)
Θ = 1.37 MeV
Θ = 2.07 MeV
$_{82}Pb^{198}$
P (E) (1/MeV)
0.05
0.04
0.03
0.02
0.01
0
100
120
140
160
180
E (MeV)
E* (MeV)
Θ = 1.37 MeV (upper scale)
Θ = 2.07 MeV (lower scale)

Fig. 41

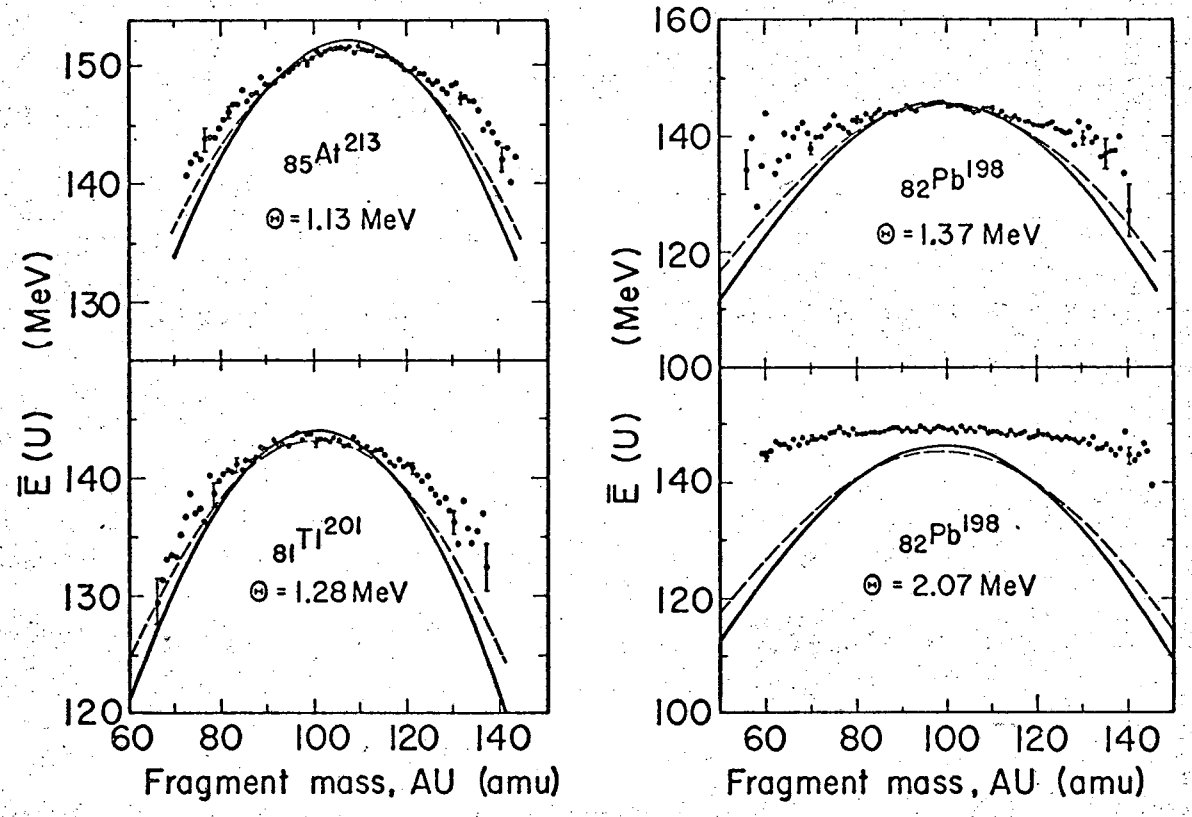
150
140
130
$_{85}At^{213}$
Θ = 1.13 MeV
Ē (U) (MeV)
140
130
120
$_{81}Tl^{201}$
Θ = 1.28 MeV
60 80 100 120 140
Fragment mass, AU (amu)
160
140
120
100
$_{82}Pb^{198}$
Θ = 1.37 MeV
Ē (U) (MeV)
140
120
100
$_{82}Pb^{198}$
Θ = 2.07 MeV
60 80 100 120 140
Fragment mass, AU (amu)
MUB-2407

Fig. 42

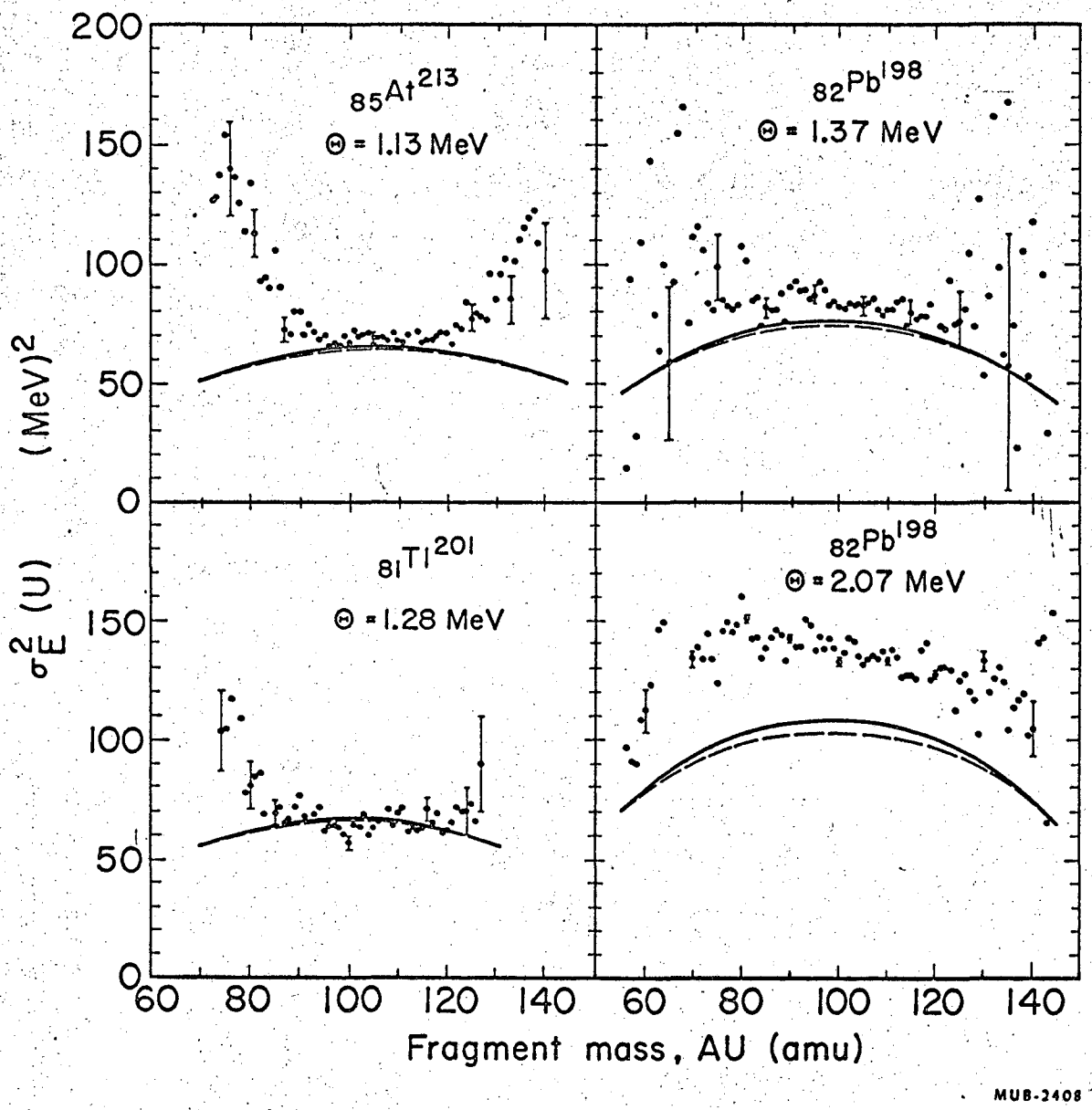
$_{85}At^{213}$
Θ = 1.13 MeV
$_{82}Pb^{198}$
Θ = 1.37 MeV
$_{81}Tl^{201}$
Θ = 1.28 MeV
$_{82}Pb^{198}$
Θ = 2.07 MeV
σ_E^2 (U) (MeV)^2
Fragment mass, AU (amu)
MUB-2408

Fig. 43

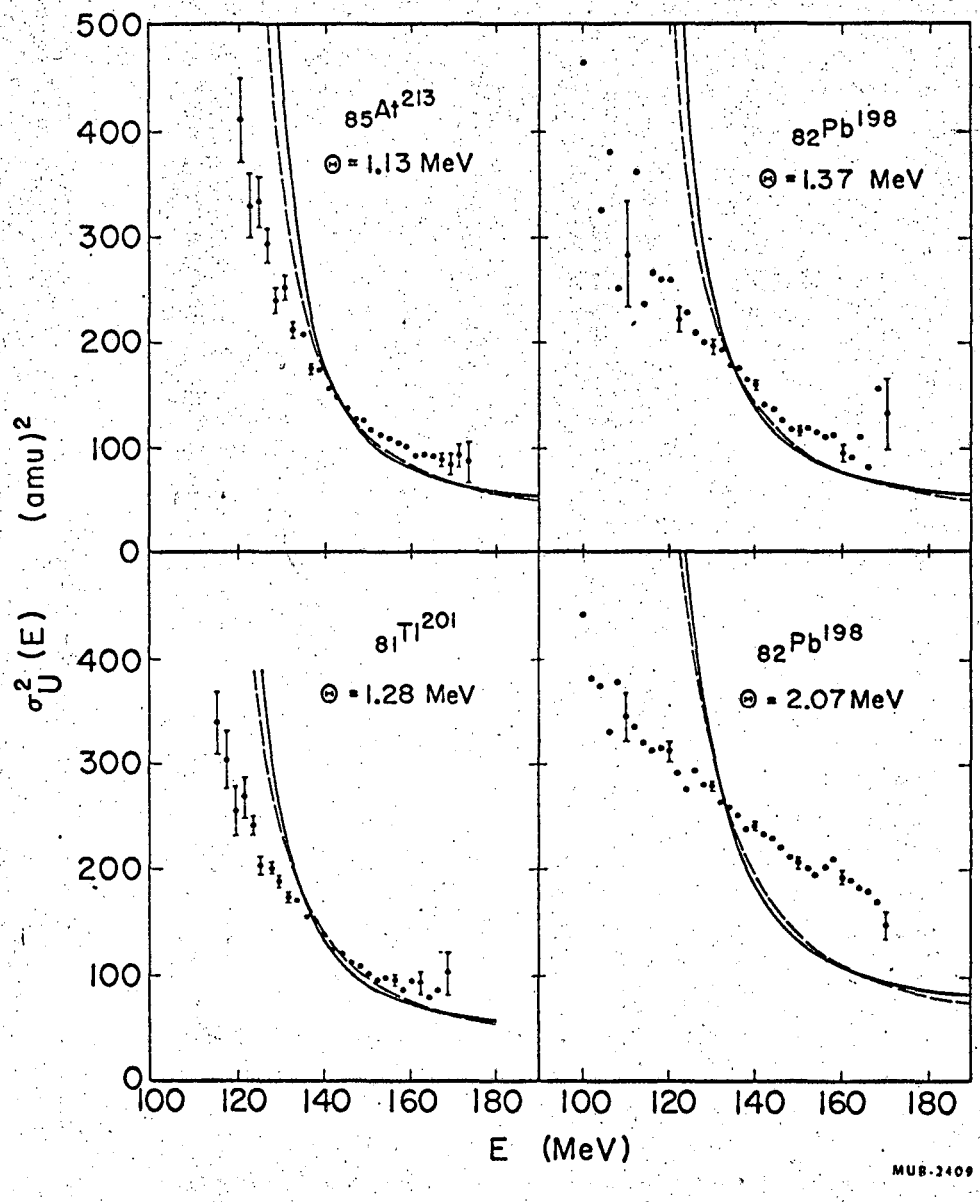
500
400
300
200
100
0
σ_U^2 (E) (amu)^2
$_{85}At^{213}$
Θ = 1.13 MeV
$_{82}Pb^{198}$
Θ = 1.37 MeV
$_{81}Tl^{201}$
Θ = 1.28 MeV
$_{82}Pb^{198}$
Θ = 2.07 MeV
100 120 140 160 180
E (MeV)
MUB-2409

Fig. 44

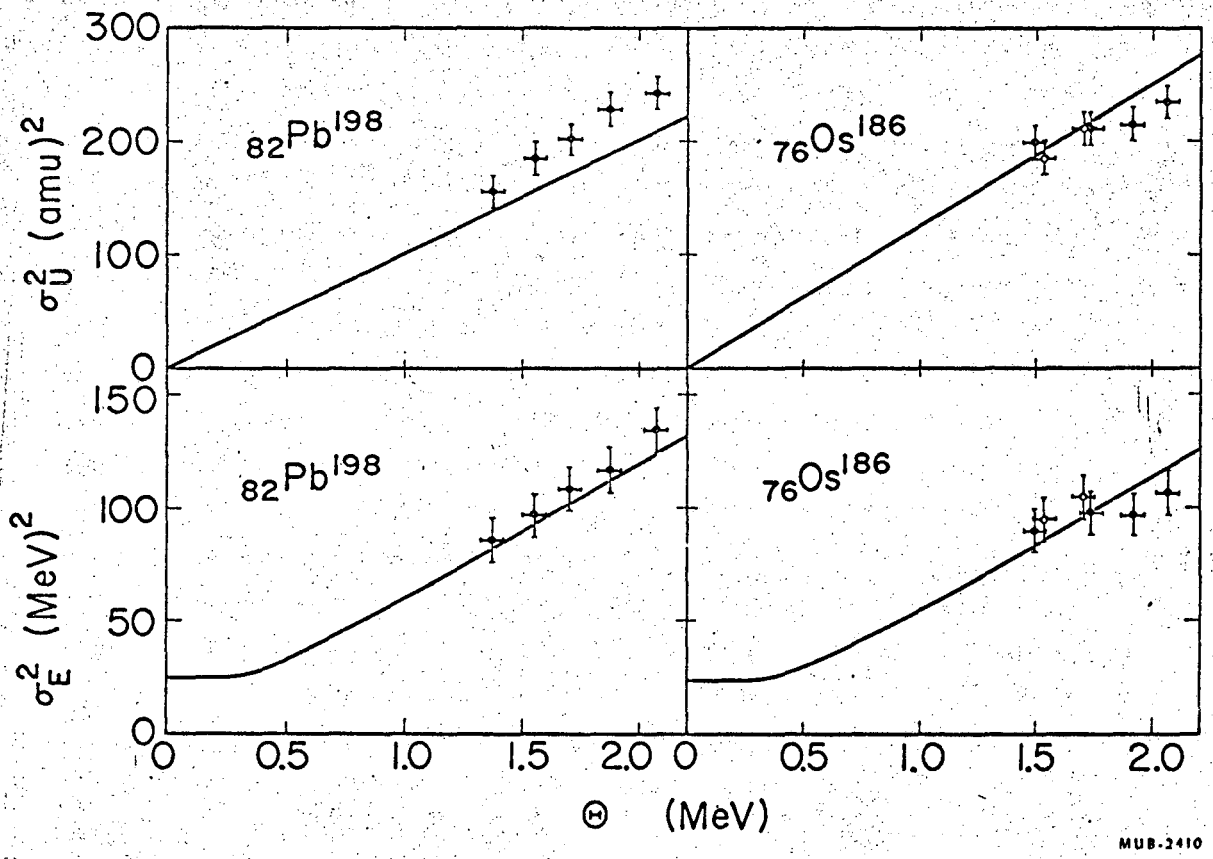
300
200
100
0
150
100
50
0
σ_U^2 (amu)^2
σ_E^2 (MeV)^2
$_{82}Pb^{198}$
$_{76}Os^{186}$
$_{82}Pb^{198}$
$_{76}Os^{186}$
0
0.5
1.0
1.5
2.0
0
0.5
1.0
1.5
2.0
Θ (MeV)
MUB-2410

Fig. 45

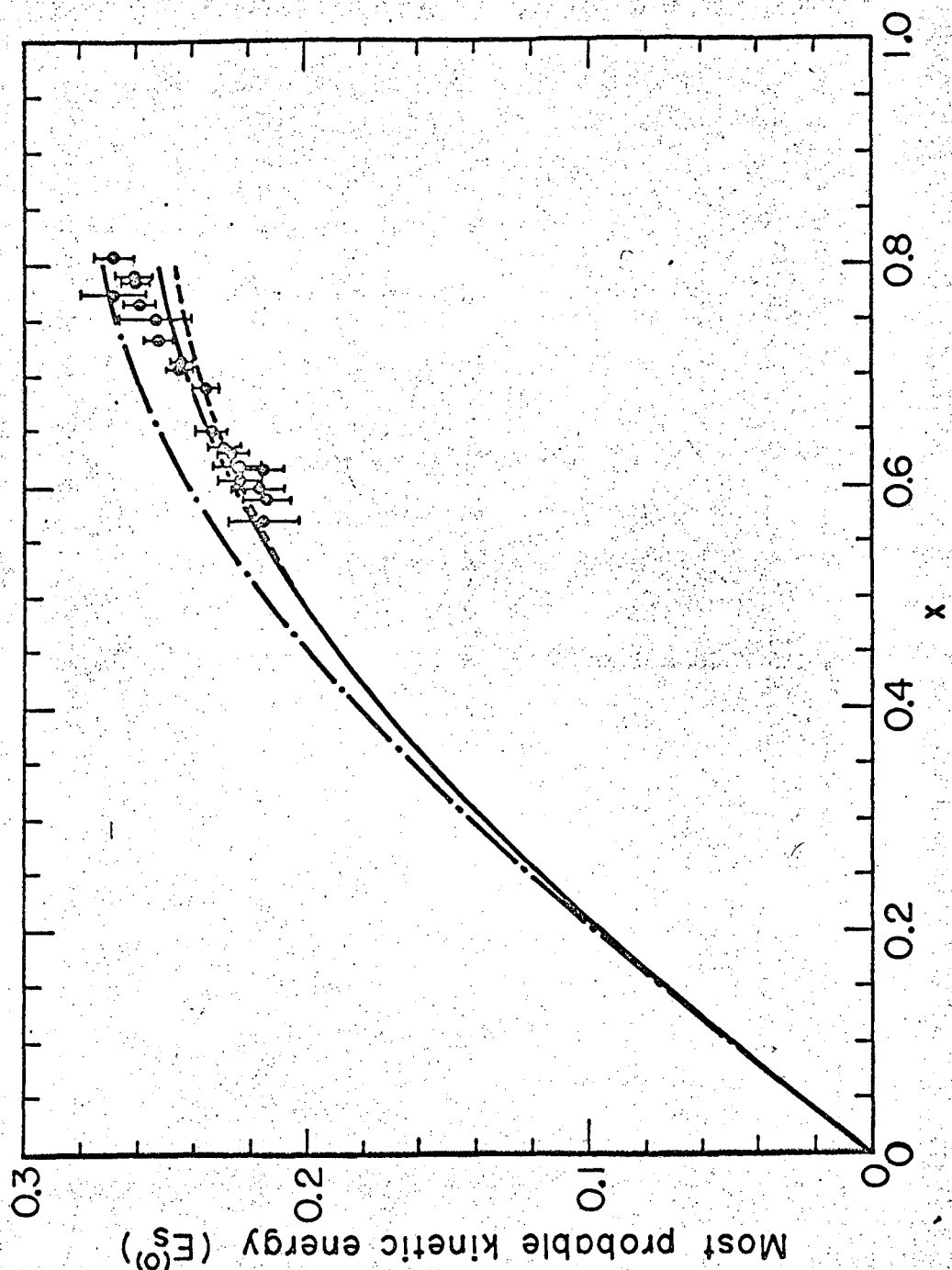

MU-29983

Fig. 46

This report was prepared as an account of Government sponsored work. Neither the United States, nor the Commission, nor any person acting on behalf of the Commission:

A. Makes any warranty or representation, expressed or implied, with respect to the accuracy, completeness, or usefulness of the information contained in this report, or that the use of any information, apparatus, method, or process disclosed in this report may not infringe privately owned rights; or

B. Assumes any liabilities with respect to the use of, or for damages resulting from the use of any information, apparatus, method, or process disclosed in this report.

As used in the above, "person acting on behalf of the Commission" includes any employee or contractor of the Commission, or employee of such contractor, to the extent that such employee or contractor of the Commission, or employee of such contractor prepares, disseminates, or provides access to, any information pursuant to his employment or contract with the Commission, or his employment with such contractor.